

University of Alberta

Cobalt-Mediated Pentadienyl/Alkyne [5+2] Cycloaddition Reactions

by

Kai Erik Oskar Ylijoki

A thesis submitted to the Faculty of Graduate Studies and Research
in partial fulfillment of the requirements for the degree of

Doctor of Philosophy

Department of Chemistry

©Kai Erik Oskar Ylijoki
Spring 2010
Edmonton, Alberta

Permission is hereby granted to the University of Alberta Libraries to reproduce single copies of this thesis and to lend or sell such copies for private, scholarly or scientific research purposes only. Where the thesis is converted to, or otherwise made available in digital form, the University of Alberta will advise potential users of the thesis of these terms.

The author reserves all other publication and other rights in association with the copyright in the thesis and, except as herein before provided, neither the thesis nor any substantial portion thereof may be printed or otherwise reproduced in any material form whatsoever without the author's prior written permission.

Examining Committee

Dr. Jeffrey M. Stryker, Department of Chemistry

Dr. Dennis G. Hall, Department of Chemistry

Dr. Frederick G. West, Department of Chemistry

Dr. Alexander Brown, Department of Chemistry

Dr. Steven M. Kuznicki, Department of Chemical Engineering

Dr. James R. Green, Department of Chemistry and Biochemistry, University of Windsor

*For my family,
whose support has been essential.*

Abstract

A new method for the preparation of seven-membered carbocycles via cobalt-mediated [5+2] cycloaddition methodology is presented. We have demonstrated that $\text{Cp}^*\text{Co}(\eta^5\text{-pentadienyl})^+$ systems undergo cycloaddition reactions with alkynes in a diastereocontrolled and high-yielding process. When acetylene is employed as the cycloaddition partner, unprecedented $\text{Cp}^*\text{Co}(\eta^2, \eta^3\text{-cycloheptadienyl})^+$ complexes were isolated as the cycloaddition product under kinetic control. These allyl/olefin species were further transformed to the thermodynamic $\text{Cp}^*\text{Co}(\eta^5\text{-cycloheptadienyl})^+$ complexes. Also described are two methods for the preparation of high-valent Co(III) $\eta^5\text{-pentadienyl}$ complexes, a compound class that has been under-reported in the literature. This work fills this void and provides a valuable view of the structural properties of $\eta^5\text{-pentadienyl}$ complexes as a function of the substitution pattern.

The incorporation of tethered pronucleophiles onto the pentadienyl ligand allowed the preparation of fused bicyclic structures of relevance to natural product synthesis. Both conjugated and unconjugated cycloheptadiene species were prepared, made possible via the differing cycloheptadienyl complex hapticity. The oxidative decomplexation of the organic products is also described. Initial steps towards a divergent pronucleophile-bearing pentadienyl synthesis were also undertaken.

The mechanism and structure/reactivity relationships for the [5+2] cycloaddition process were studied via density functional theory calculations. These investigations revealed the existence of several convergent reaction pathways on the potential energy surface, and provided a new rationale for the $\eta^2, \eta^3 \rightarrow \eta^5$ isomerization, thereby explaining the low activation barrier for the isomerization of 2-butyne cycloadducts. Of interest is

the elucidation of a radical-type pathway, calculated to be of high energy for the Cp* ligand system, yet energetically competitive in the Cp complex reaction manifold. Further, computations on the Cp system demonstrate a potentially viable pathway on the triplet energy surface, suggesting spin-forbidden transitions may play a role in the mechanism. These observations provide an explanation for the differing cycloaddition efficiencies in these two pentadienyl systems. Calculations also suggest that reaction chemoselectivity is determined during the rate-limiting alkyne complexation step; the energetics of this process being dominated by steric interactions between the pentadienyl substituents and the ancillary ligand.

Finally, initial synthetic development of a new six-electron anionic ligand template is described. Both synthetic and theoretical investigations provide insight into the ligand design and function and suggest viable new avenues of study.

Acknowledgements

I would first like to thank my family for all the support and assistance that they have provided throughout my academic career, in particular my grandparents Erkki and Ida Munnukka, who unfortunately are not here to see this work, and my parents Erkki and Eileen Ylijoki. My supervisor Prof. Jeffrey M. Stryker, whose never ending stream of suggestions ensured I always had something to contemplate and thereby ensured my continued development, also receives my full appreciation. I also thank Prof. Peter H. M. Budzelaar for permitting me to work with his group for two months and teaching me the ways of computational chemistry.

The members of the Stryker group have made my time here both educational and enjoyable and I owe much of my accomplishments to their assistance, particularly Dr. Ross Witherell, Dr. Owen Lightbody, Dr. Bryan Chan, Andrew Kirk, Jeremy Gauthier, and Jeffrey Quesnel. A very special thanks is given to Dr. Masaki Morita, who was a great help in my early days with his constant willingness to explain and/or discuss difficult concepts; much of my deeper understanding arose from these conversations. Thanks to Dr. Robin Hamilton for his patience in editing this dissertation. Also, thank you to Sebastian Böcklein and Verner Lofstrand for being willing to trust me as their research supervisor, if only for a short period of time! Thank you to Drs. Robert MacDonald and Michael Ferguson of the X-ray crystallography laboratory, whose efforts contributed significantly within. Finally, it would be impossible to perform the quality of work we accomplish at the University of Alberta without the excellent support staff, all of whom deserve credit, but special thanks are extended to Dr. Angie Morales-Izquierdo, Mark Miskolzie, Wayne Moffat, and Ryan Lister.

Table of Contents

Chapter 1: [5+2] Cycloaddition Chemistry in Organic and Organometallic Synthesis

Part A: Seven-Membered Carbocycles	1
Part B: Perezone Type-[5+2] Cycloaddition Reactions	2
I. The Perezone to Pipitzol Transformation	2
II. Intermolecular [5+2] Cycloaddition Variants	4
III. [5+2] Cycloaddition Reactions via Oxidation of Phenols	8
IV. Additional Natural Product Syntheses	10
Part C: Kojic Acid Type-[5+2] Cycloaddition Reactions	12
I. The “Cyanoethylation” of Kojic Acid	13
II. Oxidopyrylium Ylids Generated via Group Transfer	14
III. Oxidopyrylium Ylids Generated via Group Elimination	19
IV. Natural Product Syntheses	22
Part D: Vinylcyclopropane Cycloaddition Reactions	26
Part E: Rhodium-Catalyzed Vinylcyclopropane Cycloaddition Reactions	28
I. Intramolecular Cycloaddition Reactions	28
II. Intermolecular Cycloaddition Reactions	32
III. Natural Product Syntheses	35
IV. Mechanistic Studies	37
Part F: Ruthenium-Catalyzed Vinylcyclopropane Cycloaddition Reactions	38
Part G: Nickel- and Iron-Catalyzed Vinylcyclopropane Cycloaddition Reactions	39
Part H: Fischer Carbene Mediated [5+2] Cycloaddition Reactions	40

<i>Part I: Allylsilane [5+2] Cycloaddition Reactions</i>	41
<i>Part J: Metal-Mediated η^3-Pentadienyl [5+2] Cycloaddition Reactions</i>	42
<i>Part K: Metal-Mediated η^5-Pentadienyl [5+2] Cycloaddition Reactions</i>	45
<i>Part L: Conclusion</i>	48

Chapter 2: The Preparation of Cobalt(III) η^5 -Pentadienyl Complexes

<i>Part A: Project Background</i>	50
<i>Part B: High-Valent Group 9 η^5-Pentadienyl Compounds</i>	53
<i>Part C: The Synthesis of Cobalt(III) η^5-Pentadienyl Complexes</i>	57
I. <i>Synthesis of Pentadienol Substrates</i>	59
II. <i>Synthesis of η^5-Pentadienyl Complexes via Unconjugated Dienols</i> ..	62
III. <i>Synthesis of η^5-Pentadienyl Complexes via Conjugated Dienols</i>	65
<i>Part D: Summary</i>	73

Chapter 3: Cobalt-Mediated η^5 -Pentadienyl/Alkyne [5+2] Cycloaddition Reactions

<i>Part A: Introduction</i>	74
<i>Part B: Cobalt-Mediated [5+2] Cycloaddition Reactions</i>	75
<i>Part C: Results</i>	78
<i>Part D: Alkyne Surrogates</i>	85
<i>Part E: Summary and Conclusions</i>	86

Chapter 4: Synthesis of [5.3.0]- and [5.4.0]-Bicyclic Systems via [5+2] Cycloaddition Chemistry

<i>Part A: Introduction</i>	88
<i>Part B: Substrate Preparation</i>	89

<i>Part C: Cp*Co(η^5-Pentadienyl)⁺ Complex Preparation</i>	92
<i>Part D: Pentadienyl/Alkyne [5+2] Cycloaddition Reactions</i>	94
<i>Part E: Intramolecular Cyclization Reactions</i>	99
<i>Part F: Decomplexation Reactions</i>	105
<i>Part G: Intramolecular Cycloaddition Investigation</i>	108
<i>Part H: Investigations Toward Substrate Synthesis Generalization</i>	111
<i>Part I: Summary and Conclusions</i>	115

Chapter 5: Cobalt Complex Spectroscopy and Crystallography

<i>Part A: Cp*Co(η^5-Pentadienyl)⁺ Complex Characterization</i>	117
I. ¹ H NMR Spectroscopy	117
II. X-Ray Crystallography	119
<i>Part B: Cp*Co(η^2, η^3-Cycloheptadienyl)⁺ Complex Characterization</i>	124
I. ¹ H NMR Spectroscopy	124
II. X-Ray Crystallography	125
<i>Part C: Cp*Co(η^5-Cycloheptadienyl)⁺ Complex Characterization</i>	129
I. ¹ H NMR Spectroscopy	129
II. X-Ray Crystallography	131
<i>Part D: ¹H NMR Spectroscopy of Cp*Co(η^2, η^2-Cycloheptadiene) Complexes</i>	132
<i>Part E: Cp*Co(η^4-Cycloheptadiene) Complexes</i>	135
I. ¹ H NMR Spectroscopy	135
II. X-Ray Crystallography	135
<i>Part F: Summary and Conclusion</i>	136

Chapter 6: Cobalt-Mediated [5+2] Cycloaddition Reactions: A Density Functional Theory Investigation

<i>Part A: Introduction</i>	138
<i>Part B: The Mechanism of the [5+2] Cycloaddition Reaction</i>	139
<i>Part C: Variant Reaction Pathways</i>	155
<i>Part D: Reaction Selectivity</i>	161
<i>Part E: Summary and Conclusion</i>	165

Chapter 7: Tripodal Phosphine Ligand Investigation

<i>Part A: Introduction</i>	167
<i>Part B: Synthetic Investigation</i>	168
<i>Part C: DFT Investigation</i>	170
<i>Part D: Conclusion</i>	173

Chapter 8: Experimental

<i>Part A: General Experimental</i>	174
<i>Part B: Experimental Details</i>	177
I. Chapter 2	177
II. Chapter 3	187
III. Chapter 4	195
IV. Chapter 6	237
V. Chapter 7	242

Notes and References	245
-----------------------------------	-----

Appendix: Crystallographic Experimental Details	262
--	-----

List of Tables

Table 2.1: Cp*Co(η^5 -pentadienyl) ⁺ Complexes via Unconjugated Dienol Substrates	64
Table 2.2: Cp*Co(η^5 -pentadienyl) ⁺ Complexes via Conjugated Dienol Substrates	67
Table 4.1: Decomplexation Reaction Conditions	106
Table 5.1: Comparison of ¹ H NMR Data for Cp*Co(η^5 -pentadienyl) ⁺ Complexes	118
Table 5.2: Selected Bond Lengths, Bond and Diehedral Angles and Substituent Deviation from Planarity for Cp*Co(η^5 -pentadienyl) ⁺ Complexes	120
Table 5.3: Comparison of ¹ H NMR Data for Cp*Co(η^2, η^3 -cycloheptadienyl) ⁺ Complexes	125
Table 5.4: Selected Bond Lengths and Angles for Cp*Co(η^2, η^3 -cycloheptadienyl) ⁺ Complexes	128
Table 5.5: Comparison of ¹ H NMR Data for Cp*Co(η^5 -cycloheptadienyl) ⁺ Complexes	130
Table 5.6: Selected Bond Lengths and Angles for Cp*Co(η^5 -cycloheptadienyl) ⁺ Complexes	132
Table 6.1: Comparison of Alkyne Complexation TS Energies, Dihedral Angles, and C1-C5 Separations of Pentadienyl Complexes	162
Table 8.1: Thermodynamic Data for Cyclopropene Complexation	195
Table 8.2: Thermodynamic Data for Figure 6.1	238
Table 8.3: Thermodynamic Data for Note 204	239
Table 8.4: Thermodynamic Data for Figure 6.7	239
Table 8.5: Thermodynamic Data for Figure 6.6.....	240
Table 8.6: Thermodynamic Data for Figure 6.9	240
Table 8.7: Thermodynamic Data for Table 6.1	241
Table 8.8: Thermodynamic Data for Tripodal Phosphine Cycloaddition Reaction and Phosphine Deprotection	244

List of Figures

Figure 1.1: Examples of Natural Products Containing Seven-Membered Rings	1
Figure 1.2: Natural Products Synthesized via Electrochemical [5+2] Cycloaddition.....	9
Figure 1.3: Water Soluble Bidentate Phosphine and NHC Complex 159	29
Figure 5.1: C-C Bond Lengths in Pentadienyl Complexes 297d , 297b , and 366	121
Figure 5.2: X-Ray structure diagram for $[(C_5Me_5)Co(\eta^5-1\text{-phenylpentadienyl})]^+BF_4^-$	122
Figure 5.3: X-Ray structure diagram for $[(C_5Me_5)Co(\eta^5-1,4\text{-dimethylpentadienyl})]^+BF_4^-$	122
Figure 5.4: X-Ray structure diagram for $[(C_5Me_5)Co(\eta^5-1,5\text{-dimethylpentadienyl})]^+BF_4^-$	123
Figure 5.5: X-Ray structure diagram for $[(C_5Me_5)Co(\eta^5-1\text{-}(2\text{-butanoyl})\text{-pentadienyl})]^+$ BF_4^-	123
Figure 5.6: X-Ray structure diagram for $[(C_5Me_5)Co(\eta^2, \eta^3-1,5\text{-dimethylcyclohepta-}$ $\text{dienyl})]^+BF_4^-$	126
Figure 5.7: X-Ray structure diagram for $[(C_5Me_5)Co(\eta^2, \eta^3\text{-cycloheptadienyl})]^+BF_4^-$	126
Figure 5.8: X-Ray structure diagram for $[(C_5Me_5)Co(\eta^2, \eta^3\text{-cycloheptadienyl})]^+BF_4^-$	127
Figure 5.9: X-Ray structure diagram for $[(C_5Me_5)Co(\eta^2, \eta^3\text{-cycloheptadienyl})]^+BF_4^-$	127
Figure 5.10: X-Ray structure diagram for $[(C_5Me_5)Co(\eta^5\text{-cycloheptadienyl})]^+BF_4^-$..	133
Figure 5.11: X-Ray structure diagram for $[(C_5Me_5)Co(\eta^5\text{-cycloheptadienyl})]^+BF_4^-$..	133
Figure 5.12: X-Ray structure diagram for $[(C_5Me_5)Co(\eta^5\text{-cycloheptadienyl})]^+BF_4^-$..	134
Figure 5.13: X-Ray structure diagram for $[(C_5Me_5)Co(\eta^5\text{-cycloheptadienyl})]^+BF_4^-$..	134
Figure 5.14: <i>Trans</i> Relationship of Bridgehead Protons	135

Figure 5.15: X-Ray structure diagram for [(C ₅ Me ₅)Co(η^4 -[5.4.0]-bicycloundecadiene)] ⁺ BF ₄ ⁻	136
Figure 6.1: Reaction Profile for Cp*Co(η^5 -1-methylpentadienyl) ⁺ /Alkyne Cycloaddition (BP86)	142
Figure 6.2: Cp*Co(η^5 -1-methylpentadienyl) ⁺ Stationary Points	143
Figure 6.3: DFT Structure of TS2-10	148
Figure 6.4: CpCoH(η^1, η^3 -1-methylcycloheptadienyl) ⁺	148
Figure 6.5: Allyl/Olefin Isomerization Stationary Points	150
Figure 6.6: Comparison of Allyl/Olefin 2-Butyne Adducts	152
Figure 6.7: Reaction Profile for Cp*Co(η^5 -1-methylpentadienyl) ⁺ /Alkyne Cycloaddition (B3LYP)	153
Figure 6.8: DFT Structure of TS 2-4	155
Figure 6.9: Reaction Profile for CpCo(η^5 -1-methylpentadienyl) ⁺ /Alkyne Cycloaddition	156
Figure 6.10: Alternate Ring Forming Pathway	157
Figure 6.11: Triplet Surface Stationary Points	158
Figure 6.12: Alternate Ring Forming Pathway	160
Figure 6.13: Side-On Space-Filling Model of the η^5 -3-Methylpentadienyl/Alkyne Complexation TS	163
Figure 6.14: Dihedral Angle Comparison of Complexes 297a and 297j	164
Figure 7.1: (κ^3 -Trisphosphine)Co(η^5 -Pentadienyl) Complex and (κ^2 -Tris-phosphine)Co(η^5 -Pentadienyl)/Alkyne Complex	171
Figure 7.2: Alkyne Complexation TS with Tripodal Ligand	171
Figure 7.3: Transition State for PMe ₃ •BH ₃ Deprotection	172

List of Abbreviations

Å	Angstrom
Ar	Aryl
Bn	Benzyl
Boc	<i>tert</i> -Butoxycarbonyl
Bu	Butyl
Bz	Benzoyl
COSY	Correlated spectroscopy
Cp	η^5 -cyclopentadienyl
Cp*	η^5 -pentamethylcyclopentadienyl
d	Doublet
DABCO	[2.2.2]-Diazabicyclooctane
DFT	Density functional theory
DMAD	Dimethyl acetylenedicarboxylate
DMSO	Dimethylsulfoxide
Eq.	Equation
equiv.	Equivalent
Et	Ethyl
GCOSY	Gradient COSY
HF	Hartree-Fock
HMPA	Hexamethylphosphoramide
Hz	Hertz
INT	Intermediate

ⁱPr	Isopropyl
IR	Infrared
IRC	Intrinsic reaction coordinate
LAH	Lithium aluminum hydride
LDA	Lithium diisopropylamine
m	Multiplet
m-CPBA	Metachloroperbenzoic acid
Me	Methyl
MS	Mass spectrometry
NHC	N-heterocyclic carbene
NMR	Nuclear magnetic resonance
OAc	Acetate
OTf	Triflate
PCC	Pyridinium chlorochromate
PES	Potential energy surface
Ph	Phenyl
PMP	Paramethoxy benzylidene
ppm	Parts per million
py	Pyridine
R	Alkyl
RT	Room temperature
s	Singlet
SCF	Self consistent field

SV(P)	Split-valence polarization
t	Triplet
TBDMS	<i>tert</i> -Butyldimethylsilyl
^tBu	<i>tert</i> -Butyl
TCNE	Tetracyanoethylene
THF	Tetrahydrofuran
THP	Tetrahydropyranyl
TIPS	Triisopropylsilyl
TMEDA	Tetramethylethylenediamine
TMS	Trimethylsilyl
Tol	Tolyl
Trp	Trispyrazolylborate
Ts	Tosyl
TS	Transition state
TZVP	Triple-zeta valence polarization
TZVPP	Triple-zeta valence double polarization
UV	Ultraviolet
VCP	Vinylcyclopropane
X	Halide
η	Hapticity
κ	Denticity

While a range of cycloaddition schemes leading to seven-membered ring products have been developed, this chapter is limited to consideration of the [5+2] reaction manifold, discussing research in both pericyclic organic synthesis and transition metal-mediated chemistry. In the area of pericyclic synthesis, two broad categories can be delineated: reactions based on quinone systems, or “perezone-type” cycloadditions, and those based on oxidopyrylium ions, or the “kojic acid-type” cycloadditions. Metal-mediated systems can be organized in terms of the metal-ligand hapticity and the transition metal employed in the cycloaddition reaction.

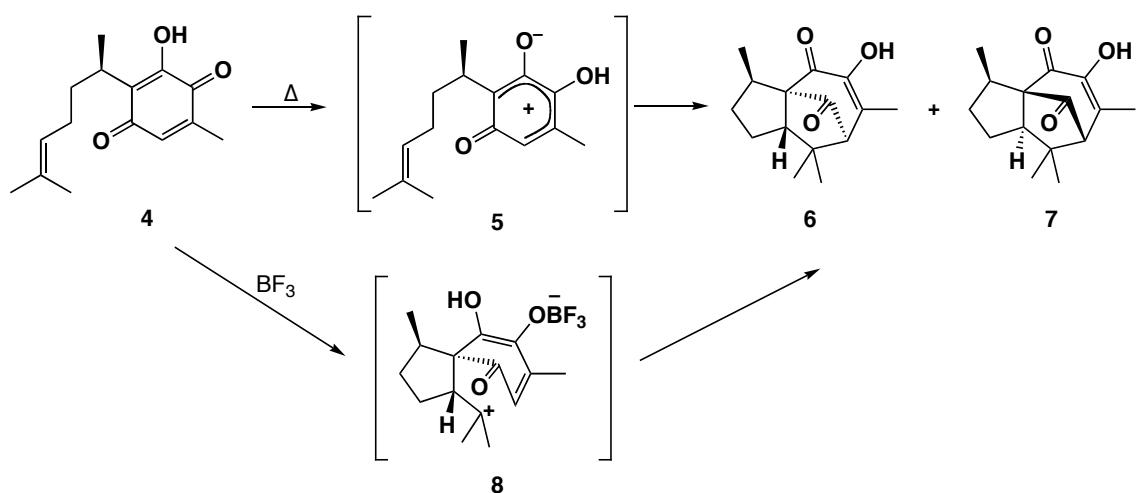
Part B: Perezone-Type [5+2] Cycloaddition Reactions

I. The Perezone to Pipitzol Transformation

Although they did not understand the nature of the process, Anschütz and Leather⁵ observed the transformation of perezone to pipitzol in 1885, the first example of [5+2] cycloaddition chemistry. They reported a reaction between the silver salt of the natural product perezone (**4**) and ethyl bromide; this reaction produced a crystalline material, isomeric with perezone. Years later, Sanders⁶ and then Remfry⁷ revisited this reaction, and both found this same transformation could be achieved by heating perezone to temperatures in excess of 200 °C. While Sanders inexplicably rejected the standard formulation of perezone (C₁₅H₂₀O₃) in favour of another, Remfry verified the original. Remfry also found that the product of this thermolysis, which he dubbed pipitzol, was a crystalline material melting at 141 °C, isomeric with perezone, thereby confirming the results of Anschütz and Leather.

It was not until 1965 that Joseph-Nathan determined the structure of pipitzol.⁸ He repeated the thermal reaction of perezone and found a 1:1 mixture of diastereomeric products resulted, dubbed α - (**6**) and β -pipitzol (**7**) (Scheme 1.1). Early mechanistic proposals were complicated by an incorrect characterization of perezone. Shortly after this initial work, structural revisions were reported,⁹ and a much simpler [5+2] cycloaddition of the pendant olefin with a pentadienyl cation intermediate **5**, itself arising from intramolecular proton transfer, was proposed, and later demonstrated to proceed in a concerted fashion.¹⁰

Scheme 1.1

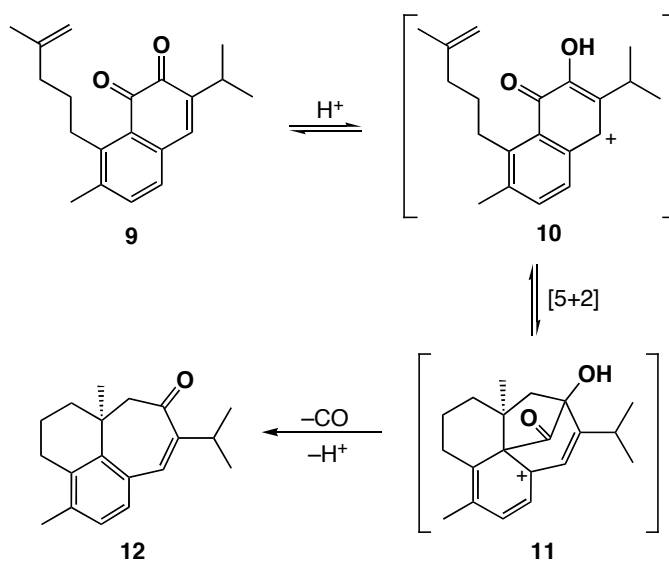


Joseph-Nathan extensively studied the stereocontrol of this transformation. He found that the cycloaddition reaction occurs at 0 °C in the presence of the Lewis acid $\text{BF}_3 \cdot \text{OEt}_2$, much lower than in the absence of acid. Further, the reaction proceeded in a diastereoselective fashion, yielding a 9:1 ratio of products favouring α -pipitzol **6**.¹¹ This selectivity arose via a change from a concerted to a stepwise mechanism involving intermediate **8**, as demonstrated by deuterium labeling experiments. Alternatively, when using $\text{AlCl}_3 \cdot \text{SEt}_2$ as the Lewis acid promoter, the selectivity was reversed, favouring β -

pipitzol in a 3:1 ratio.¹² This change in selectivity has been applied in a formal total synthesis of β -pipitzol.

A related example of an intramolecular [5+2] cycloaddition reaction occurs upon treatment of aethiopinone (**9**) with acids.¹³ When orthoquinone **9** was treated with either sulfuric acid or $\text{BF}_3 \cdot \text{OEt}_2$, cyclization product **12** was isolated in low yields (14 and 58% respectively). The authors proposed this product arises from an acid catalyzed [5+2] cycloaddition, followed by extrusion of carbon monoxide (Scheme 1.2).

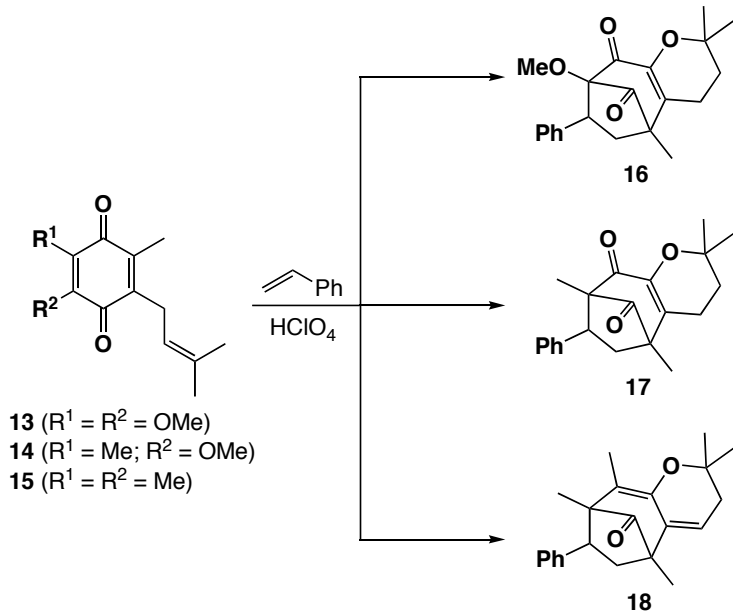
Scheme 1.2



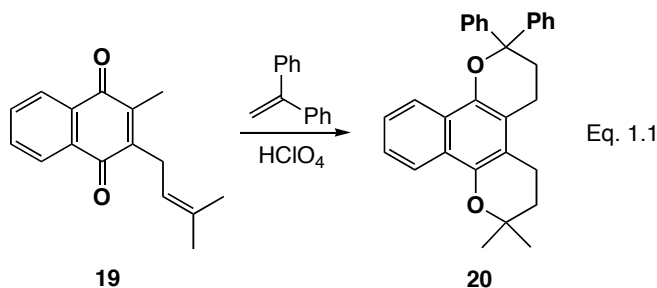
II. Intermolecular [5+2] Cycloaddition Variants

Shortly after Joseph-Nathan's seminal work on the intramolecular [5+2] cycloaddition reaction, Mamont reported the first intermolecular variants, where the acid-promoted reactions of quinones **13-15** with olefins were examined (Scheme 1.3).¹⁴ Upon reaction with styrene, the products were tricyclic compounds arising from a [5+2] cycloaddition process, proposed to occur in a stepwise fashion. The natures of R^1 , R^2 ,

Scheme 1.3



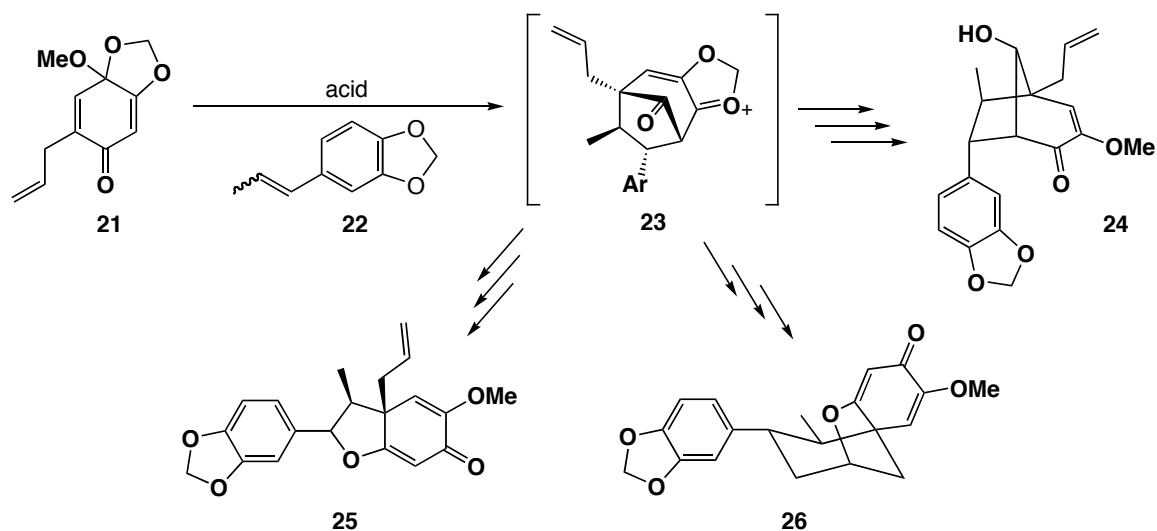
and the olefin greatly influence the course of the reaction. For instance, when the quinone is benzannulated, or when using 1,1-diphenylethene as the cycloaddition partner, the reaction does not proceed to give [5+2] products (Eq. 1.1), presumably to avoid disrupting the aromaticity and steric constraints.



Büchi further developed the intermolecular [5+2] cycloaddition of quinone-type systems.¹⁵ To overcome difficulties associated with reduced reactivity in the intermolecular reactions, the more electrophilic quinone ketals (**21**) were used. Even then, however, the product yields are still very low, typically below 50%, and the reactions result in a mixture of products. Despite these shortcomings, this process was

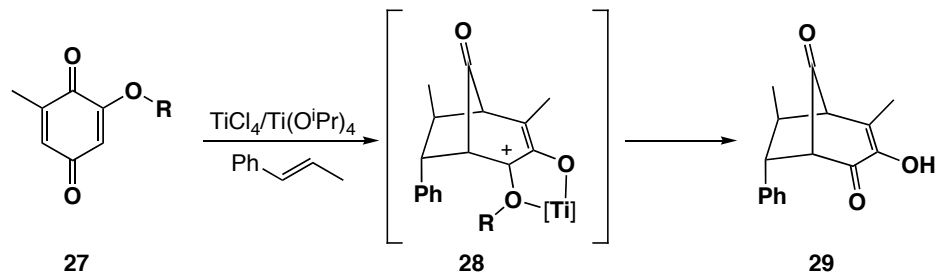
used in the syntheses of the neolignans (\pm)-guianin (**24**), (\pm)-burchellin (**25**), and (\pm)-futoenone (**26**), among others (Scheme 1.4). Each of these products was believed to arise from the cationic intermediate **23** formed upon [5+2] cycloaddition, either by nucleophilic trapping (as in the case of **24**) or by further rearrangement (**25** and **26**). This supposition was supported by the observation that bicyclic products of the type **24** are quantitatively converted to products of the type **25** under more strongly acidic conditions. Angle has studied similar isomerizations in the course of neolignan synthesis.¹⁶

Scheme 1.4



In a very elegant series of studies, Engler addressed the problem of product mixtures in these intermolecular reactions.¹⁷ By using a $\text{TiCl}_4/\text{Ti}(\text{O}^i\text{Pr})_4$ catalyst combination and selected substituents, it was possible to tune the reaction conditions to give only the bicyclic [5+2] cycloadducts in good to excellent yields. This result was rationalized by invoking cationic intermediate **28** arising from an initial [5+2] cycloaddition reaction (Scheme 1.5, simplified schematic). This intermediate functions as a branching point on the reaction pathway. Substituents R that are easily displaced (eg. R = benzyl) accelerate the rate of the reaction leading to the [5+2] adduct. The

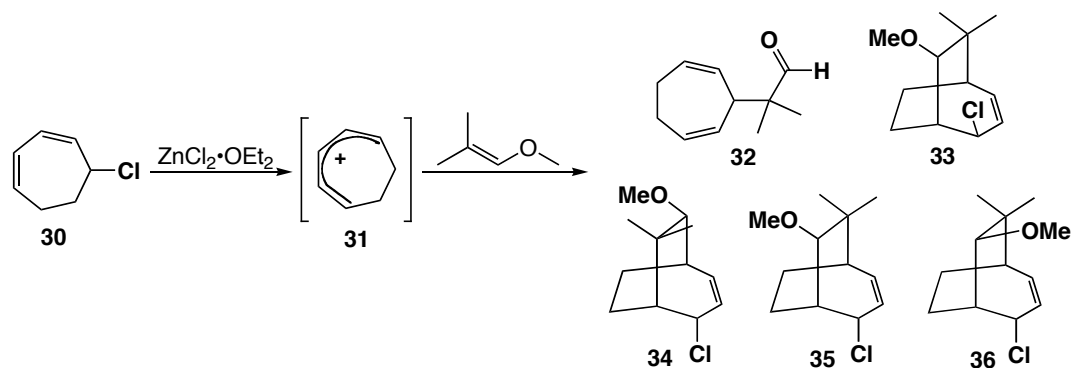
Scheme 1.5



structure of the titanium catalyst is not understood, but is likely to be $\text{TiCl}_n(\text{O}^i\text{Pr})_{4-n}$, with the exact ratio of ligands determined by the ratio of $\text{TiCl}_4:\text{Ti}(\text{O}^i\text{Pr})_4$ used in preparation. The formation of [5+2] cycloadducts is favoured by higher amounts of TiCl_4 . Recently, Grieco reported that the yields of intermolecular reactions are significantly improved by using trimethylsilyl triflate as the catalyst in the very polar solvent 3.0 M lithium perchlorate/ethyl acetate.¹⁸ This medium likely stabilizes the ionic **28**, allowing for more selective formation of the [5+2] adduct.

While not directly related to the perezone-type cycloaddition processes, the report of an intermolecular [5+2] cycloaddition reaction between cycloheptadienyl chloride **30** and 2-methyl-1-methoxy-1-propene warrants discussion here.¹⁹ When **30** and a vinyl ether are combined in the presence of $\text{ZnCl}_2 \cdot \text{OEt}_2$, five distinct products are obtained (Scheme 1.6). Four of these (**33-36**) proved to be isomers of [5+2] cycloadducts, obtained in 37% combined yield. In the proposed mechanism, initial halide abstraction generates the cycloheptadienyl cation **31**, which is trapped by the enol ether. Although this reaction can occur in either a stepwise or concerted fashion, the formation of **32** suggests that at least part of the reaction proceeds in a stepwise manner.

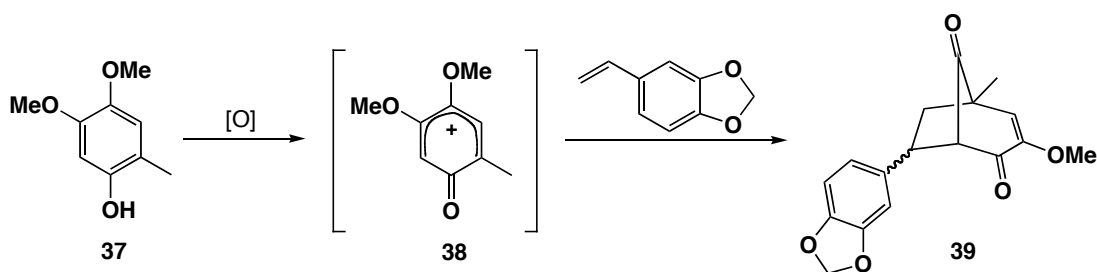
Scheme 1.6



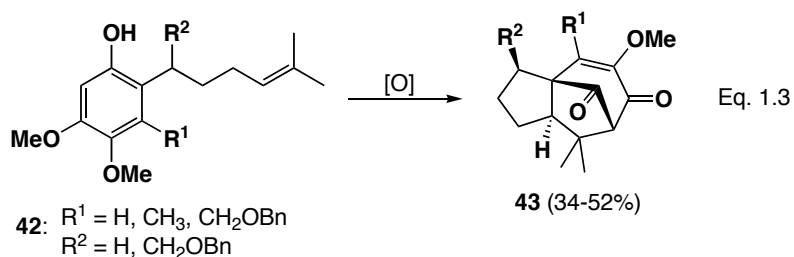
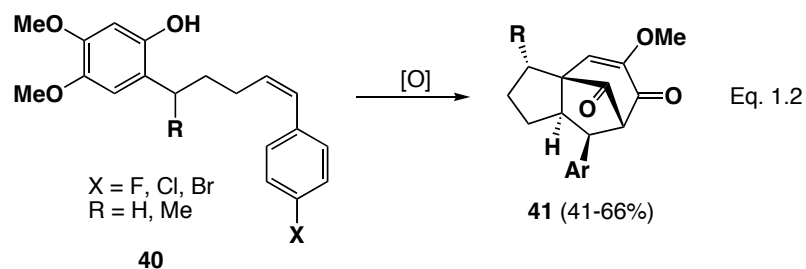
III. [5+2] Cycloaddition Reactions via Oxidation of Phenols

Yamamura has extensively studied the use of electrochemically-generated intermediates in organic synthesis,²⁰ including pentadienyl cations for both intra- and intermolecular [5+2] cycloaddition reactions.²¹ When 3,4-dimethoxy-6-methylphenol (37) was oxidized electrochemically in the presence of 3,4-methylenedioxy styrene, a mixture of *endo* and *exo* cycloadducts 39 was obtained in an approximately 3:1 ratio and an overall yield of 64% (Scheme 1.7). This work has been extended to intramolecular

Scheme 1.7

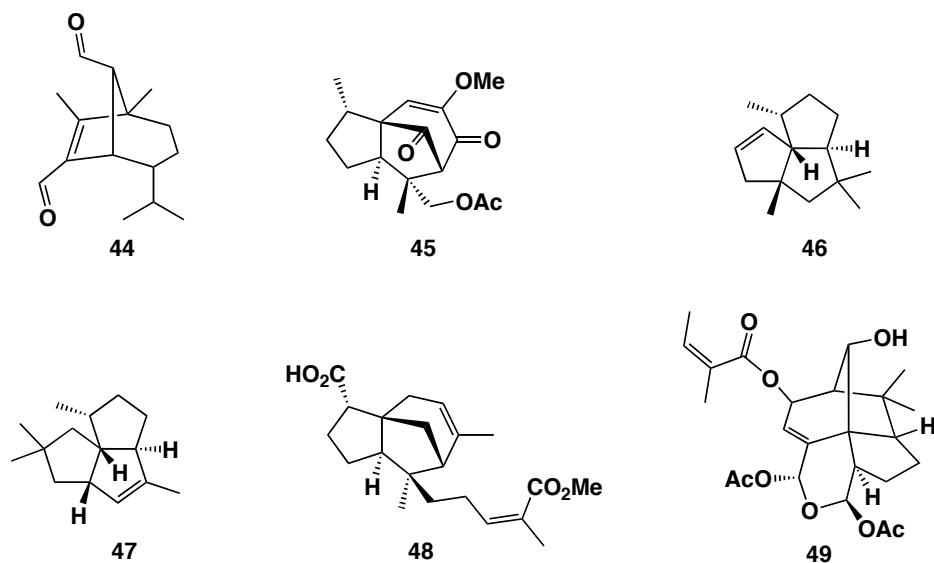


cases, including a rare use of disubstituted *Z*-olefins in [5+2] cycloaddition reactions (Eq. 1.2). Even highly substituted phenols can be used, leading to densely functionalized seven-membered ring products. For example, penta-substituted phenols of the type 42 readily form bridged-tricyclic products, albeit in low yields (Eq. 1.3).



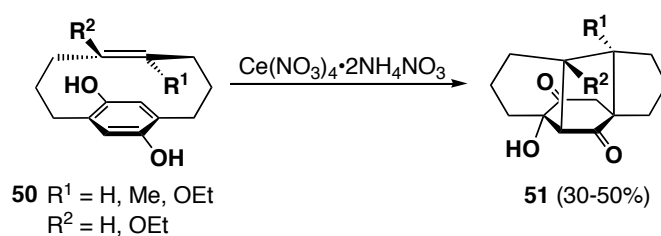
This reaction has been exploited for the total synthesis of a variety of natural products²² including neolignans **24**, **25**, and **26**, (±)-helminthosporal (**44**), (±)-8,14-cedranoxide (**45**), (±)-silphenene (**46**), (±)-pentalenene (**47**), a member of the 2-*epi*-cedrene isoprenologues (**48**), and a racemic synthesis of a highly oxygenated *Acourtia* isocedrene (**49**) (Figure 1.2). While the potential of this reaction is evident, the low product yield and often poor diastereoselectivity severely hamper the practical utility.

Figure 1.2: Natural Products Synthesized via Electrochemical [5+2] Cycloaddition



In a related reaction, Tsuji has demonstrated intramolecular [5+2] cycloaddition in bridged benzoquinone systems prepared via chemical oxidation of diphenols (Scheme 1.8).²³ The mechanism of this transformation could involve protonation of the quinone generated via oxidation, thereby aiding the cycloaddition. Alternatively, cycloaddition may proceed unaided to form an oxyallyl intermediate. In either case, the final step entails only trapping of the cation with water, followed by tautomerization.

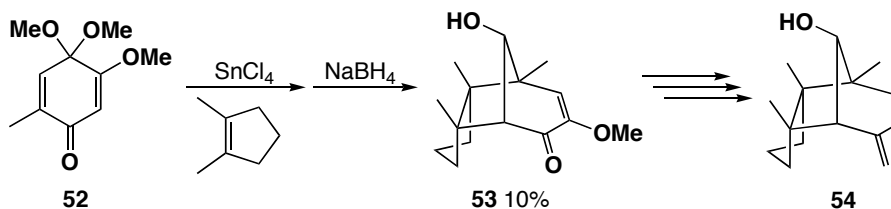
Scheme 1.8



IV. Additional Natural Product Syntheses

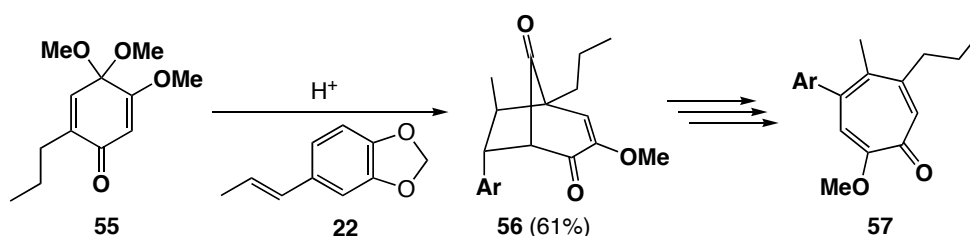
Outside of the examples described above, the perezone-type cycloaddition has not found wide spread application in the synthesis of natural compounds. Büchi, in addition to the neolignan syntheses previously noted, described the preparation of (\pm)-gymnomitrol (**54**)²⁴ and an entry into the tropolone core (**57**).²⁵ The key step in the synthesis of gymnomitrol is a [5+2] cycloaddition between ketal **52** and 1,2-dimethylcyclopentene to yield a mixture of diastereomers (Scheme 1.9). This was

Scheme 1.9



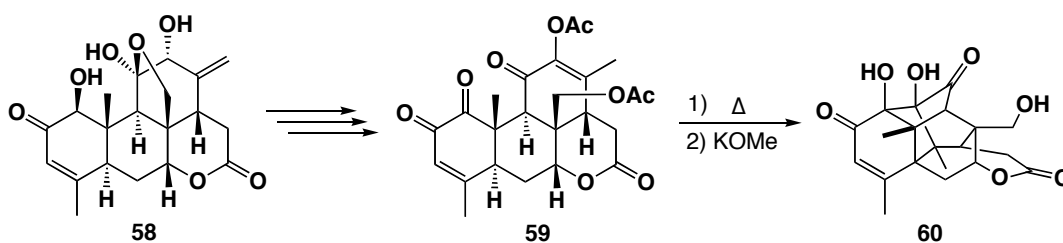
immediately reduced, with the desired diastereomer isolated in a 10% overall yield. They reasoned that the poor yield of the cycloaddition was due to the extra strain introduced by the cyclopentene ring. The tropolone synthesis made use of a cycloaddition reaction similar to that used in the neolignan syntheses (Scheme 1.10). Thus, 2,4,6-trinitrobenzenesulfonic acid promoted condensation of ketal **55** with isosafrole, produced **56** in good yield (61%) and with complete diastereocontrol.

Scheme 1.10



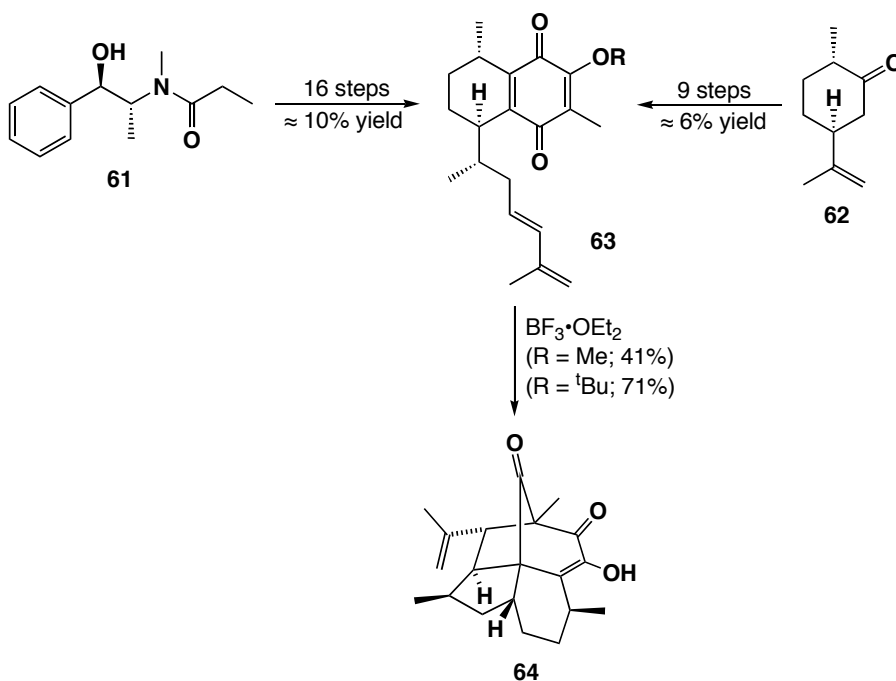
In another example, shinjulactone C (**60**) was synthesized via a [5+2] cycloaddition as a key step late in the synthesis.²⁶ Although ailanthone (**58**) can be converted directly to shinjulactone in one step by treatment with pyridine at reflux, the yield is only 8%. To investigate the mechanism and optimize the synthesis, a stepwise transformation was developed. Over five steps, **58** can be converted into the key intermediate **59**. This diketone yielded the acetylated shinjulactone C on heating in pyridine, presumably via [5+2] cycloaddition (Scheme 1.11). Deprotection provided **60** in 12% overall yield, providing little improvement.

Scheme 1.11



Finally, Rychnovsky and Harrowven have each published a synthesis of (-)-elisapterosin B (**64**)²⁷ using [5+2] cycloaddition in the final step (Scheme 1.12). In both reports, the key intermediate **63** is synthesized, each via a different strategy. Upon treatment of **63** with $\text{BF}_3 \cdot \text{OEt}_2$, an intramolecular cycloaddition occurs with complete diastereoselectivity, giving acceptable to good yields (41 or 71%).

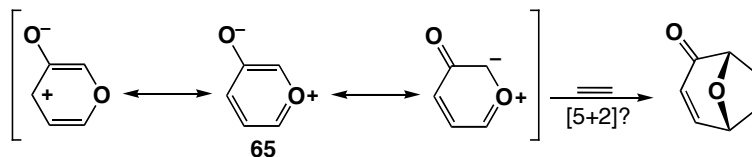
Scheme 1.12



Part C: Kojic Acid-Type [5+2] Cycloaddition Reactions

Kojic acid-type cycloaddition reactions yield products similar to those obtained via the perezone-type pathways, the only difference being a bridging oxygen atom rather than a bridging carbonyl. Mechanistically, these reactions involve the formation of an oxidopyrylium ylid (**65**) as the reactive intermediate, rather than a pentadienyl cation. As a consequence, this raises the question of whether these cycloadditions are better described in terms of a [5+2] pentadienyl cation cycloaddition, or as a [3+2] 1,3-dipolar

Scheme 1.13

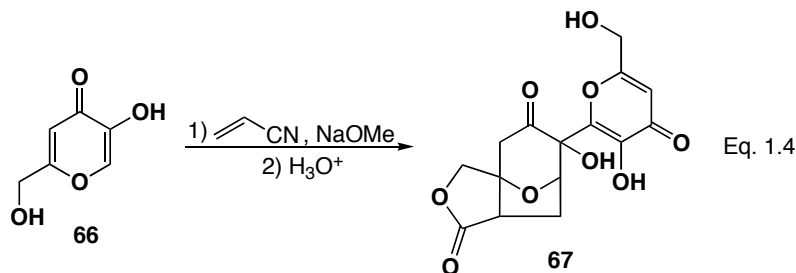


cycloaddition reaction (Scheme 1.13). With the widespread use of this class of reaction,²⁸ this discussion will be cast in terms relating to [5+2] cycloaddition chemistry. The reactions can be further classified based on how the requisite oxidopyrylium ylid is generated: by group transfer or group elimination. Additionally, these classes can in turn be divided into inter- and intramolecular subclasses. The fundamental research work will be discussed separately, with applications to synthesis grouped together. In the interest of brevity, oxidopyrylium generation through valence tautomerization^{29,30} and pathways involving metal-carbenes³¹ will not be discussed here: in the opinion of the author, these reactions are best interpreted as [3+2] cycloaddition processes. Similarly, while extensive work has been done in the field of oxidopyridinium [5+2] cycloaddition chemistry, this material will not be discussed here: the interested reader is instead directed to the applicable review.³²

I. The “Cyanoethylation” of Kojic Acid

Long after the first report of the perezone to pipitzol transformation, but before Joseph-Nathan’s elucidation of the process, Woods published on the reaction of the natural product kojic acid (**66**) with acrylonitrile³³ and β -bromopropionic acid,³⁴ isolating a product proposed to be 2-(2-hydroxymethyl-5-hydroxy-4-pyrone-6)-propionic acid. Hurd and Trofimenko, who were unable to replicate the results, isolated only kojic acid and called this result into question.³⁵ They later obtained reaction products,³⁶ however,

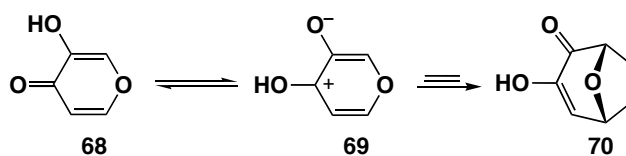
these materials analyzed as $C_{15}H_{14}O_9$, proving to be more than the result of a simple cyanoethylation (Eq. 1.4). Further investigations using α -deoxykojic acid led to product proposals requiring a complex mechanistic rationale.³⁷ Eighteen years later, the structure of the kojic acid/acrylonitrile reaction product (**67**) was correctly determined,³⁸ leading to the proposal of a [5+2] cycloaddition mechanism.



II. Oxidopyrylium Ylids Generated via Group Transfer

The early work in the cycloaddition chemistry of kojic acid led to a mechanistic proposal invoking transfer of the acidic phenolic proton to the carbonyl, generating a zwitterionic intermediate **69** (Scheme 1.14). Garst reported other early examples of this

Scheme 1.14

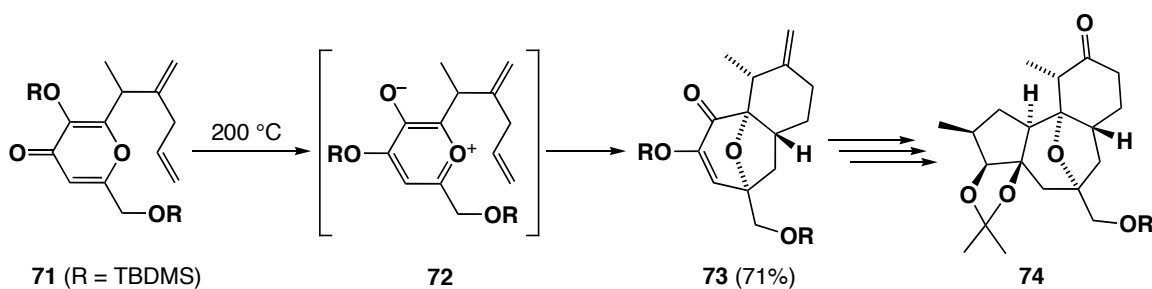


mode of oxidopyrylium ylid generation for intramolecular cycloaddition cases.³⁹ However, similar zwitterionic intermediates can be generated by other means; in fact, any group capable of equilibrium migration from one oxygen atom to the other promotes the cycloaddition reaction.

Wender investigated this possibility during model studies for the synthesis of phorbol.^{40,41} During this investigation, compounds of the type **71** bearing various oxygen

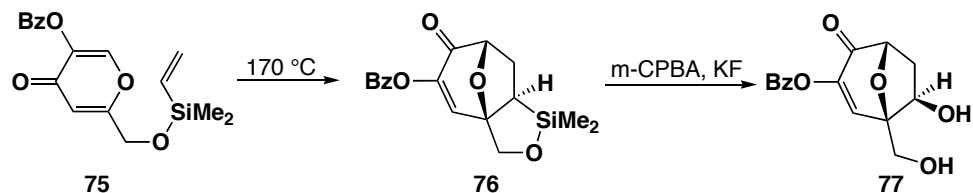
protecting groups (R) were prepared and subjected to high-temperature reaction conditions. When R = alkyl, no reaction occurs. However, when a more easily transferred group was used, cycloaddition products were obtained in good yields (71%, when R = TBDMS), with excellent stereoselectivity. Irradiation with UV light also promoted the cycloaddition, albeit in significantly reduced yield (15%). This product was elaborated to the tetracyclic intermediate **74**, a precursor to phorbol and other natural products.

Scheme 1.15

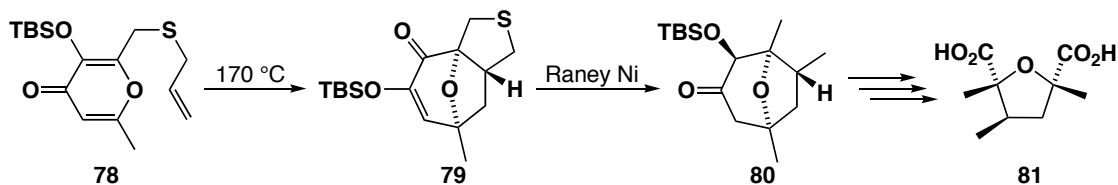


Outside of the examples discussed in the previous section, intermolecular reactions of the kojic acid-type involving the group transfer mechanism have been rare; these reactions require electronically activated alkenes (*vide infra*). This dependence on tethering for simple olefins arises from the minimization of unfavourable activation entropy in the face of a large activation enthalpy.⁴² To address this limitation, Mascareñas has used the intramolecular process to achieve formal intermolecular [5+2] cycloaddition reactions of unactivated alkenes via a temporary tethering strategy.⁴³ The temporary tethers include both silicon (Scheme 1.16, note the use of benzoyl as the migrating group) and sulphur (Scheme 1.17), which upon cleavage provide very densely functionalized seven-membered ring products.⁴⁴ Further bond cleavage leads to substituted tetrahydrofurans, a process applied to the synthesis of (±)-nemorensic acid

Scheme 1.16

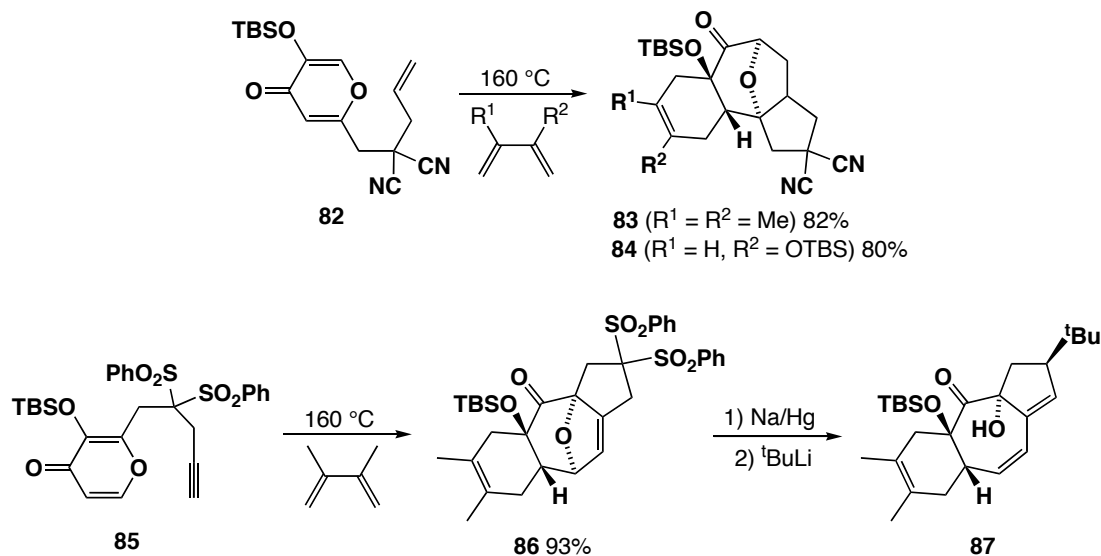


Scheme 1.17



(**81**), a unit of the natural product nemorensine. To expand the synthetic utility of this reaction, the potential of the alkene functionality in products such as **76** and **79** has been harnessed for a one-pot [5+2]/[4+2] tandem cycloaddition sequence, rapidly synthesizing highly functionalized tricyclic systems in excellent yield (Scheme 1.18).⁴⁵ Alkynes were

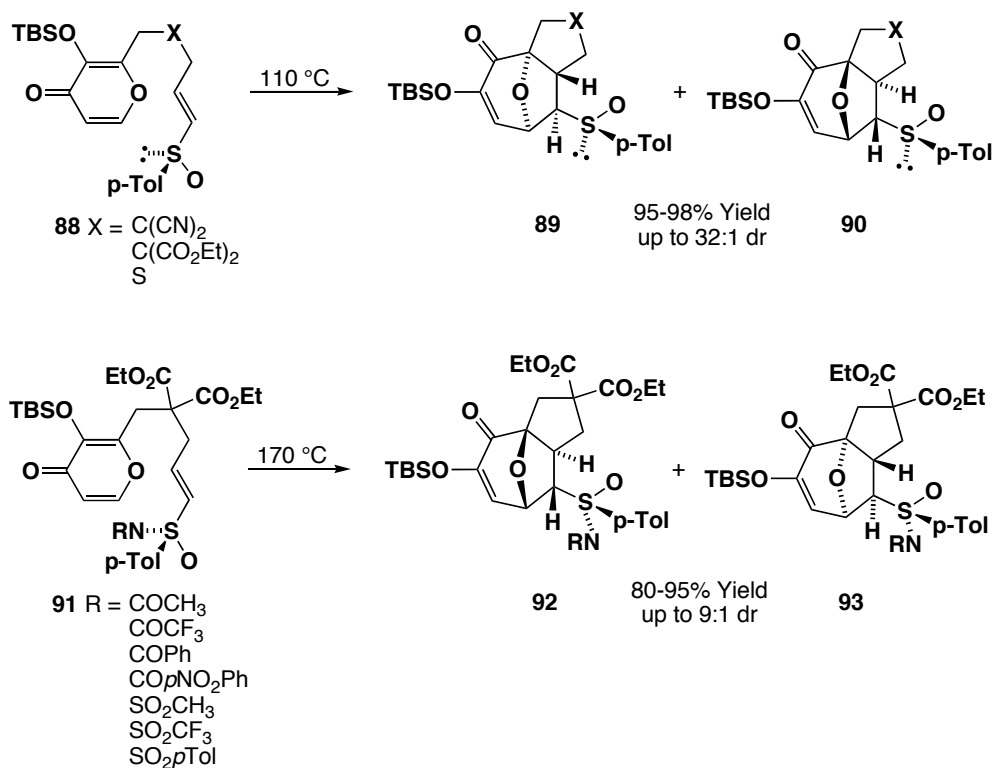
Scheme 1.18



also reactive, producing unsaturated ring products, whose functionality was further exploited, unmasking the latent hydroxyl.

Mascareñas has also demonstrated that introduction of sulfur groups can be used to control both the diastereo- and enantioselectivity of these [5+2] reactions.^{46,47} Early work with sulfinyl or sulfoxide tethers offered lower reaction temperature but only modest diastereoselectivity. However, moving the sulfinyl substituent to the terminal position of the alkene **88** provided remarkable diastereocontrol ($\approx 30:1$) and greater than 90% yields (Scheme 1.19). To obtain the complementary stereoisomer, the mismatched

Scheme 1.19

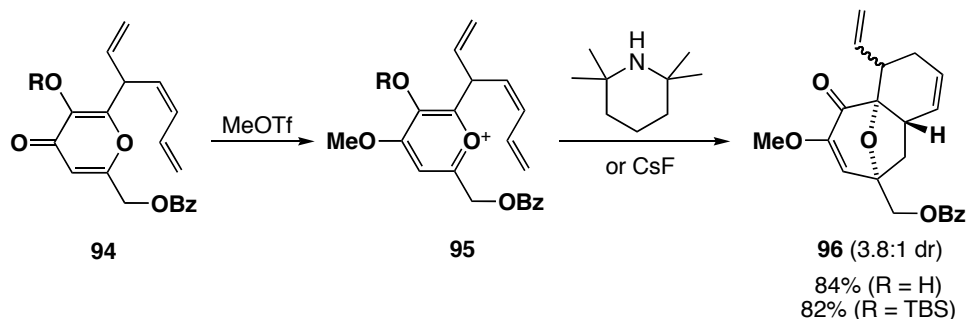


electronic arrangement required that the sulfinyl directing group be moved to the internal position of the alkene. Use of sulfoximine instead of sulfinyl groups (**91**) resulted in a switch of diastereoselectivity, with excellent diastereocontrol when R is larger than hydrogen. Simple reduction of the sulfur-directing group in **92** results in the formation of asymmetric products showing excellent enantiomeric excess. This new strategy was applied in tandem with the temporary tethering strategy, culminating in a total synthesis

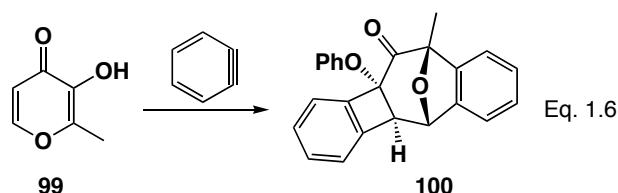
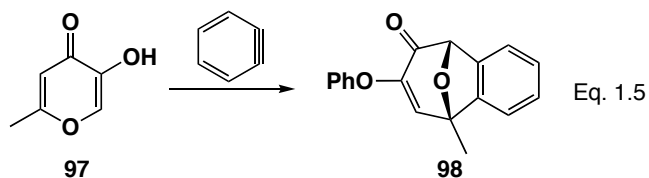
of (+)-nemorensic acid. The stereocontrol was rationalized, and later computationally verified, by assuming that the sulfoxide moiety adopts an *s-trans* conformation with respect to the sulfur lone pair, minimizing dipole-dipole interactions with the pyrone ring and disfavoring approach from the face on which the bulky Ar group points into the ring. This same rationale holds for the reversed case, where the alkenyl group is now *s-trans* with respect to the sulfoximine moiety.

The high temperature required to initiate these reactions can preclude the use of less thermally robust substrates. While Mascareñas has shown that high-valent sulfur substituents lead to reaction at lower temperatures, another approach is to form the oxidopyrylium ylid in a discrete step, circumventing the rate-limiting group transfer. Wender developed such an approach, wherein MeOTf is used to generate the methoxy pyrylium salt at mild temperature, followed by generation of the ylid using a nonnucleophilic base, such as 2,2,6,6-tetramethylpiperidine, or a fluoride source, depending on the nature of the R group (Scheme 1.20).⁴⁸ In this approach, the [5+2] cycloaddition reaction occurs smoothly at room temperature, yielding tricyclic products in greater than 80% yield as a mixture of diastereomers. The highly activated intermediates of the type **95** have also been applied successfully to intermolecular cycloadditions using both electron-deficient and strained alkenes.

Scheme 1.20



One example of using group transfer to achieve intermolecular cycloaddition with an electronically non-biased two-carbon unit has been reported.⁴⁹ When benzyne was generated in the presence of a kojic acid analogue (**97** or **99**) at 85 °C, cycloaddition occurs, incorporating two (Eq. 1.5) or three (Eq. 1.6) equivalents of benzyne. These highly functionalized, polycyclic structures were isolated in 33-36% yield.



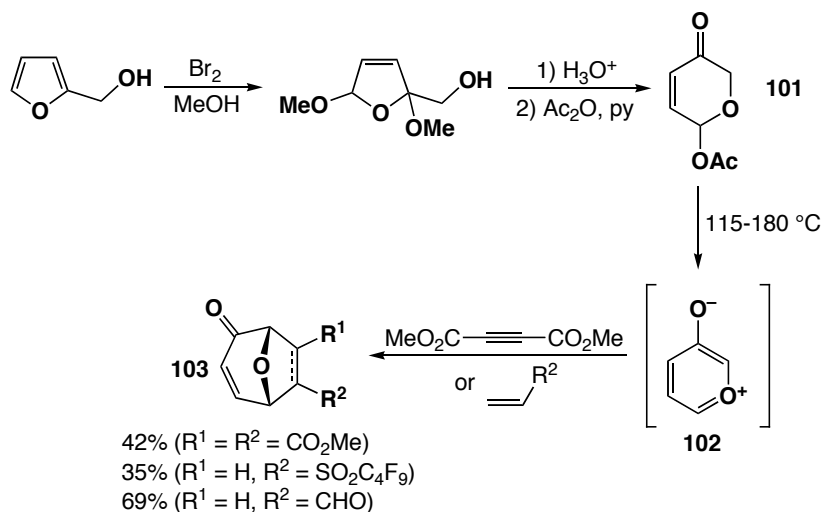
III. Oxidopyrylium Ylids Generated via Group Elimination

While group transfer to generate oxidopyrylium ylids was the earliest method developed, group elimination has found greater use in the synthetic organic community. Here, we will discuss the fundamental research performed in the area, leaving applications in total synthesis for a later section.

In 1980, Hendrickson⁵⁰ reported that the easily prepared cyclic acetoxy unsaturated ketone **101**^{51,52} can function as an oxidopyrylium precursor, presumably via a heteroatom assisted elimination of the acetate followed by enolization. Intermolecular cycloaddition reactions were demonstrated, using electron-deficient olefins and alkynes.^{53,54} These reactions occur smoothly at 115-180 °C in yields ranging from 35-69% (Scheme 1.21). This method introduced a facile new means of generating

oxidopyrylium ylids, resulting in a plethora of reports since then. In contrast to group transfer, the group elimination method has found rather extensive use in intermolecular reactions.

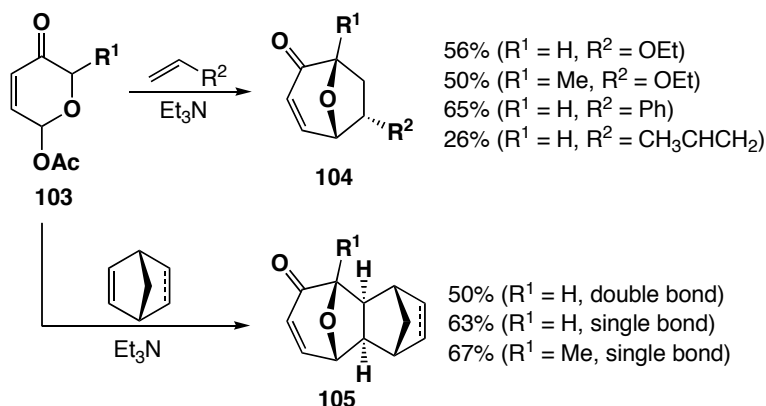
Scheme 1.21



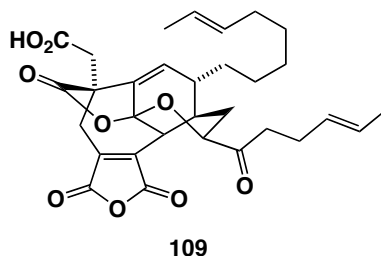
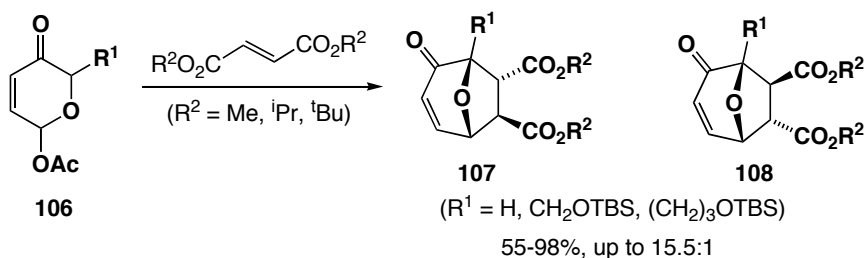
Shortly after the work of Hendrickson, Sammes⁵⁵ reported intermolecular oxidopyrylium cycloaddition reactions using the complementary electron-rich and strained olefins (*e.g.*, ethyl vinyl ether and norbornadiene); a large excess of the olefin was required to trap the dipolar intermediate and prevent dimerization (Scheme 1.22). Sammes also reported that heating the reaction could be avoided by using a base, such as triethylamine, to generate the oxidopyrylium intermediate, a strategy rapidly adopted by others.

Interestingly, the 2-substituent (R^1 in Scheme 1.23) has been shown to play a role in the stereocontrol of these reactions.⁵⁶ In the reaction of dialkyl fumarates with compounds **106**, larger R groups gave a higher degree of stereocontrol (up to 15.5:1 for $R^1 = \text{CH}_2\text{OTBS}$, $R^2 = \text{}^t\text{Bu}$), presumably due to minimizing unfavourable steric interactions in the preferred transition state geometry. These intermediates were later

Scheme 1.22



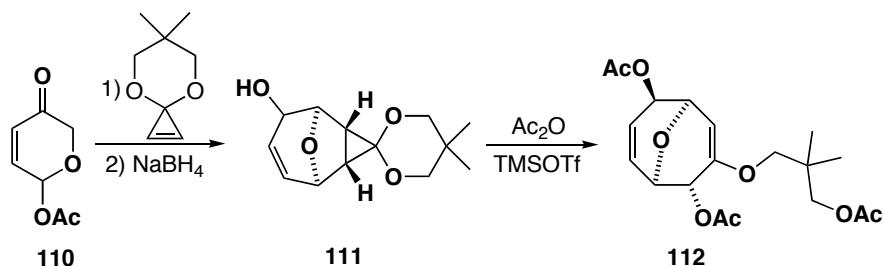
Scheme 1.23



used in studies directed toward the synthesis of phomoidride B (CP-263,114) **109**.⁵⁷

A very interesting report from Mascareñas showed that cyclopropenone acetals undergo [5+2] cycloaddition reactions smoothly at room temperature, ultimately resulting in a formal [5+3] cycloadduct (Scheme 1.24).⁵⁸ The exposure of the initial cycloadduct **111** (which was reduced to the alcohol for convenience) to acetic anhydride and a catalytic amount of TMSOTf cleaves the internal bond of the cyclopropene, generating the eight-membered ring moiety.

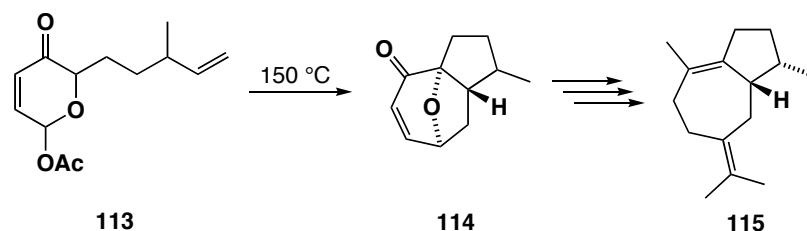
Scheme 1.24



IV. Natural Product Syntheses

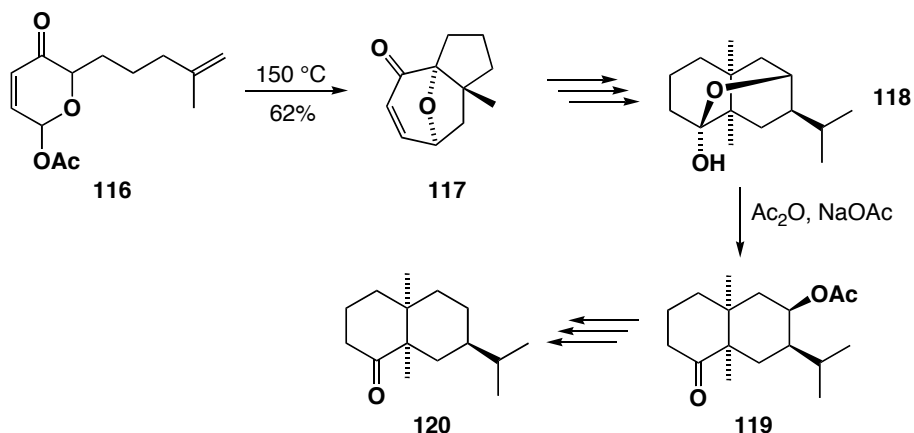
The oxidopyrylium cycloaddition reaction has been extensively applied to the total syntheses of natural products and natural product cores. In early examples, Sammes demonstrated the versatility of this chemistry through the synthesis of several natural products: (\pm)- β -bulnesene (**115**),⁵⁹ (\pm)-cryptofauronol (**118**), (\pm)-fauronyl acetate (**119**) and (\pm)-valeranone (**120**) (Schemes 1.25-1.26). In each case the intramolecular group elimination methodology was adopted, in several cases followed by skeletal rearrangements.

Scheme 1.25

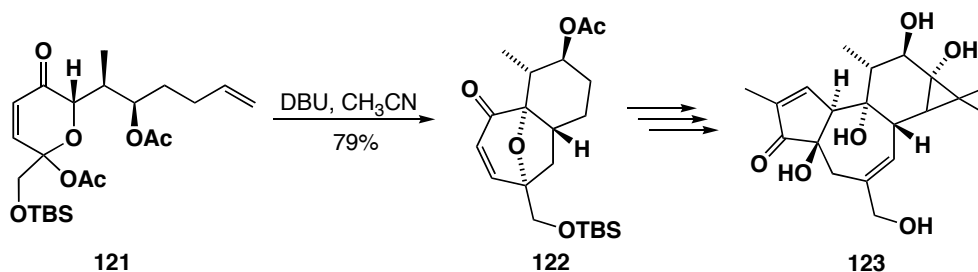


Wender, in addition to the work described above, has used this methodology in landmark asymmetric total syntheses of phorbol (**123**)⁶⁰ and (+)-resiniferatoxin (**126**) (Schemes 1.27-1.28). General approaches to the cores of the tigliane, daphnane, and ingenane families,⁶¹ the C12-hydroxy daphnetoxins and 1 α -alkyldaphnanes have also been described.

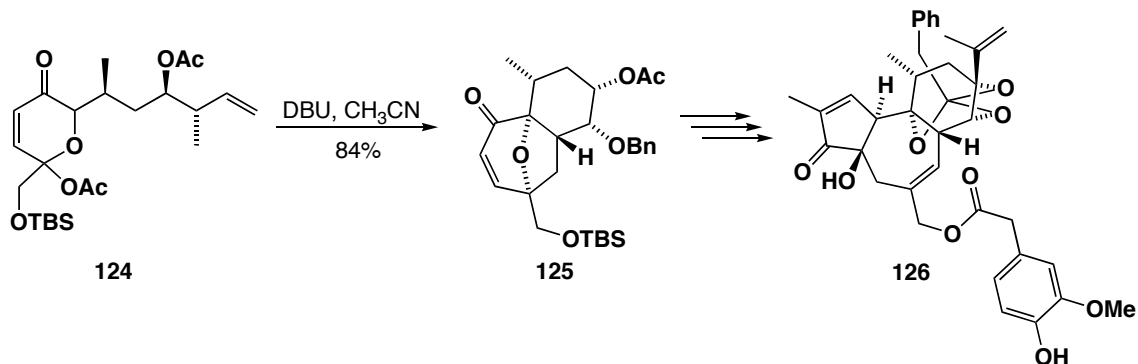
Scheme 1.26



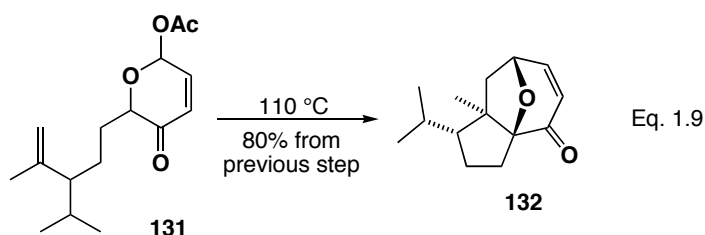
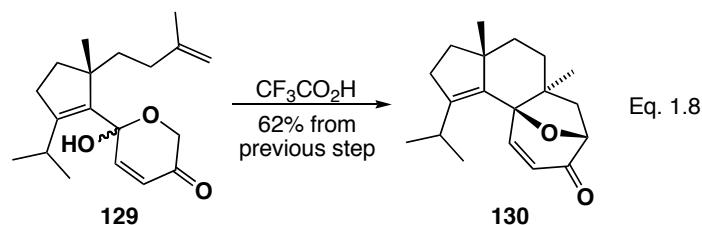
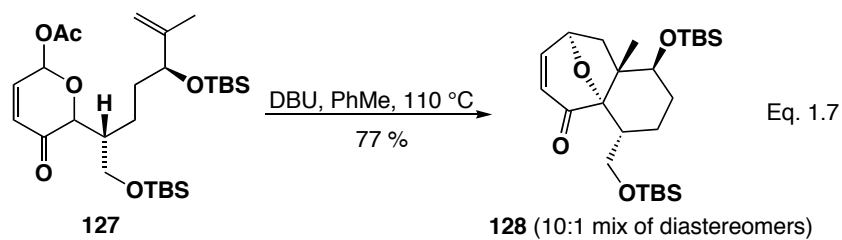
Scheme 1.27



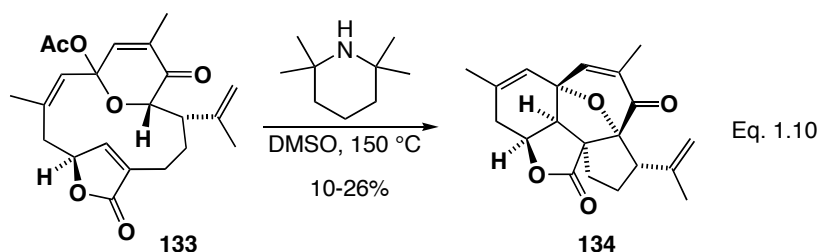
Scheme 1.28



Other examples of intramolecular oxidopyrylium cycloaddition reactions in the synthesis of advanced intermediates and natural products have been reported. Magnus has used this reaction for developing synthetic strategies applicable to the BC-ring system of taxol (Eq. 1.7),^{62a,b,63} the stereoselective synthesis of the cyanthin ring skeleton (**130**) (Eq. 1.8), and a portion of the guanacastepene skeleton (Eq. 1.9). Both Trauner⁶⁴ and

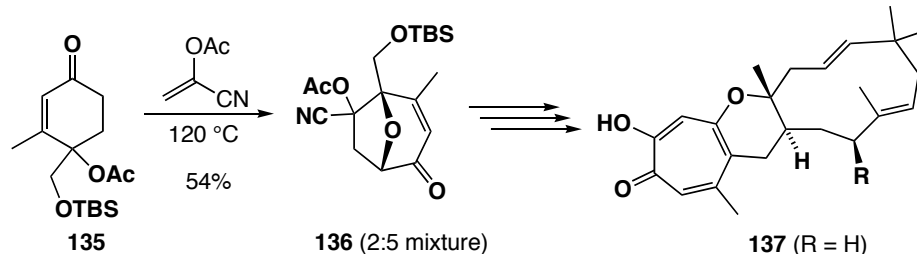


Pattenden⁶⁵ have reported biomimetic syntheses of (+)-intricarene (**134**), each using a [5+2] cycloaddition reaction of the bipinnatin J derivative **133** as the key step (Eq. 1.10).



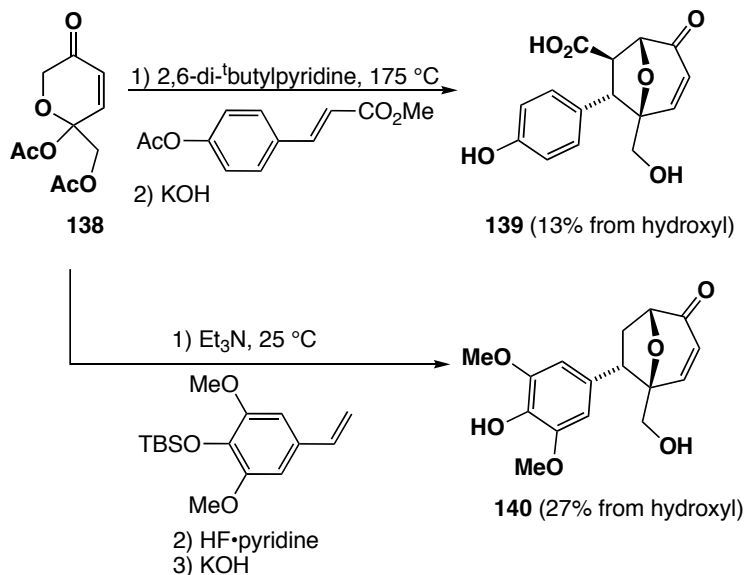
Baldwin has studied the synthesis of natural tropolone products via inter-⁶⁶ and intramolecular⁶⁷ kojic acid-type cycloaddition reactions; the intramolecular case is an uncommon example of alkyne oxidopyrylium cycloaddition. These reports include a synthesis of a deoxy-epolone B (**137**) via intermolecular cycloaddition of an oxidopyrylium ylid and α -acetoxyacrylonitrile (Scheme 1.29). The cycloaddition yielded a mixture of stereoisomers, which was of little consequence, since both were elaborated to the final product.

Scheme 1.29



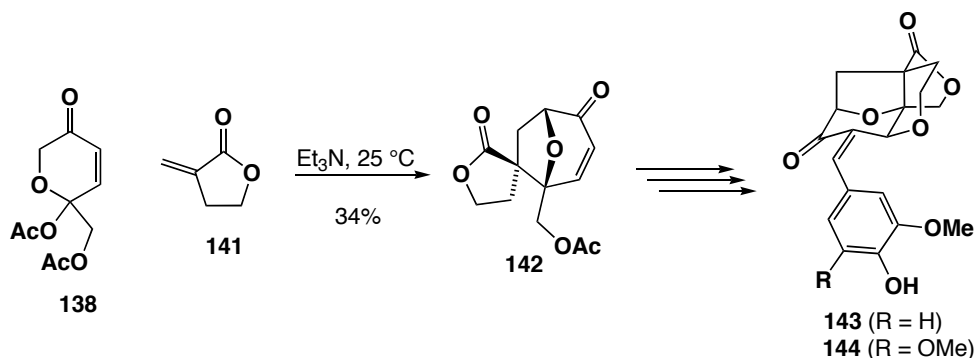
Recently, Snider reported racemic syntheses of the natural products cartormine (**139**)⁶⁸ and descurainin (**140**), along with formal biomimetic syntheses of polygalolides A (**143**) and B (**144**), all via intermolecular cycloaddition procedures (Schemes 1.30-1.31). The polygalolide syntheses in particular make use of an unconventional

Scheme 1.30

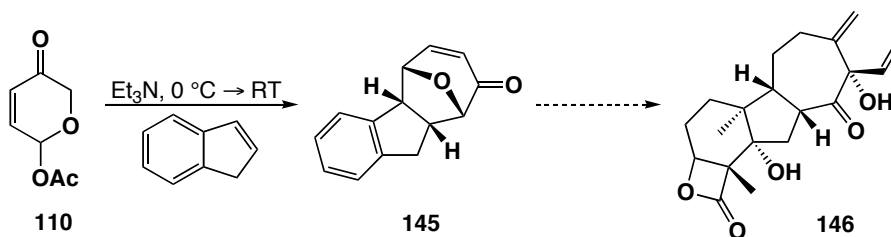


α -methylene lactone functionality in the cycloaddition reaction, giving a high degree ($\approx 90\%$) of stereocontrol. Synthetic applications from other research groups include an investigation into the synthesis of the FCCR toxin (**146**)⁶⁹ (Scheme 1.32) and model studies for a potential dictyoxetane synthesis.⁷⁰

Scheme 1.31



Scheme 1.32

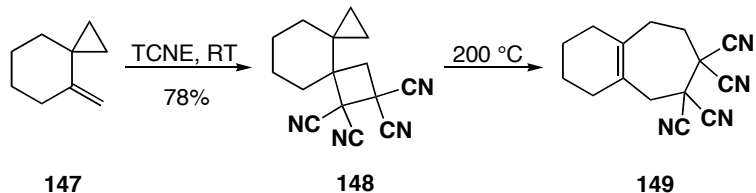


Part D: Vinylcyclopropane Cycloaddition Reactions

The Diels-Alder reaction was the most important advance in pericyclic cycloaddition chemistry, providing a powerful means to prepare six-membered carbocycles in a [4+2] fashion. Efforts to extend this to a [5+2] homologue in a strictly organic sense have met with limited success. The first report of such a reaction was in 1959,⁷¹ in which a vinylcyclopropane (VCP) and maleic anhydride reacted to produce a seven-membered carbocycle in 40% yield. Unfortunately, the results were irreproducible in the hands of others.⁷²

Vinylcyclopropanes do undergo formal [5+2] cycloaddition with the highly activated olefin tetracyanoethylene (TCNE).⁷³ In these systems, TCNE first undergoes a [2+2] cycloaddition with the olefin of the vinylcyclopropane, followed by rearrangement

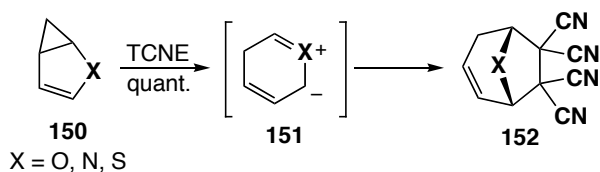
Scheme 1.33



to the formal [5+2] product (Scheme 1.33). Unfortunately, the final product yield was not reported and the reaction appears to be limited to TCNE; other activated π -systems such as dimethyl acetylenedicarboxylate (DMAD) do not lead to [5+2] products. Starting materials incorporating alternate ring sizes and dicyclopropylvinyl functionality were also explored.

Substrates wherein the vinylcyclopropane moiety is encased in a strained heterobicyclic framework also react with more success.⁷⁴ The reaction tolerates heteroatoms including oxygen, sulphur, and nitrogen and the mechanism may proceed in a fashion similar to kojic acid-type cycloaddition, through the involvement of a zwitterionic intermediate (Scheme 1.34). In these cases, however, the reaction is limited to highly activated two-carbon units such as maleic anhydride, N-phenylmaleimide, DMAD and TCNE, and many yields remain unreported.

Scheme 1.34

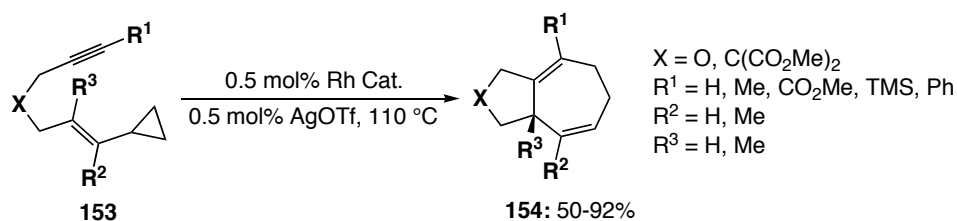


Part E: Rhodium-Catalyzed Vinylcyclopropane Cycloaddition Reactions

I. Intramolecular Cycloaddition Reactions

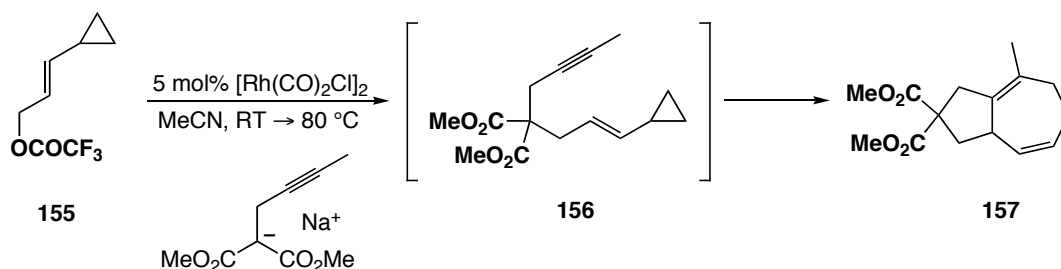
It was not until Wender reported the intramolecular rhodium-catalyzed cycloaddition of vinylcyclopropanes with alkynes that the [5+2] homologue to the Diels-Alder reaction was developed into a useful synthetic method (Scheme 1.35).⁷⁵ Initial work demonstrated that the steric and electronic effects of the alkyne substituents, as well as the nature of the tether, does not greatly control or alter the reactivity. However, some π -bond isomerization was observed with additional substitution on the alkene. These undesired transformations were eliminated by switching from Wilkinson's catalyst to

Scheme 1.35



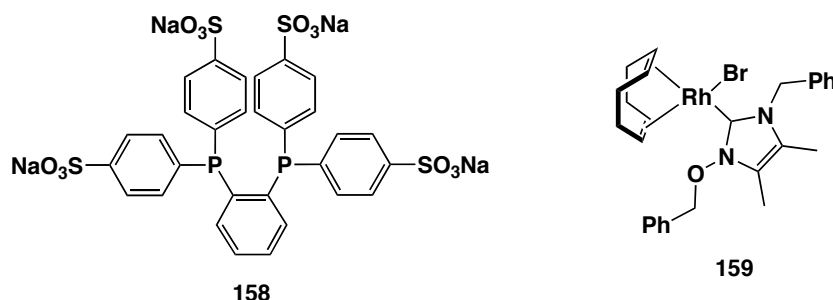
[Rh(CO)₂Cl]₂. In most cases, the reaction proceeds in excellent yield, hampered only by the volatility of some products (**154**, X = O; R¹, R², R³ = H). Martin has developed a domino-type extension of this reaction,⁷⁶ using [Rh(CO)₂Cl]₂ to catalyze an allylic alkylation followed by a [5+2] cycloaddition in one pot (Scheme 1.36).

Scheme 1.36



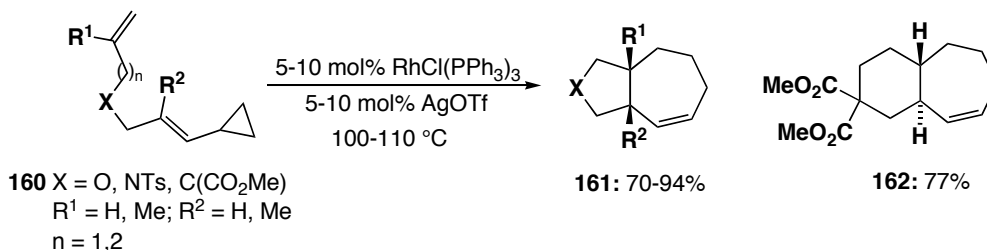
The first rhodium complex used for this transformation was Wilkinson's catalyst $[\text{RhCl}(\text{PPh}_3)_3]$.⁷⁷ Since then, however, other rhodium complexes have proven to be more effective under varying conditions. These catalysts include the aforementioned $[\text{Rh}(\text{CO})_2\text{Cl}]_2$,⁷⁸ the most versatile catalyst, $[(\text{C}_{10}\text{H}_8)\text{Rh}(\text{cod})]\text{SbF}_6$,⁷⁹ $[\text{Rh}(\text{nbd})(\text{o}-(\text{p}-(\text{NaO}_3\text{SC}_6\text{H}_4)_2\text{P})_2\text{C}_6\text{H}_4)]\text{SbF}_6$, which is water soluble (the ligand **158** is shown in Figure 1.3),⁸⁰ N-heterocyclic carbene complex **159**,⁸¹ $[\text{Rh}(\text{DIPHOS})(\text{CH}_2\text{Cl}_2)_2]\text{SbF}_6$,⁸² $[\text{Rh}(\text{dppb})\text{Cl}]_2$,⁸³ and $[\text{Rh}(\text{dppb})\text{Cl}]_2$.⁸⁴ While not always necessary, a halide abstracting agent such as AgOTf in conjunction with the rhodium catalyst generally improves the product purity.

Figure 1.3: Water Soluble Bidentate Phosphine and NHC Complex **159**

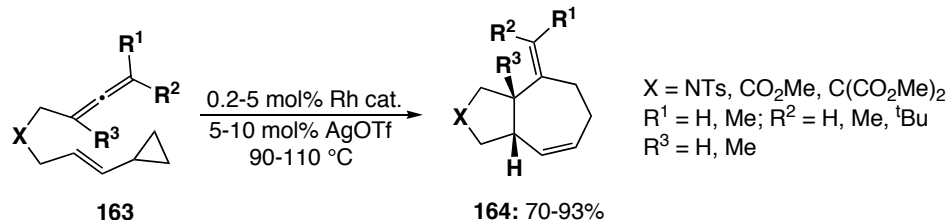


The scope of this rhodium-catalyzed process is not limited to tethered alkynes. Shortly after the original report, the first examples of intramolecular cycloaddition with alkenes were published (Scheme 1.37),⁸⁵ followed by allenes (Scheme 1.38).⁸⁶ Both of these systems displayed similar scope to the parent alkyne with regard to substituents. In

Scheme 1.37



Scheme 1.38

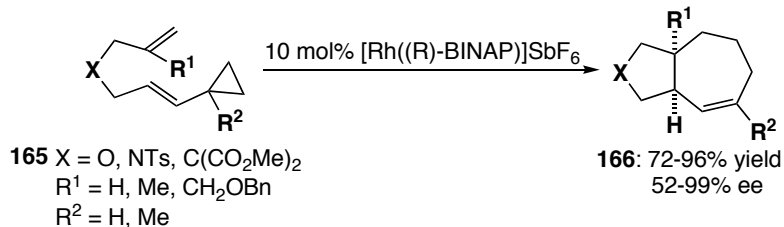


addition, these systems provided an opportunity to determine the diastereoselectivity of the reaction. Interestingly, the process was found to be completely selective, yielding only the *cis*-fused isomer **161** from three-atom tethers (in a lone example of a four-atom tether, the *trans*-fused isomer **162** prevailed). Notably, the allene system also displayed complete selectivity for the internal olefin of the allenyl moiety, with the stereochemistry of the allene being relayed to the final product with complete retention (92% ee for **164**, X = C(CO₂Me)₂, R² = ^tBu, R³ = R⁴ = H).

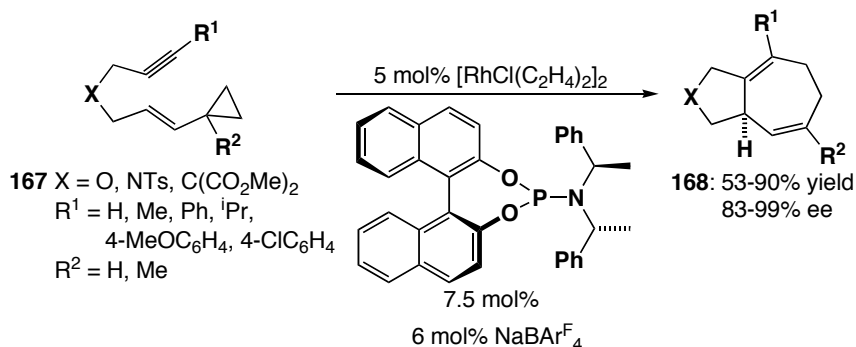
While the transfer of stereochemistry from the allenyl moiety presented a potential substrate-controlled route to asymmetric synthesis, a catalyst-controlled method is considered more general and powerful. Early investigations suggested that the use of CHIRAPHOS and derivatives might provide asymmetric catalysis, with later results indicating that BINAP was a more effective chiral phosphine (Scheme 1.39).⁸⁷ With this system, asymmetric cycloaddition reactions were performed for both alkenes and alkynes over a range of substitution patterns with ee's as high as 99%. Hayashi⁸⁸ has further advanced asymmetric induction in these systems, reporting that chiral phosphoramidite ligands result in excellent enantiomeric excess during intramolecular VCP/alkyne cycloaddition reactions (Scheme 1.40).

While a significant range of substitution patterns have already been discussed, one that has not been addressed is substitution on the cyclopropane ring, which raises the

Scheme 1.39

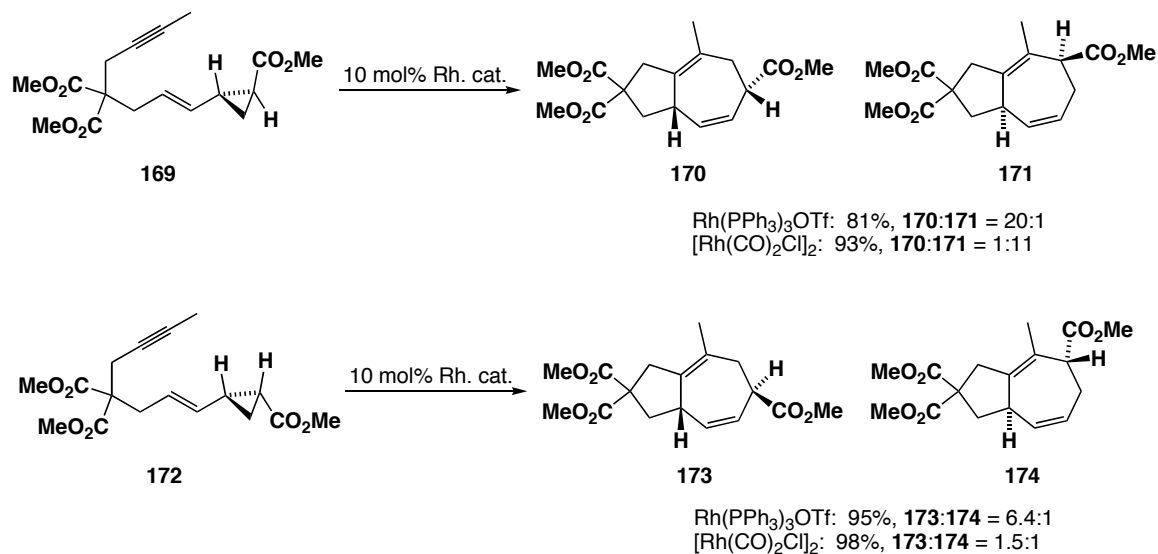


Scheme 1.40



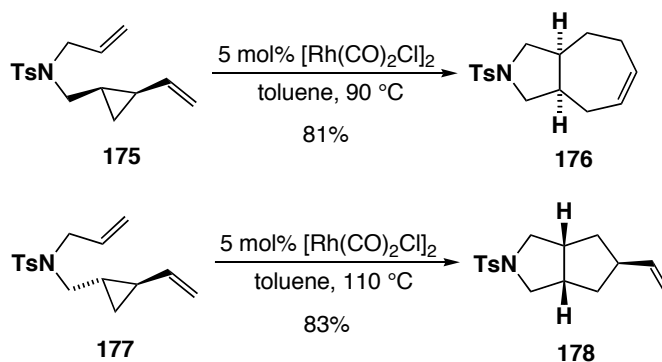
issue of regioselectivity in the cyclopropane ring-opening step. Wender has shown that careful choice of the substrate and catalyst combination allows for the selective formation of any one of the possible stereoisomers (Scheme 1.41).⁸⁹ Previous observations had shown that in *trans*-methyl substituted cyclopropane cases, the seven-membered ring product formed via RhCl(PPh₃)₃ cycloaddition arose from cleavage of the less substituted cyclopropane bond and that the initial cyclopropane configuration was translated to that of the product.⁹⁰ This preference remains true for most electron-donating groups and Wilkinson-type catalysts. When the substituent is an electron-withdrawing group, the preference for cleavage of the less substituted bond is maintained, although some of the other regioisomer can be detected. This selectivity can be completely reversed by using [Rh(CO)₂Cl]₂ as the catalyst. In *cis*-substituted substrates, the preference for cleavage of the less substituted bond is maintained, but the selectivities are not as high.

Scheme 1.41



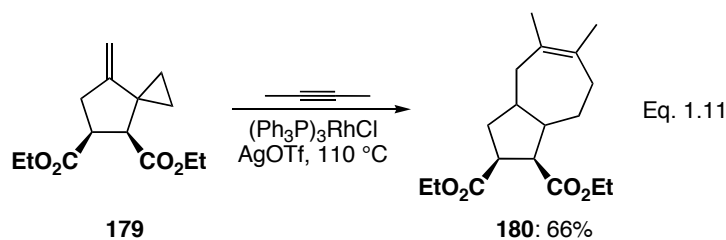
In related work, the selectivity of the reaction has been shown to depend on the regiochemical orientation of the vinylcyclopropane moiety (Scheme 1.42).⁹¹ If an internal vinylcyclopropane is used, only the *cis*-substituted substrate (**175**) leads to [5+2] products. The *trans*-system (**177**) reacts to produce a [3+2] cycloadduct.

Scheme 1.42



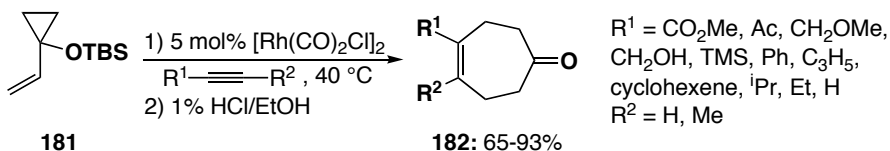
II. Intermolecular Cycloaddition Reactions

Binger and de Meijere⁹² reported the first intermolecular example of a rhodium-catalyzed [5+2] cycloaddition reaction (Eq. 1.11). This was, however, an isolated

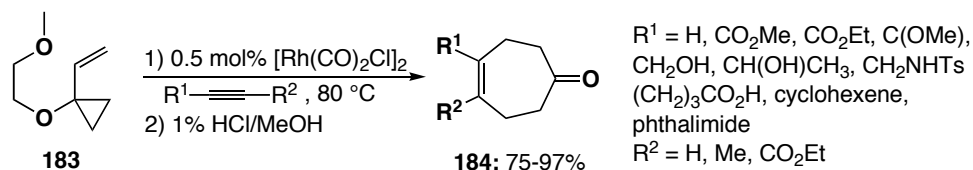


example and Wender shortly thereafter reported the first extensive study of the bimolecular reaction of alkynes and siloxyvinylcyclopropanes.⁹³ The conditions for the intramolecular cycloaddition reaction mediated by Wilkinson's catalyst were ineffective for the intermolecular cases. This difficulty was overcome by using heteroatom-substituted vinylcyclopropanes, which display a higher reaction rate, coupled with the use of the more reactive catalyst $[\text{Rh}(\text{CO})_2\text{Cl}]_2$. Under these conditions, good to excellent yields of [5+2] product (hydrolyzed to the ketone *in situ*) were obtained over a range of electron-rich, electron-poor and conjugated alkynes (Scheme 1.43). In later work, vinylcyclopropanol derivative **183** was introduced, which proved to be both economical and easily prepared on large scale, while retaining the same high level of synthetic utility (Scheme 1.44).⁹⁴

Scheme 1.43

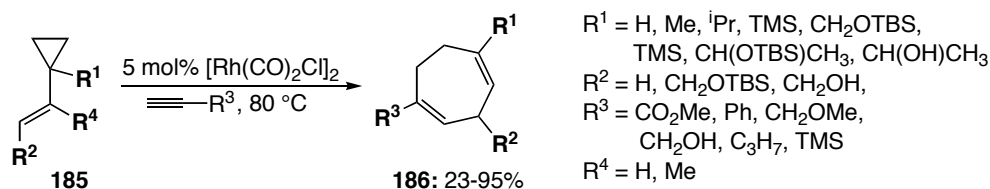


Scheme 1.44



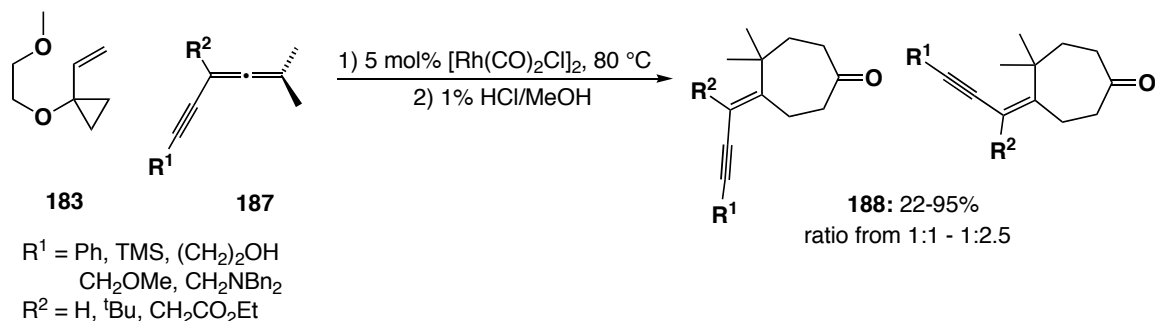
The intermolecular reaction also proceeds with sterically large groups in place of the heteroatom donors (Scheme 1.45).⁹⁵ These groups reduce the energetic differences between the conformations of the vinylcyclopropane, allowing the reactive conformer to be populated more readily. The degree of steric bulk of the substituent is directly related to the efficiency of the reaction, with ⁱPr and CH₂OTBS giving the best yields. Another noteworthy example is that of allylic alcohol **185** (R¹ = R⁴ = H, R² = CH₂OH), which undergoes [5+2] cycloaddition with methyl propiolate (R³ = CO₂Me) in 23% yield. This suggests that the cycloaddition reaction can be achieved in the absence of both activating and sterically large groups when a potentially coordinating functional group is present to help bring the VCP into the coordination sphere of the metal. This possibility remains to be further explored.

Scheme 1.45



While alkene substrates have yet to be used for intermolecular reactions, allenes that are substituted with an alkyne moiety capable of coordinating to the metal can be effectively used in cycloaddition reactions (Scheme 1.46).⁹⁶ The yields are generally

Scheme 1.46

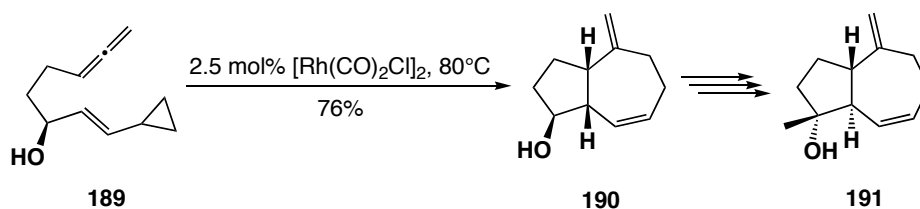


good to excellent, but the product is obtained as a mixture of isomers showing little selectivity. Other coordinating groups can be used, including alkenes and nitriles, again with excellent yields. Esters have proven to be ineffective.

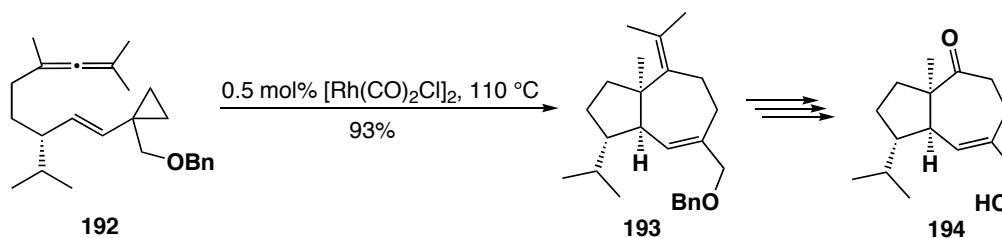
III. Natural Product Syntheses

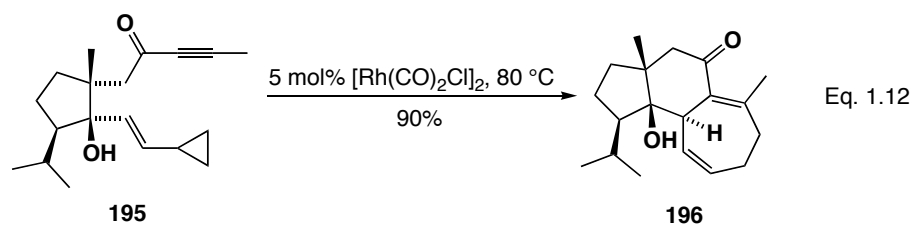
The rhodium-catalyzed [5+2] cycloaddition has been used as a key step in the synthesis of a variety of natural products and natural product core structures. The first to be reported was Wender's synthesis of (+)-dictamnol (**191**, Scheme 1.47)⁹⁷ followed shortly thereafter by a synthesis of (+)-aphanamol I (**194**, Scheme 1.48).⁹⁸ Both of these syntheses made use of the intramolecular cycloaddition reaction of allenes, constructing the bicyclic cores in one step, albeit from a densely functionalized precursor. Wender has also published a synthesis of the tricyclic core of the cyanthane diterpenes via intramolecular VCP/alkyne cycloaddition (Eq. 1.12).⁹⁹

Scheme 1.47



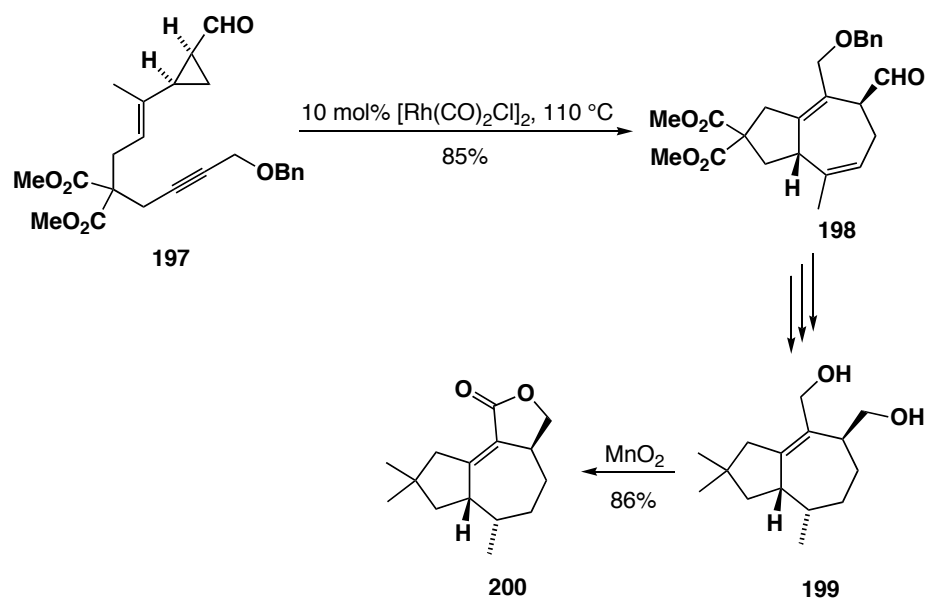
Scheme 1.48





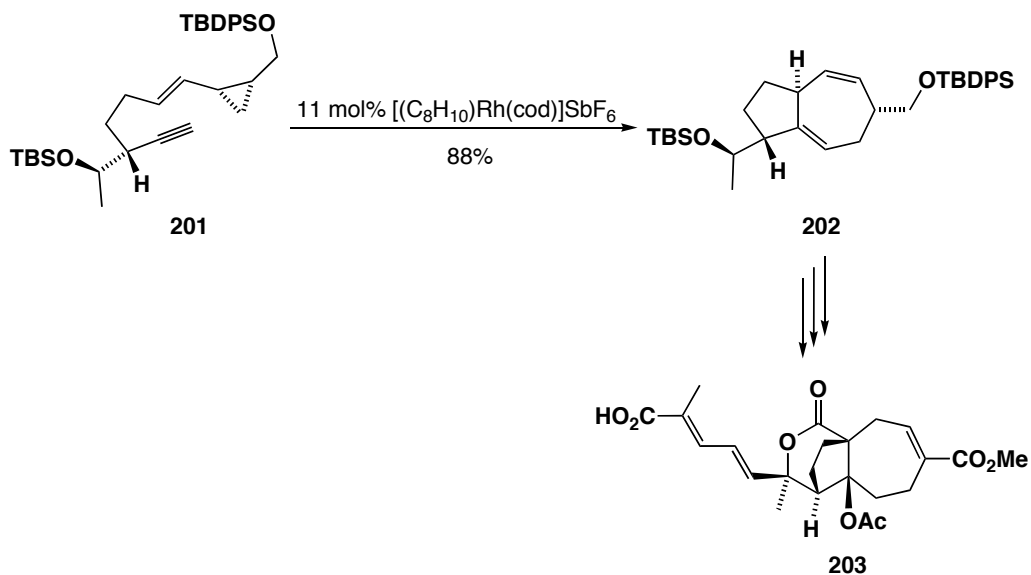
Martin applied the rhodium-catalyzed tandem alkylation/cycloaddition described earlier to the synthesis of tremulenolide A (**200**) and tremulenediol A (**199**) (Scheme 1.49).¹⁰⁰ The synthetic scheme uses the [5+2] cycloaddition as a key step in the synthesis

Scheme 1.49



of **199**, which was easily transformed into **200** by regioselective oxidation of the diol. Finally, Trost has made use of the VCP cycloaddition in the synthesis of (–)-pseudolaric acid B (**203**) (Scheme 1.50).¹⁰¹ Originally, the key cycloaddition step was attempted through Trost's ruthenium-catalyzed method (*vide infra*), developed to improve on the rhodium-conditions, but this led to product mixtures, necessitating the switch back to the Wender system.

Scheme 1.50

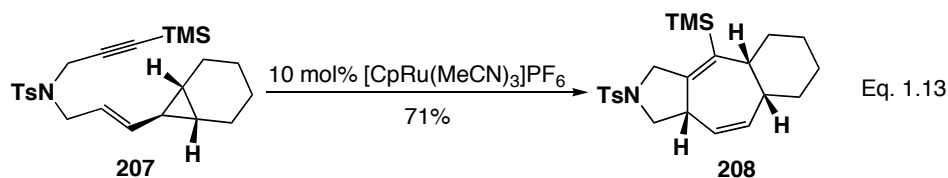
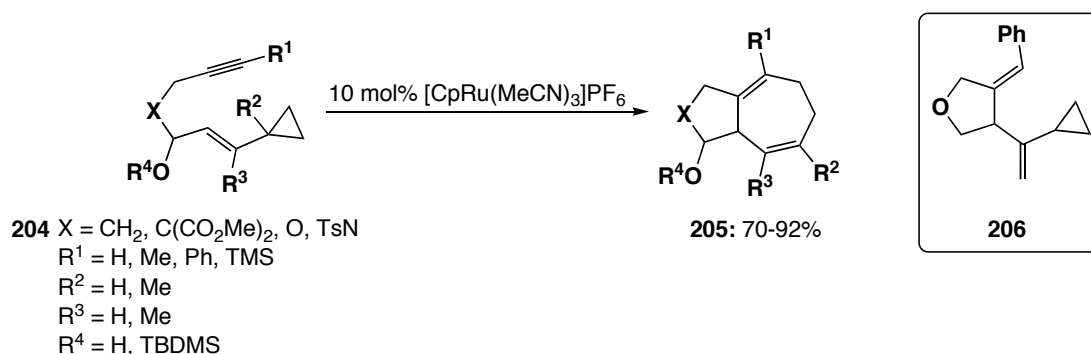


IV. Mechanistic Studies

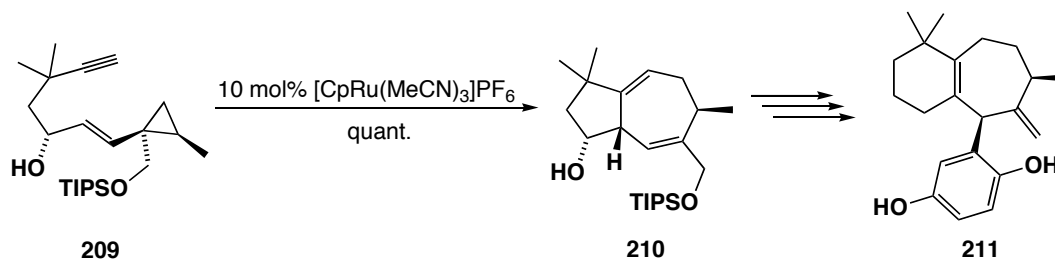
The mechanism of the $[Rh(CO)_2Cl]_2$ catalyzed VCP [5+2] cycloaddition reaction has been thoroughly modeled via DFT calculations.¹⁰² These investigations show that the reaction likely proceeds via the mechanism shown in Scheme 1.51. The reaction begins with dissociation of the rhodium-dimer, followed by coordination of the VCP. Carbonyl dissociation, followed by C-C bond activation leads to an η^1, η^3 -allyl complex, which then relaxes to a lower energy square-pyramidal form. Alkyne coordination, insertion, reductive elimination, and dissociation then lead to the final product. The rate-limiting step in these VCP cycloadditions with alkynes and allenes is the migratory insertion of the two-carbon reactant; however, in the case of alkenes, the highest energy step is subsequent reductive elimination.

of this variant is the construction of tricyclic systems of relevance to alkaloid syntheses (Eq. 1.13).¹⁰⁴ One natural product synthesis has been reported, a rather inefficient route to (+)-frondosin A (**211**) (Scheme 1.53).¹⁰⁵

Scheme 1.52

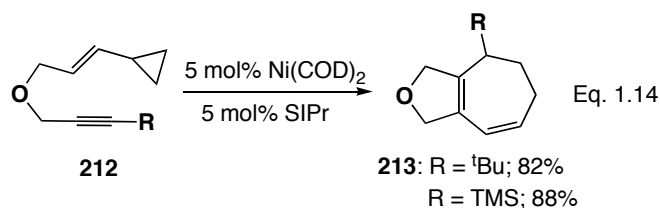


Scheme 1.53

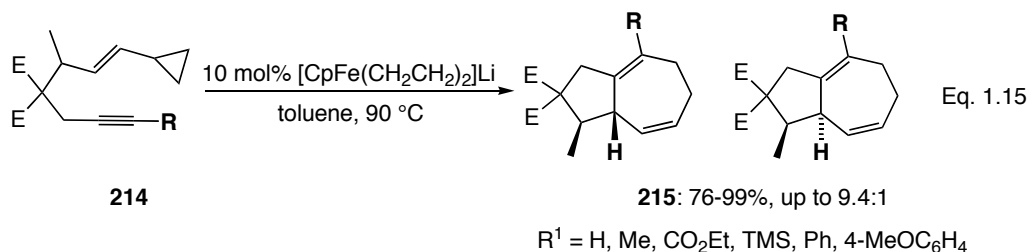


Part G: Nickel- and Iron-Catalyzed Vinylcyclopropane Cycloaddition Reactions

Louie has reported that VCP [5+2] cycloaddition reactions can be catalyzed by *in situ* prepared nickel/NHC complexes (Eq. 1.14).¹⁰⁶ Selective seven-membered ring formation was achieved with bulky alkyne substituents, with smaller substituents giving mixtures of seven-membered ring bicycles and monocyclic five-membered ring ethers.



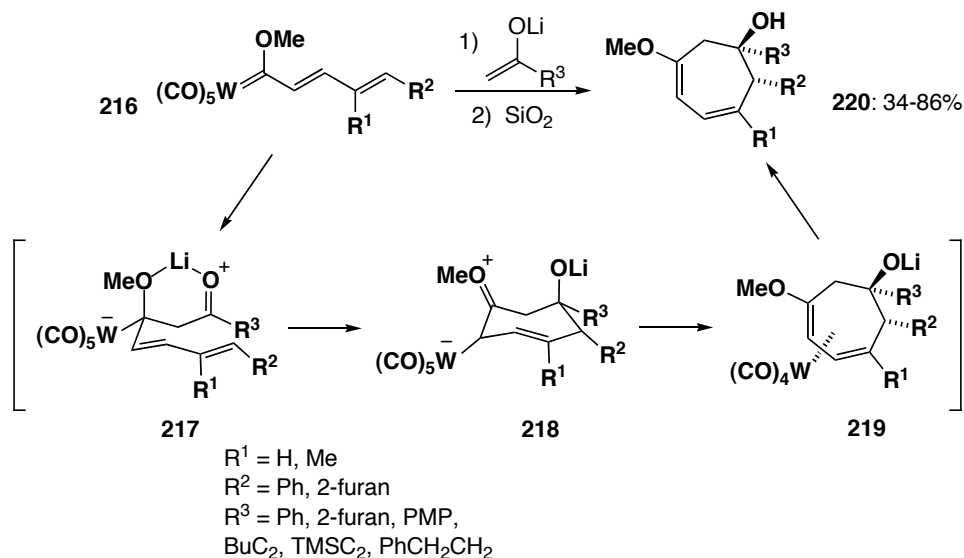
A promising iron-catalyzed VCP cycloaddition reaction¹⁰⁷ has provided an economically attractive alternative to the rhodium- and ruthenium-catalyzed systems (Eq. 1.15). The complexes $[\text{CpFe}(\text{CH}_2\text{CH}_2)_2]\text{Li}\cdot\text{tmeda}$ and $[\text{CpFe}(\text{cod})]\text{Li}\cdot(\text{MeOCH}_2\text{OMe})$ both catalyze the [5+2] cycloaddition reaction, with substrate tolerance similar to the rhodium-catalyzed system.



Part H: Fischer Carbene Mediated [5+2] Cycloaddition Reactions

Barluenga has reported a conceptually different [5+2] cycloaddition reaction of lithium enolates and Fischer carbene complexes (Scheme 1.54).¹⁰⁸ Both tungsten and chromium complexes mediate the stoichiometric reaction, with superior yields obtained in the tungsten manifold. Interestingly, the reaction occurs with complete diastereocontrol and in reasonable to good yields. The authors propose a mechanism in which the lithium enolate first adds to the carbene complex in a 1,2-fashion (**217**), followed by a 1,2-migration of the metal to induce cyclization (**218**). Decomplexation and quenching of the alkoxide completes the sequence.

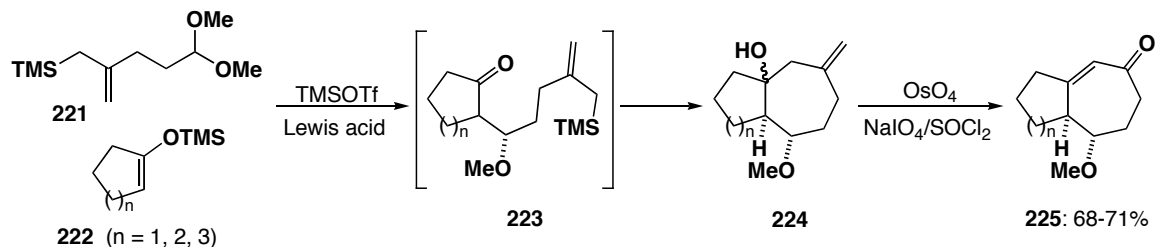
Scheme 1.54



Part I: Allylsilane [5+2] Cycloaddition Reactions

Lee reported the stepwise cycloaddition reaction of allylsilanes and silylenol ethers for the preparation of seven-membered rings in 1988.¹⁰⁹ In the presence of TMSOTf or Lewis acids such as TiCl_4 or AlCl_3 , allylsilane **221** undergoes a tandem aldol condensation/Sakurai reaction (Scheme 1.55). The cyclization product **224** is immediately converted to the enone, in overall yields of 68-71%. Recently, Tanino has

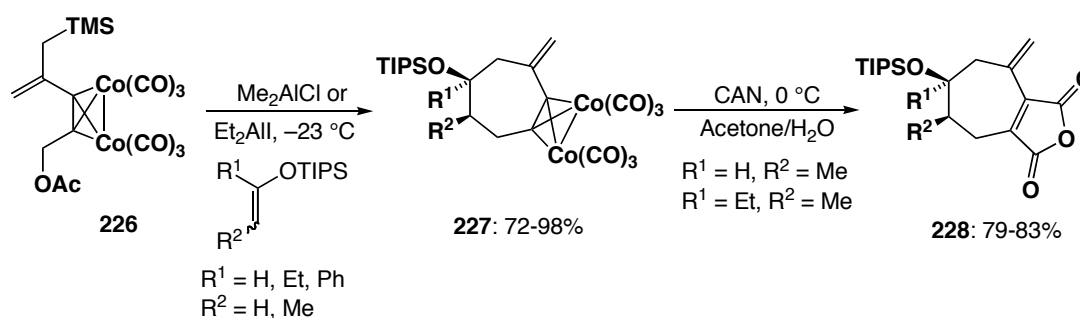
Scheme 1.55



reported a modification of this procedure wherein an allylsilane dicobalt acetylene complex is used (Scheme 1.56).^{110,111} This reaction produces mono- and bicyclic ring products in 63-98% yield with high stereoselectivity, yielding the same product

regardless of the stereochemistry of the initial silyl enoether. Decomplexation with ceric ammonium nitrate in acetone/water liberates the final organic product as a maleic anhydride derivative. The authors propose an alkylation/Sakurai reaction mechanism where a hexacarbonyldicobalt propargyl cation is the key intermediate, which undergoes the Nicholas reaction.¹¹² This reaction can therefore be conceptualized as a [5+2] cycloaddition of a cobalt-stabilized pentadienyl cation and a π -system.

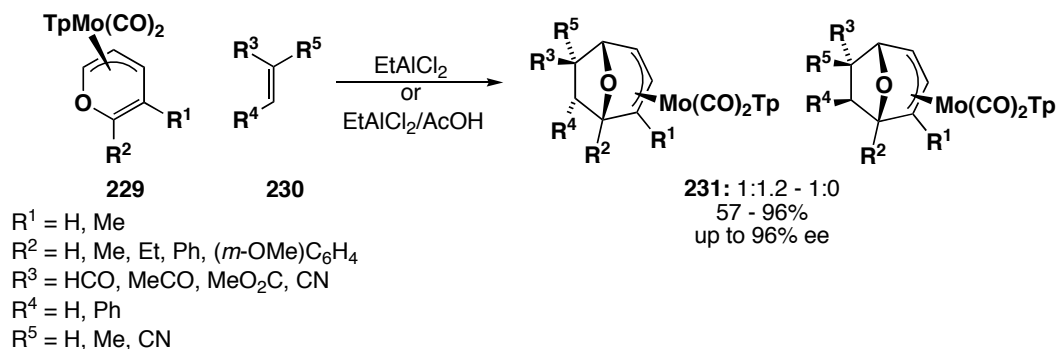
Scheme 1.56



Part J: Metal-Mediated η^3 -Pentadienyl [5+2] Cycloaddition Reactions

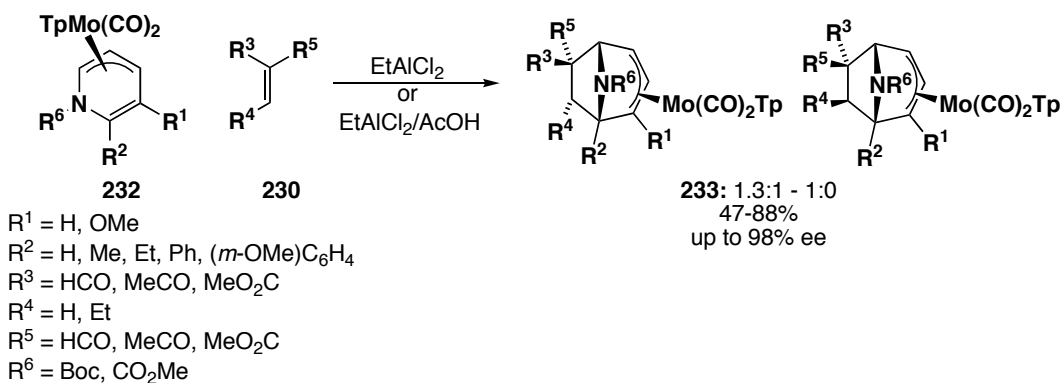
The oxidopyrylium cycloadditions and, by extension, the oxidopyridinium analogues, suffer from a lack of enantiocontrol and facial selectivity, although limited methods to achieve this control have been developed. Another means of achieving enantiocontrol in these reactions is through the use of a chiral scaffold. Liebeskind demonstrated the preparation of molybdenum allyl complexes in high enantiopurity and subsequent conversion to η^3 -pentadienyl compounds with little to no racemization.¹¹³ The η^3 -pentadienyl complexes are similar to the oxidopyrylium species described previously and readily undergo [5+2] cycloaddition reactions with electron deficient alkenes and alkynes in the presence of a Lewis acid (Scheme 1.57). Recently it was reported that for cycloaddition of 6-substituted scaffolds ($\text{R}^2 \neq \text{H}$), the presence of both

Scheme 1.57



Lewis and Brønsted acids was necessary to promote the reaction.¹¹⁴ Both oxygen and nitrogen heterocycles have been employed (Scheme 1.58), delivering seven-membered ring products in good to excellent yields, with complete facial selectivity, high *exo* regioselectivity, and high enantiopurity. The 6-substituted systems in particular lead to synthetically valuable products, with four contiguous stereocentres, one a quaternary carbon, installed in a one-pot process. The final organic product is liberated from the

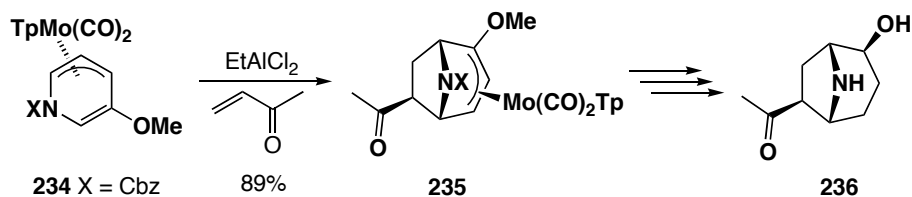
Scheme 1.58



metal through one of several procedures, including proto-, iodo-, or oxidative demetalation, all with good yields and retention of stereochemistry. The potential of this reaction class has been demonstrated by the total synthesis of the simple alkaloid (–)-Bao Gong Teng A (**236**).¹¹⁵ As of yet, however, only 5- and 6-substituted η^3 -pyranyl and η^3 -

pyridinyl systems have been thoroughly investigated, with the cycloaddition apparently limited to electron-deficient π -systems.

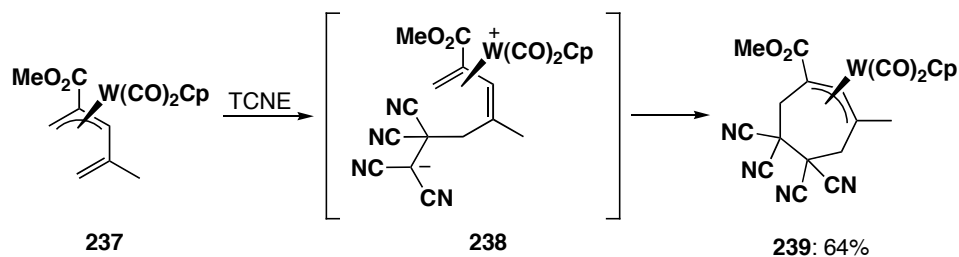
Scheme 1.59



The authors favour a mechanism wherein the electron deficient alkene or alkyne is activated by the Lewis acid (or “super Brønsted acid” in the 6-substituted cases), followed by a stepwise sequence wherein the η^3 -pentadienyl undergoes nucleophilic addition to the activated species, generating a zwitterionic intermediate. Electrophilic ring closure completes the sequence. The products slowly racemize in the presence of Lewis acid, lending credence to the proposal of a persistent zwitterionic complex lying on the reaction coordinate.

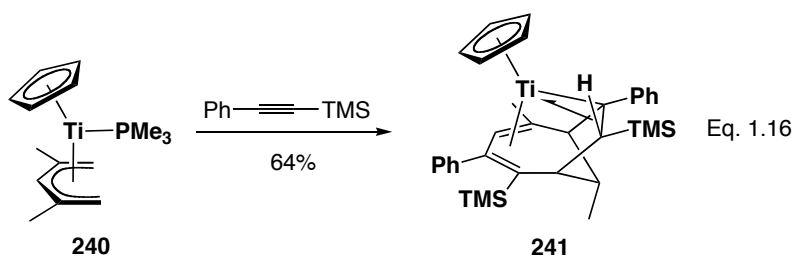
Tungsten η^3 -pentadienyl complexes also undergo [5+2] cycloaddition, presumably via a similar stepwise mechanism (Scheme 1.60).¹¹⁶ As in the molybdenum analogue, electron-deficient olefins appear to be required; only the reaction with TCNE has been reported. The most notable difference between the molybdenum and tungsten systems is the open, as opposed to closed, nature of the tungsten pentadienyl substrate.

Scheme 1.60



Part K: Metal-Mediated η^5 -Pentadienyl [5+2] Cycloaddition Reactions

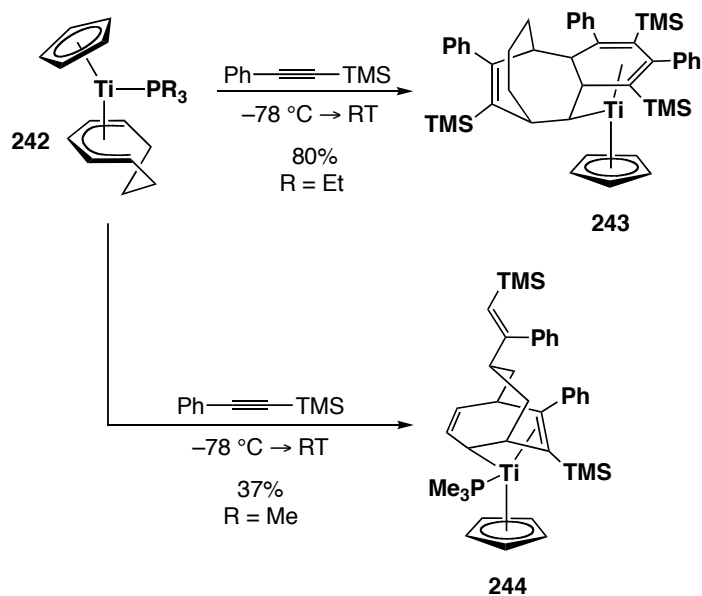
Transition-metal η^5 -pentadienyl complex cycloadditions discussed in this section, while fundamentally important, have not yet reached a level of development where the methodology can be applied to complex molecule synthesis. Ernst was first to demonstrate [5+2] cycloaddition reactivity using pentadienyl complexes adopting an η^5 -coordination mode.¹¹⁷ He observed that the titanium 2,4-dimethyl pentadienyl complex **240** incorporates two equivalents of trimethylsilyl phenylacetylene to yield the bridged



cycloheptadiene complex **241**; attempts to limit the incorporation of alkyne to one equivalent were unsuccessful (Eq. 1.16). During the course of investigations into C-C agostic interactions in unsaturated titanium complexes, Ernst also reported [5+2] cycloaddition reaction products formed from the reactions of titanium η^5 -cyclooctadienyl complex **242** and alkynes.¹¹⁸ These cycloaddition reactions also proceed by incorporation of two or three alkyne units, depending on the nature of the phosphine ligand (Scheme 1.61), yielding complex multicyclic structures. Ernst proposed that a [5+2] cycloaddition reaction is involved in the isomerization of a zirconium alkyne complex **246**; however, no characterization data was provided to support this conclusion (Scheme 1.62).¹¹⁹

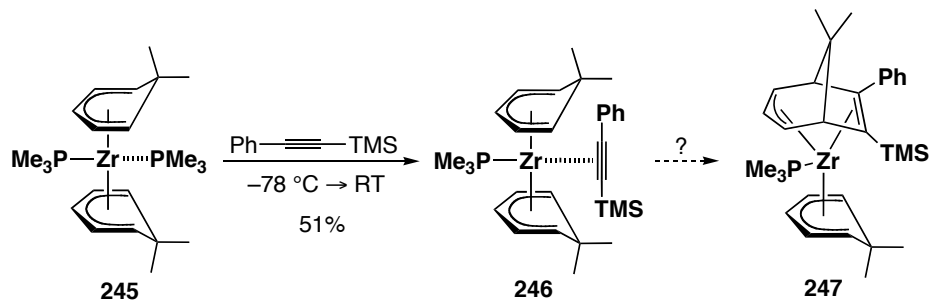
Shortly after Ernst's initial report, Kreiter¹²⁰ and Sheridan¹²¹ independently demonstrated similar reactivity in η^5 -manganese carbonyl complexes. Each determined

Scheme 1.61

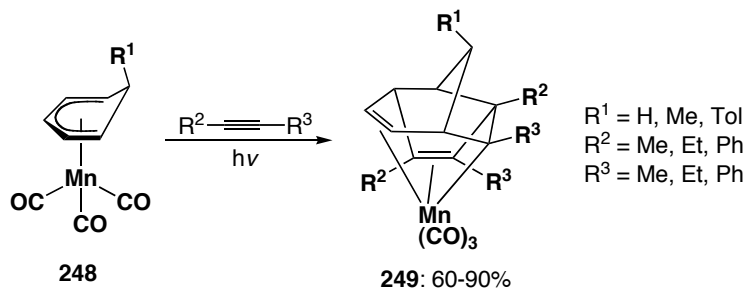


that irradiation of complexes of the type **248** in the presence of alkyne leads to cycloaddition products, generally incorporating two alkyne units to make multicyclic systems of the type **249** in good to excellent yield (Scheme 1.63).

Scheme 1.62

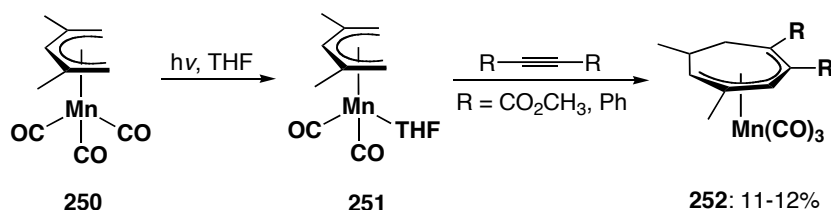


Scheme 1.63



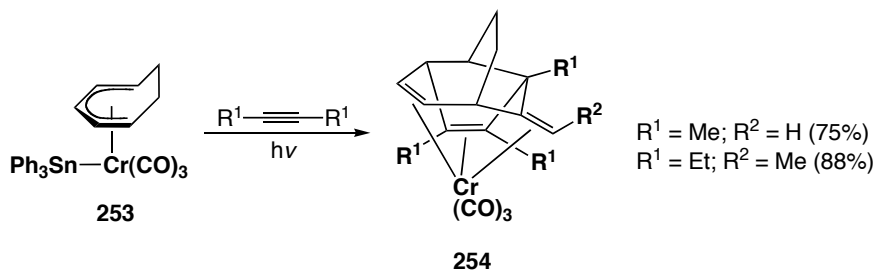
Kreiter determined that the role of the light is to generate a vacant site on the metal by liberating one equivalent of CO (Scheme 1.64). This was demonstrated via photolysis in THF in the absence of alkyne to produce the mono-THF complex **251**. When complex **251** was exposed to alkyne in the absence of light, the expected cycloaddition products **252** were obtained.

Scheme 1.64



When attempts were made to limit the incorporation of alkyne to one unit, the yields were significantly reduced. Improved yields (up to 40%) can be obtained by conducting the reaction under a CO atmosphere. Sheridan harnessed the potential of the monocyclization product by incorporating two different alkyne units, demonstrating the intermediacy of the monoinsertion product on the pathway to the final [5+2], *homo*[5+2] products. The less than impressive yield of the selective initial cycloaddition limits the overall yield. Sheridan has also shown that chromium/tin bimetallic complexes will mediate this reaction (Scheme 1.65),¹²² with the undesirable production of an equivalent of triaryltin hydride, generated via hydride abstraction from the cycloaddition product.

Scheme 1.65



Part L: Conclusion

Although a great deal of [5+2] cycloaddition chemistry has been developed, each reactivity motif is limited by inherent drawbacks. The early work in the areas of perezone-type and kojic acid-type cycloaddition chemistry is limited by the necessity of using a cyclic system by fixing the geometry of the pentadienyl cation in the former, or allowing the formation of the oxidopyrylium ylid in the latter. Liebeskind's molybdenum-mediated chemistry also shares this limitation. Despite harnessing the potential of the latent functional group in the resultant heteroatom bridge, this thermal chemistry cannot be applied to simple acyclic substrates, although the work of Tanino presents interesting opportunities for further development. In addition, the use of electronically biased or strained π -systems is necessary to achieve efficient intermolecular cycloaddition reactivity. Although elegant formal intermolecular processes have been developed via tethering protocols, these add potentially undesirable steps and extraneous functionality into a synthetic sequence.

The vinylcyclopropane cycloaddition reaction became useful after the pioneering work of Wender, demonstrating the potential of metal-mediated cycloaddition procedures, allowing the [5+2] reaction to proceed beyond cyclic systems. While the tremendous value of this reaction is obvious, the efficiency of the catalytic process is purchased at the cost of multistep substrate synthesis and building strain into the starting materials, later released to provide a thermodynamic driving force. This necessity, coupled with the potentially prohibitive cost associated with rhodium (and lower, but not insignificant, cost of ruthenium) make this procedure less attractive, particularly at large scale.

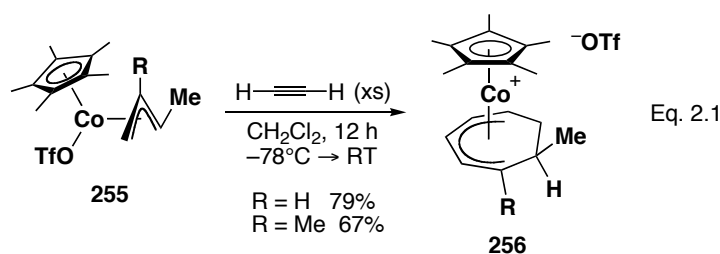
Metal-mediated η^5 -pentadienyl cycloaddition processes avoid some of the drawbacks of the vinylcyclopropane system, but are hampered by an absence of product selectivity, generally giving only higher-order cycloaddition products in synthetically useful yields. It is these shortcomings of the metal-mediated [5+2] cycloaddition reaction (*i.e.*, substrate complexity, product selectivity, yield, and material expense) that the work presented in this thesis begins to address. Presented here is a new stoichiometric [5+2] cycloaddition manifold that proceeds in exceptionally high yields, makes use of simple, inexpensive, easily prepared and unstrained starting materials, proceeds with excellent product selectivity, and allows the isolation of novel and unprecedented products during the course of the reaction.¹²³

Chapter 2: The Preparation of Cobalt(III) η^5 -Pentadienyl Complexes

Part A: Project Background

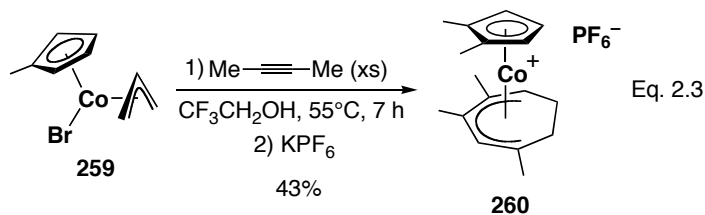
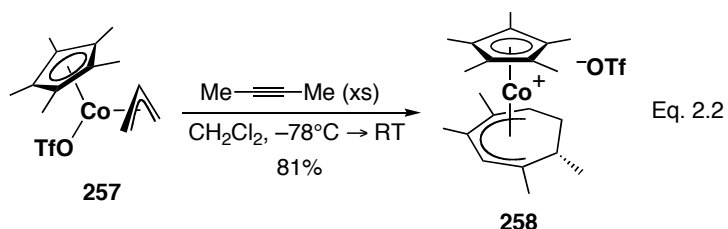
The preparation of seven-membered ring compounds via metal-mediated cycloaddition methodology has long been a topic of interest in the Stryker group. Initially, it was reported that sterically hindered half-sandwich iridium allyl complexes undergo unique cycloaddition reactions with alkynes in a [3+2+2] fashion, generating metal-bound η^5 -cycloheptadienyl compounds.¹²⁴ This was a fundamentally interesting and novel reaction manifold, although the shortcomings of the system were significant. The prohibitive cost of stoichiometric iridium chemistry aside, the greatest limitation was the inability to use acetylene or mono-substituted alkynes in the reaction, presumably due to the propensity of terminal alkynes to rearrange to vinylidenes upon coordination to late transition-metal systems.

Cobalt, which is also a Group 9 metal, presented an obvious possibility for addressing these shortcomings. A report published during the early stages of the investigation on reactions of cobalt allyl complexes suggested that even in the presence of excess alkyne, a [3+2] cycloaddition to give cyclopentadienyl complexes was the predominant reaction pathway.¹²⁵ However, Stryker and coworkers found that in a non-coordinating solvent, the reaction preferentially proceeds to seven-membered ring products via the [3+2+2] pathway, analogous to that observed in the iridium system (Eq. 2.1).¹²⁶ The cobalt system, clearly more attractive in terms of cost in stoichiometric



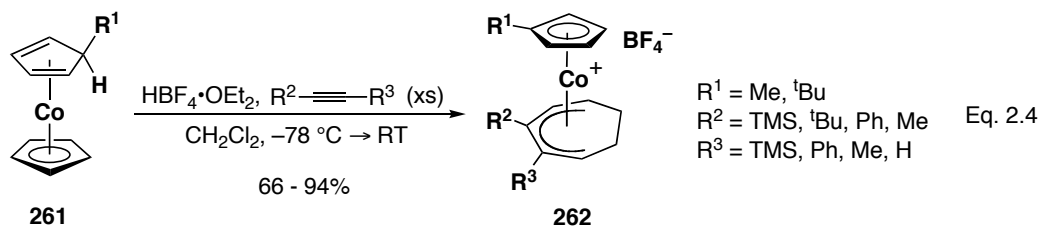
synthesis, also extends the scope of the cycloaddition to include unsubstituted alkynes. Unfortunately, the higher degree of steric crowding at the smaller cobalt centre prevents reactions with large internal alkynes, cyclizations that were successful in the iridium system.

Of greater interest, however, was the isolation of products arising from an unexpected alternative and more complicated reaction path for internal alkynes, now referred to as the anomalous [3+2+2] cycloaddition reaction.¹²⁷ These products, while still η^5 -cycloheptadienyl complexes, exhibited substitution patterns inconsistent with the insertion of two alkyne units in a contiguous fashion (Eq. 2.2 and 2.3). Isotopic labelling



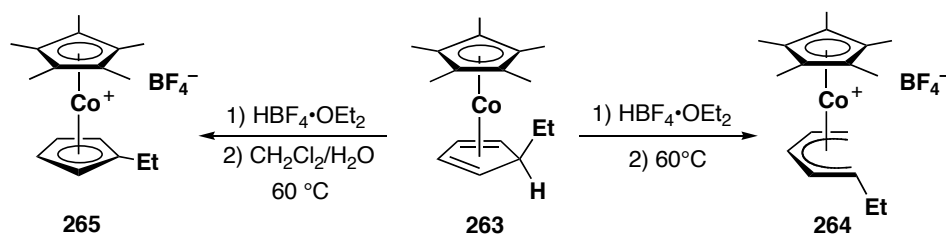
experiments with doubly ¹³C(*sp*)-labelled 2-butyne proved that methyl migration does not occur, confirming noncontiguous alkyne insertion. In Eq. 2.3, the cycloheptadienyl complex arises from C-C bond activation of the ancillary cyclopentadienyl ligand, concomitant with the [3+2] coupling of the original allyl and 2-butyne, generating a new

1,2-dimethylcyclopentadienyl ligand. Complexes such as **258** and **260** can only be rationalized in terms of a [5+2] ring expansion/cycloaddition pathway. This process was subsequently developed into emerging synthetic methodology unto itself (Eq. 2.4).¹²⁸



Spencer has shown that cyclopentadiene complexes **263** undergo C-C bond activation when exposed to acid at elevated temperatures, yielding open η^5 -pentadienyl complexes, whereas under less than rigorously dry conditions, dehydrogenation to form cobaltocenium derivatives predominates (Scheme 2.1).¹²⁹ While the anomalous [3+2+2]

Scheme 2.1



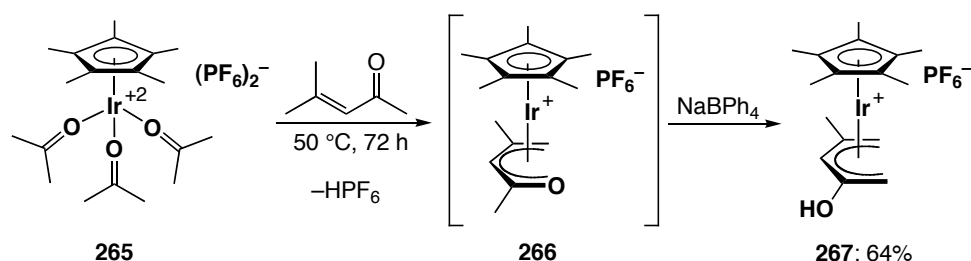
cycloaddition and [5+2] ring expansion/cycloaddition reactions occur at temperatures lower than those required to achieve the Spencer-type C-C bond activation, the possibility of an η^5 -pentadienyl/alkyne cycloaddition embedded in the ring expansion reaction mechanism was considered worthy of investigation, despite the electronically saturated cobalt centre, which suggested that pentadienyl/alkyne coupling would be unlikely.

Part B: High-Valent Group 9 η^5 -Pentadienyl Compounds

To investigate the potential cycloaddition reactivity of cationic half-sandwich cobalt(III) η^5 -pentadienyl complexes, a convenient synthesis needed to be identified. To our great surprise, very few examples of cobalt η^5 -pentadienyl compounds have been reported, and of these only a handful are of the cobalt(III) oxidation state. In fact, very few Group 9 η^5 -pentadienyl complexes have been reported in general, despite the long history¹³⁰ of pentadienyl research.

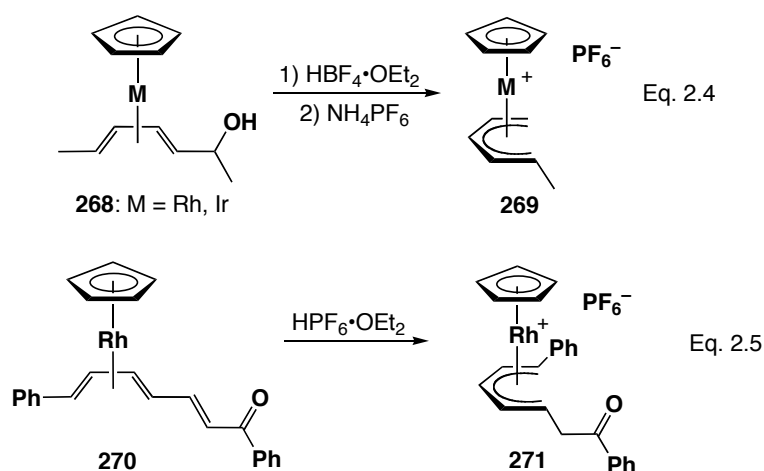
Maitlis and coworkers reported the first such complex, in iridium.¹³¹ They found that the dicationic iridium tris(solvento) complex **265** reacts with mesityl oxide at 50 °C to produce the η^5 -oxapentadienyl complex **266**. This compound slowly isomerizes to the 2-hydroxy- η^5 -pentadienyl complex **267**, isolated in 64% yield. The authors proposed a partial dissociative isomerization mechanism, wherein the oxygen-bearing end of the pentadienyl moiety dissociates, undergoes an acid-mediated tautomerization to the enol form and recoordinates; the whole process favoured by the soft-soft interaction of iridium with the olefin moiety, rather than the harder carbonyl.

Scheme 2.2



Soon after the Maitlis report, Powell¹³² published the preparation of η^5 -pentadienyl complexes of both rhodium and iridium (Eq. 2.4). Pentadienyl complexes **269** were prepared using a penta-1,3-dienyl alcohol complexation/dehydration sequence,

a protocol first developed by Pettit¹³³ for the preparation of cationic iron η^5 -pentadienyl tricarbonyl complexes. The yields, where reported, were in the range of 75%. Similarly, protonation of rhodium hexatriene compound **270** gave the 1-methyl- η^5 -pentadienyl compound **271** in 84% yield (Eq. 2.5).

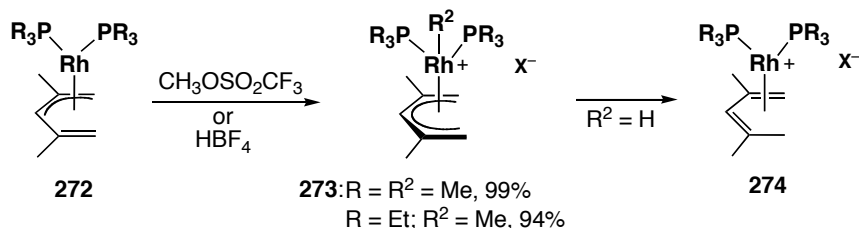


Bleeke¹³⁴ has reported η^5 -pentadienyl complexes prepared via methylation or protonation of η^3 -pentadienyl rhodium(I) and iridium(I) complexes (Schemes 2.3 – 2.4). Methylations of complexes **272** proceed readily to give the cationic Rh(III) complexes **273** in near-quantitative yield and the corresponding Ir(III) compounds in yields as high as 74%. In contrast, protonation of the rhodium complexes **272** initially yields unstable η^5 -pentadienyl compounds, which undergo rapid hydride migration to the pentadienyl ligand, producing thermally unstable rhodium-diene complexes. The analogous iridium complexes yield isolable η^5 -pentadienyl compounds upon protonation.

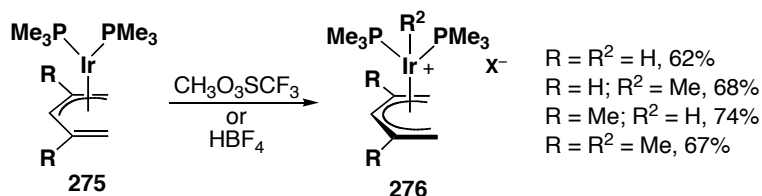
Recently, Müller¹³⁵ reported the preparation of rhodium and iridium pentadienyl complexes of the heavier Group 9 metals via hydride abstraction from metal-bound diene complexes. The product distribution varies with the solvent, giving only half-sandwich complexes **279** in acetone and THF and mixtures of **279** and **280** in CH_2Cl_2 . Low-valent,

half-open iridium and rhodium complexes **281** were prepared via the addition of 2,4-dimethylpentadienyl potassium. Attempts to form the cationic open metallocene complexes from **281** via hydride abstraction failed.

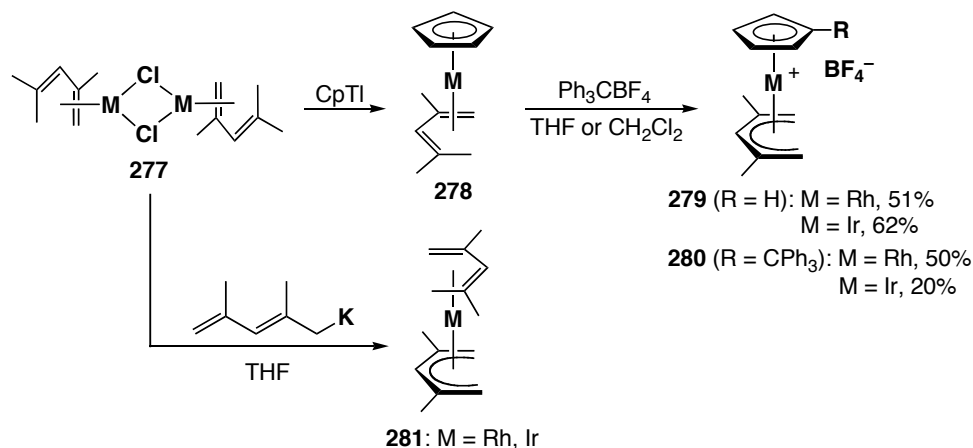
Scheme 2.3



Scheme 2.4



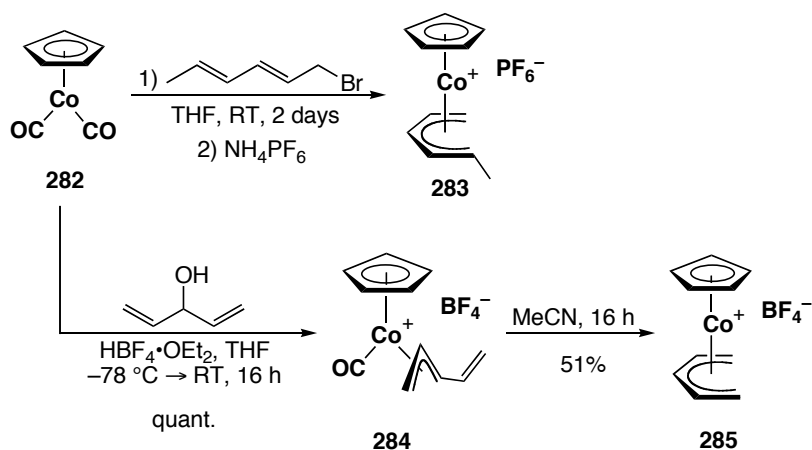
Scheme 2.5



Reports of cobalt pentadienyl complexes are primarily of low-valent Co(I) and Co(II) complexes.¹³⁶ High-valent Co(III) complexes are rare. Powell reported the preparation of $[CpCo(\eta^5\text{-1-methylpentadienyl})]PF_6$ **283** from $CpCo(CO)_2$ (Scheme 2.6), but no characterization data were provided to support this claim.^{132a} In the Stryker group,

Kirk investigated the preparation of Co(III) η^5 -pentadienyl compounds from protonation of CpCo(CO)₂ (**282**) in the presence of 1,4-pentadienyl alcohols.¹³⁷ These reactions showed initial formation of η^3 -pentadienyl monocarbonyl complexes **284**. These

Scheme 2.6

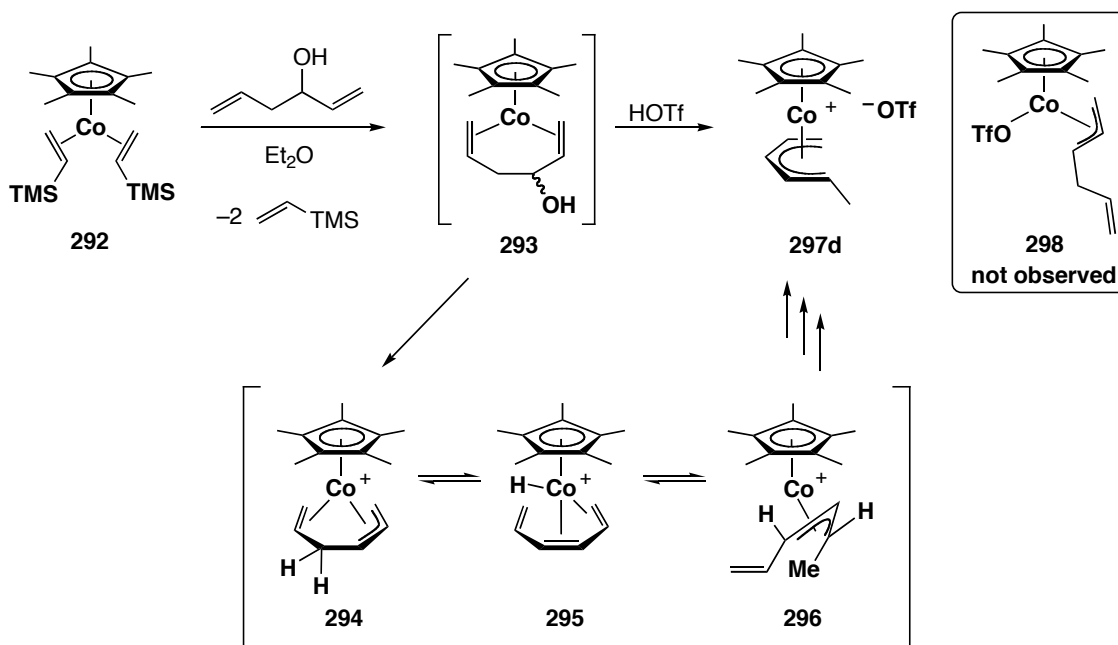


products could be further transformed to the desired η^5 -pentadienyl complexes, but required reaction conditions harsher than those reported by Powell. However, in acetonitrile at room temperature, facile conversion to the η^5 -pentadienyl compound was observed in reasonable yield, suggesting that the bromide ion present under Powell's conditions assists the dissociation of the second carbonyl ligand, presumably by $\eta^3 \rightarrow \eta^1$ isomerization and nucleophilic addition.

Ernst¹³⁸ reported the first fully-characterized Co(III) pentadienyl complexes (**287**), prepared via hydride abstraction from Co(I) diene precursors (Eq. 2.6). Spencer, in addition to the Cp*Co(η^5 -1-ethylpentadienyl)⁺ complex **264** described earlier, reported the interesting complex Cp*Co(η^5 -*anti*-1-propylpentadienyl)⁺BF₄⁻ **289**, also via C-C bond activation (Eq. 2.7).¹³⁹ Similarly, Koelle and Herberich observed C-C bond activation of a cyclobutadiene ligand by protonation, giving the 1,2,3-trisubstituted η^5 -pentadienyl complex **291** (Eq. 2.8).¹⁴⁰ This is novel, albeit not general, methodology,

(**292**) undergoes rapid exchange with 1,5-hexadiene-3-ol, presumably generating 1,5-diene complex **293** *in situ*, followed by protonation upon addition of triflic acid (Scheme 2.7). However, upon work-up, the reaction yielded a mixture containing η^5 -pentadienyl complex **297**, but none of the desired η^3 -allyl complex **298**, indicating that an olefin isomerization had occurred on the metal.

Scheme 2.7



The formation of the η^5 -pentadienyl complex is not entirely surprising. Upon protonation and dehydration of **293**, the direct product is expected to be allyl/olefin complex **294**. Olefin dissociation and subsequent β -hydride elimination/reinsertion yields complex **296**; further olefin isomerization via $\eta^3 \rightarrow \eta^1$ slipping, hydride transfers, and subsequent reassociation of the olefin leads to η^5 -1-methylpentadienyl complex **297d**. Interestingly, the 1-*anti*- η^5 -pentadienyl isomer is also accessible from this pathway, but is not seen. If the *anti*-isomer were formed, it would likely undergo a similar isomerization sequence to yield the thermodynamically favoured *syn*-isomer.

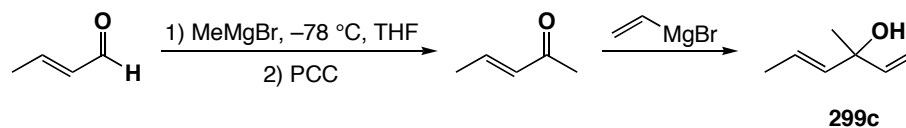
The preparation of η^5 -pentadienyl complexes via isomerization of 1,5-hexadienyl substrates is interesting from a fundamental molecular dynamics viewpoint, but it does not constitute a general pathway for the synthesis of this structural class. From the mechanistic proposal in Scheme 2.7, it is apparent that the β -hydride elimination/insertion steps present opportunities for $\eta^3 \rightarrow \eta^1$ isomerization and decomposition via subsequent σ -bond homolysis, leading to the low yield. This complication can be avoided by using an organic substrate where the two olefins are in a 1,4- rather than 1,5-arrangement. The required 1,4-dien-3-ols are easily prepared via addition of vinyl Grignard reagents to aldehydes. Many such substrates have been reported in the literature, often for use in Nazarov cyclization¹⁴¹ chemistry.

The use of 1,4-pentadienol substrates is a novel variation of the literature method of 2,4-diene-1-ol dehydration; both methods were thus investigated.¹⁴² Both the author and R. Witherell¹⁴³ conducted the research in this area and as such, only the substrates prepared for the author's contribution are discussed explicitly; however, in several areas of the discussion, significant overlap with Witherell's work is unavoidable.

I. Synthesis of Pentadienol Substrates

The 1,4-dienol class of substrates was first prepared, targeting compounds selected to evaluate a range of synthetically-relevant pentadienyl substitution patterns. 3-Methyl-1,4-pentadiene-3-ol (**299a**)¹⁴⁴ and *E*-1-phenyl-1,4-pentadien-3-ol (**299b**)¹⁴⁵ are literature compounds, each readily prepared in one step by addition of vinyl Grignard to ethyl acetate and *trans*-cinnamaldehyde, respectively. *E*-3-Methyl-1,4-hexadiene-3-ol **299c** was previously unreported, but was prepared via a simple three-step procedure

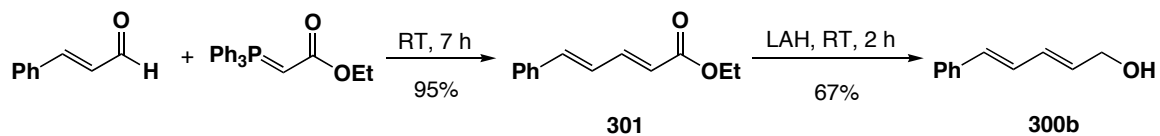
Scheme 2.8



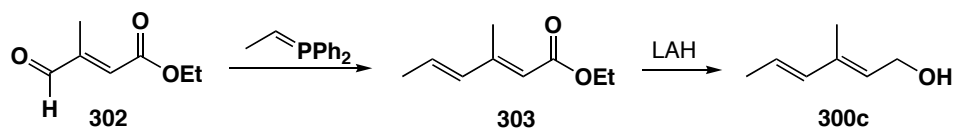
(Scheme 2.8). Although the use of 3-penten-2-one would have saved a step, crotonaldehyde was on hand and used simply for expedience. The crude products that were isolated from the preparation of dienols **299a** and **299c** remained contaminated by side products that could not be separated by chromatography. The impurities presumably arise from the acid sensitivity of these substrates, dehydrating to form doubly allylic, tertiary carbocations that undergo cyclization and/or oligomerization. As such, these products were carried forward without further purification.

The corresponding 1,3-dienol substrates were prepared in collaboration with S. Böcklein, a visiting diploma student from Germany, and V. Lofstrand, a fourth year undergraduate researcher, both working under the author's direction. These compounds fall into two groups: those selected for direct comparison with corresponding 1,4-dienol substrates, and those bearing substitution patterns not explored previously. In the first category fall commercially available *E,E*-2,4-hexadiene-1-ol (**300a**) and the literature compound *E,E*-5-phenyl-2,4-pentadien-1-ol (**300b**).¹⁴⁶ In the second are literature compounds *E,E*-3-methyl-2,4-hexadien-1-ol (**300c**),¹⁴⁷ *E,E*-2-methyl-2,4-hexadien-1-ol (**300d**),¹⁴⁸ *E,E*-3,5-heptadien-2-ol (**300e**)¹⁴⁹ and *E*-2-methyl-3,5-hexadien-2-ol (**300f**).¹⁵⁰ The syntheses of these substrates are outlined in Schemes 2.9 – 2.12 and Eq. 2.9. The preparation of *E,E*-2-methyl-2,4-hexadien-1-ol **300d** called for reduction of ester **304** with lithium aluminum hydride (LAH) deactivated with isopropanol.¹⁴⁸ This was ineffective in our hands, although the use of fully active LAH proved adequate.

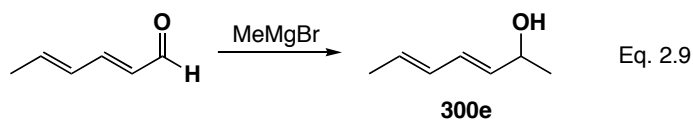
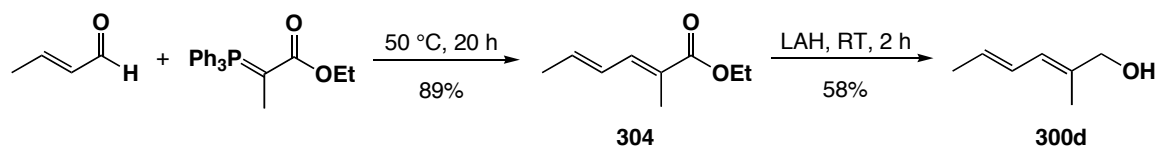
Scheme 2.9



Scheme 2.10

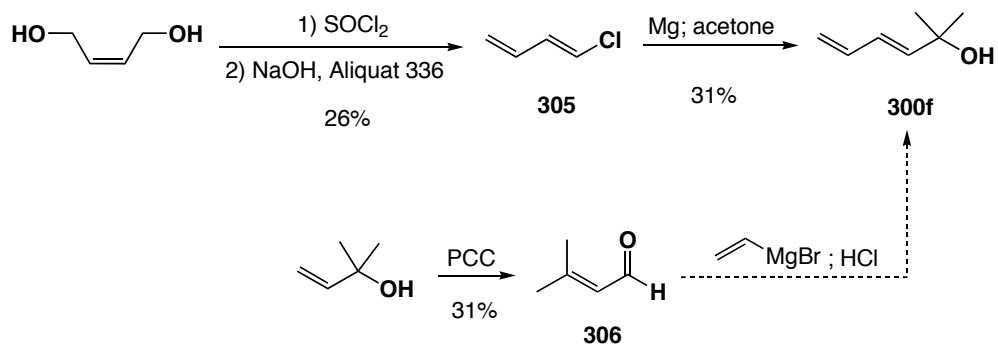


Scheme 2.11



Two routes for the preparation of *E*-2-methyl-3,5-hexadien-2-ol **300f** were attempted: one from *cis*-2-buten-1,4-diol¹⁵¹ and the other from 2-methyl-3-buten-2-ol.¹⁵² Only the former proved successful (Scheme 2.12). Chlorination of *cis*-2-buten-1,4-diol and subsequent NaOH-mediated elimination under catalytic phase transfer conditions

Scheme 2.12

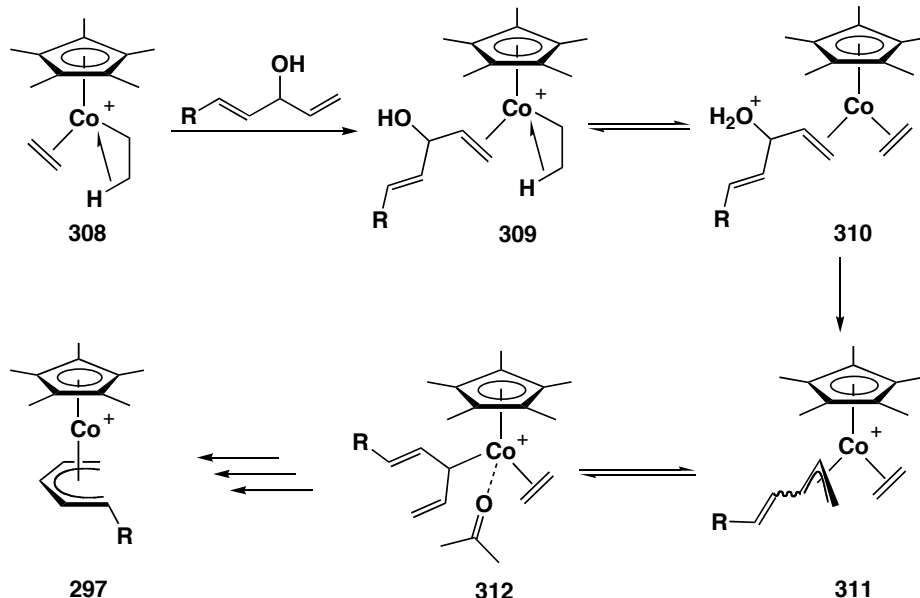


yielded 1-chloro-1,3-butadiene **305**.¹⁵³ Conversion to the Grignard reagent and quenching with acetone completed the synthetic sequence. Alternatively, PCC oxidation of 2-methyl-3-buten-2-ol produced the conjugated aldehyde **306**, which was converted to the non-conjugated dienol by Grignard vinylation. Reportedly, this product isomerizes under acidic conditions to the desired conjugated material; however, in our hands, only complex reaction mixtures were obtained.

II. Synthesis of η^5 -Pentadienyl Complexes via Non-conjugated Substrates

We initially investigated the preparation of η^5 -pentadienyl complexes from non-conjugated dienol substrates. Witherell^{142,143} developed reaction conditions wherein $\text{Cp}^*\text{Co}(\text{CH}_2\text{CH}_2)_2$ (**307**) was dissolved in acetone, cooled to -78 °C, and treated with the dienol (1.1 equiv.), followed a short time later by addition of $\text{HBF}_4 \cdot \text{OEt}_2$ (1 equiv.). Gradual warming to ambient temperature over approximately 16 hours and purification by bench top chromatography provided the red η^5 -pentadienyl cation. Tetrahydrofuran, acetone and dichloromethane were tested as reaction solvents, with acetone proving the highest yielding, presumably due to the transient stabilization of unsaturated intermediates and assisting $\eta^5 \rightarrow \eta^3 \rightarrow \eta^1$ isomerization processes. Significant amounts of a blue material were separated during purification, presumably consisting of one or more paramagnetic Co(II) decomposition products. The η^5 -pentadienyl complexes were obtained in spectroscopic purity (NMR), with subsequent crystallization yielding analytically pure samples. When we extended this methodology to η^5 -pentadienyl complexes bearing pro-nucleophilic tethers (Chapter 4), only decomposition products were observed, attributed to competitive off-metal reactions between the organic

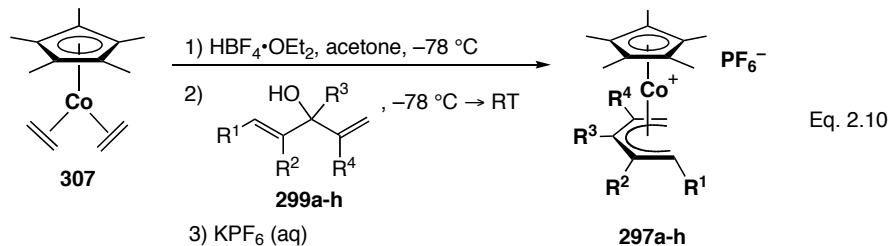
Scheme 2.13



substrate and acid. To address this problem, an alternative procedure became necessary.

Brookhart¹⁵⁴ thoroughly investigated the protonation of Cp*Co(CH₂CH₂)₂ **307**, demonstrating that the cationic adduct exists as rapidly equilibrating cationic agostic ethyl species (*e.g.*, **308**). We reasoned that prior addition of the acid directly to **307** should sequester the proton, minimizing competing off-metal reaction pathways. While this method successfully eliminated difficulties encountered with pro-nucleophilic substrates, the yields of simple alkyl- and arylated η^5 -pentadienyl complexes were not appreciably affected. Despite this, the new method has been employed as our standard procedure, giving reasonable to good yields (Table 2.1). Once formed, the products are remarkably stable, allowing bench top chromatography and recrystallization, and have demonstrated indefinite stability to air and moisture in the solid-state at room temperature. At temperatures above 60 °C in solution, minor decomposition has been observed, with complete decomposition occurring at temperatures in excess of 100 °C, likely a result of facile σ -bond homolysis arising from reversible $\eta^5 \rightarrow \eta^3 \rightarrow \eta^1$

Table 2.1: Cp*Co(η^5 -pentadienyl)⁺ Complexes via Unconjugated Dienol Substrates



Entry	Substrate	297 / yield (%)	Entry	Substrate	297 / yield (%)
1 ^a		 37	5		 67
2 ^a		 80	6 ^a		 54
3 ^a		 41	7		 59
4		 75	8		 30

^a Anion exchange (Step 3) omitted.

isomerizations. Counterion exchange from hexafluorophosphate to tetrafluoroborate was performed in many cases, providing improved crystallinity and product purity during low temperature two-solvent crystallization procedures. It was later determined that two-chambered liquid diffusion was a highly effective crystallization method for these systems, eliminating the need for anion exchange.

The product yield decreases significantly with increasing substitution, likely due to slower substrate coordination, allowing increased competition from proton exchange and off-metal reaction pathways such as cyclization and oligomerization. This was further demonstrated by Witherell's attempt to use *E*-1-phenyl-2,4-dimethyl-1,4-pentadien-3-ol,¹⁵⁵ from which he obtained no η^5 -pentadienyl complex formation. Of all the substrates explored, that one would be expected to give rise to the most stable carbocation upon protonation and loss of water.

A reasonable mechanistic pathway (Scheme 2.13) for this transformation involves initial exchange of the labile ethylene in the activated ethyl agostic complex with, presumably, the less substituted end of the dienol substrate. Proton transfer from the metal to the hydroxyl may occur directly or, more likely, via solvent mediation. Elimination of water yields η^3 -pentadienyl complex **311**, most likely as a mixture of *syn* and *anti* isomers. Configurational isomerization can occur via $\eta^3 \rightarrow \eta^1$ isomerization, with the strong preference for the acetone medium suggesting solvent assistance (*e.g.*, **312**). Subsequent dissociation of the remaining olefin and recoordination of the pendant arm yields the final η^5 -pentadienyl complex.

III. Synthesis of η^5 -Pentadienyl Complexes via Conjugated Dienols

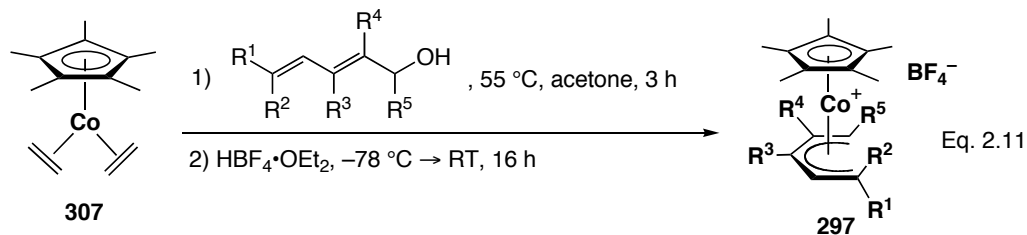
The difficulties associated with the non-conjugated pentadienol methodology (*i.e.*, the potential for substrate degradation via competitive pathways and decreasing yield with higher substitution) limit the scope of this reaction. We reasoned that employing the more traditional pre-coordination of a conjugated dienol substrate should improve the yield of the protonolysis and/or allow the preparation of complexes not accessible by the

routes described above.

Direct olefin exchange¹⁵⁶ between Cp*Co(CH₂CH₂)₂ (**307**) and *E,E*-5-phenyl-2,4-dien-1-ol (**300b**) at 60 °C in a sealed vessel under inert atmosphere was unsuccessful, returning mainly starting material. Upon heating the reactants in acetone at reflux under a mineral oil bubbler, allowing irreversible loss of ethylene, the exchange proceeded to completion, as determined by ¹H NMR spectroscopy; low-temperature protonolysis produced η^5 -1-phenylpentadienyl complex **297b**. During exchange, the sample rapidly developed some paramagnetic impurity, which significantly broadens the NMR spectrum. After three hours, the coordinated ethylene had completely disappeared, evolving into a new set of resonances, tentatively assigned to an intermediate Cp*Co(η^4 -1-phenyl-1,3-dien-4-ol) complex by comparison to analogous rhodium complexes.¹³² The spectrum was further complicated by the diastereomeric mixture of diene complexes formed; therefore, no further attempt was made to isolate or characterize this intermediate. With the exchange conditions defined, a range of η^5 -pentadienyl complexes **297** were prepared by *in situ* protonation at low temperature following thermal exchange (Table 2.2). Contrary to expectations, it is immediately apparent that this method results in yields comparable to our previous strategies, as exemplified by Entries 1 and 2.

The reactions to prepare η^5 -pentadienyl complexes **297c** and **297i** (Entries 3 and 4), produced mixtures of *syn* and *anti* isomers. Heating these mixtures to 60 °C in acetone failed to encourage convergence to one product and led only to decomposition at higher temperatures. Powell observed preferential formation of the presumably less stable *anti* isomer during the preparation of rhodium pentadienyl complexes (Scheme

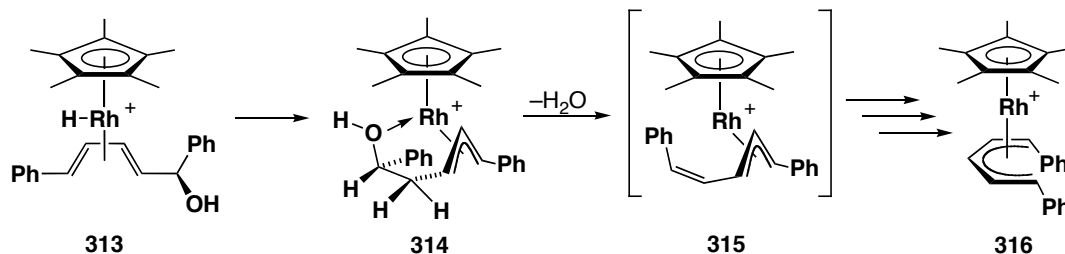
Table 2.2: Cp*Co(η^5 -pentadienyl)⁺ Complexes via Conjugated Dienol Substrates



Entry	Substrate	297 / yield (%)
1		 87
2		 81
3		 61 3:1 <i>syn/anti</i>
4		 22 1:1 <i>syn/anti</i>
5 ^a		 60

^a Followed by heating at 40 °C for 30 h.

Scheme 2.14



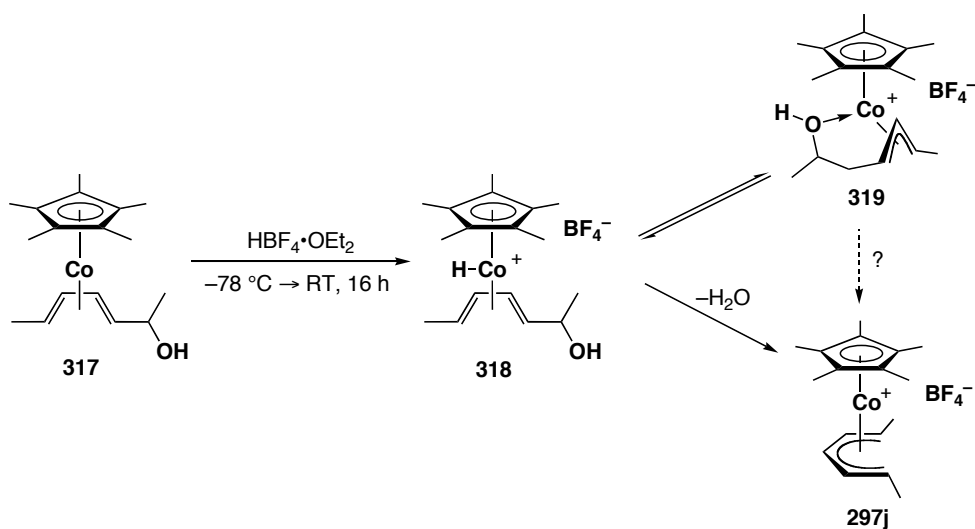
2.14).¹³² In that case, however, the intermediate rhodium-diene complex was prepared as a pure single diastereomer via reduction of an η^4 -pentadienone complex. Mechanistically, it was proposed that hydride migration initially generates the chelated η^3 -pentadienyl complex **314**, which undergoes stereospecific elimination of water to generate *Z*-olefin **315**. Subsequent *anti/syn* allyl isomerization and rotation about the single bond allowing olefin recoordination yields an η^5 -pentadienyl product with the less thermodynamically preferred *anti* substituent.

This mechanistic rationale is not relevant to our observations. In the case of Powell's reaction, the alcohol stereocentre controls the stereochemistry of the elimination product. The *syn/anti* stereochemical mixture in our complexes is observed at the end of the pentadienyl complex opposite the hydroxyl group and must involve *cis/trans* isomerization of the terminal double bond. Interestingly, a correlation between the number of equivalents of $\text{HBF}_4 \cdot \text{OEt}_2$ and ratio of pentadienyl isomers was observed, as determined by ^1H NMR spectroscopy. With precisely one equiv. of acid, only a minor amount of the *anti* isomer is formed (approx. 7:1 *syn/anti*). At 1.5 equiv. of acid, the ratio shifts to 1.3:1, with only decomposition observed at higher acid stoichiometry. The decomposition is likely the result of the protonolysis of reactive intermediates, but it is curious that the amount of acid would have an effect on the geometry of the final

products. The isomeric ratios for the initial pentadienol substrates **300c** and **300d** were 1:1 and 2:1 *E:Z*, respectively, and may provide an explanation of this result if differential complexation of the isomers occurs.¹⁵⁷

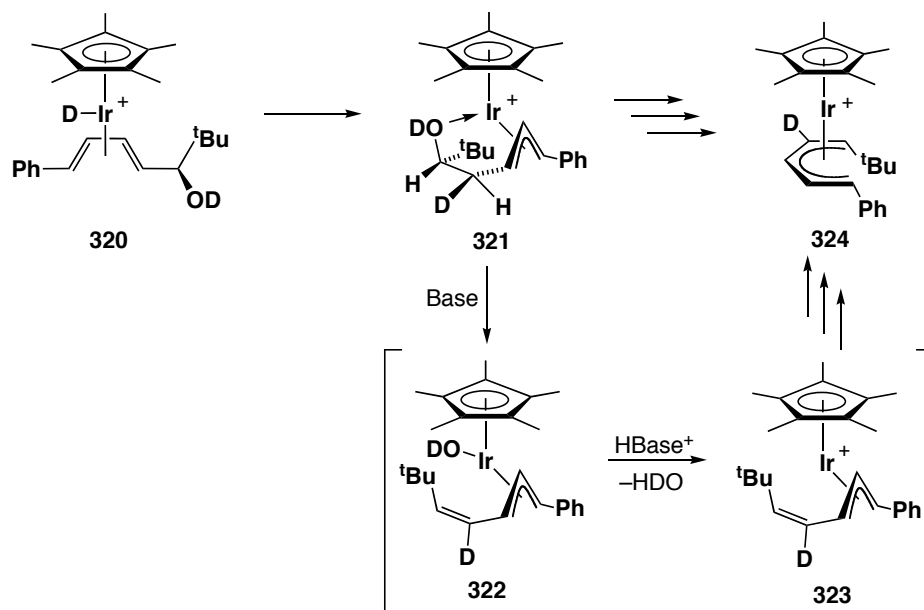
Some mechanistic insight into this problem was obtained from the synthesis of η^5 -1,5-dimethylpentadienyl complex **297j**. The protonation initially provided two products, the desired η^5 -pentadienyl complex and an intermediate tentatively assigned as the chelated Cp*Co(η^3 -allyl) complex **319** (Scheme 2.15). Complete conversion to the η^5 -pentadienyl product was only obtained upon heating at 40 °C for 30 hours. The allyl complex **319** arises from hydridocobalt intermediate **318** via competitive migration of hydride to the diene in preference to proton migration to oxygen and elimination of water. The proposed hydroxyl coordination inhibits protonation at oxygen and conformational constraints may retard the reversibility of hydride migration. Powell has observed related products during rhodium and iridium η^5 -pentadienyl complex preparation, exhibiting the same thermal conversion behaviour.^{132c}

Scheme 2.15



Whether the η^3 -allyl complex is a necessary intermediate on the pathway to η^5 -pentadienyl complexes or simply a competitive kinetic product is unclear. The iridium η^5 -pentadienyl complex prepared from deuterium-labelled acid^{132c} proceeds with complete incorporation of the deuterium label in the final pentadienyl product consistent with the intermediacy of the η^3 -allyl complex (Scheme 2.16). This suggests that the allyl complex is an intermediate in the overall process; reversible hydride insertion is expected to yield a non-labelled product. From analogous experiments using rhodium, mixtures of the labeled and unlabelled products are observed, making reversible hydride insertion and proton transfer a likely mechanistic pathway on this energy surface. If the group trend continues, cobalt is anticipated to incorporate increased amounts of β -hydride elimination.

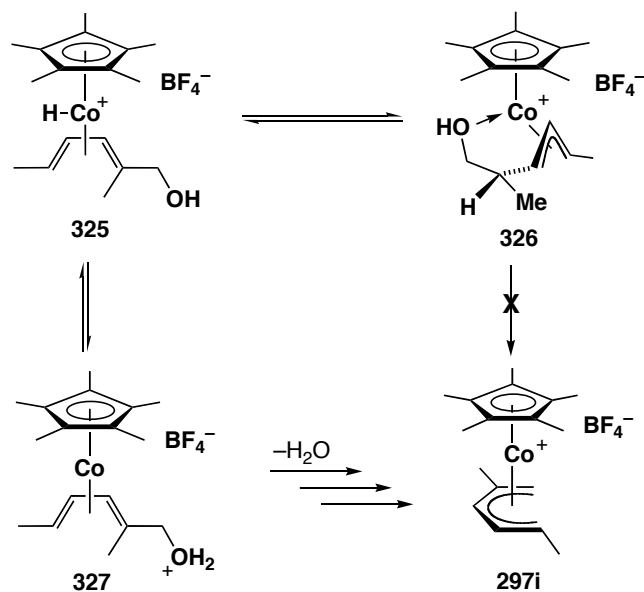
Scheme 2.16



The low yield obtained for η^5 -pentadienyl complex **297i** (Entry 4) also suggests that the intermediate formation of the η^3 -allyl complex is important mechanistically

(Scheme 2.17). Initial protonation of diene complex **325** followed by subsequent hydride insertion would result in chelated η^3 -allyl complex **326**. From this intermediate, *anti*-

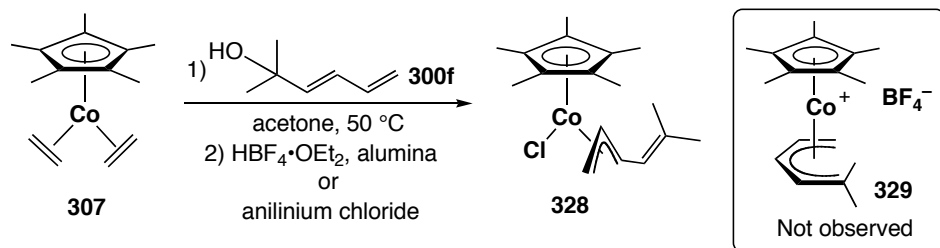
Scheme 2.17



elimination of water is not possible, meaning the only pathway for η^5 -pentadienyl complex formation is β -hydride elimination and proton transfer. From this intermediate, excess acid may encourage protonolysis of the ligand, leading to decomposition. A lower acid concentration allows the slow β -hydride elimination and equilibration to the η^5 -pentadienyl complex to occur.

The final substitution pattern targeted for synthesis was a 1,1-disubstituted pentadienyl ligand. We attempted to prepare pentadienyl complex **329** by the reaction of Cp*Co(CH₂CH₂)₂ with *E*-2-methyl-3,5-hexadien-2-ol (**300f**), under the same conditions as shown in Eq. 2.11. Unexpectedly, the reaction product proved to be unstable in air and soluble in diethyl ether, in contrast to all other η^5 -pentadienyl complexes we prepared. The procedure was repeated under inert atmosphere, with filtration through Activity IV neutral alumina to remove paramagnetic impurities (Scheme 2.18). ¹H NMR

Scheme 2.18



spectroscopy indicated that the product was an η^3 -pentadienyl complex (e.g., **328**) rather than the expected η^5 -complex, with benzene and ether solubility suggesting a neutral species. We initially proposed that the final coordination site was occupied by fluoride abstracted from the BF₄⁻ counterion, however mass spectrometry indicated that chloride ion, most likely abstracted from the Al₂O₃, was present. This observation was verified by protonolysis of conjugated diene substrate **300f** using N,N-dimethylanilinium chloride in the presence of Cp*Co(CH₂CH₂)₂. The product of this reaction was spectroscopically identical to that obtained after chromatography. This result demonstrates that cobalt(III) η^5 -pentadienyl complexes do not easily tolerate geminal terminal substitution.

To investigate the structure of the η^3 -pentadienyl complex in solution prior to halide exposure, protonolysis and inert atmosphere crystallization via layering of diethyl ether and methylene chloride was performed. Contrary to the solubility of η^3 -pentadienyl complex **328**, this product was insoluble in ether and benzene, suggesting a cationic species. The ¹H NMR spectrum had similar multiplets and coupling constants to those observed for the neutral η^3 -pentadienyl complex **328**, with the signals consistently shifted downfield, also supporting the proposal of a solvento η^3 -pentadienyl cation. Unfortunately, our attempts to isolate and further purify this compound were unsuccessful, leading only to decomposition.

Part D: Summary

$\text{Cp}^*\text{Co}(\eta^5\text{-pentadienyl})^+$ complexes can thus be prepared by oxidative proto-dehydration using either non-conjugated 1,4-pentadienol or conjugated 1,3-pentadienol substrates. Various substitution arrays can be synthesized in reasonable to good yield, although the yields decrease with increasing substrate substitution. Several of these complexes have been characterized by X-ray crystallography; these data will be discussed in Chapter 5 in the context of cyclization reactivity. The conjugated 1,3-pentadienol route results in unresolvable stereochemical mixtures in two of the cases studied, limiting to some extent the viability of this methodology. Mechanistically, the intermediacy of a hydroxy allyl complex is proposed, in accordance with literature precedent. Spectroscopic observation of this intermediate and the uncharacteristically low yield of the η^5 -1,4-dimethylpentadienyl product **297i** lend support to this proposal. Through this work, we have addressed a void in the literature concerning the synthesis of first-row late metal pentadienyl complexes. Importantly, a series of substitution patterns not previously studied in late metal systems has been prepared. Substituent arrays successfully obtained include the majority of mono- and disubstituted patterns. The 1,1-disubstitution motif could not be obtained due to product instability; this species exists as an unsaturated η^3 -pentadienyl complex readily incorporating halide ion. The non-conjugated 1,4-dienol route is most attractive for further exploration, not exhibiting competing product formation, and using pentadienol substrates that are readily prepared.

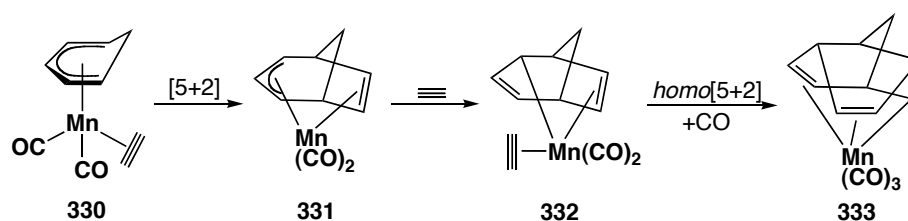
Chapter 3: Cobalt-Mediated η^5 -Pentadienyl/Alkyne [5+2]

Cycloaddition Reactions

Part A: Introduction

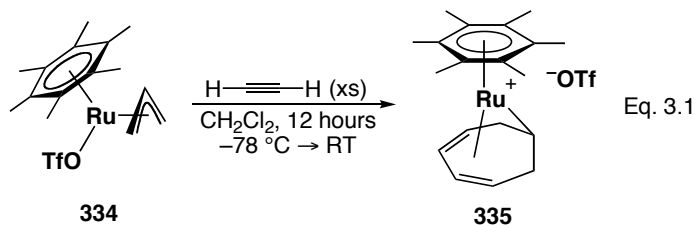
Mechanistic proposals put forth for previously reported η^5 -pentadienyl/alkyne [5+2], *homo*[5+2] cycloaddition reactions at manganese (Scheme 3.1), invoke the intermediacy of an η^2, η^3 -cycloheptadienyl complex **331**. Although no spectroscopic

Scheme 3.1



evidence was provided to support the transient formation of this compound, the unsaturated intermediate elegantly explains the formation of the multicyclic products and the difficulty associated with limiting alkyne incorporation to one equivalent. Preparations of isolable metal-bound η^2, η^3 -cycloheptadienyl products have been reported.¹⁵⁸ However, these products are invariably bridged bicyclic cycloheptadienyl complexes. Presumably, the conformational constraints imposed by the bridge inhibit β -hydride elimination, preventing isomerization to the thermodynamically favoured η^5 -cycloheptadienyl complex. Witherell has previously reviewed the literature in this area,¹⁴³ hence it will not be discussed here, other than to observe that in the one case where an unbridged η^2, η^3 -cycloheptadienyl product was reported,¹⁵⁹ the structural assignment was unsupported by adequate spectroscopic evidence and later shown to be

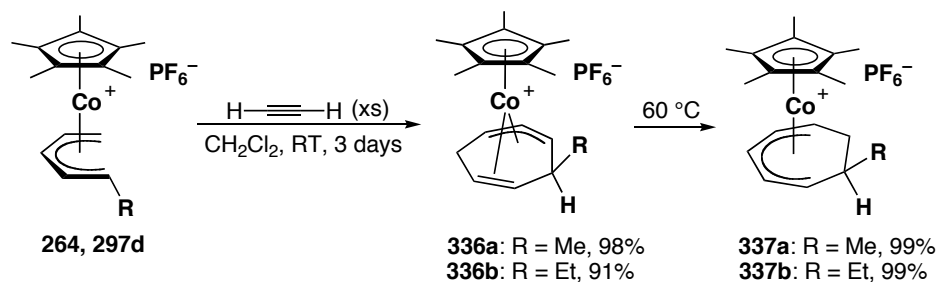
the expected η^5 -cycloheptadienyl product.¹⁶⁰ Prior to the work described here, the Stryker group reported the isolation of unprecedented $(C_6Me_6)Ru(\eta^1, \eta^4$ -cycloheptadienyl)⁺ complexes **335** (Eq. 3.1), providing the first examples of isolable monocyclic cycloheptadienyl products with hapticity diverging from the standard η^5 -coordination mode.¹⁶¹



Part B: Cobalt-Mediated [5+2] Cycloaddition Reactions

Witherell demonstrated the viability of the cobalt-mediated [5+2] cycloaddition reaction in his initial studies with $Cp^*Co(\eta^5$ -1-methylpentadienyl)⁺ complex **297d** (Scheme 3.2). The most surprising aspect of this work was the isolation of an unforeseen kinetic product formed in near quantitative yield: the η^2, η^3 -cycloheptadienyl complex

Scheme 3.2



336a arising from incorporation of one acetylene unit. In contrast to the previous reports of pentadienyl/alkyne [5+2] cycloaddition reactions, the η^2, η^3 -cycloheptadienyl product here is coordinatively saturated, leading directly to the stoichiometric control observed.

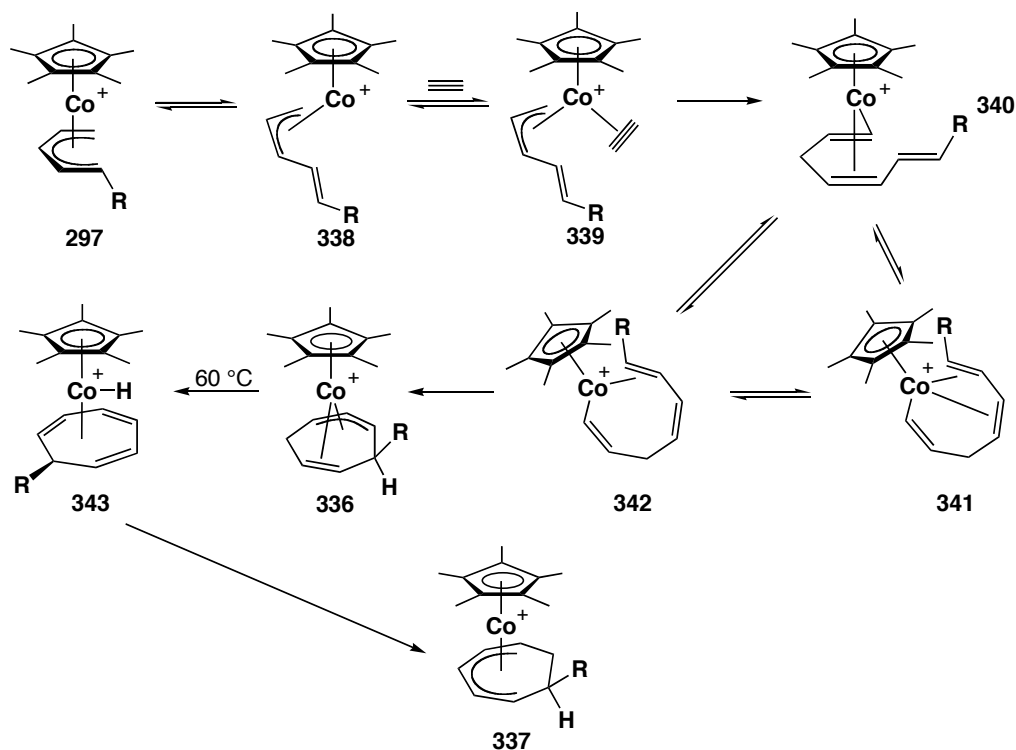
This species isomerizes to the thermodynamically preferred η^5 -cycloheptadienyl complex at elevated temperature, proving that the η^2, η^3 -cycloheptadienyl product is an intermediate on the overall [5+2] reaction pathway. The stability of this complex at room temperature also proves that the anomalous [3+2+2] cycloaddition reaction does not proceed through an η^5 -pentadienyl intermediate and that the [5+2] cycloaddition reaction operates in an independent reaction manifold.

Both the η^2, η^3 - and η^5 -cycloheptadienyl products demonstrate remarkable stability, with no decomposition in the air at room temperature in the solid state. Slow $\eta^2, \eta^3 \rightarrow \eta^5$ isomerization is observed in solution. Further investigation suggested that this reaction was only viable in 1-substituted ligand systems; substituents in other locations (*i.e.*, η^5 -pentadienyl complexes **297f-h**) exhibited severely retarded rates or a complete absence of cycloaddition reactivity.

The reaction is not limited to acetylene as the cycloaddition partner. Other alkynes such as 2-butyne, 1-pentyne and ethoxyacetylene also result in high yields, as determined by Witherell. In these cases, mild heating is needed to promote the cycloaddition reaction, preventing the isolation of the η^2, η^3 -cycloheptadienyl intermediate, which proceeds directly to the fully-conjugated product. Terminal alkynes such as 1-pentyne led to mixtures of regioisomers in a $\approx 2:1$ ratio, the slightly preferred product having the substituents in a 1,3-relationship.

A mechanistic proposal for this [5+2] cycloaddition reaction is shown in Scheme 3.3; the mechanism will be discussed in greater detail in Chapter 6. The coordinatively saturated η^5 -pentadienyl complex **297** initially isomerizes to η^3 -hapticity, freeing a site for alkyne coordination. Coordination and migratory insertion into the terminal position

Scheme 3.3



of the allyl moiety generates the unsaturated vinyl complex **340**, followed by recoordination of the terminal olefin. While this vinyl-diene intermediate may be in equilibrium with several isomers (**341** and **342**), the reactive intermediate must coordinate the terminal olefin. A second migratory insertion directly forms the experimentally observed η^2, η^3 -cycloheptadienyl complex **336**. Subsequent β -hydride elimination followed by hydride reinsertion generates the final η^5 -cycloheptadienyl product **337**.

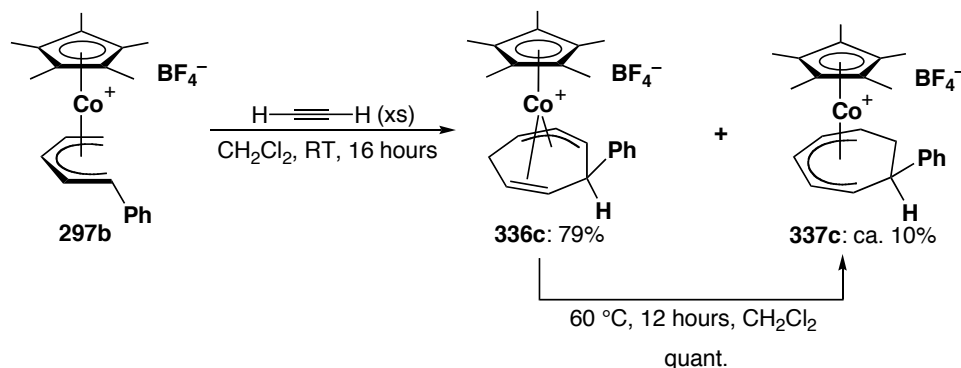
Witherell's reaction conditions involved saturating a CH_2Cl_2 solution of the η^5 -pentadienyl complex with acetylene. After approximately 19 hours at room temperature, the solvent was removed and the product purified by bench-top chromatography. While these conditions worked well, the η^5 -1-methylpentadienyl complex **297d** was accompanied by additional products arising from multiple alkyne insertion, presumably

by a [3+2+2] process. The conditions were further optimized by the author by controlling the quantity of acetylene added to the system, using canula transfer of a known volume of CH₂Cl₂ saturated with acetylene, sealing the system, and allowing the reaction to proceed for three days. Under these conditions, the competing products are not observed.

Part C: Results

To further investigate the effects of substituents on complex reactivity, 1-phenyl- η^5 -pentadienyl complex **297b** was treated at room temperature with acetylene under the optimized reaction conditions (Scheme 3.4). Surprisingly, the isolated product was an

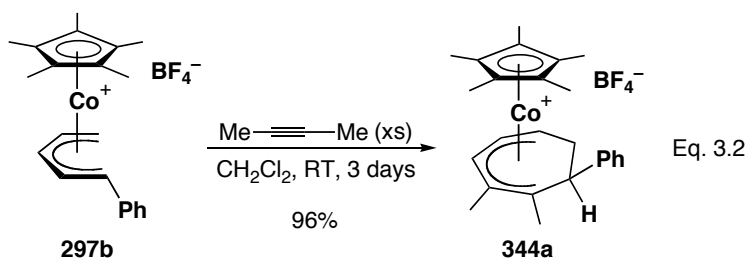
Scheme 3.4



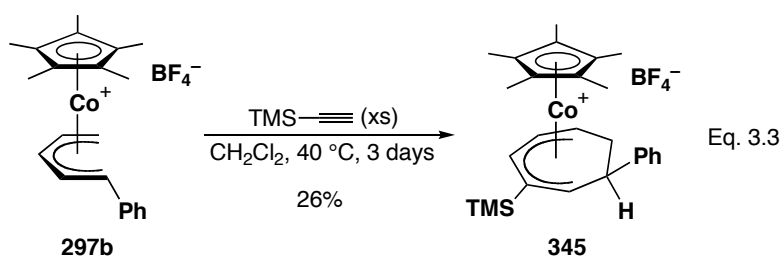
approximately 1:1 mixture of η^2, η^3 - and η^5 -cycloheptadienyl complexes **336c** and **337c**, even though the reaction was conducted at room temperature. With the higher rate of $\eta^2, \eta^3 \rightarrow \eta^5$ complex isomerization, the reaction conditions were altered to minimize reaction time, using alkyne saturation conditions to accelerate the rate such that complete conversion was obtained in 16 hours. The shorter reaction time minimized the extent of isomerization; however, approximately 10% of the η^5 -cycloheptadienyl product was still present, as determined by ¹H NMR spectroscopy, giving a combined 89% yield of thick

oily material. Due to thermal instability, crystallization of this labile intermediate was not attempted and only spectroscopic characterization was obtained. The fully conjugated η^5 -cycloheptadienyl product **337c** can be prepared in quantitative yield via controlled addition of acetylene and letting the reaction proceed for three days. Heating the resultant mixture at 60 °C for approximately 19 hours completes the isomerization. During this reaction, the colour of the solution evolves significantly, from the dark red η^5 -pentadienyl starting material to the orange-red final solution. This is likely due to the disruption of conjugation, going from the highly conjugated η^5 -1-phenylpentadienyl complex with its co-planar aromatic ring (as determined via X-ray crystallography, Chapter 5), to the η^2, η^3 -cycloheptadienyl complex. Conversion to the η^5 -isomer is again accompanied by a dramatic colour change, going from the orange-red η^2, η^3 -cycloheptadienyl complex to dark red as conjugation is reestablished.

Reaction of η^5 -1-phenylpentadienyl complex **297b** with 2-butyne also demonstrated different reactivity than the alkyl-substituted systems, which require heating to 40 °C to achieve reasonable reaction rates. η^5 -1-Phenylpentadienyl complex **297b** reacts with 2-butyne efficiently at room temperature (Eq. 3.2). Despite this lower reaction temperature, selective formation of the η^2, η^3 -cycloheptadienyl intermediate was again not possible, as the reaction proceeded directly to the fully conjugated **344a** in 96% yield.



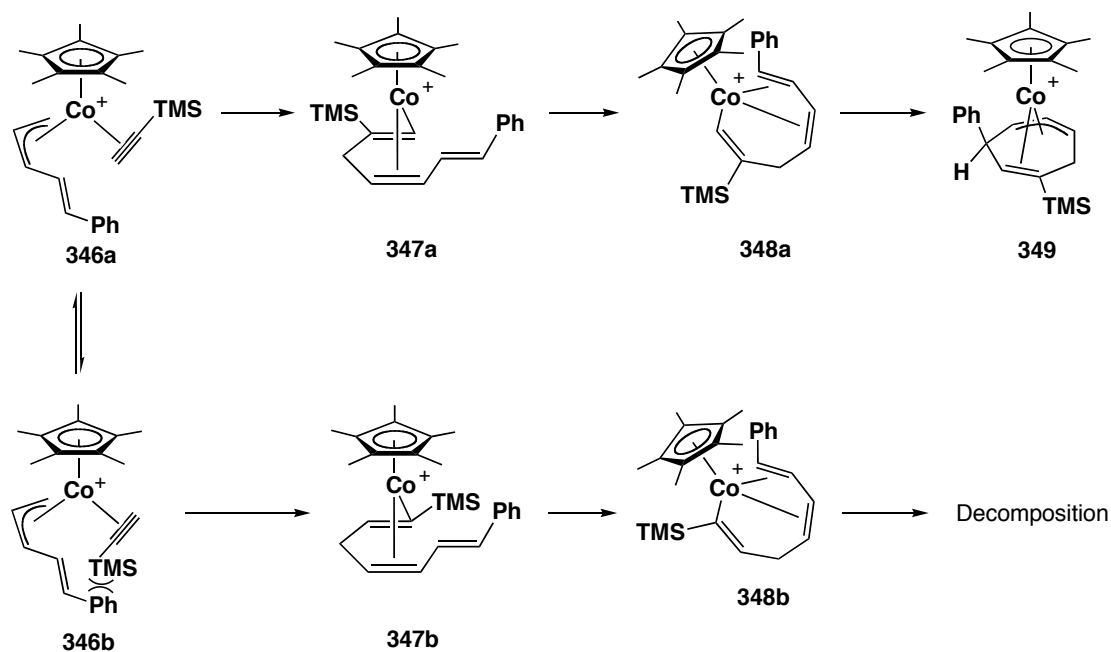
As previously described, a serious shortcoming of the [5+2] cycloaddition reaction is lack of regiocontrol with nonsymmetric alkynes. The larger size of the phenyl group in the η^5 -1-phenylpentadienyl complex suggested the possibility of exploiting steric effects to control the regiochemistry of alkyne insertion. This hypothesis was tested by the reaction with trimethylsilyl acetylene, under the assumption that the large TMS group should provide enhanced steric control. After reaction at 40 °C for 3 days (Eq. 3.3), the crude product isolated by chromatography contained significant impurities,



revealed by ^1H NMR spectroscopy. In this crude spectrum, however, signals corresponding to a single seven-membered ring product were observed, formed in 26% yield, as determined by integration against 1,3,5-trimethoxybenzene as an internal standard. Multiple recrystallizations were required to obtain an analytically pure sample. Spectroscopic and solid-state characterization clearly demonstrate that the product is a single regioisomer: η^5 -cycloheptadienyl complex **345**. While this regioselectivity is that expected from a sterically controlled alkyne insertion, the low yield suggests that the insertion remains incompletely controlled.

Steric interactions may conceivably influence the mode of alkyne complexation, but the distance between the phenyl and TMS groups in proposed alkyne intermediate **346** suggests that any effect would be small (Scheme 3.5). The initial migratory insertion may be biased towards **347b** due to stabilization by silicon in the α -position.¹⁶²

Scheme 3.5



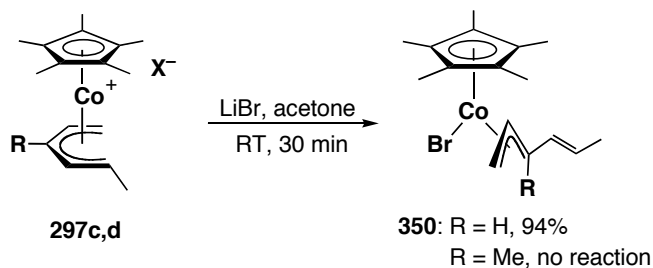
Following re-coordination of the olefin, migratory cyclization from intermediate **348b**, will be significantly impeded by steric interactions between the phenyl and TMS substituents, inhibiting C-C bond formation and increasing decomposition via σ -bond homolysis. Ring closure leading to η^2, η^3 -cycloheptadienyl complex **349** is less sterically hindered and, upon isomerization, yields the observed product. Cycloaddition reactions of 1-phenylpentadienyl **297b** using phenylacetylene or *tert*-butylacetylene returned similarly complex crude ^1H NMR spectra, again comprised of only one seven-membered ring product. Given the qualitatively poor yields of these reactions, further purification and characterization were not attempted.

Witherell's initial studies identified a connection between the η^5 -pentadienyl substitution pattern and [5+2] cycloaddition reactivity: 1-substituted complexes react readily while unsubstituted or 2-substituted complexes are unreactive. Pentadienyl complexes with multiple substituents, such as 1,2-dimethyl- or 1,2,4-trimethyl- η^5 -

pentadienyl complexes **297g** and **297h**, display significantly reduced and completely suppressed reactivity, respectively. To complete our investigation of the monsubstituted series, 3-methyl- η^5 -pentadienyl complex **297a** was treated with acetylene; no seven-membered ring products formed at any reaction temperature. These data clearly indicate that terminal substitution is critical for cycloaddition reactivity in the $\text{Cp}^*\text{Co}(\eta^5\text{-pentadienyl})^+$ complexes.

We propose that the 1-substituent assists the $\eta^5 \rightarrow \eta^3$ isomerization of the pentadienyl ligand. Witherell has demonstrated that the product of LiBr addition to η^5 -1-methylpentadienyl complex **297d** is the η^3 -pentadienyl bromide complex **350** formed via dissociation of the substituted end of the pentadienyl moiety (Scheme 3.6),¹⁴² which

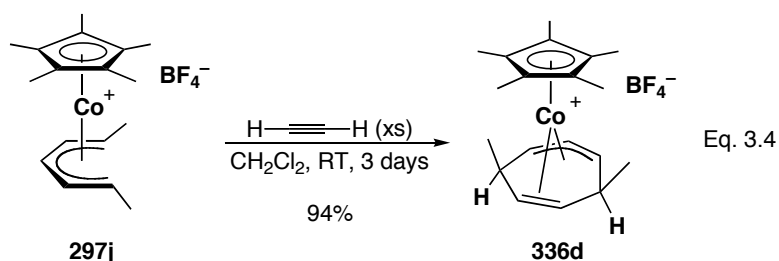
Scheme 3.6



indirectly supports this hypothesis. The η^5 -1,3-dimethyl- and η^5 -1,4-dimethylpentadienyl complexes **297c** and **297i** are thus interesting cases, bearing “activating” 1-substituents in combination with unfavourable internal substituents. Upon treatment with acetylene, η^5 -pentadienyl complexes **297c** and **297i** each returned only starting material, regardless of reaction temperature. When η^5 -1,3-dimethylpentadienyl complex **297c** was exposed to excess LiBr in THF solution, only starting material was recovered. These results clearly demonstrate that the requisite $\eta^5 \rightarrow \eta^3$ pentadienyl isomerization is suppressed by the internal substituents, preventing alkyne complexation.

Moreover, the presence of a terminal substituent is insufficient to overcome the inherently poor reactivity of 2- and 3-alkyl pentadienyl systems. The origin of this dependence will be discussed in Chapter 6.

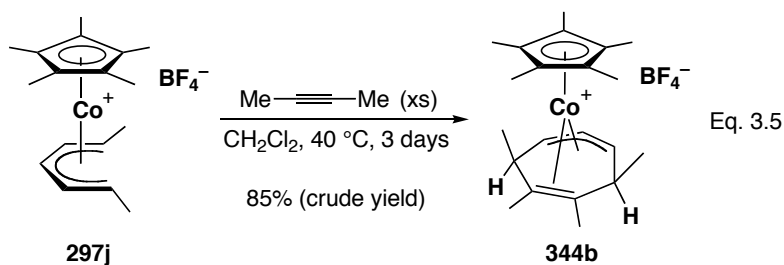
With only terminally monosubstituted compounds displaying useful reactivity, the effect of an additional terminal substituent is raised. The symmetric η^5 -1,5-dimethylpentadienyl complex **297j** readily reacts with acetylene yielding η^2, η^3 -cycloheptadienyl complex **336d** in excellent yield as a single diastereomer (Eq. 3.4).



A particularly interesting feature of the symmetric dimethyl η^2, η^3 -cycloheptadienyl complex **336d** is the proximal stereochemistry of both methyl groups. Without hydrogen atoms in the proximal position, β -hydride elimination is not possible. This complex is thus stable at 60 °C, with no $\eta^2, \eta^3 \rightarrow \eta^5$ isomerization observed, demonstrating that the isomerization process is not the result of adventitious external base. Isomerization by external acid/base reaction using diisopropylethylamine (Hünig's base) was unsuccessful. Nonetheless, a deprotonation/acidification sequence may be capable of inducing product isomerization, although this was not further investigated.

The thermal stability of **336d** also suggests that the proposed $\text{Cp}^*\text{Co}(\eta^2, \eta^3\text{-cycloheptadienyl})^+$ intermediate arising from 2-butyne cycloaddition, should be thermally stable and isolable (Eq. 3.5). As anticipated, the reaction with 2-butyne returns η^2, η^3 -cycloheptadienyl complex **344b** as the only product. Unfortunately, and not surprisingly,

although η^2, η^3 -cycloheptadienyl complex **344b** does not undergo thermal $\eta^2, \eta^3 \rightarrow \eta^5$ isomerization, slow decomposition to intractable material occurs at room temperature, preventing crystallization to analytical purity. This complex is the first example of an isolable η^2, η^3 -cycloadduct from an internal alkyne. Analogous non-conjugated adducts in the Cp series are generally obtained from η^5 -1-methylpentadienyl complexes and are surprisingly resistant to $\eta^2, \eta^3 \rightarrow \eta^5$ isomerization.¹³⁷ The potential origin of this variable reactivity will be discussed in Chapter 6.



As described in Chapter 2, the 1,1-dimethylpentadienyl complex **328** exists as an η^3 -pentadienyl complex. If the pendent olefin can coordinate in a transient fashion, [5+2] cycloaddition may still be possible, and if not, the complex could undergo a [3+2+2] cycloaddition. When the cycloaddition of the cationic analogue of η^3 -complex **328** and acetylene was attempted, however, only decomposition products were obtained. This reaction still holds considerable promise and further exploration is warranted, with direct cycloaddition of η^3 -1,1-dimethylpentadienyl chloride complex **328** in an ionizing medium being a logical first direction of study.

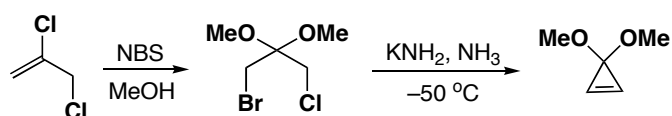
Part D: Alkyne Surrogates

The scope of the [5+2] cycloaddition reaction would be greatly extended if analogous chemistry is possible with π -systems other than alkynes. Previous workers

have shown that olefins are ineffective cycloaddition partners.¹⁴³ We explored the use of allene, proven in other [5+2] cycloaddition systems to function as an alkyne surrogate, but the reaction was unsuccessful. Witherell observed that the cycloaddition rate is significantly accelerated using electron-rich alkynes, with ethoxyacetylene demonstrating very rapid cycloaddition and the electron-poor DMAD being completely unreactive.¹⁴³ We thus considered that an electron-rich allene such as methoxyallene could be more successful. A sample of methoxyallene was prepared by isomerization of methyl propargyl ether using Schlosser's base¹⁶³ and an excess was added to the highly reactive η^5 -1-phenylpentadienyl complex **297b**. Unfortunately, cycloaddition was not observed even at elevated temperature.

Mascareñas has shown that cyclopropene acetals are effective π -systems in [5+2] cycloaddition chemistry.⁵⁸ We prepared a sample of cyclopropene dimethylacetal via bromination of 1,2-dichloropropene with NBS in MeOH, followed by potassium amide promoted cyclization/elimination (Scheme 3.8).¹⁶⁴ Isolation of the final product proved difficult, so the clean cyclopropene acetal was used as a solution in diethyl ether, with

Scheme 3.8



relative proportions determined by ¹H NMR spectroscopy. Reaction trials were conducted with approximately 10 equiv. of cyclopropene acetal relative to the η^5 -1-phenylpentadienyl complex **297b** at temperatures ranging from ambient to over 100 °C. Only starting material was isolated from these systems, except at high temperatures where pentadienyl complex decomposition occurred. The lack of reactivity was

surprising, but may be due to the electron deficient cyclopropene acetal, which may be incapable of competitive binding to the metal-centre. Cyclopropene itself, being more electron rich, may be effective. To probe this possibility, the cyclopropene complexation transition state energy was calculated computationally. While synthetic validation is still required, the 30.10 kcal/mol barrier (compared to the 26.14 kcal/mol barrier for alkyne complexation, see Chapter 6) suggests that this reaction is unlikely.

Part E: Summary and Conclusions

We have demonstrated that many Cp*Co(η^5 -pentadienyl)⁺ complexes undergo efficient [5+2] cycloaddition reactions. Moreover, the isolation of unprecedented η^2, η^3 -cycloheptadienyl intermediates demonstrates that this cycloaddition manifold is not related to the mechanism of the anomalous [3+2+2] cycloaddition reaction. The lack of substantial reactivity in all complexes other than the 1-substituted and 1,5-disubstituted cases presents a significant limitation in scope for this methodology. Despite this shortcoming, the isolation of the novel η^2, η^3 -cycloheptadienyl complexes suggests new possibilities for construction of functionalized seven-membered ring systems. η^5 -1-Phenylpentadienyl complex **297b** demonstrates that the [5+2] cycloaddition reaction is not limited to alkyl substituents, and the addition of phenyl substituents alters the reactivity of the system, lowering the activation barrier to 2-butyne reaction. Whether this is a steric or electronic effect poses interesting possibilities for the investigation of substituent effects on cycloaddition reactivity. The thermal stability of η^2, η^3 -cycloheptadienyl complexes arising from 1,5-disubstituted pentadienyl starting materials allows access to the kinetic η^2, η^3 -cycloheptadienyl adduct of 2-butyne cycloaddition,

previously only observed spectroscopically. This thermal stability also verifies our proposal that β -hydride elimination/reinsertion is involved in the $\eta^2, \eta^3 \rightarrow \eta^5$ isomerization mechanism, eliminating the possibility of adventitious base mediation.

The cycloaddition reaction is currently limited to alkynes, with alkyne surrogates such as olefins, allenes and cyclopropene acetals being ineffective. Electronic effects in the alkyne complexation step may be the cause of this reduced reactivity. If electron-rich cyclopropenes can be successfully used, the potential for development of a formal [5+3] cycloaddition pathway is high. The product formed upon successful cycloaddition will be unsaturated, unlike the η^2, η^3 -cycloheptadienyl complexes described above. This unsaturated species may activate the three-membered ring, releasing strain via ring-expansion and, as such, would present a novel cycloaddition pathway for the preparation of eight-membered ring compounds.

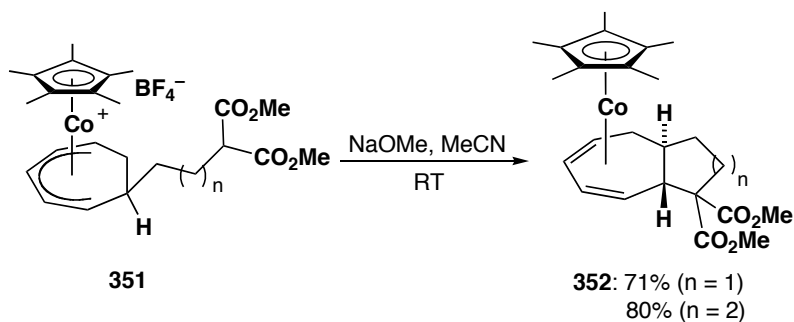
Chapter 4: Synthesis of [5.3.0]- and [5.4.0]-Bicyclic Systems

via [5+2] Cycloaddition Chemistry

Part A: Introduction

The hydrocarbon ligand hapticity in organometallic complexes in large part determines the extent to which such complexes can be further functionalized. Before this work, the only known coordination modes for unbridged cycloheptadienyl species were η^5 - and η^1, η^4 -hapticities; the reactivity potential of the new η^2, η^3 -cycloheptadienyl species is unknown. The η^5 -cycloheptadienyl products obtained via [3+2+2] cycloaddition had previously been extended to bicyclization chemistry (Scheme 4.1) by

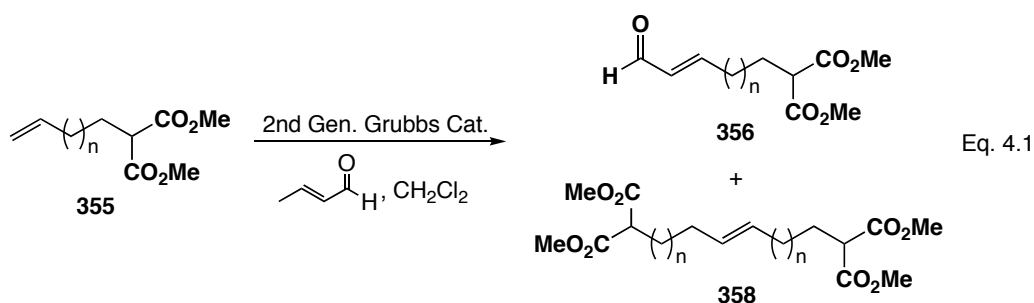
Scheme 4.1



harnessing the potential of the cationic π -complex to undergo nucleophilic addition reactions. In this way, five- and six-membered fused ring systems **352** were constructed via the intramolecular addition of tethered nucleophiles.¹⁴³ The η^2, η^3 -cycloheptadienyl systems are expected to give rise to the complementary non-conjugated cycloheptadiene products by selective alkylation of the allyl moiety.

The α,ω -bromoolefins undergo alkylation using *in situ*-generated potassium dimethylmalonate in good yields.¹⁶⁷ Interestingly, formation of dialkylated products is minimal, despite the one-pot conditions. It is likely that K_2CO_3 is insufficiently basic for deprotonation of the monoalkylated species; the addition of the alkyl group raises the pK_a by approximately 1.5 units or more. For comparison, the pK_a of dimethyl malonate is 15.9 while the related monoalkylated ethyldimethyl malonate is 18.5 (values measured in DMSO).¹⁶⁸

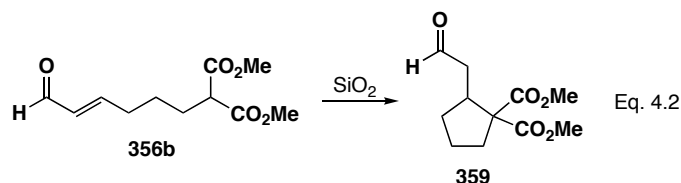
Cross metathesis of malonyl olefins **355** with crotonaldehyde led to formation of α,β -unsaturated aldehydes **356**.¹⁶⁹ In early trials, mixtures of aldehyde **356** and dimerized starting material **358** were obtained (Eq. 4.1). Contrary to expectations, use of



the less sterically hindered acrolein as the metathesis partner was detrimental to the overall reaction. The 1H NMR spectrum showed a large fraction of undimerized starting material remained, indicating that the catalyst had been poisoned. Whether this poisoning was due to the acrolein itself or an impurity was not investigated beyond confirming homogeneity via 1H NMR spectroscopy. The reaction is successfully driven to completion with three equiv. of crotonaldehyde, providing the desired enal free of dimerized olefins.

Preparation and isolation of aldehyde **356a** was straightforward and proceeded in good yield. In contrast, while 1H NMR spectroscopy of the crude cross-metathesis

product indicated complete conversion to aldehyde **356b**, chromatography resulted in product decomposition. The decomposition product is tentatively assigned as the cyclic aldehyde **359**, arising from an acid-catalyzed intramolecular Michael addition (Eq. 4.2). Attempts to prevent this cyclization reaction by neutralizing the stationary phase with



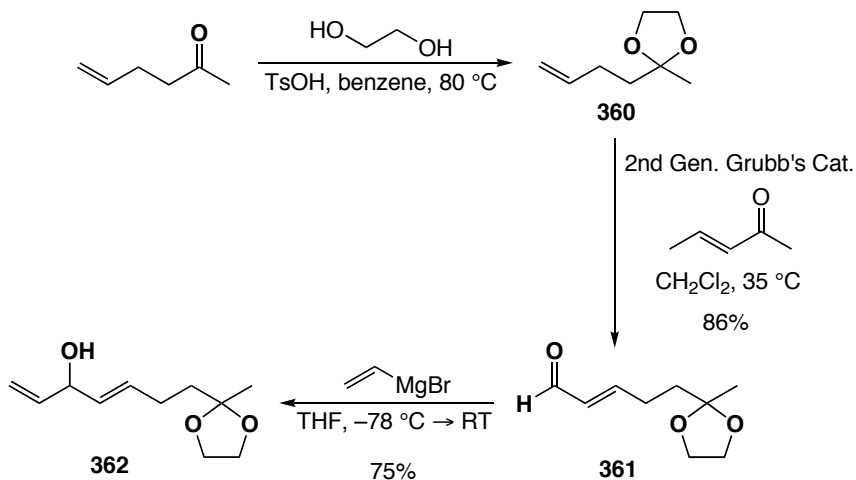
triethylamine were unsuccessful. Further investigation revealed that aldehyde **356b** is also unstable in solution, decomposing under the metathesis reaction conditions, yielding the same cyclic product **359** over prolonged reaction time. Optimization studies determined that a 10% catalyst loading reduces the reaction time to 90 minutes, permitting complete conversion prior to decomposition. The crude material was then used without purification, other than removing excess crotonaldehyde under Schlenk vacuum. These aldehydes exhibit thermal instability, decomposing slowly over time even when stored at $-30\text{ }^{\circ}\text{C}$ in the dark, and were carried forward immediately.

Vinyl Grignard reacts with these aldehydes readily, providing 1,4-dienol products **357a** and **357b**. The order of addition affects the product yield, with addition of the aldehyde to the Grignard reagent providing the best results, likely from minimizing competing 1,4-addition pathways. To prevent acid-catalyzed product decomposition, triethylamine-neutralized silica gel was employed for the chromatographic purification. In the absence of this additive, slight decomposition on the column was observed.

To vary the pro-nucleophilic tether, dienol acetal **362** was prepared from 1-hexen-5-one by initial acid catalyzed acetal formation under standard Dean-Stark conditions (Scheme 4.3).¹⁷⁰ Subsequent cross metathesis and vinyl Grignard addition completes the

synthetic sequence. This reaction series was straightforward, lacking the complications discussed for the previous cases.

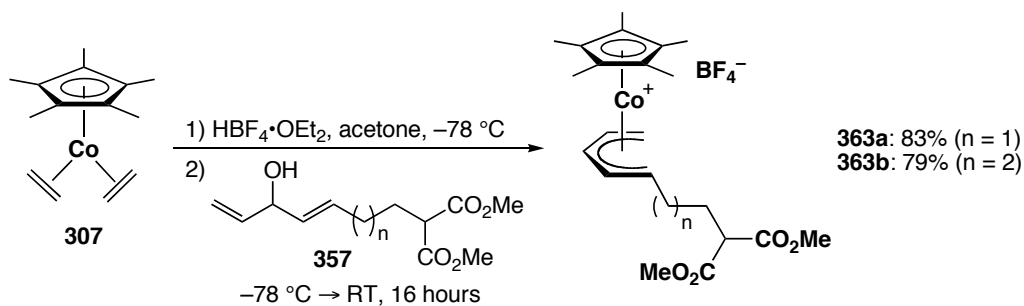
Scheme 4.3



Part C: Cp*Co(η^5 -Pentadienyl)⁺ Complex Preparation

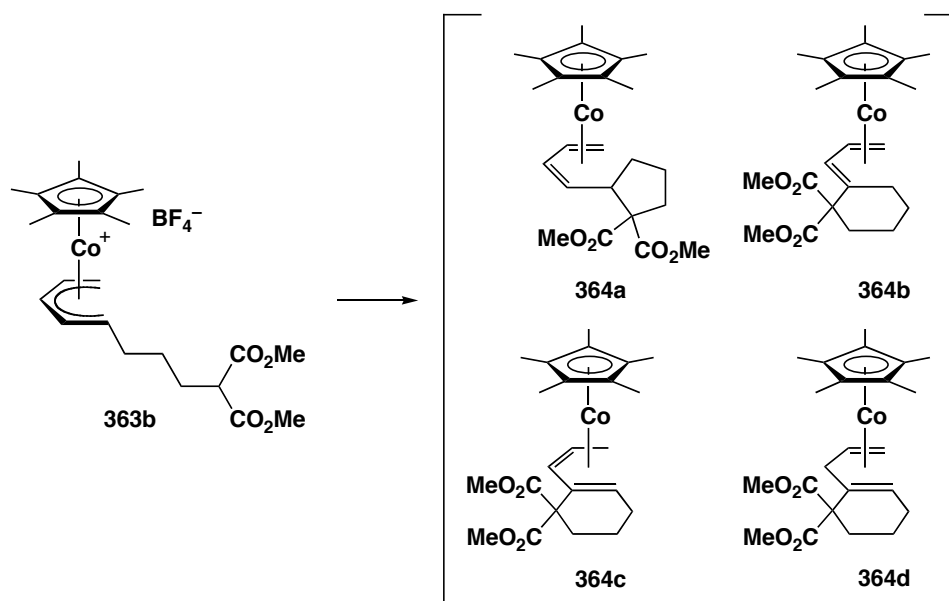
The order of substrate and acid addition to Cp*Co(CH₂CH₂)₂ was critical to optimize the preparation of pentadienyl complexes bearing tethered pro-nucleophiles. Under the pre-protonation conditions previously described, the preparation and chromatographic isolation of the two-carbon tethered η^5 -pentadienyl complex **363a** was straightforward and proceeded in good yield (Scheme 4.4). The preparation of the three-

Scheme 4.4



carbon tethered η^5 -pentadienyl complex **363b** was equally straightforward, but a pure sample could not be obtained; the ^1H NMR spectrum was significantly broadened by paramagnetic impurities even after repeated chromatographic cycles. Slow decomposition was observed, both in solution and in the solid-state, and is likely related to this purification difficulty. It is reasonable to assume that the same type of intramolecular cyclization observed for aldehyde **356b** is possible for pentadienyl complex **363b**. Such a cyclization could in principle lead to a variety of different Co(I) diene products (Scheme 4.5). An attempt to prepare the proposed cyclization

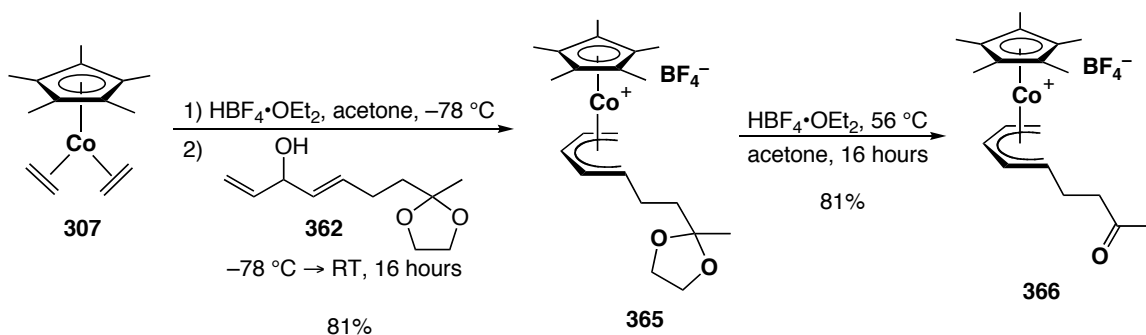
Scheme 4.5



complex(es) intentionally by deprotonation using Hünig's base under inert atmosphere resulted in a complex mixture and was not further explored. The proposed Co(I) products are susceptible to air oxidation, and 1,4-diene complexes (**364d**) lacking electron-withdrawing groups are thermally unstable;¹⁷¹ both factors could contribute to the slow decomposition observed. Given the purification difficulties, η^5 -pentadienyl complex **363b** was taken forward without characterization.

Competitive acetal deprotection during preparation of η^5 -pentadienyl complex **365** from 1,4-dienol **362** was a concern, yet preparation and isolation was accomplished readily (Scheme 4.6). Partial deprotection was observed during crystallization,

Scheme 4.6



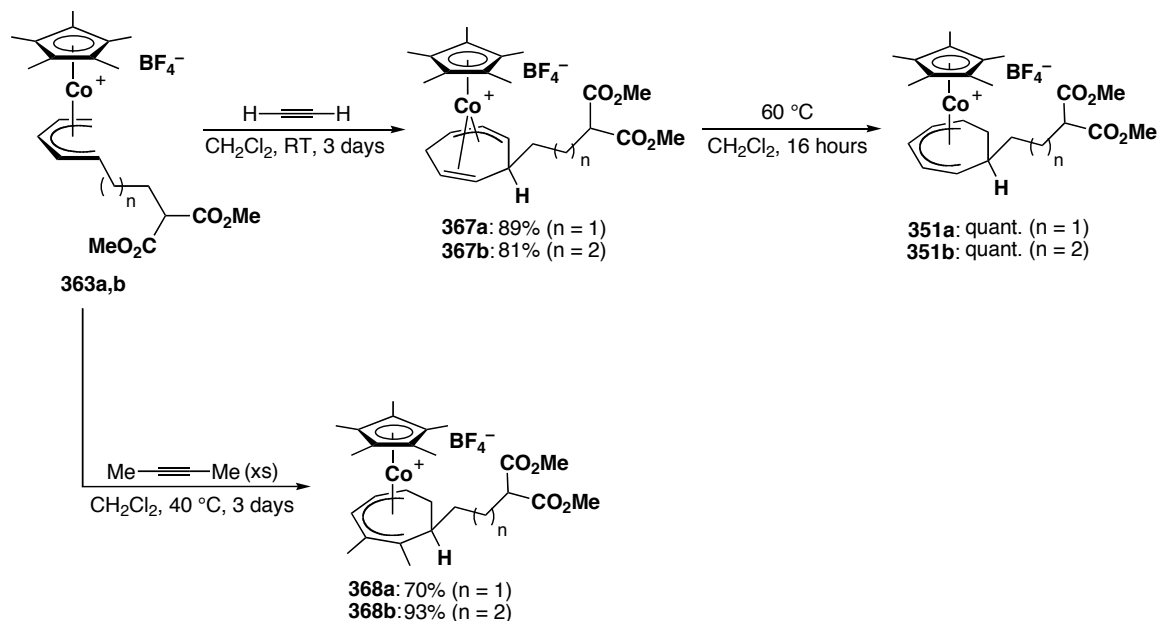
presumably catalyzed by acidic impurities introduced in the deuterated chloroform. Subsequent crystallizations, where potential for contamination was avoided, proceeded without difficulty.

Deprotection of η^5 -pentadienyl complex **365** was easily achieved by treatment with catalytic $\text{HBF}_4 \cdot \text{OEt}_2$ in wet acetone at reflux. Initial deprotection trials were conducted with 1 μL of acid, regardless of sample size; the clean reaction proceeded slowly, requiring 3-4 days for complete conversion. Adding water was detrimental, causing increased decomposition. Increasing the quantity of acid to 10 μL regardless of sample size significantly accelerated the reaction rate, with complete conversion obtained overnight.

Part D: η^5 -Pentadienyl/Alkyne [5+2] Cycloaddition Reactions

Both η^5 -pentadienyl complexes **363a** and **363b** react with acetylene to produce excellent yields of [5+2] cycloaddition products (Scheme 4.7). In the case of the three

Scheme 4.7

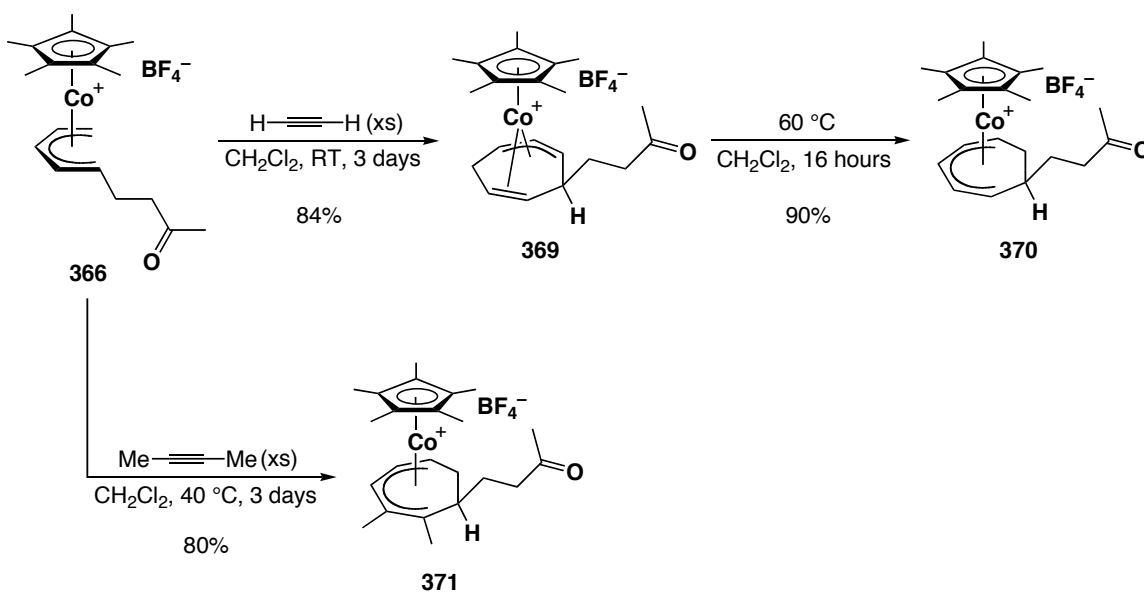


carbon-tethered η^5 -pentadienyl complex **363b**, the η^2, η^3 -cycloheptadienyl product **367b** was obtained in analytical purity, indicating that the decomposition observed for the η^5 -pentadienyl starting material (Eq. 4.2) is not a factor for the [5+2] cycloaddition product. Both η^2, η^3 -cycloheptadienyl complexes **367a** and **367b** exhibit high thermal stability, with no decomposition or $\eta^2, \eta^3 \rightarrow \eta^5$ isomerization observed at room temperature. Thermal isomerization to the fully conjugated η^5 -isomers **351a** and **351b** is readily achieved at 60°C in quantitative yield. The products from the isomerization are identical to those arising from [3+2+2] cycloaddition reactions of $\text{Co}(\eta^3\text{-allyl})$ complexes bearing tethered pro-nucleophiles and were not further explored. Cycloaddition reactions with 2-butyne are also efficient, providing η^5 -cycloheptadienyl complexes **368a** and **368b**, from sequential cycloaddition and isomerization under the reaction conditions.

Upon treatment of η^5 -pentadienyl ketone complex **366** with acetylene, η^2, η^3 -cycloheptadienyl complex **369** is obtained in good yield (Scheme 4.8). Crystallization

provided X-ray quality crystals (Figure 5.5). Isomerization to the η^5 -cycloheptadienyl complex **369** proceeded cleanly and in excellent yield. The corresponding [5+2] cycloaddition with 2-butyne, however, does not consistently provide cycloheptadienyl product of spectroscopic homogeneity. The additional byproduct, formed in approximately 10% yield, is tentatively assigned as a cobaltocenium complex on the basis of ^1H NMR spectroscopy. Qualitative observations gathered over the series of synthetic trials indicate that a higher concentration of 2-butyne suppresses this side reaction, returning spectroscopically pure material.

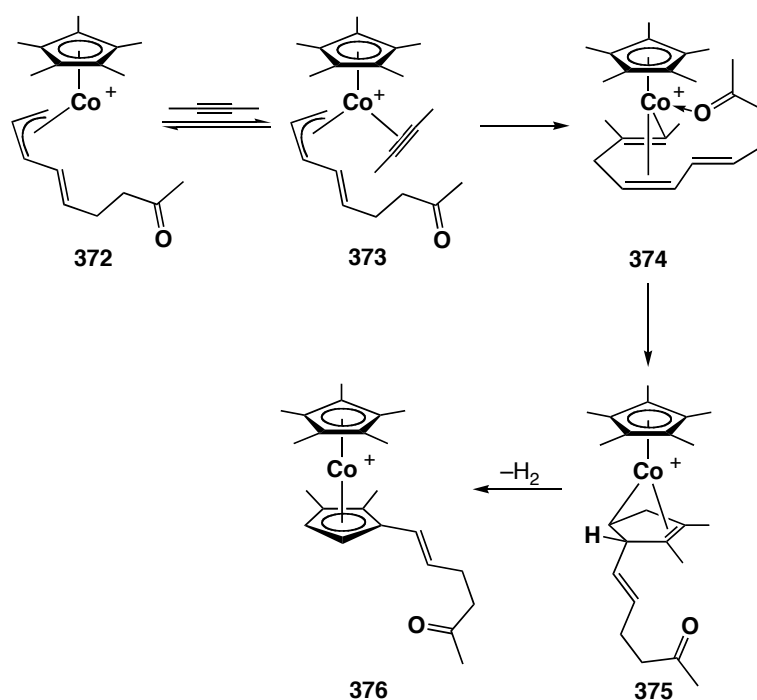
Scheme 4.8



Witherell¹⁴³ also observed the formation of cobaltocenium derivatives during the reaction of 2-butyne with Cp*Co(η⁵-1-methylpentadienyl)⁺ **247d** at 60 °C. This byproduct was avoided by lowering the reaction temperature to 40 °C. Witherell proposed that this product is the result of a competitive [3+2] cycloaddition, arising from steric hindrance between methyl groups, which inhibits pendant olefin reassociation following alkyne insertion. The η⁵-pentadienyl ketone complex **366** is prone to this

competitive side reaction, which occurs at lower temperature than observed from the η^5 -1-methylpentadienyl complex. A reasonable mechanistic rationale invokes equilibrium coordination of the pendant ketone moiety in an intra- or intermolecular fashion, interfering with alkyne coordination and/or reassociation of the pendant olefin (Scheme 4.9). From the [3+2] cycloadduct **375**, subsequent β -hydride elimination and extrusion of dihydrogen generates cobaltocenium complex **376**.

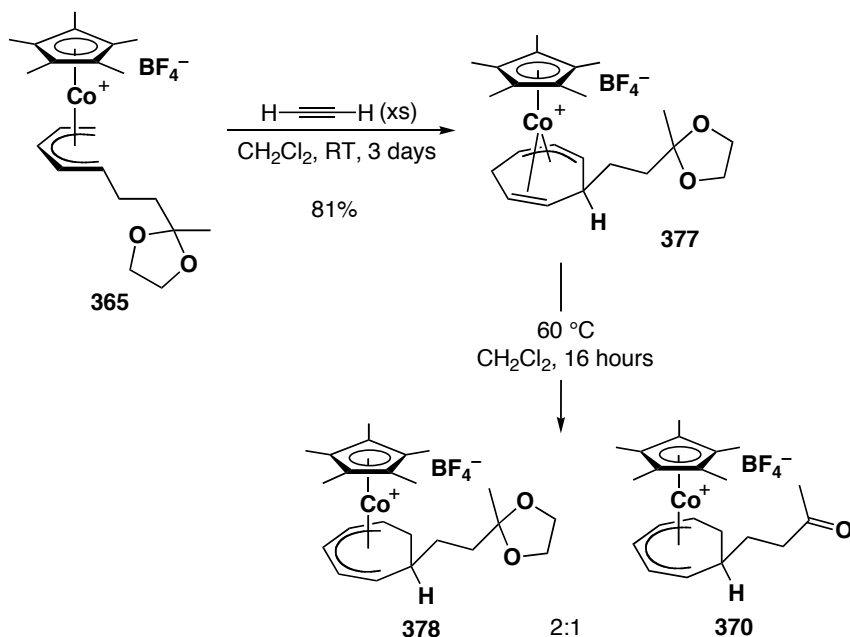
Scheme 4.9



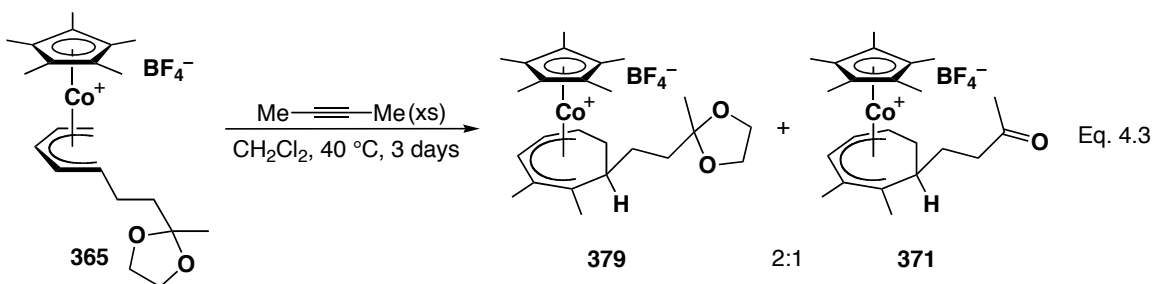
The η^5 -pentadienyl acetal complex **365** also efficiently yields η^2, η^3 -cycloheptadienyl complex **377** upon reaction with acetylene (Scheme 4.10). Thermal isomerization of η^2, η^3 -cycloheptadienyl complex **377** to the fully conjugated isomer **378**, however, also results in partial acetal hydrolysis. This same competitive process is observed during 2-butyne [5+2] cycloaddition reactions (Eq. 4.3), demonstrating the kinetic instability of the protecting group. Cyclic acetals are generally stable under

neutral conditions, but it is possible that the cationic cobalt(III) complex can function as a Lewis or Brønsted acid at elevated temperature, catalyzing the hydrolysis by adventitious water.

Scheme 4.10

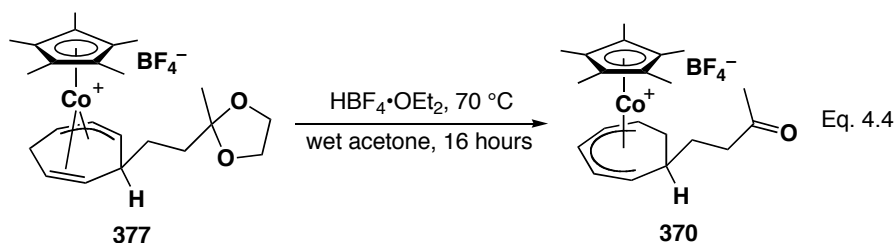


The η^5 -cycloheptadienyl product mixtures were characterized spectroscopically but are of little consequence; simple acid-catalyzed acetal hydrolysis yields the deprotected complexes **370** and **371** as the sole products. Acetal cleavage and $\eta^2, \eta^3 \rightarrow \eta^5$



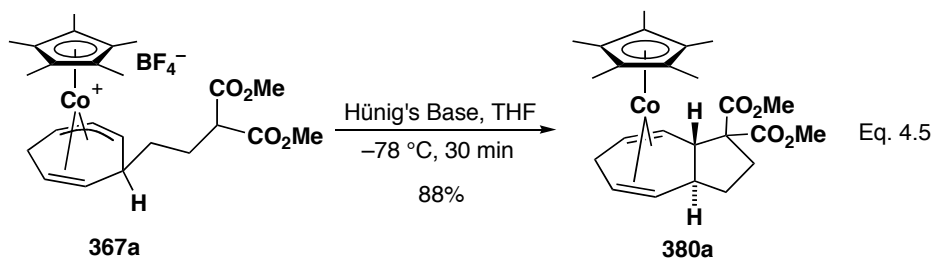
isomerization can also be achieved in one pot, rendering the transformation of η^5 -pentadienyl acetal complex **365** to η^5 -cycloheptadienyl complex **370** a one-step procedure (Eq. 4.4). The high-level of efficiency for the individual steps makes this a

potentially powerful synthetic procedure for the construction of functionalized seven-membered rings.



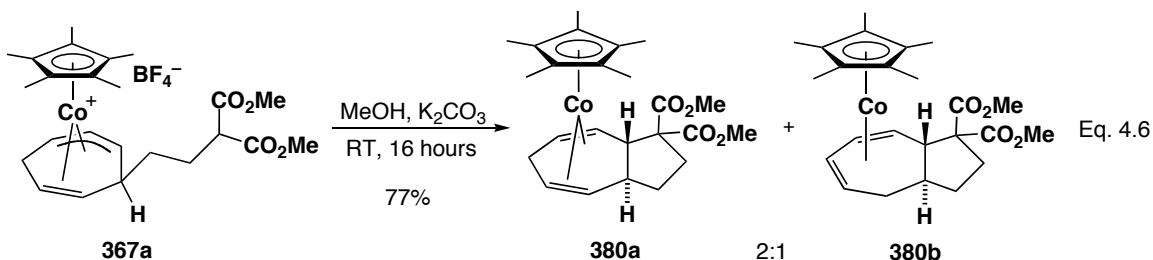
Part E: Intramolecular Cyclization Reactions

With the pro-nucleophile bearing η^2, η^3 - and η^5 -cycloheptadienyl complexes in hand, we turned our attention to intramolecular cyclization reactions, anticipating similar reactivity as that found for the [3+2+2] cycloaddition analogues **351** (Scheme 4.1). Initially, η^2, η^3 -cycloheptadienyl complex **367a** was deprotonated using excess NaOMe in acetonitrile at room temperature. The ^1H NMR spectrum of the crude bicyclic reaction product **380a** displayed significant byproduct formation, unlike the previously explored η^5 -cycloheptadienyl species. To optimize the conditions, THF was used as an alternate solvent and amine bases were evaluated, with Hünig's base giving the best results (Eq. 4.5). Improved purity was attained by cooling to $-78\text{ }^\circ\text{C}$. Unfortunately, when this chemistry was later revisited, this result was irreproducible, giving no reaction or severe



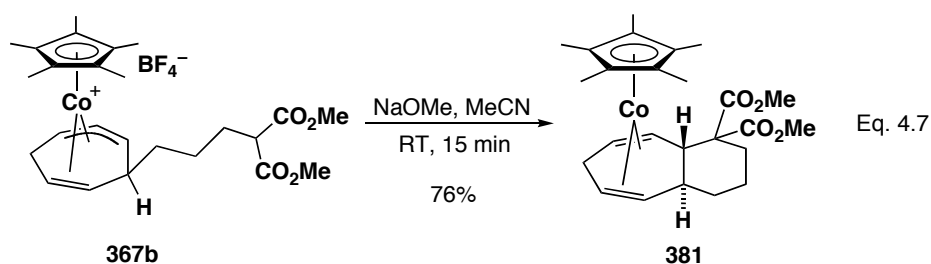
decomposition under nominally identical conditions. Freshly distilled solvent and rigorously purified Hünig's base were prepared, but to no avail. We conclude this initial

positive reactivity was the result of impurities in the starting material, solvent, or base. We have not explored this system further, but have since optimized the reaction under different conditions. Dissolution of η^2, η^3 -cycloheptadienyl complex **367a** in MeOH with one equiv. of K_2CO_3 yields a 2:1 mixture of the tentatively characterized bicyclic product **380a** and the fully-conjugated isomer **380b** (Eq. 4.6). Complex **380b** is identical to that



obtained via cyclization of the η^5 -cycloheptadienyl complex **351a**, in turn obtained from the [3+2+2] cycloaddition. In wet MeOH, the cyclization yields only the conjugated product **380b**, homogeneous by NMR.

Surprisingly, NaOMe in MeCN effectively cyclizes the three-carbon tethered η^2, η^3 -cycloheptadienyl complex **367b** (Eq. 4.7). Subsequent crystallization from pentane



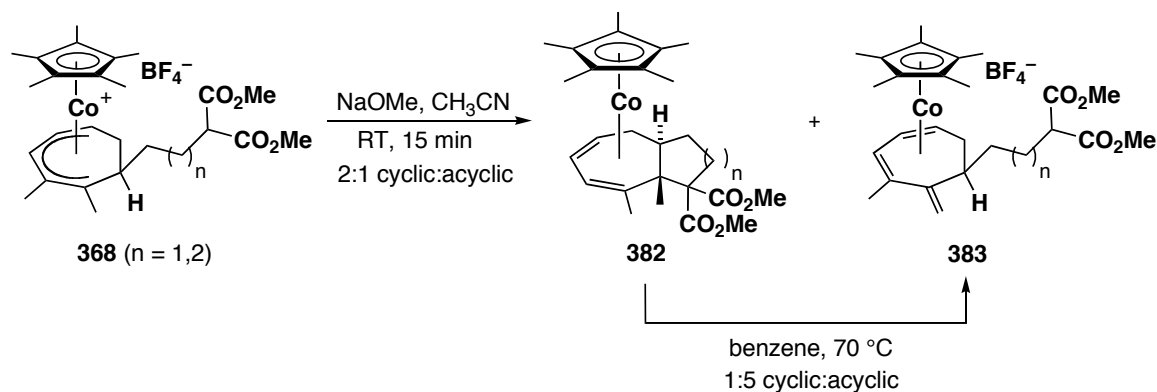
at $-35\text{ }^\circ\text{C}$ provides spectroscopically pure product. η^2, η^3 -Cycloheptadienyl complex **367b** is only sparingly soluble in THF, necessitating the use of MeCN. Not surprisingly, Hünig's base was ineffective in this chemistry.

The thermal stabilities of bicyclic complexes **380a** and **381** vary significantly. The [5.4.0]-bicyclic system **381** is stable for indefinite periods of time in the solid state at

–35 °C under a nitrogen atmosphere. Conversely, the [5.3.0]-bicyclic **380a** decomposes slowly to unidentified products at both room temperature and –35 °C. ¹H NMR data suggest that this decomposition arises from re-opening of the five-membered ring.

The 2-butyne η^5 -cycloadducts **368a** and **368b** are of particular interest in this bicyclization chemistry, presenting the possibility of introducing a quaternary carbon at the ring junction. When these cycloadducts were subjected to the cyclization conditions, the ¹H NMR spectrum revealed what are tentatively identified as the desired bicyclic products **382**, each accompanied by a second minor component believed to be the monocyclic triene complex **383** (Scheme 4.11). Equilibration to the thermodynamically

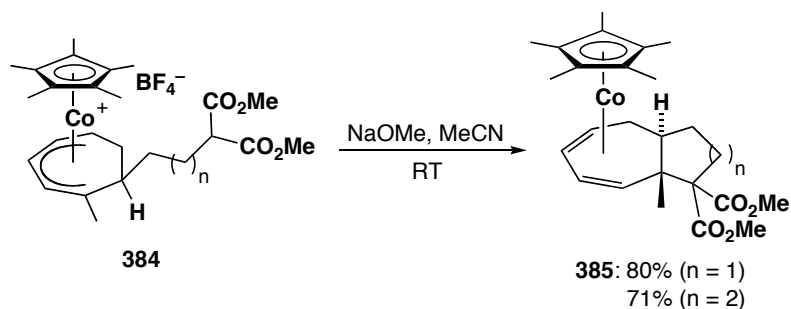
Scheme 4.11



preferred triene complex is achieved by heating the mixture to 70 °C for 16 hours, demonstrating that the bicyclization reaction is reversible under the reaction conditions. This observation is surprising in light of the clean cyclizations obtained from η^5 -cycloadducts **384**, where the bicyclic reaction products **385** are thermally stable (Scheme 4.12).¹⁴³ The only difference between these two sets of substrates is the additional methyl substituent, which ends up adjacent to the quaternary centre in the complexes made by [5+2] cycloaddition. Why this methyl group kinetically encourages the ring-opening is not clear. Due to the 1,2-eclipsing interactions between the methyl groups of

complexes **368**, the 1-methyl group will be torqued into an alignment closer to the plane of the η^5 -cycloheptadienyl moiety (a similar effect is observed for 1,2-disubstituted pentadienyl complexes (Chapter 5)), possibly favouring deprotonation over cyclization. Additionally, it is possible that the bicyclic products **385** are in equilibrium with the open, monocyclic complex; however, lacking the bias of the second methyl group, the 1-methyl group is not as well aligned with the π -system and competitive deprotonation pathways are not energetically accessible. An alternative rationale is that the additional methyl group in complexes **382** increases the rate of ring-opening through increased steric repulsion with the malonate moiety, allowing deprotonation to the thermodynamically preferred triene complex to become competitive.

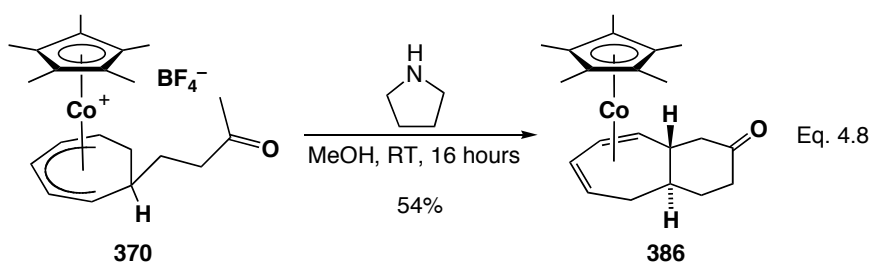
Scheme 4.12



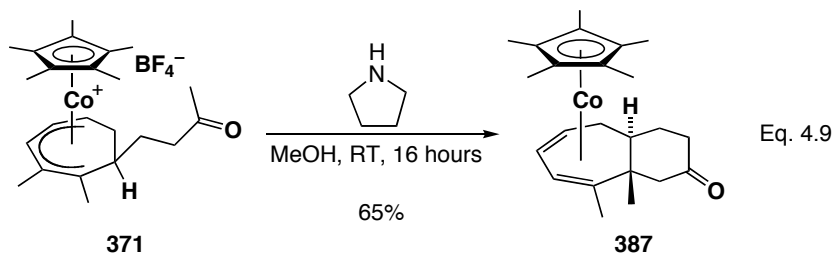
We anticipated the ketone enolate generated from η^2, η^3 - and η^5 -cycloheptadienyl complexes **369** and **371** would address this ring-opening issue by stabilizing the bicyclic adduct toward reversible nucleophilic addition. Deprotonation mediated by the strong kinetic base LDA provided no tractable product from the reaction at -78 °C in THF. This result is not surprising: competitive pathways, such as allylic deprotonation and single electron transfer reduction, are not unexpected. An attractive alternative procedure involves the generation of an enamine intermediate, methodology that has been exploited

extensively in organic aldol condensations.¹⁷² Pyrrolidine has been shown to be very effective in enamine catalysis and was selected for our investigation.¹⁷³

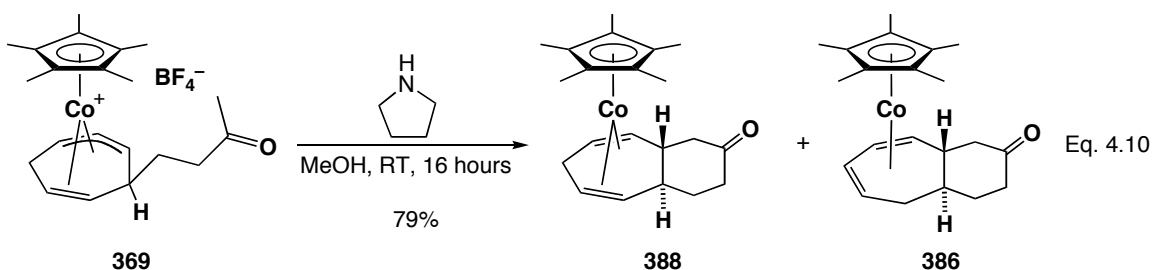
Upon treatment with stoichiometric pyrrolidine, η^5 -cycloheptadienyl complex **370** was readily converted to the bicyclic diene complex **386**, which was obtained in spectroscopic purity but moderate yield (Eq. 4.8). Further attempts to improve the yield through lower reaction temperature or the use of catalytic pyrrolidine were unsuccessful. Hydrolysis of the iminium salt occurs *in situ*, induced by the equivalent of water produced during enamine formation.



The fact that this reaction was very clean, with no evidence of equilibrium ring-opening, was encouraging. Under the same reaction conditions, dimethyl η^5 -cycloheptadienyl complex **371** also provides the desired bicyclic diene complex **387**, in which the bridgehead quaternary stereocentre is obtained as a single diastereomer (Eq. 4.9). As anticipated, the higher basicity of the enolate nucleophile inhibits the ring-opening, allowing bicyclization chemistry in the presence of the methyl group that proved to be detrimental in the malonate system.

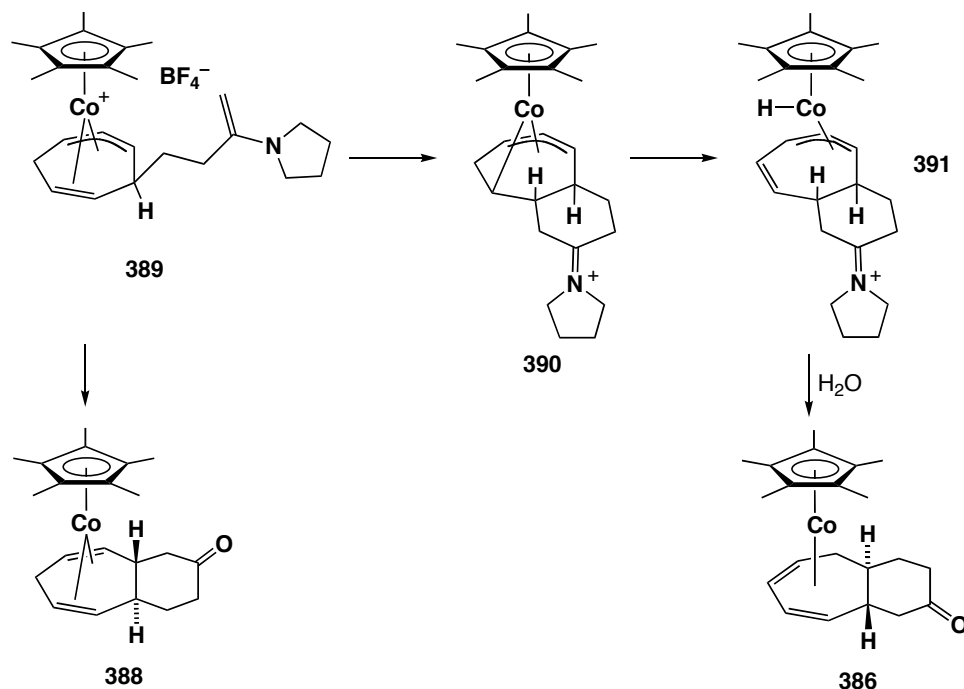


The promising results obtained with the η^5 -cycloheptadienyl complexes were unfortunately not replicated in cyclizations of the η^2, η^3 -cycloheptadienyl system **369** (Eq. 4.10). Under identical cyclization conditions, a 4:1 mixture of the desired 1,4-cycloheptadiene complex **388** and the conjugated 1,3-cycloheptadiene complex **386** was produced, as revealed by ^1H NMR spectroscopy. Reducing the reaction temperature to $-78\text{ }^\circ\text{C}$ did not limit the isomerized byproduct formation.



A mechanistic proposal for this reaction is shown in Scheme 4.13. Initial enamine formation occurs in the standard fashion. While one could argue that direct deprotonation occurs, rather than enamine formation, the pK_a value of 11.1 for pyrrolidinium¹⁷⁴ versus that of 26.5 for acetone¹⁷⁵ (both as measured in DMSO) suggests it is an unlikely possibility. Kinetic ring closure can occur at the allyl, leading directly to the non-conjugated product **388**, or at the olefin, in accordance with the Davies-Green-Mingos rules,¹⁷⁶ forming η^1, η^3 -complex **390**. Complex **390** may undergo β -hydride elimination, with the resultant cobalt allylhydride complex **391** reinserting at the terminal position of the η^3 -allyl moiety, leading to the conjugated complex **386**. Interestingly, we found that water was essential for cyclization reactivity; when dry MeOH was used, no cyclization products were obtained. Water must aid enamine formation, likely by acting as a very mild acid source.

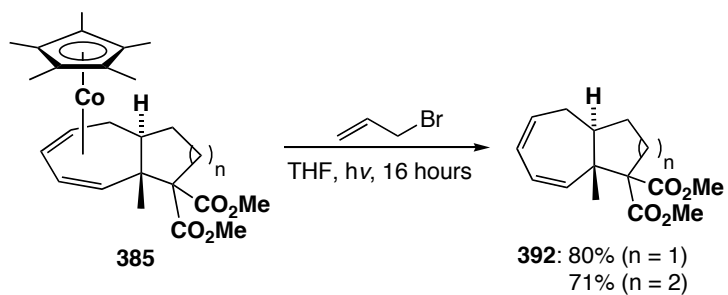
Scheme 4.13



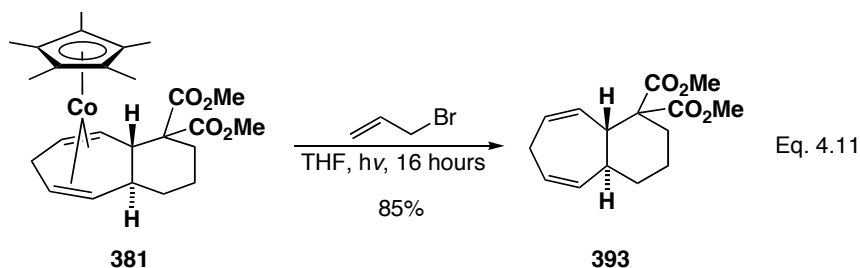
Part F: Decomplexation Reactions

Previously, decomplexation of cycloheptadiene substrates was achieved using ferrocenium ion-mediated oxidative demetallation. Unfortunately, these conditions are low-yielding and limit the synthetic applicability of this methodology. Witherell investigated the decomplexation of complexes **385** (Scheme 4.14), reporting a novel set of high-yielding photolytic demetallation conditions that we have exploited further.¹⁴³

Scheme 4.14



Malonate complex **381** was taken up in THF, treated with allyl bromide (one equiv.) and irradiated under a mercury vapour lamp. Upon work-up, the desired bicyclic organic product **393** is isolated in good yield as a spectroscopically homogeneous oil (Eq. 4.11). Unfortunately, the decomplexation of the corresponding bicyclo[5.3.0]decadiene



complex **380a** yielded a mixture of two products (Scheme 4.15). Without purification, one component of this mixture was tentatively characterized as the desired bicyclic product **394a** by ^1H NMR spectroscopy. A second product displayed ^1H NMR

Scheme 4.15

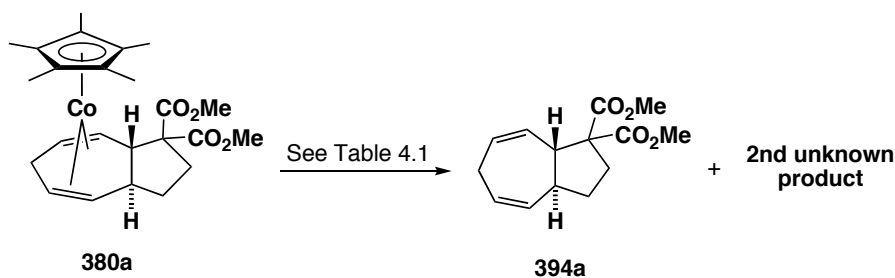
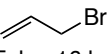
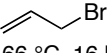
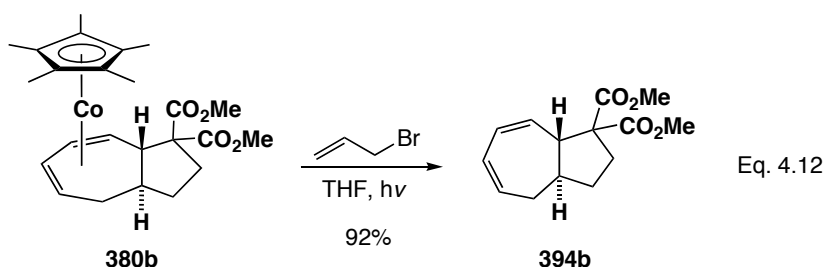


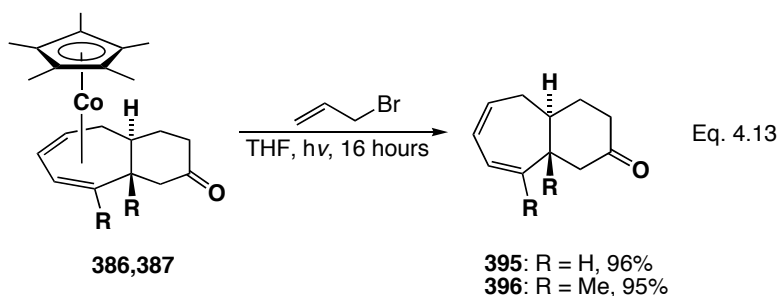
Table 4.1: Decomplexation Reaction Conditions

Entry	Conditions
1	$[\text{Cp}_2\text{Fe}]\text{PF}_6$ MeCN/Pentane, 15 min
2	 THF, hv, 16 hours
3	 THF, 66 °C, 16 hours
4	I_2 THF, 16 hours

resonances reminiscent of the uncyclized malonate tether of the starting η^2, η^3 -cycloheptadienyl complex **366a**. This suggests that the bicyclic complex **380a** is unstable under photolytic conditions, reopening the five-membered ring as previously proposed for the thermal decomposition. We explored other demetallation conditions, including ferrocenium-mediated oxidation, thermal oxidative decomplexation using allyl bromide, and iodinolysis; all conditions resulted in mixtures containing this second product. This shortcoming may be addressed by using lower pressure photolysis lamps. Surprisingly, similar difficulties are not encountered during decomplexation of complex **380b** (Eq. 4.12).



The decomplexation of η^4 -cycloheptadiene complexes **386** and **387** proceed very efficiently, providing the organic bicyclic systems **395** and **396** in excellent yields (Eq. 4.13). These exploratory reactions were conducted on very small scale. Further optimization of these decomplexation conditions on large scale is required before synthetic utility can be claimed. However, these initial results indicate these investigations are warranted and will be fruitful.



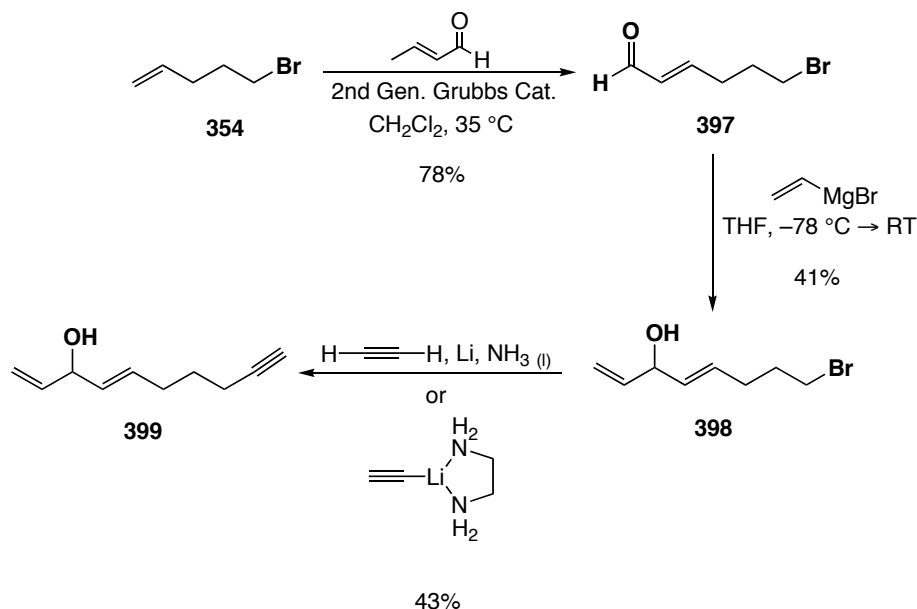
Depending on the concentration of the photolysis reactions, the colour of the solution varies afterwards: green at low concentration and red at higher concentration. When the red solution is obtained, the organic product and the red material can be separated via careful chromatography. The ^1H NMR spectrum of this red material is consistent with that reported for $\text{Cp}^*\text{Co}(\eta^3\text{-allyl})\text{bromide}$.¹²⁵ While this cycloaddition methodology is stoichiometric, the isolation of this cobalt byproduct from the decomplexation presents the possibility of metal recycling.

Part G: Preliminary Investigation of Intramolecular [5+2] Cycloaddition

Nucleophilic cyclization onto cationic cobalt intermediates is only one method of preparing bicyclic products; another is direct intramolecular [5+2] cycloaddition. This method would provide a means to control the regiochemistry of alkyne insertion, a significant advance in this methodology, especially when combined with the temporary tethering strategies described in Chapter 1. To investigate this possibility, dienynol **399** was prepared (Scheme 4.16).

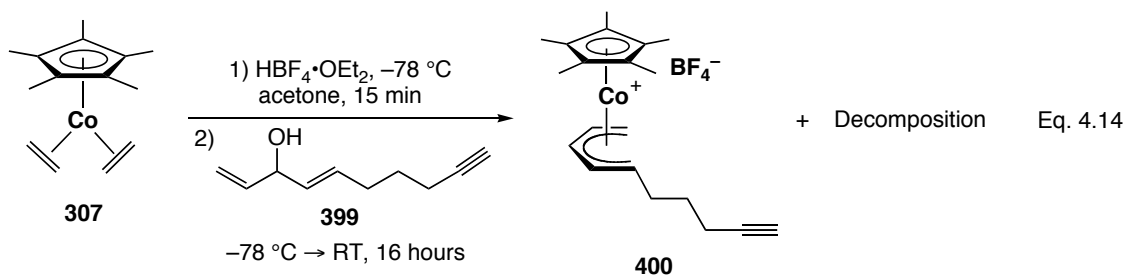
The inelegant but direct synthesis makes use of the α,ω -bromoolefin **354** described in Scheme 4.2. Subsequent cross metathesis yields aldehyde **397** using a recently published procedure.¹⁷⁷ Addition of vinyl Grignard provides bromodienol **398** in mediocre yield, possibly due to competitive reactions at the C-Br bond. From bromodienol **398**, installation of the alkyne moiety was achieved either by alkynylation using commercial lithium acetylide•EDA complex, or *in situ*-generation of lithium acetylide under dissolving metal conditions.¹⁷⁸ Both methods proceed in approximately 40% yield. For convenience, the route from commercial acetylide was used; however, *in*

Scheme 4.16



situ-generation is preferable on larger scale. With two low-yielding steps, this synthesis is less than ideal, yet sufficient to obtain enough material for exploratory cycloadditions.

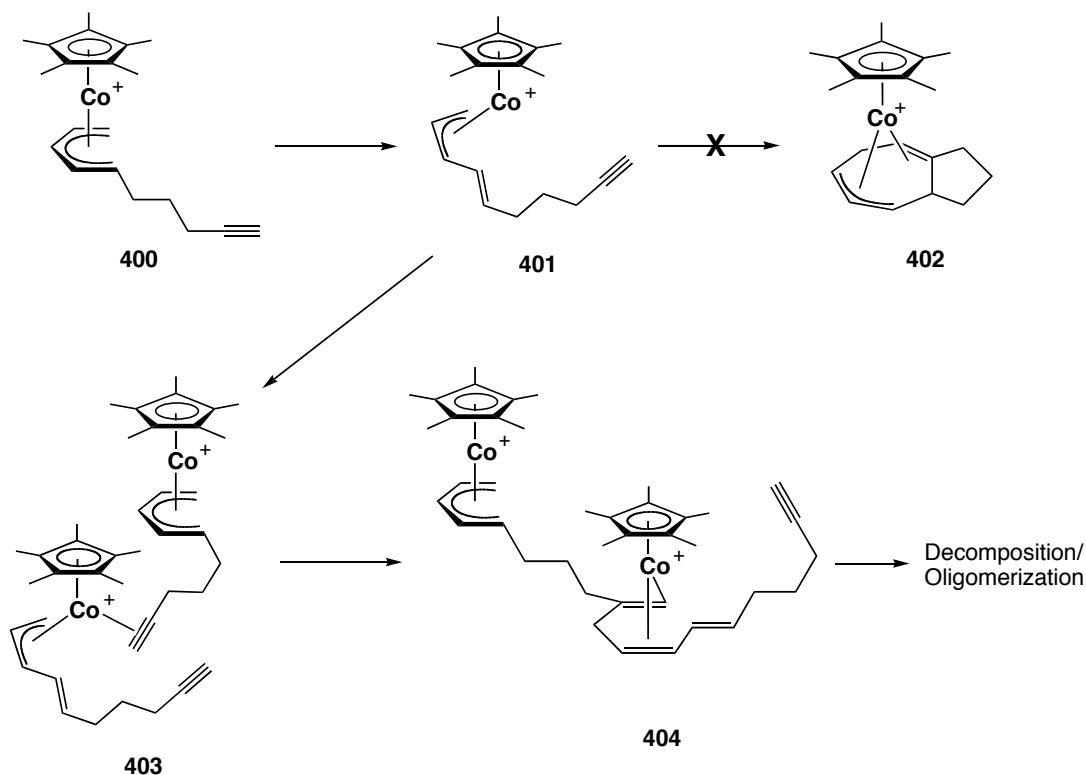
The preparation of pentadienyl complex **400** from alkynyldienol **399** led to a complex mixture of products (Eq. 4.14). One of the components in the mixture exhibited ^1H NMR resonances characteristic of the terminal methylene group of a η^5 -pentadienyl



complex. The other component(s) could not be identified. We speculate that this material consists of a mixture of products arising from intermolecular cycloaddition reaction rather than the desired intramolecular process. Intermolecular cycloaddition leading to pentadienyl “dimers” **404** leaves an η^5 -pentadienyl moiety available for further

cycloaddition reactivity, potentially leading to oligomerization (Scheme 4.17).

Scheme 4.17



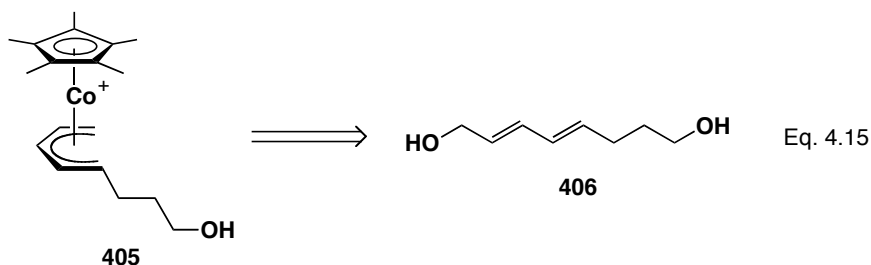
Intramolecular processes are generally kinetically preferred to intermolecular reactions. In this particular case, however, the intramolecular process appears to be significantly disfavoured. This is due to the *syn* configuration of the pentadienyl substituent. For intramolecular reaction, the alkyne substituent must eventually coordinate to the metal centre. Upon $\eta^5 \rightarrow \eta^3$ dissociation to form intermediate **401**, the *trans*-stereochemistry of the alkene clearly inhibits the pendent alkyne from binding.

One method to address this shortcoming is the incorporation of a longer tether, with more freedom to coordinate at the metal. This, however, would be accompanied by the unfavourable entropy of large-ring formation, resulting in similar competitive reactivity. We originally targeted the preparation of a complex with two geminal alkynyl

groups, both *syn* and *anti*, to overcome this difficulty. However, the difficulty preparing the model substrate $\text{Cp}^*\text{Co}(\eta^3\text{-1,1-dimethylpentadienyl})^+$ complex **328**, suggests that η^5 -pentadienyl complexes with geminal substituents will not be stable.

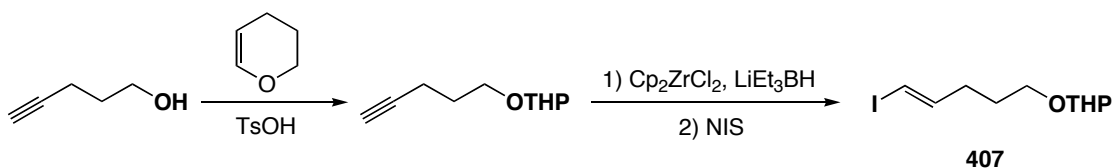
Part H: Investigations in Generalization of Substrate Synthesis

The substrate syntheses presented in Part B, while effective for preparing a limited range of η^5 -pentadienyl complexes, is too linear for the construction of more complex substrates. A superior strategy allows for the preparation of an advanced intermediate that could be further elaborated in a divergent fashion. Such an intermediate complex requires a functional handle on the substrate to permit facile incorporation of a range of pro-nucleophiles. The η^5 -pentadienyl complex **405** fulfills these conditions. This complex can in principle be prepared from diene diol substrate **406**; here we summarize our ultimately fruitless attempt to prepare this substrate.

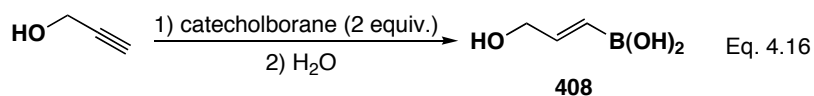


We first envisioned that diendiol **406** could arise from Suzuki-Miyaura coupling of vinyl iodide **407** and boronic acid **408** (Scheme 4.18 and Eq. 4.16). The vinyl iodide

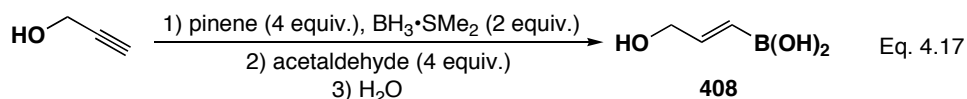
Scheme 4.18



fragment has been reported previously,¹⁷⁹ prepared by acid-catalyzed protection of 1-pentyne-5-ol, followed by hydrozirconation and quenching with N-iodosuccinimide. The preparation of boronic acid fragment **408** proved to be more difficult. While previously reported,¹⁸⁰ preparative details were not published; Prof. W. R. Roush kindly provided them upon request.¹⁸¹ Recently, an independent preparative procedure was published.¹⁸² Hydroboration of propargyl alcohol with two equivs. of catecholborane, followed by aqueous work-up, yields the desired hydroxy boronic acid (Eq. 4.16). Unfortunately, we were unable to separate the boronic acid from the catecholborane hydrolysis byproduct.

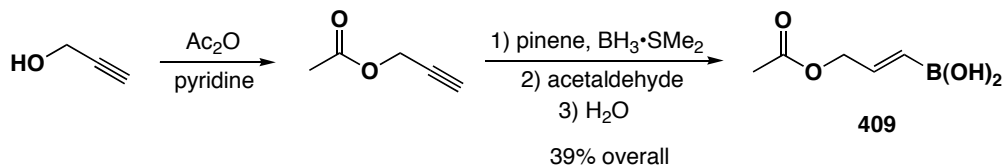


To eliminate this purification problem, we adapted a procedure reported by Hall and coworkers.¹⁸³ Hydroboration of propargyl alcohol with phenyl borane, followed by conversion to the boronic ester and subsequent hydrolysis, yields hydroxy boronic acid **408** (Eq. 4.17). This reaction was again plagued by purification difficulties: we were



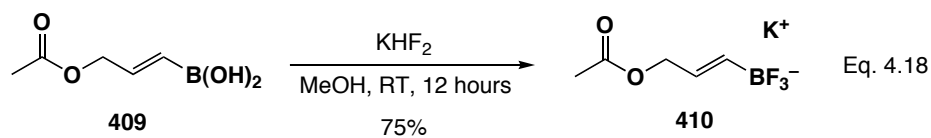
unable to separate the boric acid generated in the work-up. Protection of the alcohol as an acetate eliminates the formation of boric acid and relatively pure boronic acid **409** was isolated, as indicated via ¹H and ¹¹B NMR spectroscopy.

Scheme 4.19



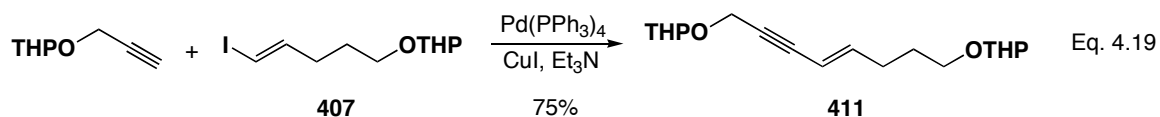
Suzuki-Miyaura coupling of the two fragments under palladium-catalyzed conditions with KOH was entirely unsuccessful, with the ^1H NMR spectrum suggesting wholesale decomposition. The use of TIOH, known to improve the yield of Suzuki-Miyaura coupling reactions,¹⁸⁴ was not effective in our reaction system.

Boronic acids are notoriously difficult to purify, possibly preventing clean coupling reactivity. In contrast, vinyl trifluoroborates are generally easy-to-purify crystalline compounds; Molander has demonstrated their utility in Suzuki-Miyaura coupling reactions.¹⁸⁵ Using the reaction conditions developed by Vedejs, boronic acid **409** was converted to trifluoroborate **410** and the product was crystallized to analytical purity (Eq. 4.18).¹⁸⁶ Cross-coupling with vinyl iodide under Molander's conditions was



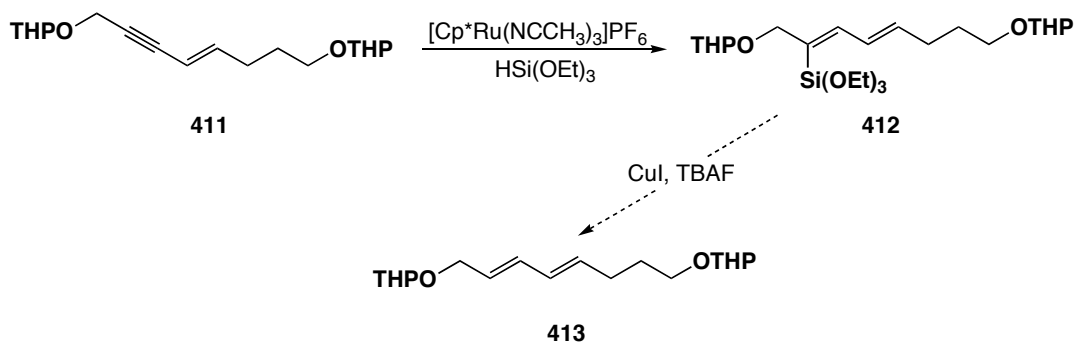
again attempted; only decomposition products were obtained. In hindsight, it became apparent that the choice of acetate as a protecting group was unwise, since vinyl acetates readily undergo Tsuji-Trost allylation reactions under palladium-catalyzed conditions.¹⁸⁷ It is highly likely that this competing reaction pathway is the source of the various byproducts observed in the ^1H NMR spectra.

Our second route to diene diol **406** was based on the Sonogashira coupling reaction. Through coupling of the previously described vinyl iodide fragment **407** and protected propargyl alcohol, enyne **411** was prepared (Eq. 4.19). The original intention

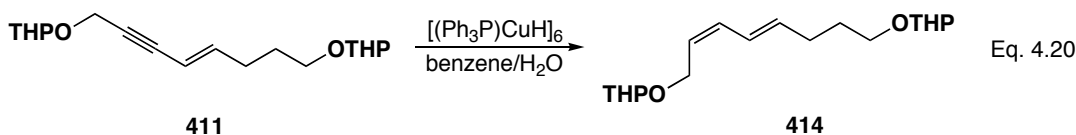


was to reduce the alkyne via ruthenium-catalyzed hydrosilylation/protodesilylation (Scheme 4.20),¹⁸⁸ leading to the *trans*-olefin **413**. We prepared the $[\text{Cp}^*\text{Ru}(\text{NCMe})_3]\text{PF}_6$ catalyst,¹⁸⁹ but observed only partial reduction of the triple bond. As such, we chose to pursue a less costly reduction methodology.

Scheme 4.20



Stryker and coworkers have previously reported alkyne reduction using stoichiometric $[\text{CuH}(\text{PPh}_3)]_6$ in the presence of water to yield *cis*-alkenes.¹⁹⁰ While the *trans*-alkene geometry is preferred, at the time of this work, we believed isomerization of the *cis*-alkene would occur during pentadienyl complex preparation. However, the *syn/anti* product mixtures obtained from *E/Z* mixtures of conjugated dienols described in Chapter 2 (Table 2.2) renders this assumption questionable. Complete reduction was accomplished using two equiv. of $[\text{CuH}(\text{PPh}_3)]_6$ (12 equiv. hydride), as determined by ^1H NMR spectroscopy (Eq. 4.20). This substrate, however, was neither isolated nor further

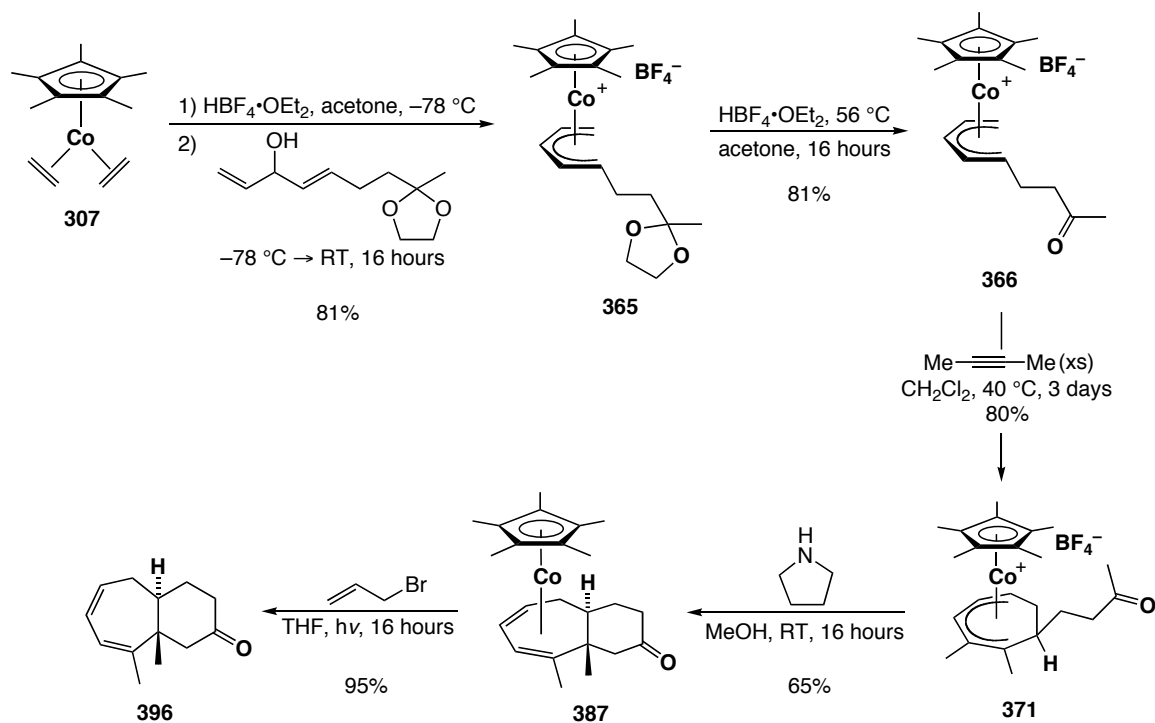


characterized. At this point in the author's research, it was concluded that the utility of the Cp^* ancillary ligand in [5+2] cycloaddition chemistry had been nearly exhausted and our efforts were better applied to other problems.

Part I: Summary and Conclusion

Bicyclic seven-membered ring compounds have been prepared through multistep synthesis, featuring the cobalt-mediated [5+2] cycloaddition and cyclization of tethered pro-nucleophiles as key transformations (Scheme 4.21). The simple ketone system

Scheme 4.21



provided the best results. The tethered malonate pro-nucleophile was plagued by problems with cyclization reversibility, resulting either in decomposition during decomplexation, or the formation of unwanted triene byproducts during cyclization reactions. This difficulty was nicely addressed by using the ketone-derived enamine nucleophile; this system is not prone to competitive deprotonation, allowing preparation of [5.4.0]-bicyclic systems in reasonable yields, including angular methylated product **396**, with complete diastereocontrol. A preliminary investigation into the formation of

bicyclic systems via intramolecular [5+2] cycloaddition chemistry was unsuccessful, with only complex product mixtures obtained.

Significant progress towards the development of a divergent pentadienyl synthon has been made. This work is incomplete, yet may prove to be a valuable area of exploration and diversification for both pentadienyl synthesis and bicyclization chemistry. Once a suitable new ancillary ligand system has been identified, this work should be revisited.

Chapter 5: Cobalt Complex Characterization: Spectroscopy and Crystallography

*Part A: Cp*Co(η^5 -Pentadienyl)⁺ Complex Characterization*

I. ¹H NMR Spectroscopy

The η^5 -pentadienyl complexes prepared for this work constitute the largest collection of Group 9 pentadienyl complexes known, with a substituent array of a scope not previously studied. As such, this set presents a valuable opportunity to examine the pentadienyl structural properties in relation to the substituent pattern. Rigorous characterizations of all complexes have been obtained, including a number of solid-state structures.

The ¹H NMR data for the η^5 -pentadienyl complexes described in Chapters 2 and 4 are gathered in Table 5.1. For the purposes of this discussion, the protons are labeled from H1-H5, where C1 is the terminus bearing a substituent, or absent that, closest to it. When the data are examined, several commonalities among all species are evident. The H3 of the η^5 -pentadienyl moiety appears furthest downfield, generally resonating at ≈ 6.4 ppm. When the adjacent positions are unsubstituted, a triplet multiplicity ($J \approx 7.0$ Hz) is always observed, despite the lack of symmetry. The protons at the C2 and C4 positions are further upfield, at 5.1 and 5.0 ppm respectively, with that closest to the substituent being slightly deshielded. In C3-substituted complexes **297a** and **297c**, H4 appears as a broad triplet, suggesting that the terminal methylene protons are significantly distorted from co-planarity. This conclusion is supported by solid-state structures of related complexes. The terminal protons are most diagnostic for pentadienyl characterization.

Table 5.1: Comparison of ^1H NMR Data (ppm and Hz in CDCl_3) for $\text{Cp}^*\text{Co}(\eta^5\text{-pentadienyl})^+$ Complexes

	$\text{H}_{1\text{anti}}$ $J_{1\text{anti-2}}$ $J_{1\text{anti-1syn}}$	$\text{H}_{1\text{syn}}$ $J_{1\text{syn-2}}$ $J_{1\text{syn-1anti}}$	H_2 $J_{2-1\text{anti}}$ $J_{2-1\text{syn}}$ J_{2-3}	H_3 J_{3-2} J_{3-4}	H_4 $J_{4-5\text{anti}}$ $J_{4-5\text{syn}}$ J_{4-3}	$\text{H}_{5\text{anti}}$ $J_{5\text{anti-4}}$ $J_{5\text{anti-5syn}}$	$\text{H}_{5\text{syn}}$ $J_{5\text{syn-4}}$ $J_{5\text{syn-5anti}}$
297a	1.72 11.9 3.1	3.25 9.5 3.0	4.91 10.6 10.6 -	- - -	4.91 10.6 10.6 -	1.72 11.9 3.1	3.25 9.5 3.0
297c-syn	2.12 11.9 -	- - -	4.89 11.9 -	- - -	4.68 11.2 11.2 -	1.74 11.6 3.6	3.11 9.7 3.6
297c-anti	- - -	4.65 7.0 -	4.65 - 9.0 -	- - -	4.81 10.4 10.4 -	2.09 11.5 3.5	3.23 9.6 3.4
297b	2.98 12.8 -	- - -	6.23 12.8 - 7.1	6.78 7.2 7.2	5.16 11.1 9.4 7.5	2.06 11.7 3.3	3.34 9.6 3.4
297i-syn	2.18 12.4 -	- - -	5.25 12.2 - 7.2	6.38 6.9 -	- - - -	1.41 - 4.0	2.85 - 4.0
297i-anti	- - -	3.89 8.4 -	4.98 - 8.0 8.0	6.41 7.2 -	- - - -	1.43 - 3.8	2.97 - 3.6
297j	2.06 12.5 -	- - -	5.04 12.1 - 7.0	6.48 7.0 7.0	5.04 12.1 - 7.0	- - -	2.06 12.5 -
363a	2.05 - ^a -	- - -	5.07 11.7 - 6.9	6.31 7.0 7.0	4.96 11.7 9.6 9.8	1.77 12.5 3.9	3.21 9.6 3.4
365	1.96 10.7 -	- - -	5.13 11.9 - 6.8	6.46 6.9 6.9	5.03 11.8 9.7 7.1	1.65 - ^a -	3.20 9.5 3.4
366	2.01 - ^b -	- - -	5.18 11.9 - 6.8	6.33 7.0 7.0	4.98 11.5 9.8 7.2	1.80 11.8 3.3	3.18 9.6 3.5

^a Signal overlaps those of other protons. ^b Multiplet is poorly resolved.

The *syn* and *anti* protons at the 1- and 5-positions are inequivalent, with the *anti* protons significantly shielded, presumably due to the anisotropic field of the π -system or metal. The terminal methylene protons appear as doublets of doublets, with one strong *syn/anti* coupling and one weak geminal coupling ($J \approx 12$ Hz, 3 Hz). This characteristic signal allows differentiation between the *syn*- and *anti*-isomers of η^5 -pentadienyl complexes **297c** and **297i**. Alkyl and aryl substituents generally appear at chemical shifts typical of allylic sp^3 -hybridized and aromatic protons. These observations are in agreement with the previously reported Co(III) pentadienyl structures.^{129,138-140}

II. X-Ray Crystallography

Single crystal X-ray structures have been obtained for η^5 -pentadienyl complexes **297b**, **297d**, **297f-h**, **297i**, **297j**, and **366** encompassing both Witherell's¹⁴³ and the author's work; the pertinent interatomic lengths and angles are gathered in Table 5.2 with crystal structure diagrams for complexes **297b**, **297i**, **297j**, and **366** provided as Figures 5.2-5.5. Despite significant effort, we have been unable to grow X-ray quality crystals of any complex with a C3 substituent, yet several general structural trends are still evident. The Co-C bond lengths of the pentadienyl moiety vary, with the Co-C1 and Co-C5 lengths being the longest (≈ 2.1 Å), and the Co-C3 bond the shortest (≈ 2.0 Å), a common distortion in pentadienyl complexes with highly compact metal orbitals.¹³⁰ As anticipated, the pentadienyl substituents are located approximately 0.2 Å out of the pentadienyl plane, bent up towards the metal, in agreement with the previously reported complexes.¹³⁰⁻¹³⁸ With adjacent substituents, as in 1,2-dimethyl or 1,2,4-trimethylpentadienyl complexes **297g** and **297h**, the internal substituent is distorted

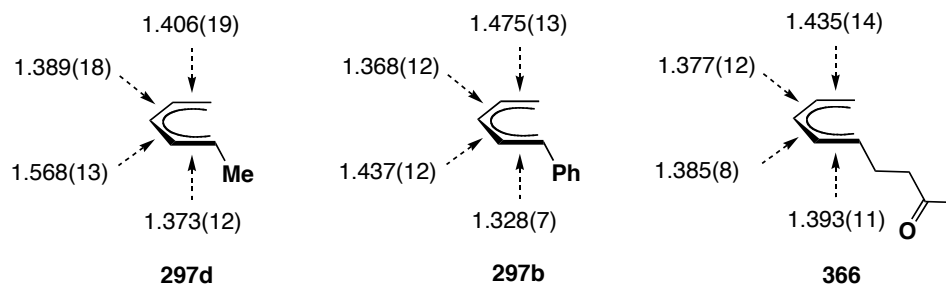
Table 5.2: Selected Bond Lengths (Å), Bond and Dihedral Angles (deg) and Substituent Deviation from Planarity (Å) for Cp*Co(η^5 -pentadienyl)⁺ Complexes

	297d	297f	297g	297h	297b	297i	297j	366
Co-C1	2.176(3)	2.189(11)	2.195(7)	2.181(2)	2.223(3)	2.144(3)	2.191(2)	2.173(4)
Co-C2	2.018(5)	2.058(13)	2.086(7)	2.090(2)	2.083(6)	2.043(3)	2.043(7)	2.027(4)
Co-C3	2.082(11)	2.005(5)	2.007(6)	2.060(3)	2.034(10)	2.034(3)	2.015(4)	1.995(6)
Co-C4	2.037(3)	2.043(8)	2.00(2)	2.067(2)	2.038(4)	2.124(3)	2.043(3)	2.036(5)
Co-C5	2.054(9)	2.212(8)	2.147(19)	2.086(3)	2.073(12)	2.108(5)	2.191(2)	2.152(5)
C1-C2	1.373(12)	1.428(16)	1.398(14)	1.405(4)	1.328(7)	1.369(4)	1.382(5)	1.393(11)
C2-C3	1.568(13)	1.429(15)	1.430(10)	1.426(3)	1.437(12)	1.433(5)	1.406(4)	1.385(8)
C3-C4	1.389(18)	1.392(10)	1.46(2)	1.420(4)	1.368(12)	1.397(5)	1.406(4)	1.377(12)
C4-C5	1.406(19)	1.526(11)	1.378(14)	1.418(3)	1.475(13)	1.502(7)	1.382(5)	1.435(14)
C1-C5	2.654	2.810	2.840	2.822	2.860	2.649	2.878	2.880
C1-C2-C3	122.4(10)	123.8(11)	120.5(8)	121.5(2)	125.6(6)	125.9(3)	125.9(3)	125.6(6)
C2-C3-C4	131.6(7)	126.9(8)	124.4(9)	126.5(2)	127.4(8)	124.0(3)	124.3(4)	127.2(7)
C3-C4-C5	124.5(4)	120.0(7)	126.6(14)	123.0(2)	120.9(6)	116.3(4)	125.9(3)	123.5(7)
Dihedral	1.4(2)	11.90(19)	9.55(16)	10.28(17)	7.6(3)	1.98(14)	0.36(6)	7.4(3)
Deviation	0.293(7)	0.227(14)	0.239(18)	0.190(5)	0.103(13)	0.211(6)	0.255(4)	0.379(9)
			0.323(17)	0.329(5)		0.188(6)		
				0.149(4)				

farther out of plane, presumably to minimize steric interactions. Substituents compress the C-C-C bond angle on which they reside, an extreme example being 1,4-dimethyl complex **297i**, where the C3-C4-C5 bond angle is $\approx 9.0^\circ$ smaller than the C1-C2-C3 or C2-C3-C4 angles; however, the crystal selected for X-ray diffraction study was disordered and this value may be exaggerated.¹³⁸ The dihedral angle between the two η^5 -coordinated ligands varies significantly with substituent pattern, ranging from 11.90° for $\text{Cp}^*\text{Co}(\eta^5\text{-2-methylpentadienyl})^+$ (**297f**) to 0.36° in the $\text{Cp}^*\text{Co}(\eta^5\text{-1,5-dimethylpentadienyl})^+$ (**297j**) case. This deviation is likely the result of steric repulsion between the ancillary ligand substituents and pentadienyl substituents. The fact that the highest and lowest angles are associated with unreactive and reactive complexes respectively is suggestive, and the potential correlation will be examined computationally in Chapter 6.

The pentadienyl C-C bond lengths vary, yet are suggestive of a reactivity trend. The reactive $\text{Cp}^*\text{Co}(\eta^5\text{-1-methylpentadienyl})^+$ (**297d**) and $\text{Cp}^*\text{Co}(\eta^5\text{-1-ethylpentadienyl})^+$ (**264**) complexes exhibit a distortion toward η^2, η^3 -coordination (Figure 5.1). The very reactive $\text{Cp}^*\text{Co}(\eta^5\text{-1-phenylpentadienyl})^+$ (**297b**) displays a more extreme distortion, with bond lengths characteristic of an η^1, η^4 -coordination mode. Unreactive complexes do not exhibit these distortions, being much closer to the 1.39 Å

Figure 5.1: C-C Bond Lengths in Pentadienyl Complexes **297d**, **297b**, and **366**



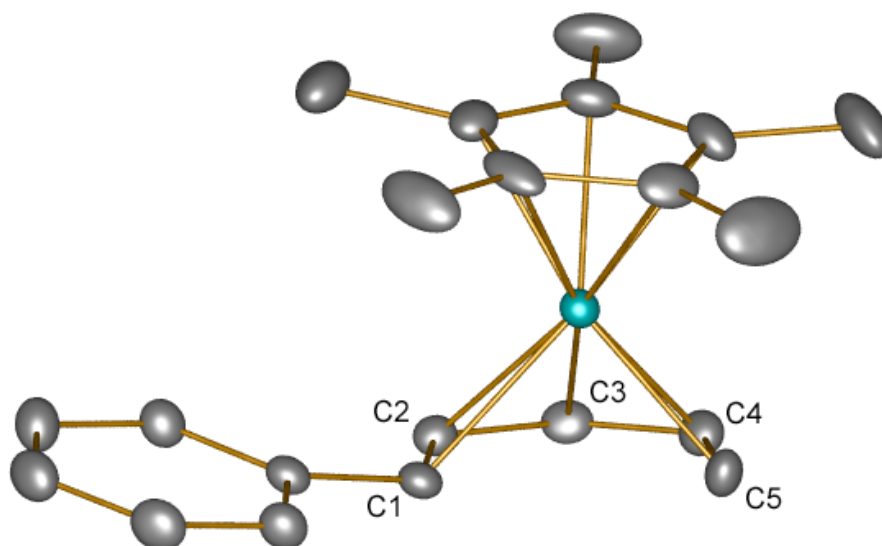


Figure 5.2: X-Ray structure diagram for $[(C_5Me_5)Co(\eta^5\text{-1-phenylpentadienyl})]^+BF_4^-$ (**297b**) with non-hydrogen atoms represented by thermal ellipsoids at the 20% probability level. Final residuals: $R_1 = 0.0534$, $wR_2 = 0.1601$.

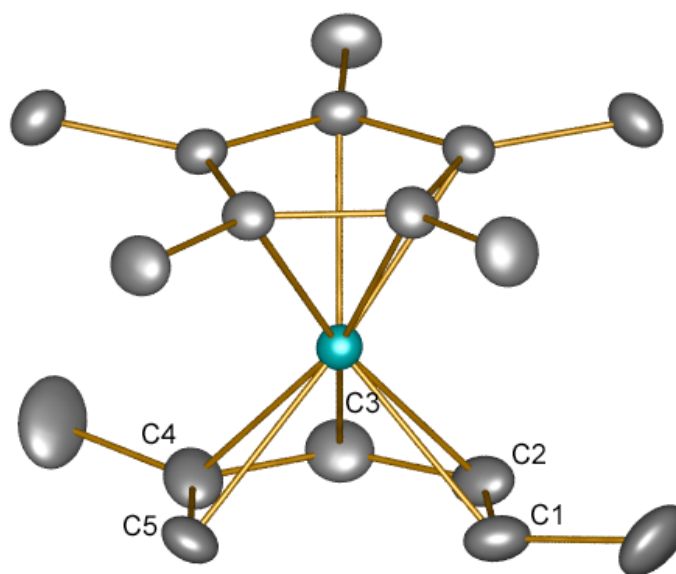


Figure 5.3: X-Ray structure diagram for $[(C_5Me_5)Co(\eta^5\text{-1,4-dimethylpentadienyl})]^+BF_4^-$ (**297i**) with non-hydrogen atoms represented by thermal ellipsoids at the 20% probability level. Final residuals: $R_1 = 0.0440$, $wR_2 = 0.1162$.

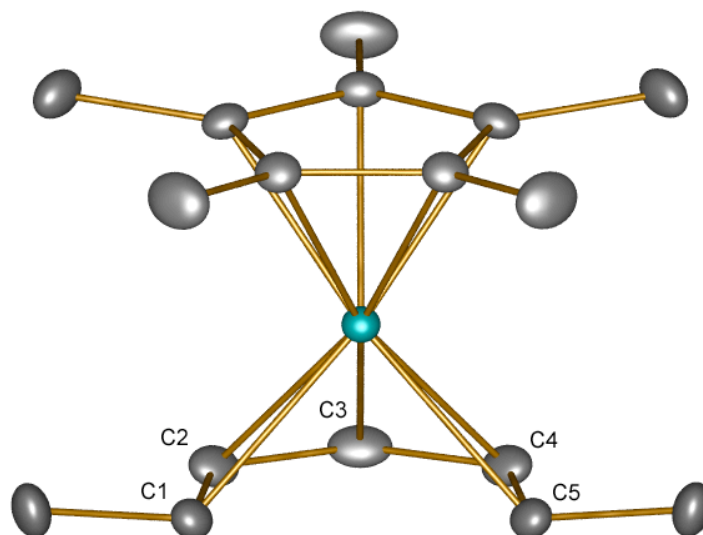


Figure 5.4: X-Ray structure diagram for $[(C_5Me_5)Co(\eta^5\text{-}1,5\text{-dimethylpentadienyl})]^+BF_4^-$ (**297j**) with non-hydrogen atoms represented by thermal ellipsoids at the 20% probability level. Final residuals: $R_1 = 0.0312$, $wR_2 = 0.0781$.

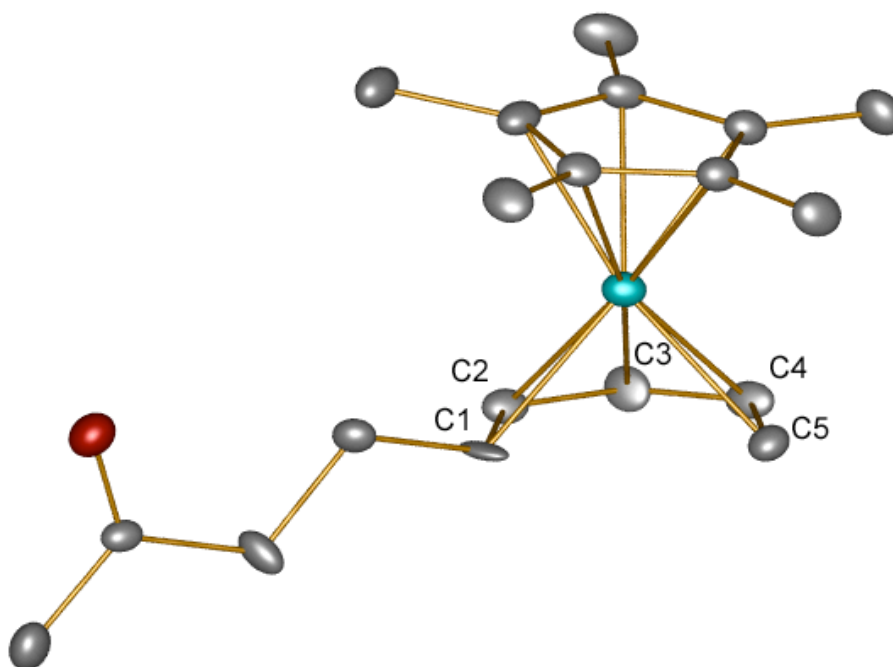


Figure 5.5: X-Ray structure diagram for $[(C_5Me_5)Co(\eta^5\text{-}1\text{-}(2\text{-butanoyl})\text{-pentadienyl})]^+BF_4^-$ (**366**) with non-hydrogen atoms represented by thermal ellipsoids at the 20% probability level. Final residuals: $R_1 = 0.0363$, $wR_2 = 0.0953$.

C-C bond lengths expected of η^5 -hapticity.¹³⁸ However, the η^5 -pentadienyl ketone complex **366** is both reactive and undistorted. As such, there does not appear to be a consistent relationship between the C-C bond lengths and the reactivity of the pentadienyl complexes. The origin of the distortions is most likely the result of crystal packing forces.

Part B: Cp*Co(η^2, η^3 -Cycloheptadienyl)⁺ Complex Characterization

I. ¹H NMR Spectroscopy

Spectroscopically, the η^2, η^3 -cycloheptadienyl complexes differ significantly from their η^5 -cycloheptadienyl isomers, allowing clear differentiation between the two potential [5+2] reaction products (Table 5.3). In the η^2, η^3 -cycloheptadienyl species, the furthest downfield resonance occurs at ≈ 3.9 ppm and corresponds to the allyl position distal to the substituent, manifesting as a doublet of triplets ($J \approx 8.0$ Hz, 4.0 Hz) from vicinal coupling to the methylene and allyl methine protons. The allyl terminus proximal to the substituent, a doublet of doublets at ≈ 3.6 ppm ($J \approx 7.5$ Hz, 3.8 Hz), is further upfield. The central allyl proton appears as a triplet at ≈ 3.3 ppm ($J \approx 7.5$ Hz). The large difference between the chemical environments of the cycloheptadienyl faces causes the geminal pair of the unsubstituted methylene group to be very characteristic of these species, with the *endo* proton appearing as a doublet of triplets ($J \approx 14.1$ Hz, 8.4 Hz) at ≈ 3.1 ppm, and the *exo* proton at ≈ 2.0 ppm as a doublet of broad triplets ($J \approx 14.1$ Hz, 4.3 Hz). The olefin protons occur at ≈ 2.8 ($J \approx 7.3$ Hz, $J \approx 4.9$ Hz) and 2.4 ppm ($J \approx 6.3$ Hz, 4.6 Hz), significantly shielded by coordination to the metal, with the proton closest to the substituent experiencing additional shielding. The remaining sp^3 -methine proton

resonance is close to that of the geminal pair *endo* proton, at ≈ 2.2 ppm.

Table 5.3: Comparison of ^1H NMR Data (ppm and Hz in CDCl_3) for $\text{Cp}^*\text{Co}(\eta^2, \eta^3\text{-cycloheptadienyl})^+$ Complexes.

	H₁	H₂	H₃	H_{4endo}	H_{4exo}	H₅	H₆	H₇
	J_{1-2}	J_{2-1}	J_{3-2}	$J_{4endo-4exo}$	$J_{4exo-4endo}$	$J_{5-4endo}$	J_{6-5}	J_{7-6}
	J_{1-7}	J_{2-3}	$J_{3-4endo}$	$J_{4endo-3}$	J_{4exo-3}	J_{5-6}	J_{6-7}	J_{7-1}
			J_{3-4exo}	$J_{4endo-5}$	J_{4exo-5}	J_{5-4exo}		
336c	4.10	3.51	4.06	3.30	2.31	3.02	2.75	3.40
	7.3	7.7	8.2	14.1	13.9	7.5	6.0	4.2
	4.0	7.7	8.2	8.6	4.4	7.5	6.0	4.2
		4.1	8.6	4.4	4.8			
336d	3.59	3.42	3.59	-	2.34	2.38	2.38	2.34
	7.6	7.7	7.6	-	-	-	-	-
	3.8	7.7	-	-	^a	-	-	^a
		3.8	-	-	3.2	3.2		
344b	3.67	3.12	3.67	-	2.69	-	-	2.69
	7.4	7.4	7.4	-	-	-	-	-
	4.5	7.4	-	-	4.4	-	-	4.4
		4.5	-	-	-	-		
367a	3.60	3.30	3.92	3.10	2.04	2.83	2.42	2.16
	7.6	7.6	8.3	14.1	14.1	7.3	6.6	3.7
	3.8	7.6	8.3	8.5	4.3	7.3	4.5	3.7
		4.1	8.5	4.3	4.9			
367b	3.58	3.34	3.96	3.15	2.10	2.87	2.36	2.18
	7.6	7.6	8.4	14.3	14.4	7.1	6.3	3.7
	3.8	7.6	8.4	8.7	4.1	7.1	4.7	3.7
		4.0	8.7	4.1	5.4			
369	3.69	3.33	3.91	3.10	2.11	2.86	2.49	2.21
	7.5	7.6	8.4	14.1	^b	7.2	6.4	^b
	3.7	7.6	8.4	8.4	-	7.2	4.6	-
		4.0	8.4	-	4.8			
377	3.58	3.34	3.93	3.12	2.06	2.87	2.36	2.17
	7.5	7.6	^b	14.2	14.1	7.7	6.2	3.7
	3.7	7.6	-	8.3	4.2	7.7	4.8	3.7
		-	8.3	4.2	4.8			

^a Multiplet is poorly resolved. ^b Signal overlaps those of other protons.

II. X-Ray Crystallography

The η^2, η^3 -cycloheptadienyl complexes are unprecedented; therefore the solid-

state structures are of particular interest for both fundamental issues and structural confirmation. The cyclic framework is numbered from C1-C7, starting from the substituent and continuing around the allyl moiety. The pertinent bond lengths and angles for the $\text{Cp}^*\text{Co}(\eta^2, \eta^3\text{-cycloheptadienyl})^+$ complexes are gathered in Table 5.4, with structural representations of complexes **336d**, **367b**, **369**, and **377** provided as Figures 5.6-5.9. The Co-C2 and Co-C4 allyl terminal bond lengths (2.1 Å) are generally the

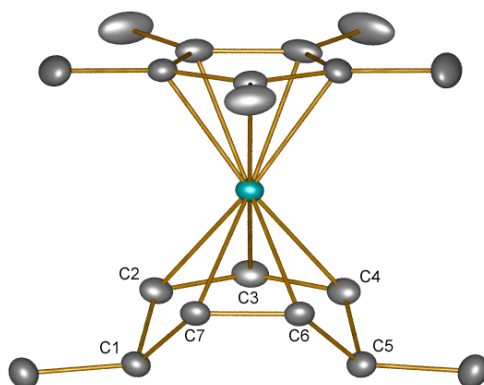


Figure 5.6: X-Ray structure diagram for $[(\text{C}_5\text{Me}_5)\text{Co}(\eta^2, \eta^3\text{-1,5-dimethylcycloheptadienyl})]^+\text{BF}_4^-$ (**336d**) with non-hydrogen atoms represented by thermal ellipsoids at the 20% probability level. Final residuals: $R_1 = 0.0312$, $wR_2 = 0.0781$.

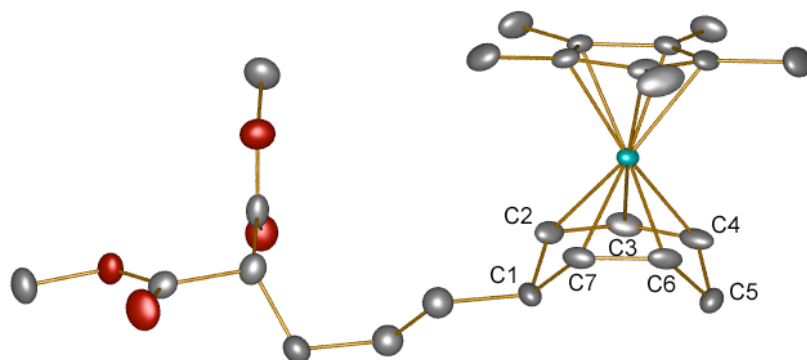


Figure 5.7: X-Ray structure diagram for $[(\text{C}_5\text{Me}_5)\text{Co}(\eta^2, \eta^3\text{-cycloheptadienyl})]^+\text{BF}_4^-$ (**367b**) with non-hydrogen atoms represented by thermal ellipsoids at the 20% probability level. Final residuals: $R_1 = 0.0549$, $wR_2 = 0.1584$.

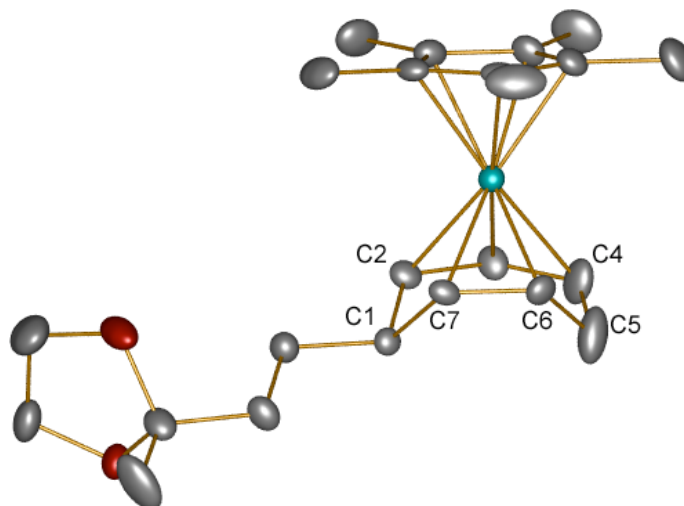


Figure 5.8: X-Ray structure diagram for $[(C_5Me_5)Co(\eta^2,\eta^3\text{-cycloheptadienyl})]^+BF_4^-$ (**377**) with non-hydrogen atoms represented by thermal ellipsoids at the 20% probability level. Final residuals: $R_1 = 0.0582$, $wR_2 = 0.1601$.

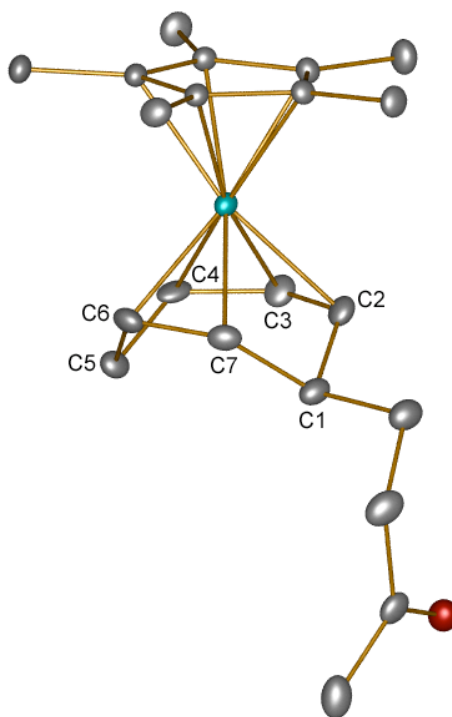


Figure 5.9: X-Ray structure diagram for $[(C_5Me_5)Co(\eta^2,\eta^3\text{-cycloheptadienyl})]^+BF_4^-$ (**369**) with non-hydrogen atoms represented by thermal ellipsoids at the 20% probability level. Final residuals: $R_1 = 0.0613$, $wR_2 = 0.1641$.

Table 5.4: Selected Bond Lengths (Å) and Angles (deg) for Cp*Co(η^2, η^3 -cycloheptadienyl)⁺ Complexes

	336a	336b	336d	367b	377	369
Co-C2	2.148(3)	2.101(2)	2.107(2)	2.104(4)	2.107(4)	2.100(3)
Co-C3	2.083(3)	2.062(2)	2.022(2)	2.068(4)	2.050(4)	2.056(3)
Co-C4	2.157(5)	2.136(4)	2.111(2)	2.122(9)	2.186(5)	2.135(6)
Co-C6	2.076(3)	2.081(2)	2.1205(19)	2.057(4)	2.104(4)	2.082(3)
Co-C7	2.090(2)	2.103(2)	2.118(2)	2.097(4)	2.116(4)	2.103(3)
C1-C2	1.508(4)	1.513(3)	1.517(3)	1.504(6)	1.527(5)	1.530(5)
C2-C3	1.372(5)	1.396(3)	1.411(4)	1.365(6)	1.396(6)	1.393(5)
C3-C4	1.426(6)	1.517(5)	1.401(3)	1.301(10)	1.376(6)	1.377(6)
C4-C5	1.396(7)	1.480(6)	1.516(3)	1.496(13)	1.402(7)	1.490(7)
C5-C6	1.590(8)	1.448(5)	1.516(3)	1.595(10)	1.479(7)	1.547(6)
C6-C7	1.393(6)	1.374(3)	1.377(3)	1.393(6)	1.372(6)	1.372(5)
C7-C1	1.476(5)	1.515(3)	1.516(3)	1.507(6)	1.513(5)	1.499(6)
C1-C2-C3	122.7(4)	124.6(2)	125.7(2)	124.5(4)	124.4(4)	124.2(3)
C2-C3-C4	121.7(4)	120.0(2)	123.5(2)	127.2(5)	124.5(4)	126.0(4)
C3-C4-C5	132.0(5)	126.3(3)	125.6(2)	123.9(7)	126.3(5)	122.2(5)
C4-C5-C6	100.2(4)	98.0(3)	99.96(16)	101.5(7)	108.3(5)	103.2(4)
C5-C6-C7	115.9(4)	120.0(3)	121.8(2)	117.7(4)	118.9(4)	119.4(4)
C6-C7-C1	124.3(4)	123.8(2)	122.0(2)	122.4(4)	123.4(4)	122.2(3)
C7-C1-C2	105.3(2)	99.68(15)	100.41(16)	99.6(3)	99.7(3)	99.9(3)

longest, with the central Co-C3 bond (2.0 Å) the shortest. These bond lengths are significantly longer than those for Cp*Co(η^3 -allyl) halide complexes (≈ 2.08 Å) and may be due to the cationic metal being a weaker π -donor. The olefin Co-C bond lengths are similar to those of the allyl termini. The C2-C3 and C3-C4 bond lengths (≈ 1.4 Å) are consistent with those observed for Cp*Co(η^3 -allyl) halide complexes. The C6-C7 olefin bond is the shortest (≈ 1.3 Å). The remaining C-C distances are consistent with single bonds (1.5 Å). The bond angles of the saturated carbons (C4-C5-C6 and C7-C1-C2) are consistently the smallest ($\approx 100^\circ$). The C1-C2-C3, C2-C3-C4, and C3-C4-C5 angles are similar and generally the largest ($\approx 124^\circ$), and the C5-C6-C7 and C6-C7-C1 angles are slightly smaller ($\approx 121^\circ$).

Part C: Cp*Co(η^5 -cycloheptadienyl)⁺ Complex Characterization

I. ¹H NMR Spectroscopy

The ¹H NMR spectra of the η^5 -cycloheptadienyl complexes are unsurprisingly similar to those of their corresponding η^5 -pentadienyl complexes; Table 5.5 gathers compiles the data for those prepared by the author and they are in good agreement with previously reported examples. The central proton of the η^5 -moiety is again the furthest downfield (≈ 6.6 ppm), exhibiting doublet or triplet multiplicity ($J \approx 7.0$ Hz), depending on substitution. The protons flanking the central position are further upfield (≈ 5.3 and 4.6 ppm), with those closer to the ring substituent resonating at slightly lower field. The termini of the η^5 -moiety differ slightly in chemical shift, with that closer to the substituent arriving at ≈ 4.0 ppm ($J \approx 8.0$ Hz, 4.0 Hz), with the other downfield at ≈ 4.3 ppm ($J \approx 9.0$ Hz, 3.4 Hz). Similar to the η^2, η^3 -cycloheptadienyl system, the geminal

Table 5.5: Comparison of ^1H NMR Data (ppm and Hz in CDCl_3) for $\text{Cp}^*\text{Co}(\eta^5\text{-cycloheptadienyl})^+$ Complexes.

	H₁	H₂	H₃	H₄	H₅	H_{6endo}	H_{6exo}	H₇
	J_{1-2}	J_{2-1}	J_{3-2}	J_{4-3}	J_{5-4}	$J_{6endo-6exo}$	$J_{6exo-6endo}$	$J_{7-6endo}$
	J_{1-7}	J_{2-3}	J_{3-4}	J_{4-5}	$J_{5-6endo}$	$J_{6endo-7}$	J_{6exo-5}	J_{7-6exo}
					J_{5-6exo}	$J_{6endo-5}$	J_{6exo-7}	J_{7-1}
337c	4.32	5.42	6.90	5.16	4.52	2.99	2.30	1.78
	8.1	7.1	6.3	8.6	9.3	16.7	16.7	11.6
	4.5	7.1	6.3	8.6	3.7	10.4	3.7	5.2
					3.7	4.2	3.7	5.2
344a	-	-	6.75	4.83	4.52	3.25	2.39	1.30
	-	-	-	8.3	9.2	16.5	16.6	12.8
	-	-	7.4	8.3	3.4	12.8	4.8	4.0
				3.4	3.1	4.8	-	-
345	3.93	-	6.73	5.25	4.79	3.06	2.36	1.48
	-	-	-	7.5	9.5	17.1	17.0	10.8
	4.2	-	6.9	8.8	3.6	11.1	3.6	4.8
				3.6	4.2	3.6	4.8	4.8
368a	-	-	6.59	4.69	4.36	2.48	2.34	0.02
	-	-	-	8.4	9.1	16.7	16.7	12.8
	-	-	7.4	8.4	3.3	11.9	3.1	4.7
				3.3	2.8	3.1	-	-
368b	-	-	6.58	4.68	4.34	2.42	2.30	0.00
	-	-	-	8.5	9.3	16.9	17.1	^a
	-	-	7.3	8.5	3.1	11.7	3.6	-
				3.1	2.9	3.6	-	-
370	4.08	5.34	6.63	4.94	4.34	2.40	2.06	0.56
	8.0	7.2	6.5	8.3	9.2	^b	17.0	^a
	3.8	7.2	6.5	8.3	3.7	-	3.5	-
				3.7	-	3.5	-	-
371	-	-	6.49	4.60	4.34	2.45	2.25	-0.01
	-	-	-	7.8	9.1	16.7	16.6	9.7
	-	-	7.3	7.8	3.3	11.8	3.2	4.5
				3.3	3.0	3.2	-	-
378	4.00	5.30	6.64	4.94	4.34	2.32	2.02	0.57
	8.2	7.4	6.3	7.9	8.6	16.6	16.5	^a
	4.1	7.4	6.3	7.9	4.0	9.6	3.7	-
				4.0	4.7	3.7	-	-
379	-	-	6.55	4.66	4.35	2.45	2.30	-0.01
	-	-	-	8.7	9.2	16.8	16.8	11.8
	-	-	7.2	8.7	3.4	12.2	3.6	4.2
				3.4	3.2	3.6	-	-

^a Multiplet is poorly resolved. ^b Signal is overlapping those of other protons.

pair at C6 is very characteristic, with the *endo* and *exo* protons resonating very close in chemical shift (≈ 2.4 and 2.0 ppm respectively). The methine proton is also very characteristic, appearing very far upfield, often close to 0 ppm, presumably due to the conformation of the cycloheptadienyl ring placing the proton within the anisotropic shielding field of the π -system.

II. X-Ray Crystallography

The η^5 -cycloheptadienyl complexes proved to be difficult to crystallize, generally powdering out of solution, with only four compounds studied crystallographically (Figures 5.10-5.13). Pertinent bond lengths and angles are gathered in Table 5.6. The carbons are numbered from the η^5 -moiety closest to the substituent and around the unsaturated carbons. In these complexes, the Co-C1 bond (2.1 \AA) is longest, with the rest being significantly shorter (2.0 \AA). As a result, the η^5 -moiety is not planar. This may be a function of the substitution pattern, since the previously reported $\text{Cp}^*\text{Co}(\eta^5\text{-2,3-dimethylcycloheptadienyl})^+$ complex does not exhibit this distortion.¹⁹¹ The pentadienyl C-C bond lengths are significantly longer ($\approx 1.4 \text{ \AA}$) than those of the $\text{Cp}^*\text{Co}(\eta^5\text{-2,3-dimethylcycloheptadienyl})^+$ complex ($\approx 1.3 \text{ \AA}$). The C-C-C bond angles are again compressed by the presence of a substituent, as observed in the pentadienyl complexes and the $\text{Cp}^*\text{Co}(\eta^5\text{-2,3-dimethylcycloheptadienyl})^+$ complex. The dihedral angles between the η^5 -coordinated ligand planes are all greater than 10° , with TMS complex **345** showing the largest angle of 13.77° . These deviations are likely due to steric repulsion between the substituents and the ancillary ligand, as was observed in the pentadienyl systems.

Table 5.6: Selected Bond Lengths (Å) and Angles (deg.) for Cp*Co(η^5 -Cycloheptadienyl)⁺ Complexes

	344a	345	378	370
Co-C1	2.216(2)	2.084(2)	2.117(5)	2.118(3)
Co-C2	2.061(3)	2.056(2)	2.040(2)	2.025(2)
Co-C3	2.040(3)	2.063(2)	2.027(2)	2.056(3)
Co-C4	2.026(3)	2.033(2)	2.035(2)	2.032(2)
Co-C5	2.072(3)	2.099(2)	2.049(2)	2.085(2)
C1-C2	1.419(3)	1.424(3)	1.470(5)	1.413(4)
C2-C3	1.422(4)	1.435(3)	1.407(4)	1.414(4)
C3-C4	1.400(5)	1.418(3)	1.410(4)	1.422(4)
C4-C5	1.427(4)	1.410(3)	1.418(4)	1.411(4)
C5-C6	1.490(4)	1.497(3)	1.391(5)	1.475(4)
C6-C7	1.508(4)	1.517(3)	1.517(10)	1.537(4)
C7-C1	1.544(4)	1.535(3)	1.452(15)	1.504(4)
C1-C2-C3	117.9(3)	115.7(2)	116.5(3)	119.7(2)
C2-C3-C4	124.7(2)	124.5(2)	124.9(2)	122.3(2)
C3-C4-C5	126.7(2)	126.5(2)	124.6(2)	127.2(2)
C4-C5-C6	127.3(3)	130.0(2)	138.4(3)	130.0(3)
C5-C6-C7	108.6(2)	110.3(2)	106.9(6)	111.8(2)
C6-C7-C1	108.5(2)	108.73(19)	113.0(7)	109.4(2)
C7-C1-C2	117.4(2)	121.3(2)	126.7(6)	123.6(2)
Dihedral	10.9(2)	13.77(18)	11.75(12)	11.88(19)

Part D: ¹H NMR Spectroscopy of Cp*Co(η^2, η^2 -cycloheptadiene) Complexes

The non-conjugated Co(I) cycloheptadiene complex **381** prepared from nucleophilic addition to η^2, η^3 -cycloheptadienyl complex **367b** is easily distinguished spectroscopically. The most striking feature of this spectrum is the doubly allylic geminal pair, each proton clearly identified as a doublet of triplets, the *endo* proton at \approx 3.1 ppm ($J \approx$ 13.0 Hz, 8.0 Hz) and the *exo*, located beneath the π -system, at \approx 2.4 ppm ($J \approx$ 13.0 Hz, 4.0 Hz). By two-dimensional proton spectroscopy, the geminal protons correlate to olefin protons appearing at \approx 2.0 and 1.5 ppm. These two olefin protons do

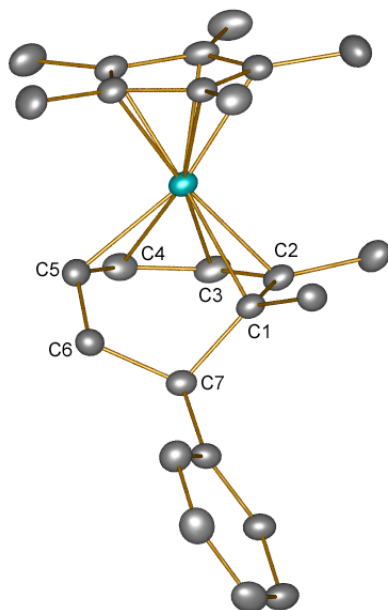


Figure 5.10: X-Ray structure diagram for $[(C_5Me_5)Co(\eta^5\text{-cycloheptadienyl})]^+BF_4^-$ (**344a**) with non-hydrogen atoms represented by thermal ellipsoids at the 20% probability level. Final residuals: $R_1 = 0.0479$, $wR_2 = 0.1374$.

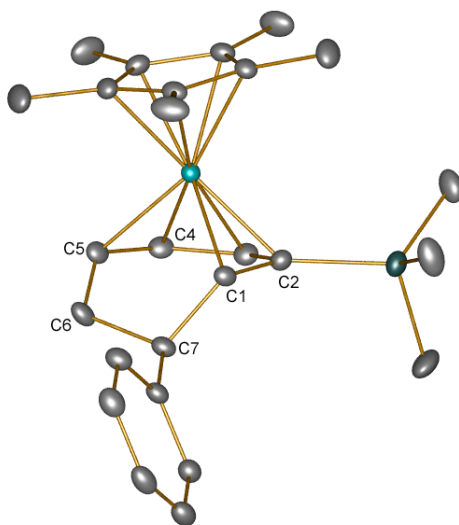


Figure 5.11: X-Ray structure diagram for $[(C_5Me_5)Co(\eta^5\text{-cycloheptadienyl})]^+BF_4^-$ (**345**) with non-hydrogen atoms represented by thermal ellipsoids at the 20% probability level. Final residuals: $R_1 = 0.0313$, $wR_2 = 0.0884$.

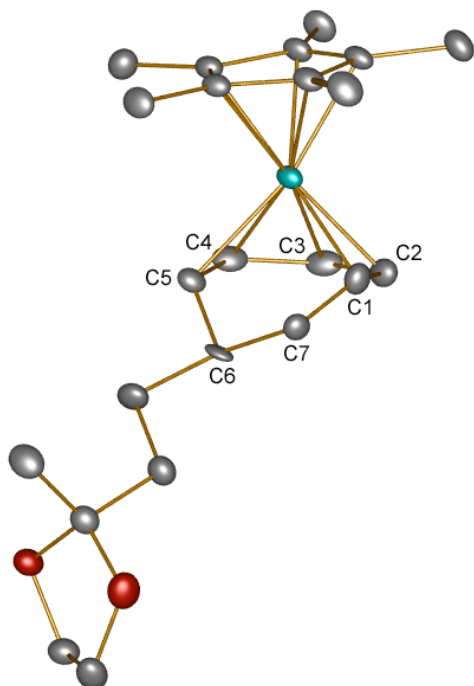


Figure 5.12: X-Ray structure diagram for $[(C_5Me_5)Co(\eta^5\text{-cycloheptadienyl})]^+BF_4^-$ (**378**) with non-hydrogen atoms represented by thermal ellipsoids at the 20% probability level. Final residuals: $R_1 = 0.0436$, $wR_2 = 0.1189$.

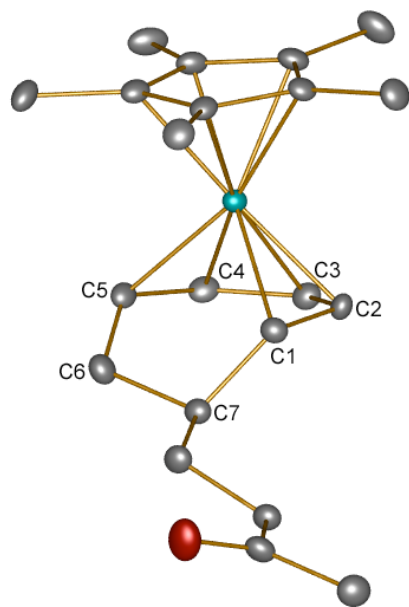
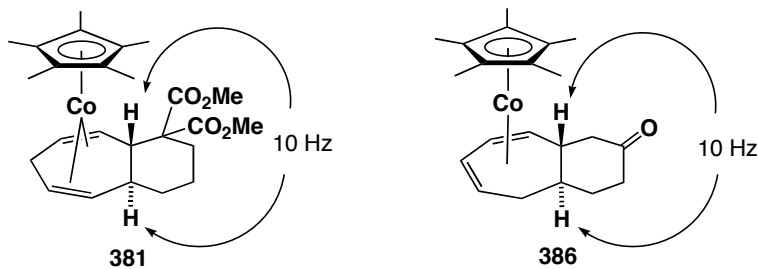


Figure 5.13: X-Ray structure diagram for $[(C_5Me_5)Co(\eta^5\text{-cycloheptadienyl})]^+BF_4^-$ (**370**) with non-hydrogen atoms represented by thermal ellipsoids at the 20% probability level. Final residuals: $R_1 = 0.0361$, $wR_2 = 0.0961$.

not correlate to each other, establishing that the diene is non-conjugated. The remaining olefin protons resonate at ≈ 2.0 and 1.6 ppm. The 10 Hz coupling constant between the bridge head protons at ≈ 3.1 and 1.5 ppm is consistent with the *trans* stereochemical assignment of the ring-fusion (Figure 5.14).

Figure 5.14: *Trans* Relationship of Bridgehead Protons



Part E: Cp*Co(η^4 -cycloheptadiene) Complexes

I. ^1H NMR Spectroscopy

The conjugated cycloheptadiene complexes differ markedly from the non-conjugated isomer, making spectroscopic differentiation simple. The internal protons of the diene are the furthest downfield (≈ 3.9 and 3.8 ppm). The remaining diene protons resonate upfield at ≈ 2.0 and 1.6 ppm, likely due to significant contribution from a Co(III) resonance form. The geminal pair adjacent to the diene is further upfield relative to the non-conjugated isomer, with the *endo* proton resonating at ≈ 1.4 ppm and the *exo* at ≈ 1.0 ppm. The *trans* ring-fusion is again established by the ≈ 10 Hz coupling of the bridgehead protons (≈ 1.2 and 0.5 ppm) (Figure 5.14).

II. X-Ray Crystallography

Only one Co(I) complex was characterized crystallographically during the course

of this work: conjugated bicyclic diene complex **386** (Figure 5.15). This structure clearly proves the *trans* geometry of the ring-fusion. The six-membered ring is angled away from the metal and is locked in a chair conformation. The Co-C1 and Co-C4 bond distances (1.9 Å) are slightly longer than the Co-C2 and Co-C3 distances (2.0 Å), and the C1-C2 and C3-C4 bond lengths (1.42 Å) are longer than the C2-C3 distance (1.40 Å), again suggesting significant contribution from a Co(III) resonance form.

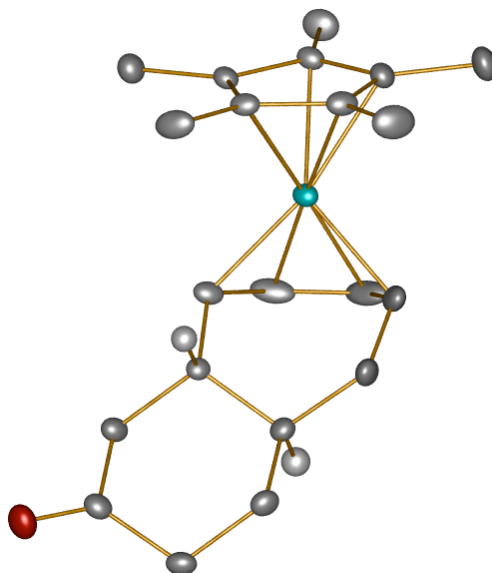


Figure 5.15: X-Ray structure diagram for $[(C_5Me_5)Co(\eta^4\text{-}[5.4.0]\text{-bicyclopentadiene})]^+BF_4^-$ (**386**) with non-hydrogen atoms represented by thermal ellipsoids at the 20% probability level. Final residuals: $R_1 = 0.0294$, $wR_2 = 0.0778$.

Part F: Summary and Conclusion

The η^5 -pentadienyl and η^5 -cycloheptadienyl complexes are unsurprisingly very similar spectroscopically and crystallographically. Despite the large number of η^5 -pentadienyl complexes that have been crystallographically characterized, a general structure/reactivity relationship cannot be elucidated; although compelling hapticity distortions and variations in dihedral angle are observed. These possibilities are

examined in greater detail in Chapter 6.

The η^2, η^3 -cycloheptadienyl complexes are unprecedented and their structures provide insight into this binding mode. The Co-C bond distances of the allyl moiety are longer than those of neutral Co(III) allyl complexes,^{142,143} suggesting diminished back-donation from the metal. To the best of our knowledge, thermally stable, crystallographically characterized Co(III) olefin complexes are not known. This suggests that the stronger bonding mode of the allyl moiety holds the weakly donating olefin in the coordination sphere of the metal, encouraging binding to the high-oxidation state metal. This also suggests that the olefin moiety could be hemi-labile; we will also explore this possibility in Chapter 6.

η^5 -Cycloheptadienyl complexes are well known^{123,126-128,137,143,191} and the data reported here are consistent with previous examples. Interestingly, the Co-C bonding appears to be substituent dependent, leading to a longer Co-C1 bond in C7 substituted complexes. The crystallography and spectroscopy for Co(I) diene complex **386** suggest significant contribution from a Co(III) resonance form.

Chapter 6: Cobalt-Mediated [5+2] Cycloaddition Reactions:

A Density Functional Theory Investigation

Part A: Introduction

The advent of electronic structure theory and the accompanying computational software packages, coupled to powerful and affordable computer hardware, has made high-level theoretical calculations a routine part of chemical research. This situation has increased our understanding of numerous fundamental reaction pathways, allowing chemists to model transformations difficult, or impossible, to observe experimentally. Of the many levels of theory developed, density functional theory (DFT) has displayed the greatest promise.¹⁹² When Hohenberg and Kohn demonstrated that electron density uniquely defines the energy of a molecular system,¹⁹³ a theoretical framework was established for solving molecular energy equations in a much simpler fashion than post-Hartree-Fock (HF) methods. Early orbital-free DFT methods were severely limited; the problems were rooted in their poor description of kinetic energy. Later, this difficulty was addressed by reintroduction of orbital calculations using the Kohn-Sham kinetic energy approximation.¹⁹⁴ When this approximation is applied, the total energy of a molecular system is broken down into basic components: kinetic, Coulombic attraction between the electrons and nucleus, Coulombic repulsion between electrons, and an exchange-correlation term. With the kinetic energy described by the Kohn-Sham approximation and the Coulombic terms given by their classical expressions, functional development relies only on derivation of exchange-correlation energy expressions. The

exchange-correlation term is a relatively small contributor to the overall energy, making the overall functionals less sensitive to slight errors. These non-interacting particle DFT functionals have proven to be highly accurate in reproducing experimental structures and energies.

The exchange-correlation functional is derived in an empirical fashion, and those developed are divided into two main categories: the hybrid and nonhybrid functionals. In HF theory, correlation energy is ignored and exchange energy calculated exactly. Hybrid functionals incorporate some of this exact exchange, while nonhybrid functionals do not. With the multitude of functionals available, the difficulty for a researcher is deciding which to use. Unfortunately, there is no *a priori* way to decide which functional is best in any situation. In practice, computations are often performed with multiple functionals, preferably one from each class, and the results compared, wherever possible, with experimental data.

Part B: The Mechanism of the [5+2] Cycloaddition Reaction

A DFT investigation of the cobalt-mediated [5+2] cycloaddition reaction mechanism (Scheme 3.3) was undertaken in collaboration with Prof. Peter H. M. Budzelaar. To determine the sensitivity of the results to functional choice, we studied the system with both the nonhybrid BP86¹⁹⁵ and hybrid B3LYP¹⁹⁶ functionals as implemented in *Turbomole* Version 5.¹⁹⁷ Both functionals are widely used in computational transition metal research and have proven highly accurate in specific cases. The following discussion will refer to values computed using the BP86 functional when not indicated otherwise, with the B3LYP data being described only when matters of

significant interest or deviation arise.

In the interest of minimizing computational cost, exploratory work and rough optimization of intermediates (INT) and transition states (TS) was conducted with the relatively small SV(P)^{198,a} basis set, with final geometries optimized at the larger TZVP^{199,b} basis set level. Improved single-point energies were obtained from these geometries at the TZVPP^{200,c} level with a COSMO solvent correction ($\epsilon = 9.1$)^{201,d} applied. The known difficulty with obtaining accurate solution-state entropies for bimolecular associative complexation reactions from gas-phase calculations was addressed by approximating the entropy component as 2/3 of that calculated in the gas-phase.^{202,203} Vibrational analyses^e were performed to confirm the nature of all stationary points and to calculate thermal corrections (enthalpy and entropy for 273 K, 1 bar, gas phase) to produce the final free energy values.

Initial exploratory work was performed with the unsubstituted CpCo(η^5 -pentadienyl)⁺ and CpCo(η^5 -1-methylpentadienyl)⁺ complexes to minimize computational cost. However, to eliminate ligand effects as a variable, we concluded that the final calculations were best performed with the Cp* ligand set. Cp*Co(η^5 -1-methylpentadienyl)⁺ was chosen as the complex for study given the high level of activity associated with 1-substituted complexes. The reaction profile computed is shown in Figure 6.1 with stationary point figures shown in Figure 6.2.

^a SV(P) is a split-valence (*i.e.*, double-zeta) basis set incorporating a polarization function on all non-hydrogen atoms.

^b TZVP is a triple-zeta valence basis set incorporating a polarization function on all atoms.

^c TZVPP is a triple-zeta valence basis set with double polarization, where the second polarization function is of higher angular momentum than the first.

^d COSMO is used to correct for the effect of a polarizing medium.

^e A vibrational analysis maps the energy surface by calculating the eigenvalues for all of the vibrational degrees of freedom in the molecule, thereby proving the nature of the stationary point (*i.e.*, a minimum (INT) will have zero negative eigenvalues and a saddle-point (TS) will have one negative eigenvalue).

The $\text{Cp}^*\text{Co}(\eta^5\text{-1-methylpentadienyl})^+$ complex and acetylene were both optimized and taken as reference for all other stationary point energies. The transition state energy (TS0-1) for alkyne complexation was calculated as 26.14 kcal/mol, corresponding to a dissociative interchange type pathway.²⁰⁴ At the TS, the substituted arm of the pentadienyl complex is nearly completely dissociated and swings further away as the alkyne approaches. Attempts to locate a local minimum corresponding to the unsaturated complex **338** were unsuccessful, returning only η^5 -coordinated complexes. An intrinsic reaction coordinate (IRC)^a calculation to trace the connection of TS0-1 to the starting η^5 -pentadienyl complex was unsuccessful, likely due to the potential energy surface (PES) being flat in this region (convergence on this stationary point was also very slow). An informal connection was established by minimization upon following the vibrational coordinate associated with approach of alkyne. The possibility of a high-spin intermediary state was probed, with compelling results. When the η^5 -pentadienyl complex is optimized in the triplet electronic configuration, the substituted arm of the pentadienyl complex dissociates, presumably to allow population of a higher energy orbital on the cobalt centre. However, the energy of this triplet species was calculated to be higher than TS0-1. These data suggest that the proposal of a coordinatively unsaturated intermediate preceding the trapping of alkyne is incorrect. The resultant alkyne complex INT1 has an optimized energy of 10.69 kcal/mol.

Transition states corresponding to alkyne insertion at both ends of the allyl moiety were located. That leading to productive insertion at the terminus (TS1-2, 20.10 kcal/mol) is slightly lower in energy than the internal position (TS1-9, 20.47 kcal/mol).

^a An IRC calculation maps the lowest energy pathway between two stationary points (*i.e.*, TS→INT) and formally establishes a connection.

Figure 6.1: Reaction Profile for $\text{Cp}^*\text{Co}(\eta^5\text{-1-methylpentadienyl})^+/\text{Alkyne Cycloaddition}$ (BP86/TZVPP Free Energies (kcal/mol))

142

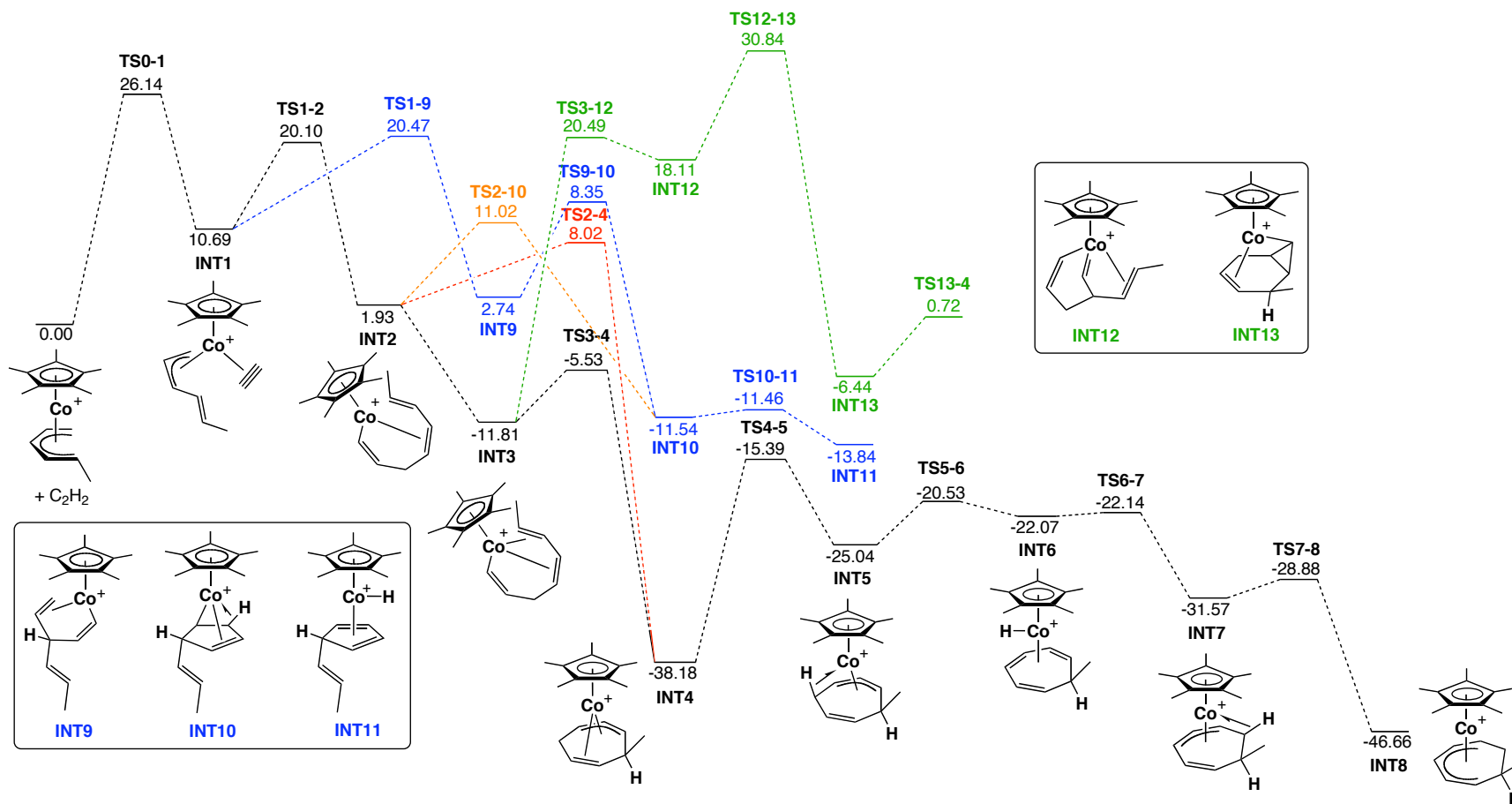
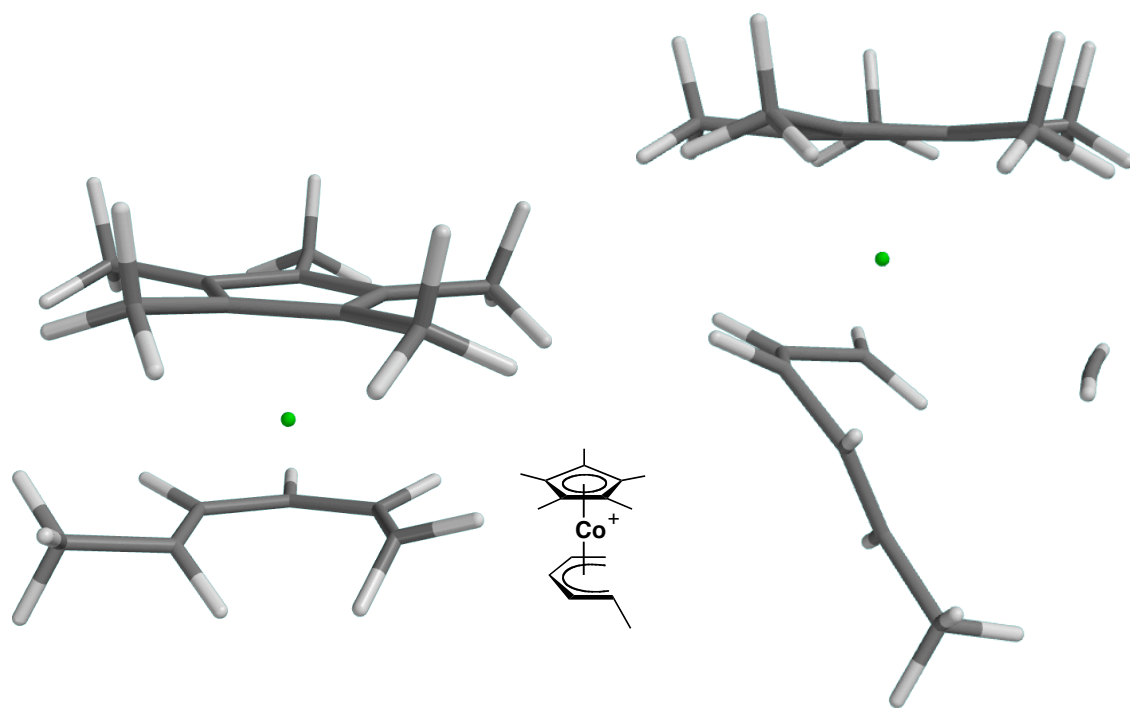
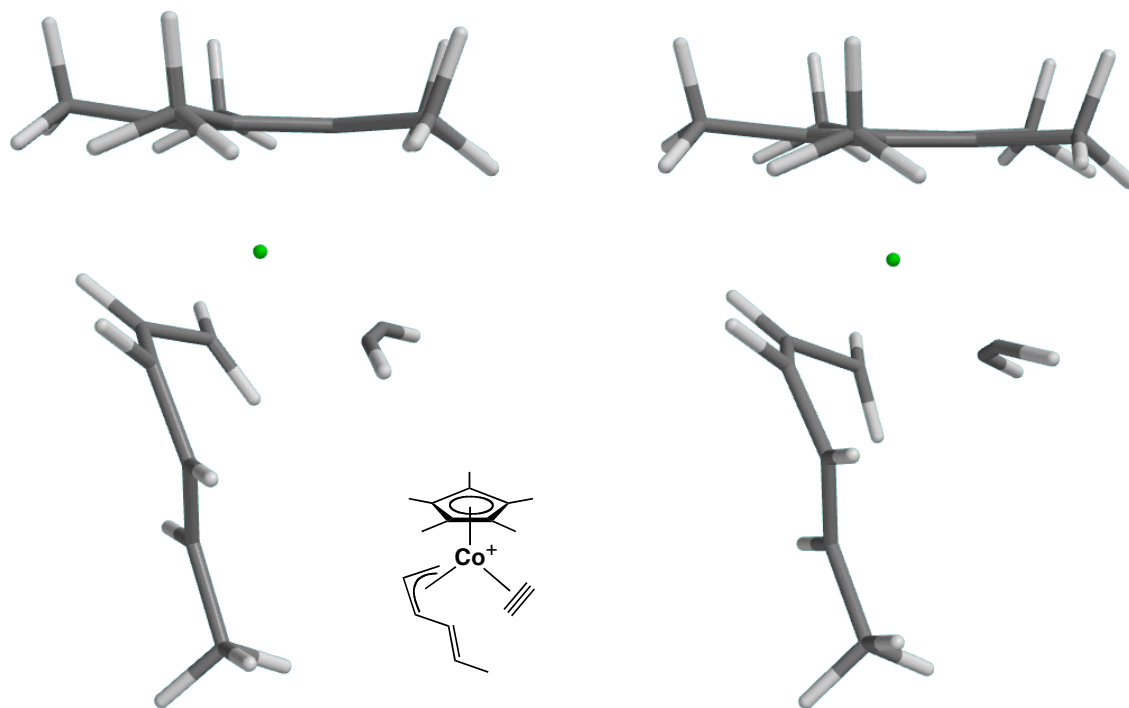


Figure 6.2: $\text{Cp}^*\text{Co}(\eta^5\text{-1-methylpentadienyl})^+$ Stationary Points (BP86/TZVP)



$\text{Cp}^*\text{Co}(\eta^5\text{-1-methylpentadienyl})^+$

TS0-1



INT1

TS1-2

Figure 6.2: Cp*Co(η^5 -1-methylpentadienyl)⁺ Stationary Points (BP86/TZVP) (cont.)

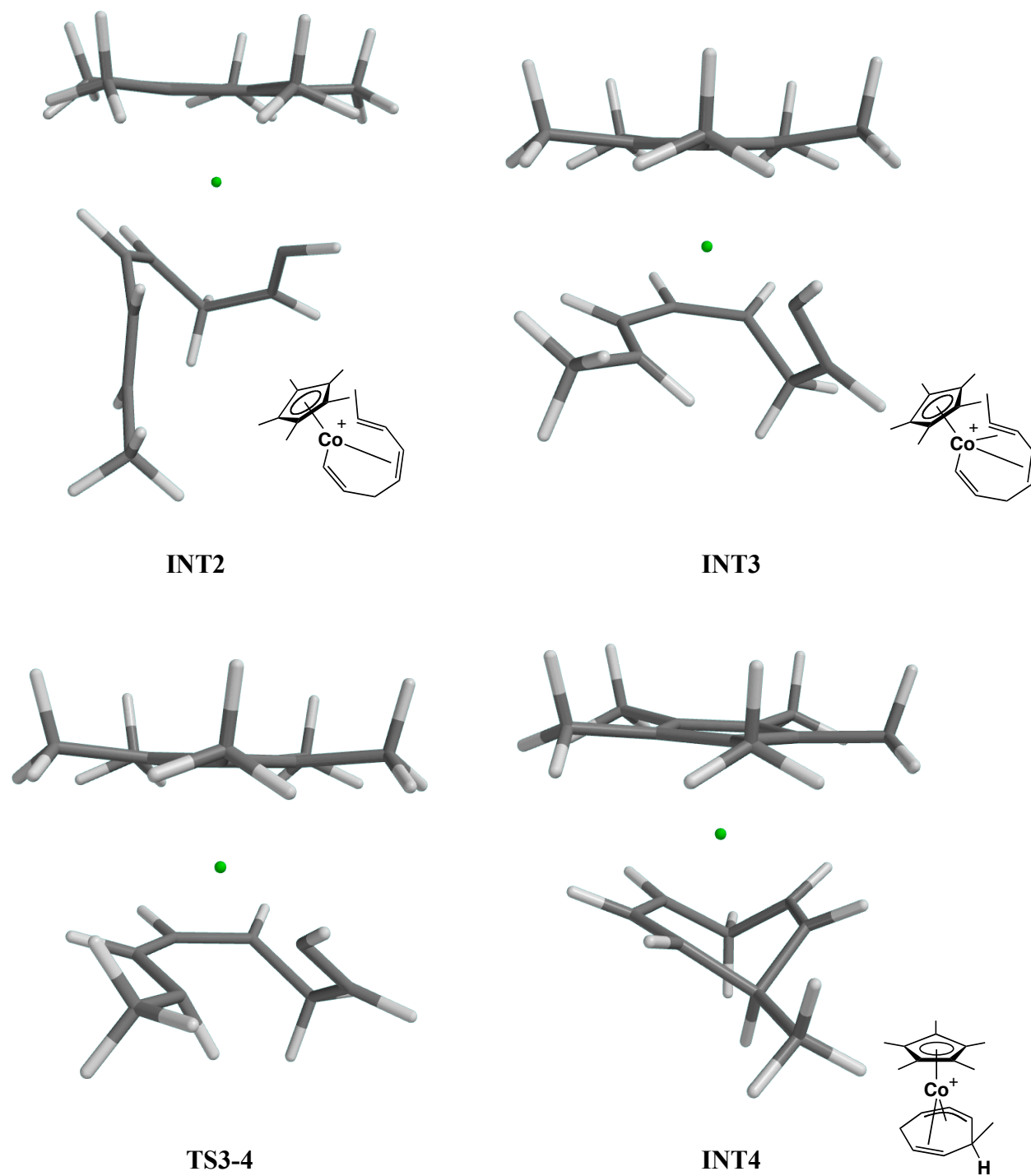
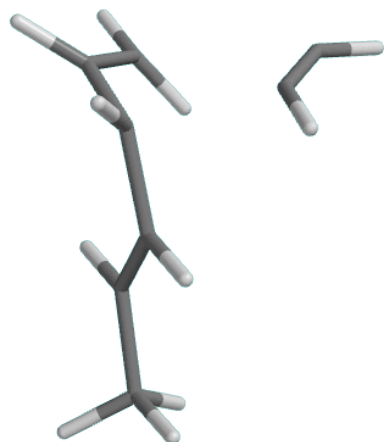
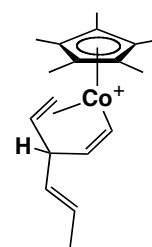
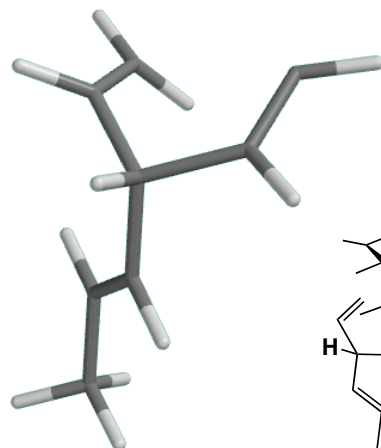


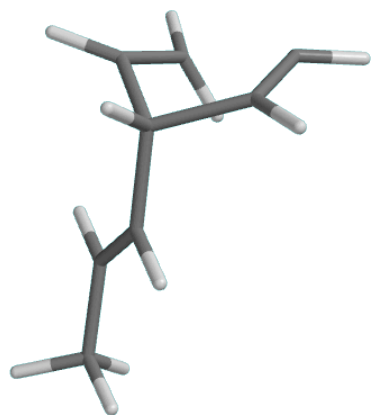
Figure 6.2: Cp*Co(η^5 -1-methylpentadienyl)⁺ Stationary Points (BP86/TZVP) (cont.)



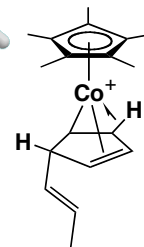
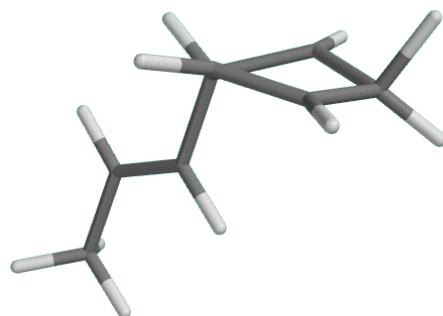
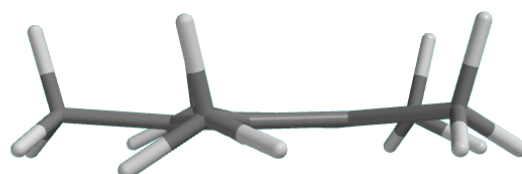
TS1-9



INT9

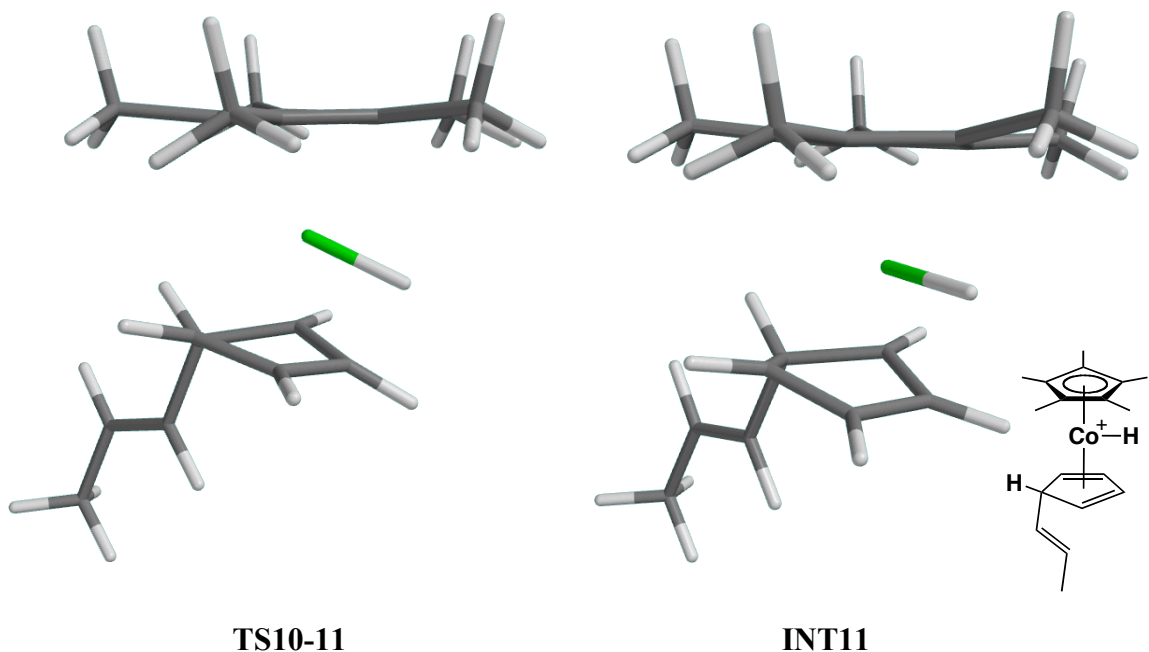


TS9-10



INT10

Figure 6.2: Cp*Co(η^5 -1-methylpentadienyl)⁺ Stationary Points (BP86/TZVP) (cont.)



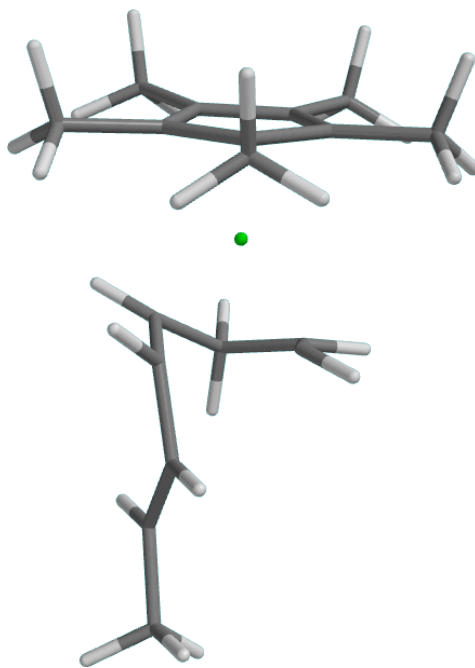
The products of these two insertions (INT2, 1.93 kcal/mol and INT9, 2.47 kcal/mol) are also very close in energy. With such a small difference in TS energies, both modes of insertion may be active. Since we do not observe the formation of products via TS1-9, this step may exist in equilibrium, however, the 34.31 kcal/mol barrier for the reverse process (INT11→INT1) makes this an unlikely possibility. It is more likely that the energy difference between the two TS's is higher than calculated. We explored this region of the energy profile further, locating TS9-10 (8.35 kcal/mol), corresponding to a five-membered ring forming process (Figure 6.2). This TS leads to agostic hydride complex INT10; attempts to locate an unsaturated intermediate were unsuccessful. TS10-11 (-11.46 kcal/mol) leads to the formation of hydride complex INT11 (-13.84 kcal/mol). Spencer and Nehl have shown that from this point, formation of cobaltocenium type products via dehydrogenation is possible.^{125,129} Since placing

compounds of varying charge on the same scale is complicated, we did not explore this portion of the PES further.

Locating the unsaturated product of the first insertion step (INT2, 1.03 kcal/mol) proved difficult and was eventually achieved by locating a geometry closely approximating the minimum by an IRC calculation, followed by further minimization. Perhaps tellingly, initial minimization attempts proceeded directly to the saturated product (INT3), where the pendant olefin is recoordinates to the cobalt-centre; efforts to locate a TS for this transformation were unsuccessful. These data suggest that the PES in this region is flat and the energy barrier to recoordination of the olefin is very low. This observation is not surprising; rotation about C-C single bonds and approach of π -systems to unsaturated metal centres are achievable with little energy cost. Not surprisingly, the saturated INT3 was calculated as a more stable complex than the unsaturated analogue (-11.81 kcal/mol). From INT3, TS3-4 (-5.53 kcal/mol) leads to the kinetic η^2, η^3 -cycloheptadienyl product (INT4) at an energy of -38.18 kcal/mol. From INT2, TS2-10 (11.02 kcal/mol) was also located, leading into the non-productive cyclopentenyl pathway previously described (Figure 6.3).

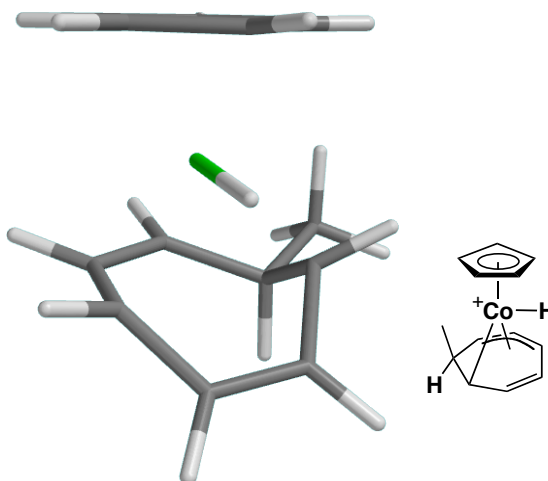
From the allyl/olefin complex, INT4, isomerization to the η^5 -cycloheptadienyl complex was investigated. An $\eta^3 \rightarrow \eta^1$ hapticity change, freeing a coordination site for β -hydride elimination, was investigated by constraining the Co to H separation to shorter distances. Surprisingly, the β -hydride elimination pathway located had an energy barrier of 37.91 kcal/mol (BP86/SV(P)) and did not lead to formation of the proposed η^4 -cycloheptatriene complex **343** (INT6). Instead, the intermediate located was a high-oxidation state Co(V) η^1, η^3 -cycloheptadienyl hydride complex (Figure 6.4). Presumably

Figure 6.3: DFT Structure of TS2-10 (BP86/TZVP)



due to constraints imposed by the cyclic system, $\eta^3 \rightarrow \eta^1$ isomerization is thus disfavoured. While Co(V) species have been proposed as reaction intermediates²⁰⁵ and isolable Co(V) complexes have been reported,²⁰⁶ the high activation barrier makes this pathway unlikely.

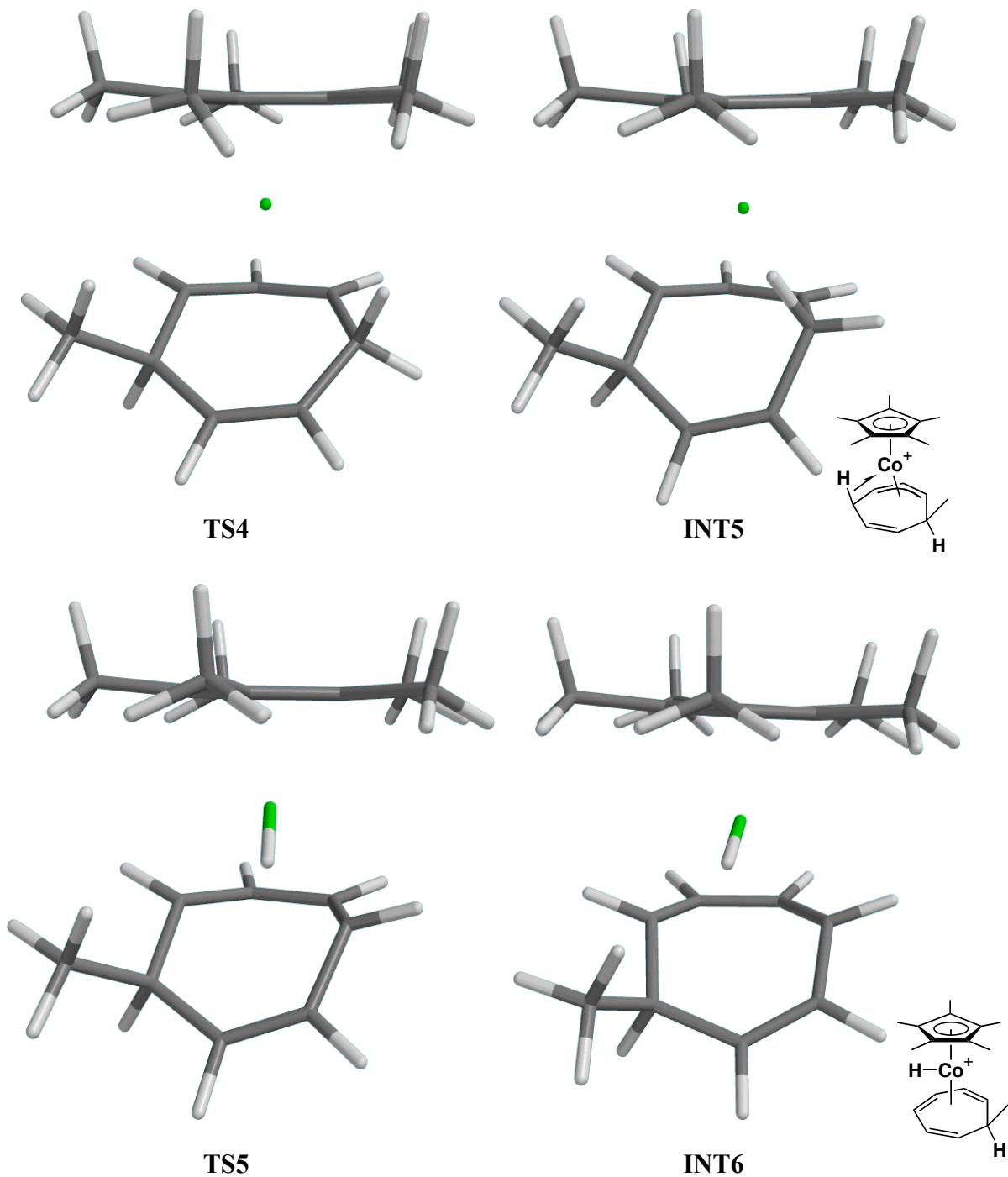
Figure 6.4: CpCoH(η^1, η^3 -1-methylcycloheptadienyl)⁺ (BP86/SV(P))



Alternatively, a coordination site for β -hydride elimination can be freed by olefin dissociation from the η^2, η^3 -cycloheptadienyl complex (Figure 6.5). Modelling this pathway leads to TS4-5, corresponding to dissociation of the olefin ligand, concomitant with the methylene hydrogen rotating towards the metal centre. This pathway has an energy barrier of 22.79 kcal/mol, significantly lower than the $\eta^3 \rightarrow \eta^1$ isomerization pathway, but still high enough to account for isolating the non-conjugated intermediate. This TS leads to INT5 (-25.04 kcal/mol), an agostic complex not previously proposed on the reaction coordinate. This agostic species is connected to cycloheptatriene cobalt hydride complex INT6 (-22.07 kcal/mol) via TS5-6 (-20.53 kcal/mol). TS6-7 (-22.14 kcal/mol),²⁰⁷ connects the hydride complex to a second agostic hydride species (INT7, -31.57 kcal/mol). This agostic species dissociates via TS7-8 (-28.88 kcal/mol), leading to the thermodynamic η^5 -cycloheptadienyl complex INT8. The product energy was optimized at -46.66 kcal/mol, 8.48 kcal/mol lower than the kinetic η^2, η^3 -cycloheptadienyl product.

The dissociative hydride elimination mechanism differs from our previously proposed route and presents a solution to a somewhat troubling experimental observation. Full $\eta^2, \eta^3 \rightarrow \eta^5$ isomerization of acetylene [5+2] cycloadducts can only be achieved at temperatures in excess of 60 °C. However, η^2, η^3 -cycloheptadienyl complexes arising from 2-butyne cycloaddition isomerize rapidly and quantitatively at the 40 °C reaction temperature. Kirk demonstrated that in the Cp series, the corresponding 2-butyne η^2, η^3 -cycloheptadienyl products are unexpectedly thermally stable.¹³⁷ This observation was not easily explained; however, this new mechanistic proposal provides an elegant rationale. The tetra-substituted olefin moiety in the η^2, η^3 -cycloheptadienyl complex

Figure 6.5: Allyl/Olefin Isomerization Stationary Points (BP86/TZVP)



experiences significant steric repulsion from the large Cp* ligand (less so in the Cp series) (Figure 6.6). This repulsion encourages olefin dissociation, raising the energy of

Figure 6.5: Allyl/Olefin Isomerization Stationary Points (BP86/TZVP) (cont.)

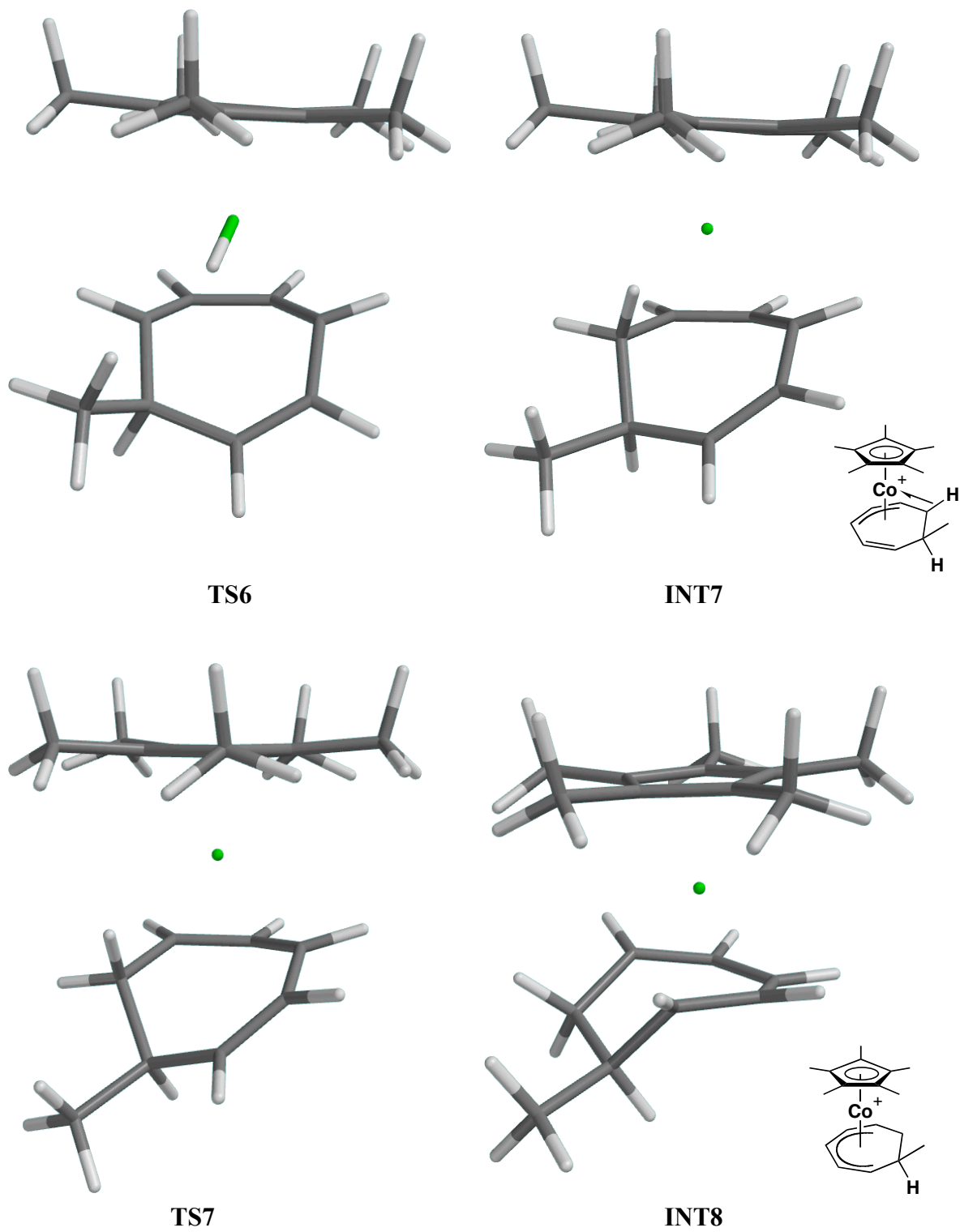
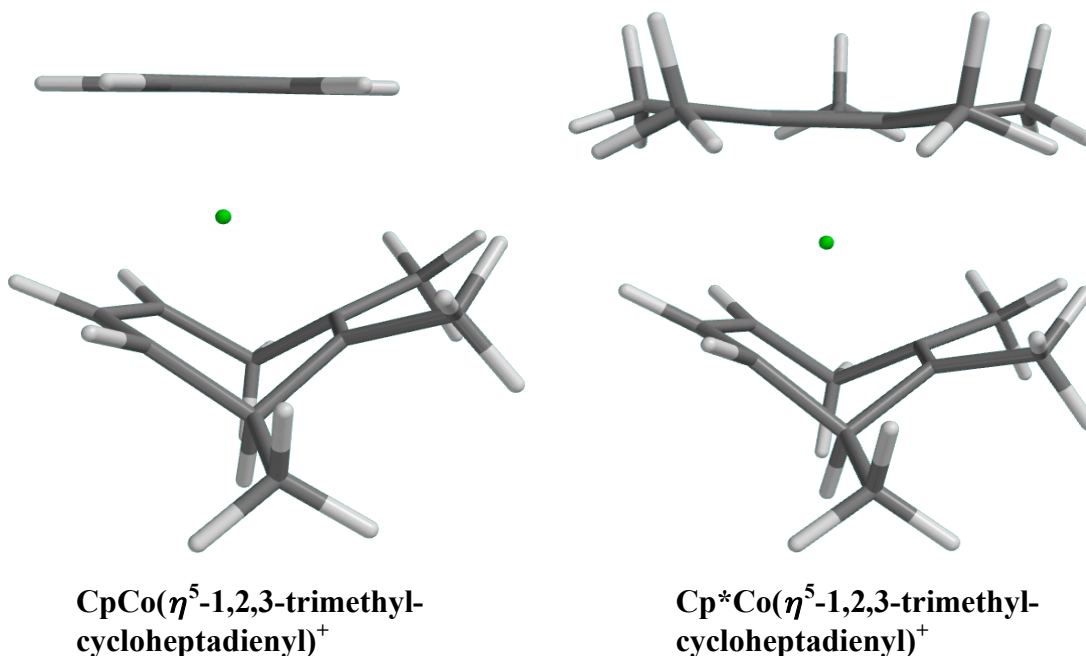


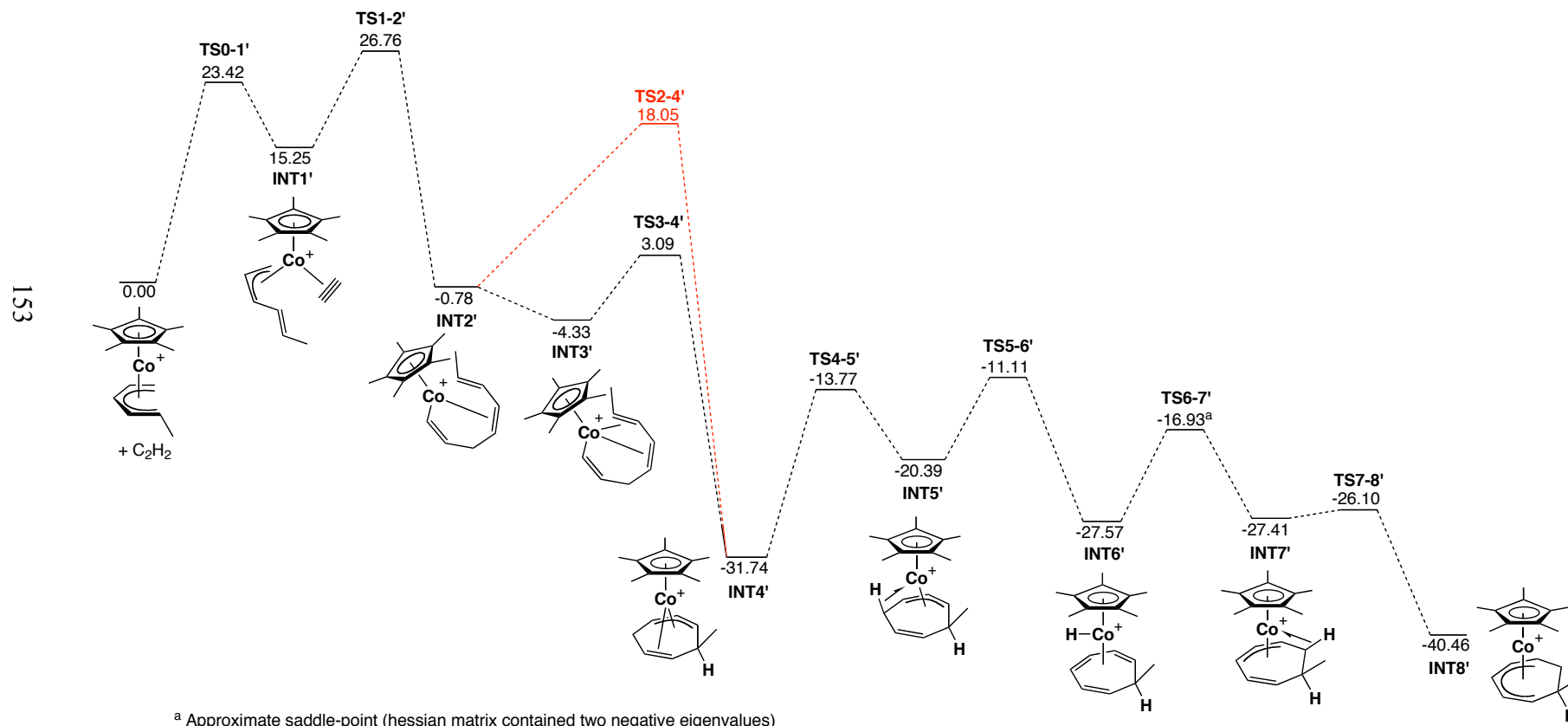
Figure 6.6: Comparison of Allyl/Olefin 2-Butyne Adducts (BP86/TZVP)



the allyl/olefin intermediate. This proposal is borne out in calculations for $\text{CpCo}(\eta^2, \eta^3\text{-1,2,3-trimethylcycloheptadienyl})^+$ and $\text{Cp}^*\text{Co}(\eta^2, \eta^3\text{-1,2,3-trimethylcycloheptadienyl})^+$ complexes: the complex energies are -23.06 and -18.42 kcal/mol, and the average Co-olefin bond distances are 2.218 and 2.170 Å respectively. The $\eta^2, \eta^3 \rightarrow \eta^5$ isomerization barriers for the 2-butyne cycloadducts are 27.16 and 19.03 kcal/mol respectively, with the Cp complex being 8.13 kcal/mol higher.

The potential energy surface generated from B3LYP calculations agrees reasonably well with that obtained from BP86, except in the region surrounding TS1-2' for alkyne insertion (Figure 6.7). The TS energy, 26.76 kcal/mol, was 6.66 kcal/mol higher than that computed via BP86 and predicted to be the rate-limiting step. Similar divergence between the BP86 and B3LYP functionals has been previously observed,²⁰⁸ there ascribed to an artifact of the relative closeness of the singlet and triplet energy

Figure 6.7: Reaction Profile for $\text{Cp}^*\text{Co}(\eta^5\text{-1-methylpentadienyl})^+/\text{Alkyne}$ Cycloaddition (B3LYP/TZVPP Free Energies (kcal/mol))



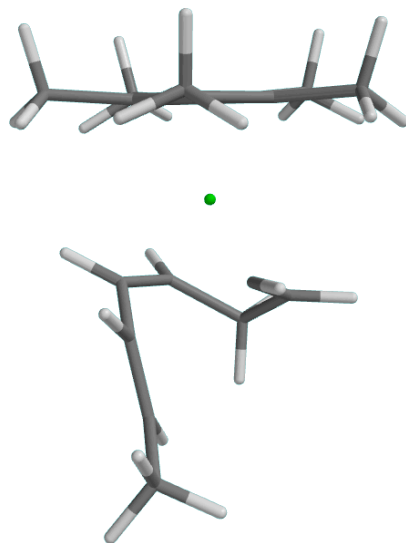
surfaces. Studies of DFT functionals and their use in spin-crossing systems have focused on the high- and low-spin states of Fe(II) and Fe(III) complexes.²⁰⁹ These studies suggest that nonhybrid functionals predict low-spin states that are too stable by approximately 13 kcal/mol (RPBE/COSMO solvent correction).²¹⁰ Alternatively, hybrid functionals over-stabilize high-spin states.²¹¹ Reducing the incorporation of HF exchange, as in the B3LYP* hybrid functional, minimizes these problems, yet results in non-generalizable functionals and does not present an ideal solution to the problem. Rate-limiting alkyne complexation best agrees with our experimental data, therefore we believe the BP86 results are most accurate.

While the computed mechanism fits our experimental observations well, it is immediately apparent that the 26.14 kcal/mol activation barrier calculated for alkyne complexation is high for a facile, room temperature, reaction. The barrier calculated for thermal $\eta^2, \eta^3 \rightarrow \eta^5$ isomerization is 22.79 kcal/mol, 3.35 kcal/mol lower than the room temperature process. The two-thirds entropy solvation correction had the effect of lowering the alkyne complexation energy barrier (TS0-1) by only 2.29 kcal/mol (Ziegler^{202a} has observed decreases of ≈ 4 kcal/mol during olefin complexation to Group 4 metals). Placing an intermolecular reaction on the same scale as intramolecular processes, without accounting for concentration or other effects, may be the source of this discrepancy.

Part C: Alternative Reaction Pathways

As noted, an unexpected second accessible TS state (TS2-4) was located from unsaturated INT2, at an energy of 8.02 kcal/mol (Figure 6.1). This TS corresponds to a C1-C6 bond formation (Figure 6.8), but an IRC leads directly to the allyl/olefin product INT4, passing through points resembling a six-membered carbocyclic diradical²¹² and a six-membered carbocycle fused to a cyclopropane moiety, akin to those shown in Figure 6.10. Unfortunately, these species were not local minima and could not be individually optimized. The inability to locate a TS leading from INT2 to INT3 makes it impossible to say with certainty which reaction mechanism is preferred. However, it is likely the INT2 to INT3 barrier is significantly lower than the 6.09 kcal/mol alternate possibility.

Figure 6.8: DFT Structure of TS 2-4 (BP86/TZVP)



During initial investigations in the Cp system, we encountered an additional variant on this reaction surface (Figure 6.9) that could not be located in the Cp* series. Along with cyclization transition state TS2-4", we located TS2-4a", a TS corresponding to the direct bond formation between C1 and C7 (Figure 6.10). This TS does not lead to the η^2, η^3 -cycloheptadienyl complex normally observed in these reactions, but to the

Figure 6.9: Reaction Profile for $\text{CpCo}(\eta^5\text{-1-methylpentadienyl})^+/\text{Alkyne Cycloaddition}$ (BP86/TZVPP Free Energies (kcal/mol))

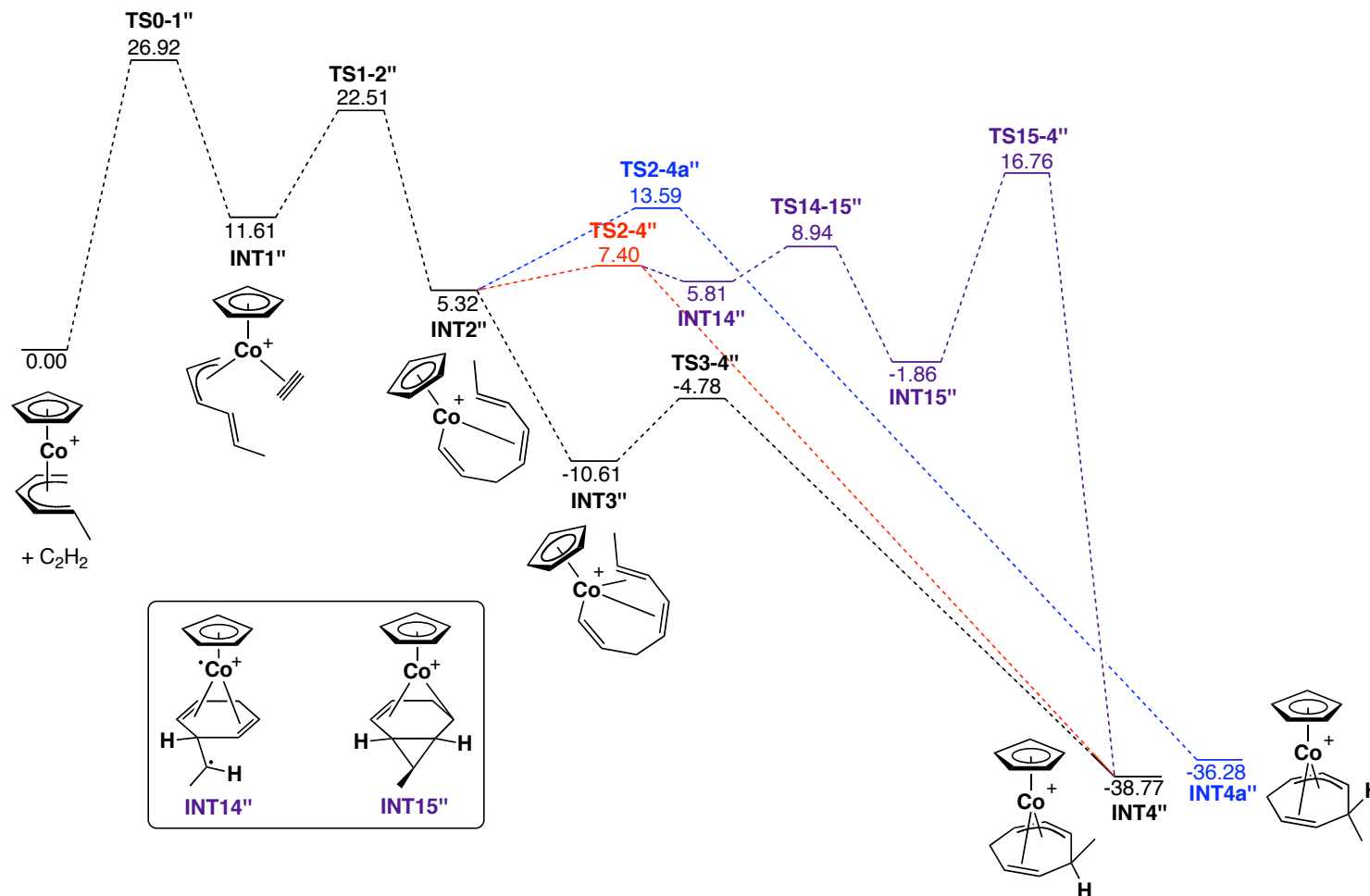
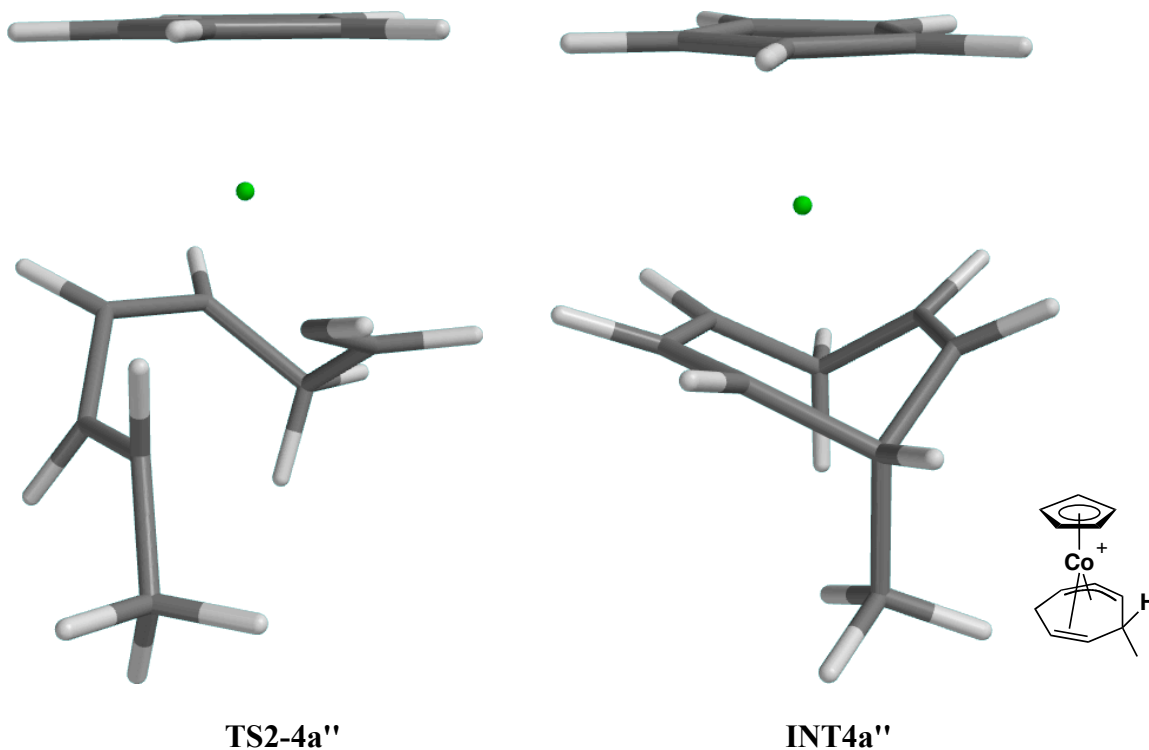


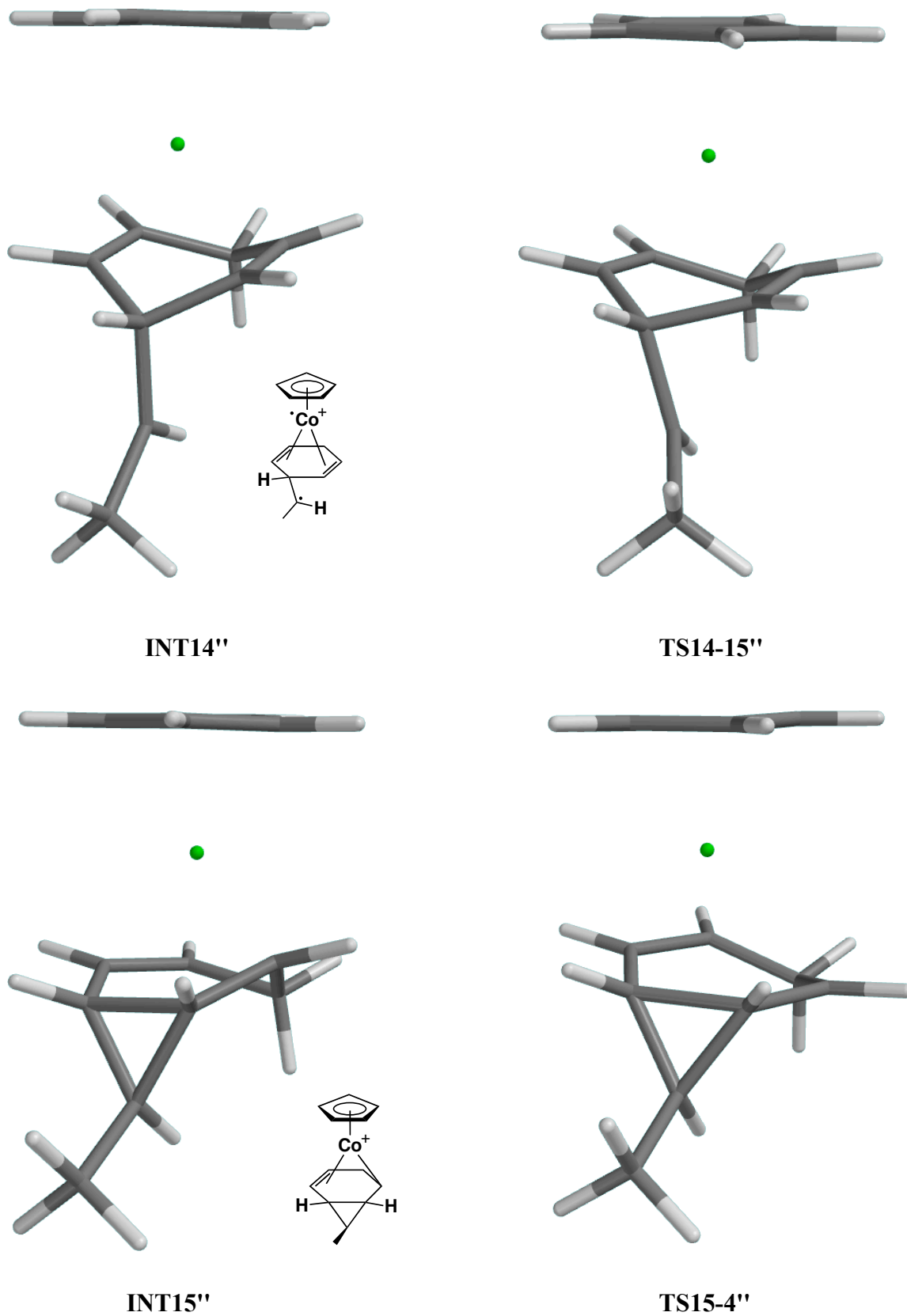
Figure 6.10: Alternate Ring Forming Pathway (BP86/TZVP)



opposite diastereomer INT4a''. Kirk observed the formation of minor products that were very tentatively assigned to those of the unusual diastereomer,²¹³ suggesting there is a possibility that this reaction pathway is accessible in some systems. However, the 8.27 kcal/mol energy barrier makes it unlikely under room temperature conditions, particularly given the barrierless cascade to INT3''.

The diradical nature of the species lying on the IRC connecting TS2-4'' to INT4'' prompted us to investigate the triplet surface in this region. Interestingly, species analogous to those observed on the Cp* singlet surface IRC were now optimized as local minima on the Cp triplet surface (Figure 6.11). Tracing the PES from TS2-4'' leads to six-membered carbocycle INT14'', a complex containing a trigonal planar carbon centre where an unpaired electron is situated. From here, TS14-15'' leading to fused

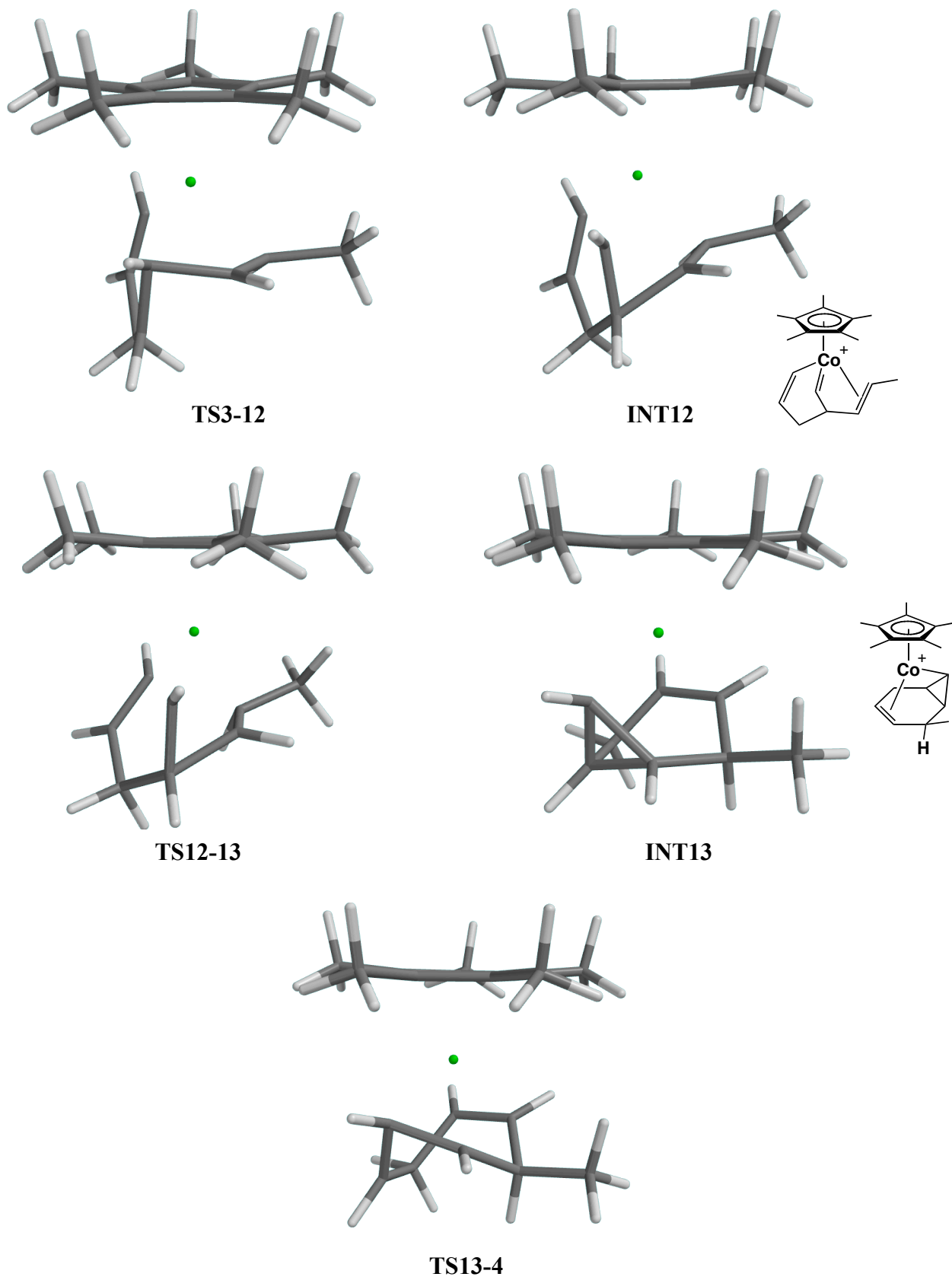
Figure 6.11: Triplet Surface Stationary Points (BP86/TZVP)



cyclopropane system INT15" was located. Cleavage of the C1-C6 bond via TS15-4" leads to the experimentally observed η^2, η^3 -cycloheptadienyl product. The structural similarity between the species on the singlet IRC profile and the intermediates located on the triplet surface is compelling. It is likely that the singlet and triplet PES's are close in energy, raising the possibility that spin-crossings play a role in the reaction mechanism. A corresponding triplet reaction pathway could not be located in the Cp* system, suggesting the higher field ligand stabilizes the singlet-state. Potential competition between reaction pathways in the Cp reaction manifold may be a factor contributing to the low cycloheptadienyl product yield: generation of radical intermediates, particularly in chlorinated solvents, could lead to significant reaction byproducts.

A third seven-membered ring-forming pathway was found in the Cp* manifold, albeit at significantly higher energy (Figure 6.1). This alternate path diverges via TS3-12 (20.49 kcal/mol), leading to cobalt-carbene complex INT12 (18.11 kcal/mol) (Figure 6.12). Reductive elimination via TS12-13 (30.84 kcal/mol) leads to bicyclic [4.1.0] complex INT13 (-6.44kcal/mol). Carbon-carbon bond cleavage via TS13-4 yields the experimentally observed η^2, η^3 -cycloheptadienyl product. Given the high energy barrier, this pathway is probably not accessible. However, cobalt-carbene complexes have been implicated in cyclopentadienyl ring-expansion/[5+2] cycloaddition chemistry;²¹⁴ therefore the identification of such a path in the pentadienyl/alkyne [5+2] cycloaddition reaction is interesting.

Figure 6.12: Alternate Ring Forming Pathway (BP86/TZVP)



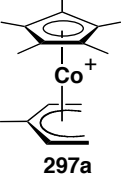
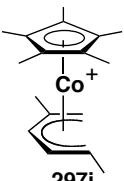
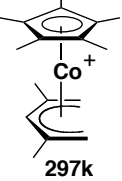
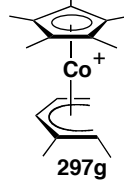
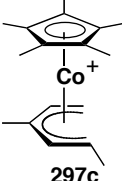
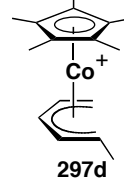
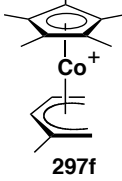
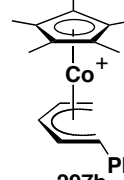
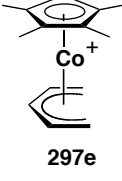
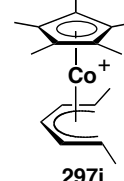
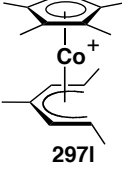
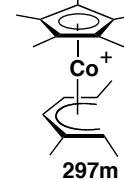
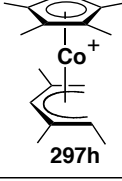
Part D: Reaction Selectivity

As determined from the reaction coordinate of the Cp* system (Figure 6.1), the rate-limiting step appears to be complexation of alkyne. Therefore, while theoretically interesting, the diverging reaction pathways computed are not pertinent to the observed reaction selectivity. We thus computed the acetylene coordination TS geometries for all of the relevant η^5 -pentadienyl complex substitution patterns and ranked them by decreasing relative energy (Table 6.1). This ranking coincides with our experimental observations: the reactive η^5 -1-phenyl-, η^5 -1-methyl-, and η^5 -1,5-dimethylpentadienyl complexes have low TS energies (Entries 10-12), and all of the unreactive species higher. For comparison, we also computed the complexation TS energies for substituted pentadienyl complexes not yet investigated for [5+2] cycloaddition chemistry: η^5 -2,4-dimethyl- (**297k**), η^5 -1,3,5-trimethyl- (**297l**) and η^5 -1,2,5-trimethylpentadienyl (**297m**) complexes (Entries 2, 6, and 13).

From these data, it is immediately apparent that 3-substituents are strongly detrimental to the reaction, raising the activation energies by ≈ 5 kcal/mol (Entry 1 vs. 5, Entry 3 vs. 10, Entry 6 vs. 12). When the space-filling model TS structure for 3-substituted complex **297a** is examined (Figure 6.13), it is evident that the 3-substituent is forced into the space of the Cp* ligand at the TS. This steric interaction will raise the TS energy. Analogous interactions of 1- and 2-substituents with the ancillary ligand are less problematic and not a significant factor.

For the reaction profile calculation, the η^5 -pentadienyl complexes were taken as the reference point for comparison; therefore the computed activation energy differences may be a result of geometric variation in the η^5 -pentadienyl ground states themselves and

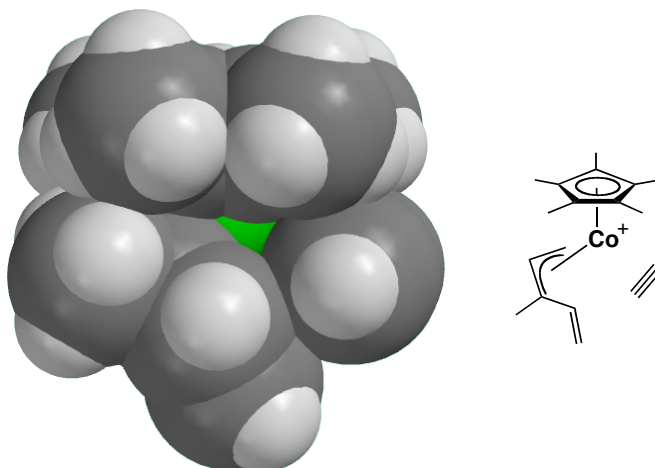
Table 6.1: Comparison of Alkyne Complexation TS Energies, Dihedral Angles, and C1-C5 Separations of η^5 -Pentadienyl Complexes

Entry	Pentadienyl	TS Energy/Dihedral/C1-C5 (kcal·mol ⁻¹ /deg./Å) ^a	Entry	Pentadienyl	TS Energy/Dihedral/C1-C5 (kcal·mol ⁻¹ /deg./Å) ^a
1		34.57 / 11.07 / 2.78	8		28.24 / 7.84 / 2.86 (1.98 / 2.65)
2		32.28 / 13.67 / 2.77	9		26.44 / 9.40 / 2.84 (9.55 / 2.84)
3		30.53 / 8.57 / 2.84	10		26.15 / 7.27 / 2.87 (1.4 / 2.65)
4 ^b		30.26 / 11.58 / 2.79 (11.90 / 2.81)	11 ^c		25.58 / 7.52 / 2.92 (7.6 / 2.86)
5		29.96 / 9.82 / 2.81	12		24.32 / 1.55 / 2.93 (0.36 / 2.88)
6		29.64 / 3.29 / 2.90	13		23.88 / 3.67 / 2.91
7		28.38 / 10.37 / 2.82 (10.28 / 2.82)			

^a X-ray structure data is in parentheses ^b Pentadienyl hessian matrix contained one negative eigenvalue

^c TS hessian matrix contained two negative eigenvalues.

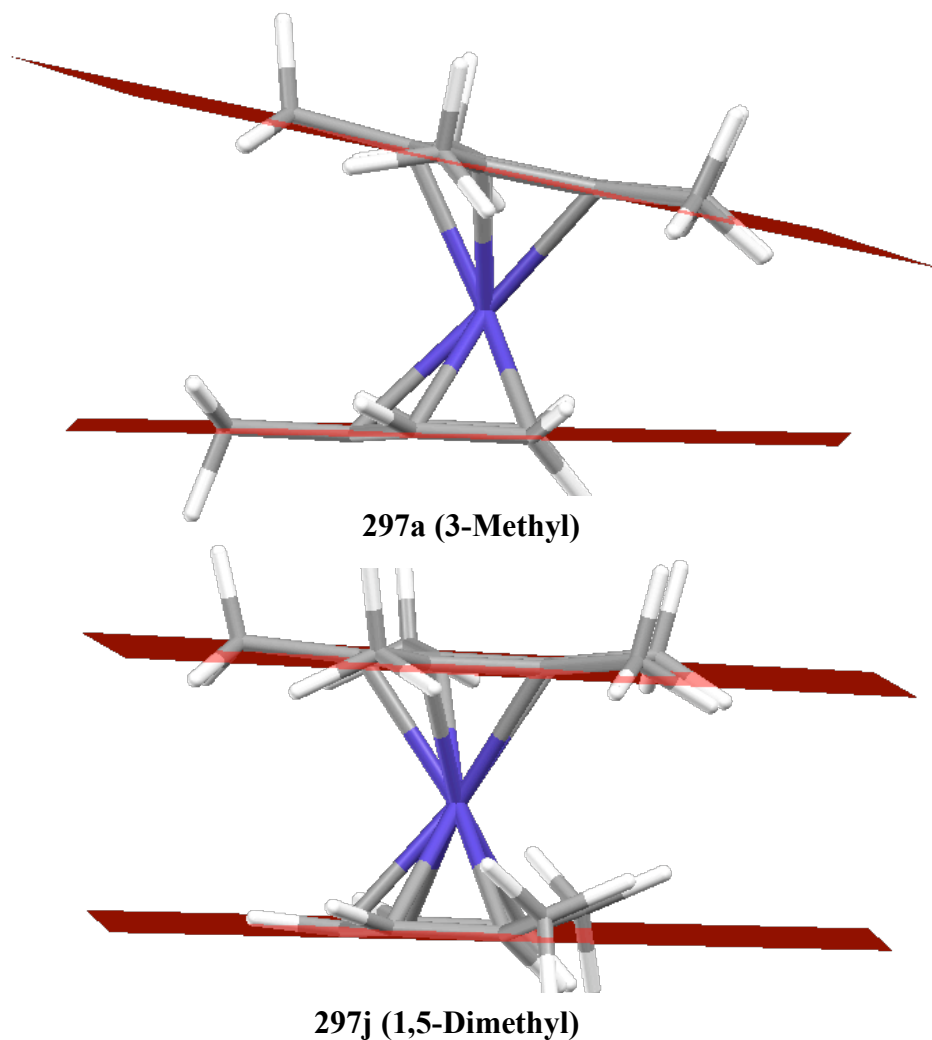
Figure 6.13: Side-On Space-Filling Model of the η^5 -3-Methylpentadienyl/Alkyne Complexation TS (BP86/TZVP)



not a TS effect. The optimized structures of the highest activation energy and unreactive $\text{Cp}^*\text{Co}(\eta^5\text{-3-methylpentadienyl})^+$ complex **297a** and the low energy and reactive $\text{Cp}^*\text{Co}(\eta^5\text{-1,5-dimethylpentadienyl})^+$ complex **297j** were compared. Figure 6.14 shows a side-on comparison of these two complexes. The most obvious structural difference between the species is the dihedral angle between the planes defined by the Cp^* ligand and the η^5 -pentadienyl moiety: 11.07° for the unreactive 3-methyl complex **297a**, and 1.55° for reactive 1,5-dimethyl species **297j**. When the dihedral angles are calculated for the other η^5 -pentadienyl structures, they fall into a series where the reactive complexes have smaller dihedral angles and the unreactive species, while not entirely consistent, are larger. It should be noted that these computational data are most often in good agreement with those determined via X-ray crystallography (Table 6.1).

The unsubstituted η^5 -pentadienyl complex **297e** has a significant 9.82° dihedral, and is taken as the electronically ideal angle between the planes of interest. Substituents at the terminal positions distort the planes toward smaller angles (Entries 6, 12, 13), while

Figure 6.14: Dihedral Angle Comparison of Complexes **297a** and **297j** (BP86/TZVP)



internal substituents lead to larger angles (Entries 1, 2). For alkyne coordination leading to [5+2] cycloaddition, the unreactive complexes with large dihedral angles (*e.g.*, **297a**, **297f**) must initially distort to a coplanar, higher energy, arrangement. Terminal substituents force the η^5 -pentadienyl planes into an initial high-energy alignment, resulting in a corresponding lower TS barrier. The η^5 -1,3,5-trimethylpentadienyl complex **297i** (Entry 6) is predicted to have a high TS energy, despite the small dihedral angle enforced by the terminal substituents. This example demonstrates the significant 3-

substituent steric effect previously noted. Experimental evidence suggests that 1,2,4-trisubstituted pentadienyl complexes are unreactive. Therefore, the prediction that η^5 -1,2,5-trimethylpentadienyl complex **297m** (Entry 13) has a lower TS than the η^5 -1,5-dimethylpentadienyl complex **297j** (Entry 12) is particularly interesting. The dihedral angle between the pentadienyl planes in trisubstituted complex **297m** is 3.67°. Experimental validation of this result would provide significant support for our reactivity proposal.

Ernst has proposed that substituents on the internal carbons of η^5 -pentadienyl ligands improve overlap between the compact, high-oxidation state metal orbitals and the pentadienyl ligand.¹³⁰ A measure of this improved overlap is the C1-C5 separation, where longer distances signify weaker and more reactive Co-C bonds. When calculated, the lowest TS energy complexes consistently have the longest separations, including the hypothetical 1,2,5-trimethyl complex **297m**. The exception to this is the 1,3,5-trimethyl complex **297l**, which has a long C1-C5 separation and a high TS energy, again highlighting the significant inhibitory effect of the 3-substituent.

Part E: Summary and Conclusion

The reaction mechanism of the [5+2] cycloaddition reaction has been computationally explored and several potential reaction pathways, some ancillary ligand-dependant, have been elucidated. In the Cp* system, both standard olefin coordination/insertion and singlet diradical pathways are found, with the former clearly more favourable. Cp systems exhibit these mechanistic possibilities and an additional triplet diradical pathway not located for the higher-field Cp* ligand. This suggests that

Cp* stabilizes the singlet state, ensuring that the reactions remain on the singlet energy surface. These competing reaction pathways offer a rationale for the lower product yield for [5+2] cycloadditions in CpCo(η^5 -pentadienyl)⁺ series: diradical intermediates are highly reactive and may undergo a range of intramolecular and intermolecular side-reactions, including reaction with the CH₂Cl₂ solvent.

The rate-limiting step for the cycloaddition reaction is initial alkyne complexation. Comparison of the η^5 -3-methyl- and η^5 -1,3-dimethylpentadienyl structures with their corresponding alkyne complexation TS's revealed that the steric interaction between the 3-substituent and the ancillary ligand is potentially responsible for the low reactivity of these systems. 1,5-Substituents raise the η^5 -pentadienyl complex's energy, resulting in a correspondingly lower TS energy. Evidence supporting Ernst's proposal that internal substituents reduce reactivity by improving metal/pentadienyl overlap was also obtained.

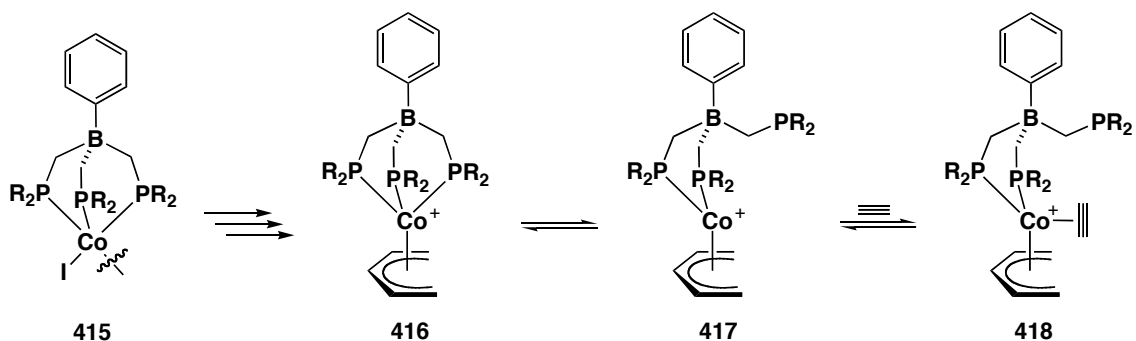
In addition to confirming our experimental observations, we have predicted the structure and reactivity of two pentadienyl complexes not yet reported. The 1,2,5-pentadienyl complex **297m** is predicted to have a complexation TS energy lower than the known reactive 1,5-pentadienyl complex. Our experimental observations of [5+2] cycloaddition had suggested that trisubstituted complexes are uniformly unreactive, yet computational investigations suggest a direction for research we would not have considered otherwise. If this proves to be accurate, a pathway to significant extension of the [5+2] reaction scope has been elucidated, marking an equally significant use of theory to make unexpected, yet synthetically useful, predictions.

Chapter 7: Tripodal Phosphine Ligand Investigation

Part A: Introduction

Tolerating pentadienyl substituents only at the C1 and C5 positions limits the scope of the cobalt-mediated [5+2] cycloaddition reaction. DFT investigations suggest this limitation is the result of high transition state energies for dissociative alkyne coordination. Pentadienyl $\eta^5 \rightarrow \eta^3$ isomerization is only one possibility for vacant site generation; ancillary ligand isomerization is a second possibility. While not impossible,²¹⁵ $\eta^5 \rightarrow \eta^3$ isomerization of Cp and Cp* ligands is not generally facile. Indenyl ancillary ligands ring slip readily, however the preferred (η^5 -indenyl)Co(CH₂CH₂)₂ starting material for η^5 -pentadienyl synthesis is thermally unstable.²¹⁶ Peters has reported a novel class of anionic tripodal phosphine ligands **415**.²¹⁷ We hypothesize that these ligands can undergo reasonably facile $\kappa^3 \rightarrow \kappa^2$ isomerization, thereby freeing a coordination site at the metal. Subsequent alkyne coordination and insertion may occur in a fashion analogous to the Cp* system (Scheme 7.1).

Scheme 7.1



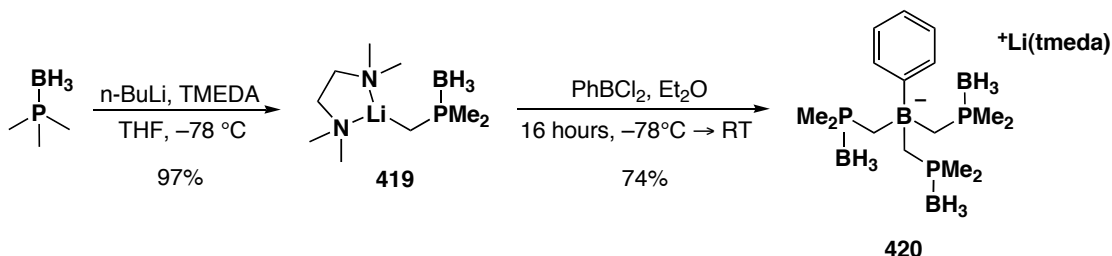
Part B: Synthetic Investigation

Peters has prepared tripodal phosphine cobalt halide dimers of the type **415** (R = Ph, ⁱPr). We investigated sodium amalgam reduction of these species in the presence of ethylene, butadiene, or 2-butyne, but these reactions did not yield tractable products. The X-ray structures of cobalt complexes **415** suggest that the large Ph or ⁱPr substituents encapsulate the cobalt atom and prevent coordination of the π -system after reduction. The significantly less sterically crowded complex **415** (R = Me) may be small enough to permit olefin coordination, however, the requisite tripodal phosphine ligand has not been reported.

We assumed that this ligand could be prepared in a fashion analogous to that used for the Ph and ⁱPr analogues. We prepared $\text{LiCH}_2\text{P}(\text{CH}_3)_2$ ²¹⁸ and quenched it with PhBCl_2 in a 3:1 molar ratio. Only intractable mixtures were obtained, with attempts to purify the product via crystallization or complexation to CoCl_2 unsuccessful. A report from the Peters group²¹⁹ on bisphosphinodiaryl borate ligand preparation noted that attempts to prepare the dimethylphosphino ligand were unsuccessful. This observation was attributed to the propensity of phosphorous and trivalent boron to form strongly bound Lewis acid/base pairs. Similar reactivity has been observed in aluminum systems.²²⁰ Protection of the phosphine as a borane adduct eliminated the synthetic difficulties. We adapted this solution to the tripodal system, preparing the $\text{Me}_3\text{P}\cdot\text{BH}_3$ complex,²²¹ followed by deprotonation with $\text{BuLi}\cdot\text{TMEDA}$ at $-78\text{ }^\circ\text{C}$ (Scheme 7.2). The resultant $\text{TMEDA}\cdot\text{LiCH}_2(\text{Me})_2\text{P}\cdot\text{BH}_3$ salt **419** was initially isolated to confirm product formation through NMR spectroscopy, and was thereafter used *in situ*. Subsequent addition of PhBCl_2 and crystallization from hexane yielded analytically pure tripodal

borate complex **420**, characterized by NMR spectroscopy, mass spectrometry and elemental analysis.

Scheme 7.2

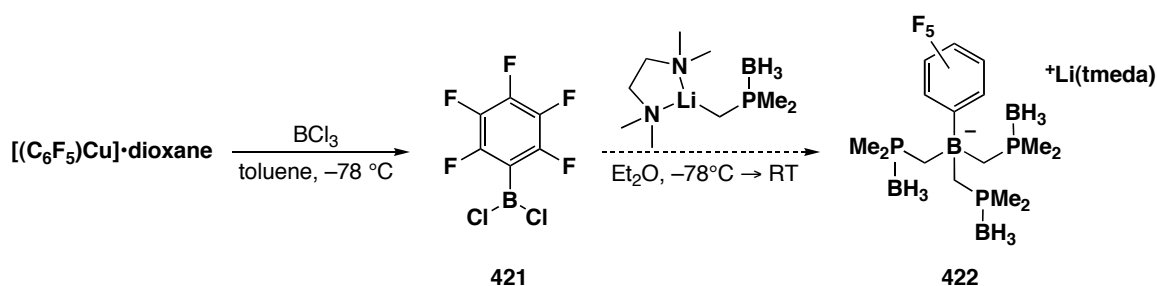


Peters reported considerable difficulty removing the borane protecting group(s). We encountered similar difficulties, obtaining no reaction or decomposition under various deprotection conditions (competitive borane decomplexation using DABCO, protonolysis with acids such as $\text{HBF}_4 \cdot \text{OEt}_2$, TFA, and MeOH). We attempted to exploit the hydridic nature of the borane adduct for a novel deprotection procedure with little success: hydride acceptors such as acetone, crotonaldehyde, and benzaldehyde failed to react. Only with paraformaldehyde was any reactivity observed. In the ^{31}P NMR spectrum of the crude reaction product, resonances in the region corresponding to phosphine oxides were observed, implying cleavage of the borane-protecting group. Careful exclusion of oxygen did not eliminate the formation of these products and their oxide identity is unconfirmed.

This resistance to common deboration conditions is surprising. We propose that electron donation from the anionic boron raises the phosphine basicity. Therefore, the incorporation of an electron withdrawing aryl borate group (*e.g.*, **422**) should lower the basicity, perhaps enough to render the adducts reactive. The pentafluorobenzene transfer agent $[(\text{C}_6\text{F}_5)\text{Cu}]_4$ was prepared from $\text{C}_6\text{F}_5\text{Br}$ and CuBr via Grignard reaction,²²²

then added to BCl_3 to give the known $(\text{C}_6\text{F}_5)\text{BCl}_2$ (Scheme 7.3).²²³ As reported, a mixture of the mono-, di-, and triarylated boron compounds is obtained. We were unable to isolate the monoarylated product in pure form and the product yield was very low. An improved method for the ligand synthesis is clearly required, yet was considered beyond the scope of our current objectives. This is an area that may be suited for further investigation by subsequent researchers.

Scheme 7.3



Part C: DFT Investigation

The unexpected complications during tripodal ligand synthesis prompted a brief DFT evaluation of this ligand to help determine if this direction for synthetic exploration is justified theoretically. We first studied the proposed alkyne complexation mechanism (Scheme 7.1). To reduce computational cost, the aryl moiety of the tripodal ligand is modeled as a methyl group. In our proposed reaction pathway, phosphine arm dissociation liberates a coordination site. We were unable to locate a TS corresponding to such a step, and the unsaturated κ^2 -product could not be structurally optimized in either singlet or triplet electronic states. Similarly, a TS corresponding to alkyne complexation could not be found. The η^5 -pentadienyl/alkyne complexation product was, however, located as a minimum (Figure 7.1). Surprisingly, the alkyne coordination is

Figure 7.1: (κ^3 -Trisphosphine)Co(η^5 -Pentadienyl) Complex and (κ^2 -Trisphosphine)Co(η^5 -Pentadienyl)/Alkyne Complex (BP86/TZVP)

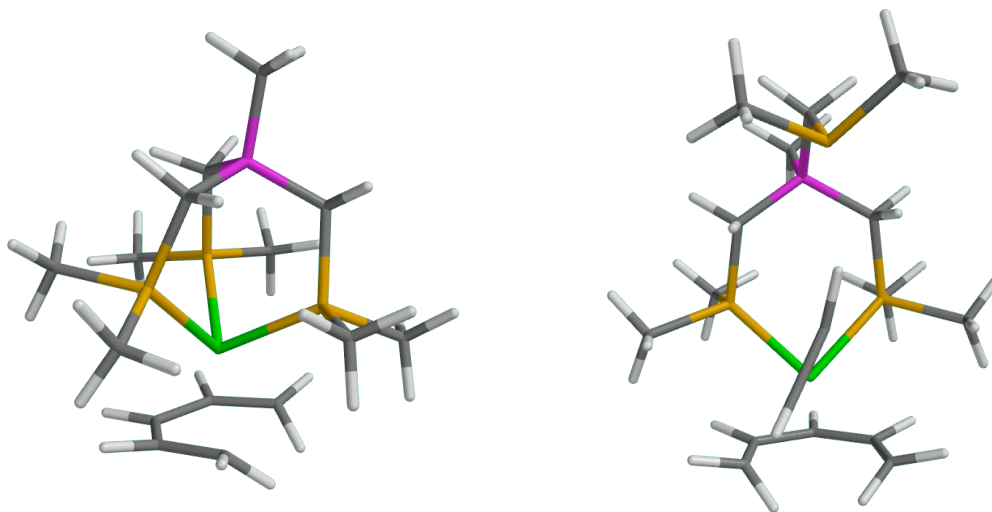
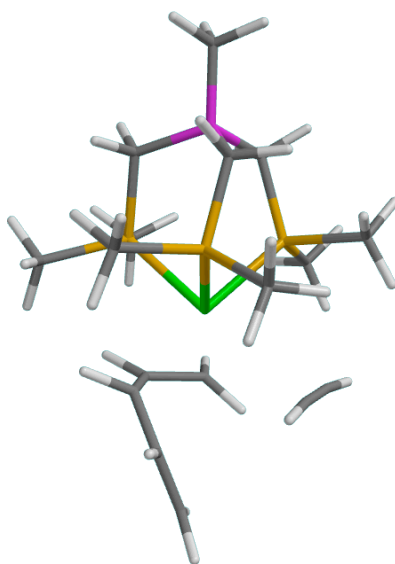


Figure 7.2: Alkyne Complexation TS with Tripodal Ligand (BP86/TZVP)

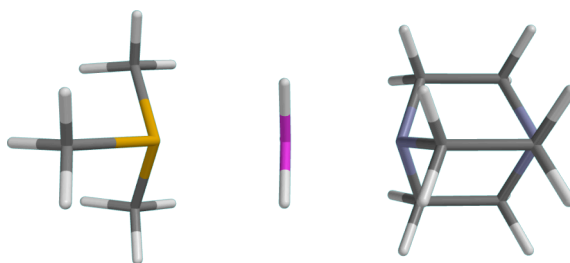


nearly vertical in comparison to the horizontal mode of the cyclopentadienyl alkyne complexes (Figure 6.2). From this intermediate, we were unable to locate a TS for alkyne insertion and the proposed intermediate products could not be optimized. For direct comparison, the tripodal phosphine alkyne complexation TS analogous to that for unsubstituted cyclopentadienyl systems (TS0-1 in Figure 6.1) was optimized (Figure 7.2).

The calculated barrier (33.12 kcal/mol) is significantly higher than that calculated for the Cp* analogues, suggesting this mechanistic pathway is not accessible. Together, these data suggest our mechanistic proposal is unlikely to be successful and the tripodal ligand system will not address the limitations of the [5+2] cycloaddition reaction. However, experimental confirmation is still required.

The tripodal borate ligands will have utility in systems beyond cycloaddition, and as such, the preparation of the tripodal dimethylphosphino methyl ligand is still of significant value. The most promising route proposed to access the methylphosphino tripodal ligand is that from deprotection of the borane complexes **420** or **422**. We computationally probed the resistance of these complexes to the widely used DABCO deprotection conditions. Geometry optimizations were conducted at the BP86/TZVP level, with improved single point energies obtained from these geometries at the BP86/TZVPP level. Solvent corrections were not applied, however a 2/3 entropy correction was used to better approximate the solution state entropy. We first optimized the TS for DABCO-mediated deprotection of Me₃P•BH₃ as a reference point, and found an activation barrier of 23.35 kcal/mol (Figure 7.3). In comparison, the energy barrier for

Figure 7.3: Transition State for PMe₃•BH₃ Deprotection (BP86/TZVP)



deprotection of borane protected ligand **420** was 27.52 kcal/mol. The higher barrier is consistent with our experimental observations. The deprotection TS energy for the perfluorinated ligand **422**, contrary to expectations, was 27.78 kcal/mol, 0.26 kcal/mol

higher than the non-flourinated ligand **420**. This finding suggests that electron donation from the borate to the phosphine atoms is not the cause of the high deprotection barrier; the barrier is thus unlikely to be decreased by the use of an electron withdrawing aryl group.

Part D: Conclusion

The preparation of η^5 -pentadienyl complexes with tripodal phosphine ligands will likely require ligands with less bulky phosphine substituents than those currently reported in the literature. A novel synthetic procedure for the dimethylphosphinomethyl tripod ligand is required. Deprotection of borane-protected trisphosphinoborate complex **420** does not currently present a viable route. Unfortunately, DFT calculations suggest that the difficulties encountered during the deprotection of borate complex **420** will not be addressed by the incorporation of an electron withdrawing aryl group on the borate ligand. While convincing theoretical support for the proposed $\kappa^3 \rightarrow \kappa^2$ isomerization mechanism could not be obtained, the potential utility of the methylated tripodal ligand in other applications justifies further synthetic efforts.

Chapter 8: Experimental

Part A: General Experimental

Reagents and Methods. All manipulations on air sensitive compounds were performed under argon or nitrogen atmosphere using standard Schlenk techniques or in a MBraun LABmaster drybox. Diethyl ether and tetrahydrofuran were distilled from sodium/benzophenone ketyl under nitrogen. Pentane was distilled from potassium/benzophenone ketyl under nitrogen. Dichloromethane and acetonitrile were distilled from calcium hydride and deoxygenated. Acetone was dried over boric oxide, degassed *via* three freeze-pump-thaw cycles, vacuum transferred and stored under nitrogen. DMSO was dried over CaH₂, distilled under nitrogen and stored in a glass storage bomb. All other reagents were used without further purification. Flash column chromatography was performed with Silicycle silica gel (40 – 63 μm), neutralized with 1 mL of triethylamine for acid-sensitive compounds. Alumina filtrations were performed with Sigma-Aldrich neutral aluminum oxide, Brockman I, standard grade, 150 mesh, 58 Å, deactivated to Activity IV with 10 wt.% water. Photolysis reactions were performed with a Hanovia 450 watt high-pressure mercury lamp filtered through Pyrex or a Rayonette UV reaction carousel. The terms “reaction bomb” or “bomb” refer to a thick walled glass vessel fitted with a Teflon vacuum stopcock capable of withstanding moderately elevated internal pressure.

IR spectra were recorded on either a Nicolet Magna 750 FTIR spectrometer or a Nic-Plan FTIR microscope. ¹H NMR, ¹³C NMR, ³¹P NMR, ¹⁹F NMR and ¹¹B NMR spectra were recorded on either a Varian Unity-Inova 300 (¹H, 300 MHz), Varian Unity-

Inova 400 (^1H , 400 MHz; ^{13}C , 100 MHz; ^{31}P , 162 MHz; ^{11}B , 128 MHz; ^{19}F , 376 MHz), Varian Mercury 400 (^1H , 400 MHz; ^{13}C , 100 MHz), Varian Unity-Inova 500 (^1H , 500 MHz; ^{13}C , 125 MHz), Varian DirectDrive 500 (^1H , 500 MHz; ^{13}C , 125 MHz), or a Varian Unity-Inova 600 (^1H , 600 MHz) spectrometer. High-resolution mass spectra, performed by the University of Alberta Mass Spectrometry Facility, were obtained on an Applied Biosystems Mariner Biospectrometry Workstation (electrospray ionization) or a Kratos Analytical MS-50G workstation (electron impact ionization) with an ionization energy of 70 eV. Elemental analyses were performed by the University of Alberta Microanalysis Laboratories, using a Carlo Erba Instruments CHSN-O EA1108 Elemental Analyzer. X-Ray diffraction data was recorded on a Bruker Platform diffractometer with a SMART 1000 CCD area detector at $-80\text{ }^\circ\text{C}$. Data collection, structure solution, and refinements were performed by Drs. Robert McDonald and Michael J. Ferguson of the University of Alberta X-Ray Crystallography Laboratory. Crystals suitable for X-ray crystallography were often grown with a technique herein referred to as “two-chambered liquid diffusion”. In this method, a small quantity of material is dissolved in a single solvent and placed in a small glass crystallization tube, then topped up with additional solvent if needed. The tube is sealed with an NMR-tube cap that is perforated once with a narrow-gauge needle. This tube is placed in a large sample vial and immersed in a second solvent in which the complex has minimal solubility. Due to the very slow diffusion rate via the pinhole, several weeks may be required to achieve complete crystallization.

All DFT geometry optimizations were performed at either the BP86¹⁹⁵/TZVP¹⁹⁹ level or the b3-lyp¹⁹⁶/TZVP level as implemented in the *Turbomole* (Version 5) computational software package.¹⁹⁷ Improved single-point energies were obtained from

the TZVP optimized geometries at the TZVPP²⁰⁰ basis set level and a COSMO solvent correction ($\epsilon = 9.1$)²⁰¹ applied. Solvent-state entropies were estimated as 2/3 the value calculated in the gas-phase.²⁰² Vibrational analyses were performed to confirm the nature of all stationary points and to obtain thermal corrections (enthalpy and entropy for 273 K, 1 bar, gas phase) to produce the final free-energy values. Atomic coordinates in the .xyz file format for all stationary points are available upon request from Prof. J. M. Stryker of the University of Alberta Chemistry Department.

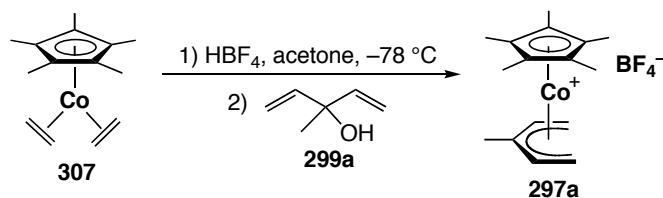
Further Notes on Spectroscopic Methods. ¹H NMR chemical shifts are reported relative to residual protiated solvent. ¹³C NMR chemical shifts are reported relative to the deuterated solvent. ³¹P NMR, ¹¹B NMR, and ¹⁹F NMR chemical shifts are reported relative to the calculated value for IUPAC reference standards (³¹P NMR: H₃PO₄, ¹¹B NMR: BF₃•OEt₂, ¹⁹F NMR: CFCl₃). All spectra were recorded at 27 °C. Values of the coupling constants are obtained directly from the spectrum. Although generally measured to ± 0.1 Hz, *J* values are self-consistent to only ± 0.5 Hz. GCOSY denotes the standard COSY experiment, acquired using field gradients. Data for the ¹H-¹H COSY or GCOSY is presented such that correlations are listed only once.

Materials. Compounds prepared by published procedures: 3-methyl-1,4-pentadiene-3-ol (**299a**),¹⁴⁴ *E*-1-phenyl-1,4-pentadien-3-ol (**299b**),¹⁴⁵ *E,E*-5-phenyl-2,4-pentadien-1-ol (**300b**),¹⁴⁶ *E,E*-3-methyl-2,4-hexadien-1-ol (**300c**),¹⁴⁷ *E,E*-2-methyl-2,4-hexadien-1-ol (**300d**),¹⁴⁸ *E,E*-3,5-heptadien-2-ol (**300e**),¹⁴⁹ *E*-2-methyl-3,5-hexadien-2-ol (**300f**),¹⁵⁰ Cp*Co(CH₂CH₂)₂ (**307**),²²⁴ 1-bromo-3-butene (**354a**),¹⁶⁶ 1-bromo-4-pentene (**354b**),¹⁶⁶

dimethyl 2-(but-3-en-1-yl)malonate (**355a**),¹⁶⁷ dimethyl 2-(pent-4-en-1-yl)malonate (**355b**),¹⁶⁷ *E*-dimethyl 2-(5-oxopent-3-en-1-yl)malonate (**356a**),¹⁴³ 2-(but-3-en-1-yl)-2-methyl-1,3-dioxolane (**360**),¹⁷⁰ *E*-6-bromohex-2-enal (**397**),¹⁷⁷ *E*-2-((5-iodopent-4-en-1-yl)oxy)tetrahydro-2*H*-pyran (**404**),¹⁷⁹ Me₃P•BH₃.²²¹

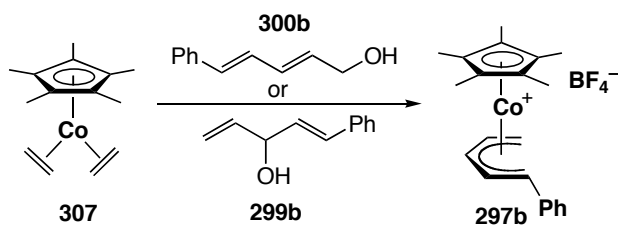
Part B: Experimental Details

I. Chapter 2



[Cp*Co(η^5 -3-methylpentadienyl)]⁺BF₄⁻ (**297a**). In the drybox, Cp*Co(C₂H₄)₂ (111 mg, 0.44 mmol) was dissolved in acetone (10 mL) and placed in a Schlenk tube equipped with a stir-bar and septum. The sealed flask was removed to the Schlenk line, cooled to –78 °C in a dry ice/acetone bath and HBF₄•Et₂O (53 μ L, 0.44 mmol) was added. Upon addition of HBF₄, an immediate colour change from red to black was observed. The reaction was allowed to stir under argon for 15 minutes, then 3-methyl-1,4-pentadien-3-ol (**299a**) (48 mg, 0.49 mmol) was added via syringe. The reaction mixture was then allowed to warm to room temperature overnight. A gradual colour change from black to red occurred. The solvent was removed *in vacuo* and the product purified on the bench by silica gel chromatography using 3% MeOH/CH₂Cl₂. The red fraction was collected and dried to yield 52 mg (37%) of product as a sticky red solid. Crystallization via two-chambered liquid diffusion using CH₂Cl₂ and Et₂O provided red crystals suitable for

combustion analysis. IR (neat, cm^{-1}): 3648 (w), 3556 (w), 2968 (w), 2920 (w), 1818 (w), 1522 (w), 1470 (m), 1383 (m), 1283 (w), 1208 (w), 1052 (s); ^1H NMR (400 MHz, CDCl_3): δ 4.91 (t, $J_{1-2} = J_{1-3} = 10.6$ Hz, 2H, H_1), 3.25 (dd, $J_{2-1} = 9.5$ Hz, $J_{2-3} = 3.0$ Hz, 2H, H_2), 2.29 (s, 3H, Me), 1.89 (s, 15H, C_5Me_5), 1.72 (dd, $J_{3-1} = 11.9$ Hz, $J_{3-2} = 3.1$ Hz, 2H, H_3); ^1H - ^1H GCOSY (400 MHz, CDCl_3): δ 4.91 (H_1) \leftrightarrow δ 3.25 (H_2), 1.89 (H_3); δ 3.25 (H_2) \leftrightarrow δ 1.89 (H_3); $^{13}\text{C}\{^1\text{H}\}$ NMR (100 MHz, CDCl_3): δ 112.3, 98.9, 97.5, 64.4, 21.0, 9.6; Electrospray MS m/z calculated for $\text{C}_{16}\text{H}_{24}\text{Co}$ ($\text{M}^+ - \text{BF}_4^-$): 275.12045; found: 275.12032 (100%); Analysis calculated for $\text{C}_{16}\text{H}_{24}\text{CoBF}_4$: C, 53.07%; H, 6.68%; found: C, 52.71%; H, 6.59%.

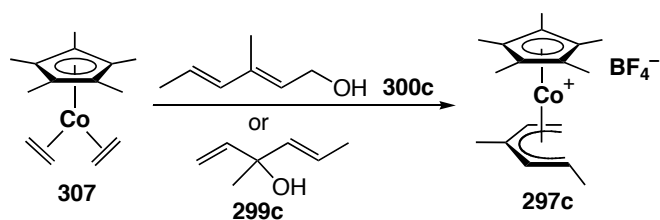


[Cp*Co(η⁵-1-phenylpentadienyl)]⁺BF₄⁻ (297b). Method 1. In the drybox, Cp*Co(C₂H₄)₂ (772 mg, 3.1 mmol) was dissolved in acetone (10 mL) and placed in a Schlenk tube equipped with a stir-bar and septum. The sealed flask was removed to the Schlenk line, cooled to -78 °C in a dry ice/acetone bath and HBF₄•Et₂O (424 μL , 3.1 mmol) was added. Upon addition of HBF₄, an immediate colour change from red to black was observed. The reaction was allowed to stir under argon for 15 minutes, then 1-phenyl-1,4-pentadiene-3-ol (**299b**) (542 mg, 3.4 mmol) in acetone (1 mL) was added via syringe. The reaction mixture was allowed to warm to room temperature overnight and a gradual colour change from black to red occurred. The solvent was removed *in vacuo* and the product purified on the bench by silica gel chromatography using 3%

MeOH/CH₂Cl₂. The red fraction was collected and dried to yield 1.03 g (80%) of product as a dark-purple solid. Crystallization via two-chambered liquid diffusion using CH₂Cl₂ and Et₂O provided black crystals suitable for combustion and X-ray analysis.

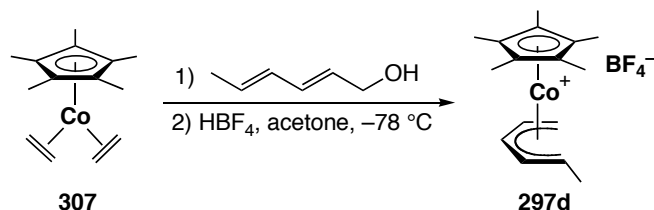
Method 2. In the dry box, a Schlenk tube was charged with Cp*Co(CH₂CH₂)₂ (89 mg, 0.36 mmol) in acetone (10 mL), then removed to the Schlenk line. To this, *E,E*-1-phenyl-1,3-pentadiene-5-ol (**300b**) (57 mg, 0.36 mmol) was added via syringe and heated to reflux under an argon atmosphere for 3 hours, resulting in a brown solution. This solution was cooled to -78 °C in a dry ice/acetone bath and HBF₄•OEt₂ (49 μL, 0.36 mmol) added, then allowed to warm gradually to room temperature overnight (≈ 16 h). The solvent was removed *in vacuo* and the residue purified on the bench by silica gel chromatography using 3% MeOH/CH₂Cl₂. The red fraction was collected and dried to yield 123 mg (81%) of product as a sticky red solid. IR (neat, cm⁻¹): 3063 (w), 2989 (w), 1486 (w), 1418 (w), 1388 (w), 1286 (w), 1262 (w), 1212 (w), 1190 (w), 1161 (w), 1054 (s), 949 (w), 878 (w), 810 (w), 759 (w), 695 (w); ¹H NMR (400 MHz, CDCl₃): δ 7.44 (m, 5H, Ph), 6.78 (t, *J*₃₋₂ = *J*₃₋₄ = 7.2 Hz, 1H, H₃), 6.23 (dd, *J*₂₋₁ = 12.8 Hz, *J*₂₋₃ = 7.1 Hz, 1H, H₂), 5.16 (ddd, *J*_{4-5anti} = 11.1 Hz, *J*_{4-5syn} = 9.4 Hz, *J*₄₋₃ = 7.5 Hz, 1H, H₄), 3.34 (dd, *J*_{5syn-4} = 9.6 Hz, *J*_{5syn-5anti} = 3.4 Hz, 1H, H_{5syn}), 2.98 (d, *J*₁₋₂ = 12.8 Hz, 1H, H₁), 2.06 (dd, *J*_{5anti-4} = 11.7 Hz, *J*_{5anti-5syn} = 3.3 Hz, 1H, H_{5anti}), 1.61 (s, 15H, C₅Me₅); ¹H-¹H GCOSY (400 MHz, CDCl₃): δ 6.78 (H₃) ↔ δ 6.23 (H₂), 5.16 (H₄); δ 6.23 (H₂) ↔ 2.98 (H₁); δ 5.16 (H₄) ↔ δ 3.34 (H_{5syn}), 2.06 (H_{5anti}); δ 3.34 (H_{5syn}) ↔ δ 2.06 (H_{5anti}); ¹³C{¹H} NMR (100 MHz, CDCl₃): δ 134.8, 129.6, 129.5, 128.7, 100.0, 98.4, 94.8, 92.5, 85.5, 64.1, 9.2; Electrospray MS *m/z* calculated for C₂₁H₂₆Co (M⁺ - BF₄): 337.13610; found: 337.13619 (100%); Analysis calculated for C₂₁H₂₆CoBF₄: C, 59.46%; H, 6.18%;

found: C, 59.58%; H, 6.29%.



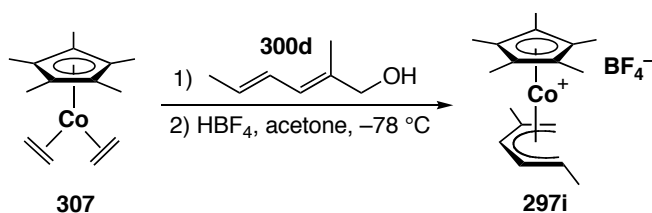
[Cp*Co(η⁵-1,3-dimethylpentadienyl)]⁺BF₄⁻ (297c). Method 1. In the drybox, Cp*Co(C₂H₄)₂ (60 mg, 0.24 mmol) was dissolved in acetone (8 mL) and placed in a Schlenk tube equipped with a stir-bar and septum. The sealed flask was removed to the Schlenk line, cooled to -78 °C in a dry ice/acetone bath and HBF₄•Et₂O (33 μL, 0.24 mmol) was added. Upon addition of HBF₄, an immediate colour change from red to black was observed. The reaction was allowed to stir under argon for 15 minutes, then *E*-3-methyl-1,4-hexadien-3-ol (**299c**) (118 mg, 0.26 mmol) was added via syringe. The reaction mixture was then allowed to warm to room temperature overnight. A gradual colour change from black to red occurred. The solvent was removed *in vacuo* and the product purified on the bench by silica gel chromatography using 3% MeOH/CH₂Cl₂. The red fraction was collected and dried to yield 29 mg (41%) of product as a sticky red solid. Crystallization via two-chambered liquid diffusion using CH₂Cl₂ and Et₂O provided red crystals suitable for combustion analysis. **Method 2.** In the dry box, a Schlenk tube was charged with Cp*Co(CH₂CH₂)₂ (16 mg, 0.063 mmol) in acetone (8 mL), then removed to the Schlenk line. To this, *E*-3-methyl-1,4-hexadien-3-ol (**300c**) (8 mg, 0.071 mmol) was added via syringe and heated to reflux under an argon atmosphere for 3 hours, resulting in a brown solution. This solution was cooled to -78 °C in a dry ice/acetone bath and HBF₄•OEt₂ (9 μL, 0.63 mmol) added, then allowed to warm

gradually to room temperature overnight (≈ 16 h). The solvent was removed *in vacuo* and the residue purified on the bench by silica gel chromatography using 3% MeOH/CH₂Cl₂. The red fraction was collected and dried to yield 11 mg (61%) of product as a 2:1 mixture of isomers **297c-syn**:**297c-anti**. Compound **297c-syn**: IR (neat, cm⁻¹): 3132, 2965, 2914, 1537, 1463, 1387, 1285, 1217, 1094, 1053, 1038, 916; ¹H NMR (400 MHz, CDCl₃): δ 4.89 (d, $J_{2-1} = 11.9$ Hz, 1H, H₂), 4.68 (t, $J_{3-4syn} = J_{3-4anti} = 11.2$ Hz, 1H, H₃), 3.11 (dd, $J_{4syn-3} = 9.7$ Hz, $J_{4syn-4anti} = 3.58$ Hz, 1H, H_{4syn}), 2.32 (s, 3H, Me), 2.12 (dq, $J_{1-2} = 11.9$ Hz, $J_{1-Me} = 6.32$ Hz, 1H, H₁), 1.82 (s, 15H, C₅Me₅), 1.74 (dd, $J_{4anti-3} = 11.6$ Hz, $J_{4anti-4syn} = 3.6$ Hz, 1H, H_{4anti}), 1.50 (d, $J_{Me-1} = 6.3$ Hz, 3H, Me); ¹³C NMR (100 MHz, CDCl₃): δ 107.01, 97.90, 97.41, 97.32, 83.13, 63.57, 21.47, 18.57, 9.42. Electrospray MS m/z calculated for C₁₇H₂₆Co (M⁺ – BF₄): 289.13610; found: 289.13587; Analysis calculated for C₁₇H₂₆CoBF₄: C, 54.29%; H, 6.97%; found: C, 53.85%; H, 7.17%. Compound **297c-anti** (partial data only): ¹H NMR (300 MHz, CDCl₃): δ 4.81 (t, $J_{3-4syn} = J_{3-4anti} = 10.4$ Hz, 1H, H₃), 4.65 (d, $J_{2-1} = 9.0$ Hz, 1H, H₂), 3.75 (quint, $J_{1-2} = J_{1-Me} = 7.0$ Hz, 1H, H₁), 3.23 (dd, $J_{4syn-3} = 9.6$ Hz, $J_{4syn-4anti} = 3.4$ Hz, 1H, H_{4syn}), 2.31 (s, 3H, Me), 2.09 (dd, $J_{4anti-3} = 11.5$ Hz, $J_{4anti-4syn} = 3.5$ Hz, 1H, H_{4anti}), 1.84 (s, 15H, C₅Me₅), 0.61 (d, $J_{Me-1} = 6.9$ Hz, 1H, Me).



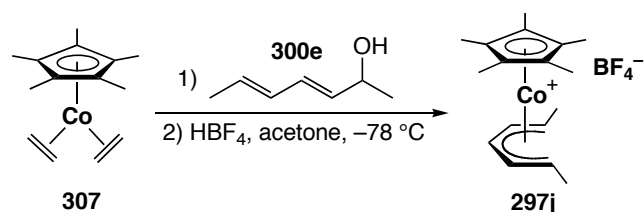
[Cp*Co(η^5 -1-methylpentadienyl)]⁺BF₄⁻ (297d**). In the dry box, a Schlenk tube was charged with Cp*Co(CH₂CH₂)₂ (**307**) (135 mg, 0.54 mmol) in acetone (5 mL), then**

removed to the Schlenk line. To this, *E,E*-2,4-hexadienol (**300a**), (55 mg, 0.56 mmol) was added via syringe and heated to reflux under an argon atmosphere for 3 hours, resulting in a brown solution. This solution was cooled to $-78\text{ }^{\circ}\text{C}$ in a dry ice/acetone bath, $\text{HBF}_4\cdot\text{OEt}_2$ (75 μL , 0.54 mmol) added, then allowed to warm gradually to room temperature overnight (≈ 16 h). The solvent was removed *in vacuo* and the residue purified on the bench by silica gel chromatography using 3% MeOH/ CH_2Cl_2 . The red fraction was collected and dried to yield 171 mg (87%) of product as a sticky red solid. The product spectra were identical with those previously reported.



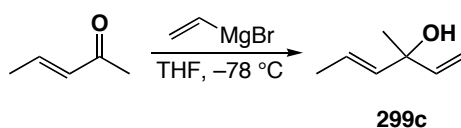
[Cp*Co(η^5 -1,4-dimethylpentadienyl)]⁺BF₄⁻ (297i**).** In the drybox, a Schlenk tube was charged with $\text{Cp}^*\text{Co}(\text{CH}_2\text{CH}_2)_2$ (89 mg, 0.36 mmol) in acetone (5 mL), then removed to the Schlenk line. To this, *E,E*-5-methyl-2,4-hexadien-6-ol (**300d**) (40 mg, 0.36 mmol) was added via syringe and heated to reflux under an argon atmosphere for 3 hours, resulting in a brown solution. This solution was cooled to $-78\text{ }^{\circ}\text{C}$ in a dry ice/acetone bath and $\text{HBF}_4\cdot\text{OEt}_2$ (49 μL , 0.36 mmol) added, then allowed to warm gradually to room temperature overnight (≈ 16 h). The solvent was removed *in vacuo* and the residue purified on the bench by silica gel chromatography using 3% MeOH/ CH_2Cl_2 . The red fraction was collected and dried to yield 25 mg (19%) of product as a sticky red solid. Material suitable for combustion and X-ray analysis was obtained via two-chambered liquid diffusion of diethyl ether into CH_2Cl_2 . In some trials the product was an

inseparable mixture of isomers **297i-syn** and **297i-anti** in a 1:1 ratio with a slightly improved (22%) yield. Compound **297i-syn**: IR (neat, cm^{-1}): 3059 (w), 2996 (w), 2964 (w), 2912 (w), 1491 (m), 1476 (m), 1451 (m), 1434 (m), 1382 (m), 1282 (w), 1056 (s), 953 (w), 928 (w), 906 (w), 849 (w); ^1H NMR (400 MHz, CDCl_3): δ 6.38 (d, $J_{3-2} = 6.9$ Hz, 1H, H_3), 5.25 (dd, $J_{2-1} = 12.2$ Hz, $J_{2-3} = 7.2$ Hz, 1H, H_2), 2.85 (d, $J_{5\text{syn}-5\text{anti}} = 4.0$ Hz, 1H, $\text{H}_{5\text{syn}}$), 2.18 (dq, $J_{1-2} = 12.4$ Hz, $J_{1-\text{Me}} = 5.9$ Hz, 1H, H_1), 2.11 (s, 3H, Me), 1.84 (s, 15H, C_5Me_5), 1.51 (d, $J_{\text{Me}-1} = 6.4$ Hz, 3H, Me), 1.41 (d, $J_{5\text{anti}-5\text{syn}} = 4.0$ Hz, 1H, $\text{H}_{5\text{anti}}$); ^1H - ^1H GCOSY (400 MHz, CDCl_3): δ 6.38 (H_3) \leftrightarrow δ 5.25 (H_2), 2.85 ($\text{H}_{5\text{syn}}$), 1.41 ($\text{H}_{5\text{anti}}$); δ 5.25 (H_2) \leftrightarrow δ 2.18 (H_1); δ 2.85 ($\text{H}_{5\text{syn}}$) \leftrightarrow δ 1.41 ($\text{H}_{5\text{anti}}$); δ 2.18 (H_1) \leftrightarrow δ 1.51 (Me); $^{13}\text{C}\{^1\text{H}\}$ NMR (100 MHz, CDCl_3): δ 112.2, 99.5, 97.6, 93.1, 87.2, 58.6, 23.1, 18.8, 9.7; Electrospray MS m/z calculated for $\text{C}_{17}\text{H}_{26}\text{Co}$ ($\text{M}^+ - \text{BF}_4$): 289.13610; found: 289.13602 (100%); Analysis calculated for $\text{C}_{17}\text{H}_{26}\text{CoBF}_4$: C, 54.29%; H, 6.97%; found: C, 53.84%, H, 7.00%. Compound **297i-anti** (partial data only): ^1H NMR (300 MHz, CDCl_3): δ 6.41 (d, $J_{3-2} = 7.2$ Hz, 1H, H_3), 4.98 (t, $J_{2-3} = J_{2-1} = 8.0$ Hz, 1H, H_2), 3.89 (dq, $J_{1-2} = 8.4$ Hz, $J_{1-\text{Me}} = 6.9$ Hz, 1H, H_1), 2.97 (d, $J_{5\text{syn}-5\text{anti}} = 3.6$ Hz, 1H, $\text{H}_{5\text{syn}}$), 2.12 (s, 3H, Me), 1.83 (s, 15H, C_5Me_5), 1.43 (d, $J_{5\text{anti}-5\text{syn}} = 3.8$ Hz, 1H, $\text{H}_{5\text{anti}}$), 0.57 (d, $J_{\text{Me}-1} = 7.0$ Hz, 3H, Me); ^1H - ^1H COSY (300 MHz, CDCl_3): δ 6.41 (H_3) \leftrightarrow δ 4.98 (H_2), 3.89 (H_1), 0.57 (Me); δ 4.98 (H_2) \leftrightarrow δ 3.89 (H_1), 0.57 (Me); δ 3.89 (H_1) \leftrightarrow δ 0.57 (Me); δ 2.97 ($\text{H}_{5\text{syn}}$) \leftrightarrow δ 1.43 ($\text{H}_{5\text{anti}}$).

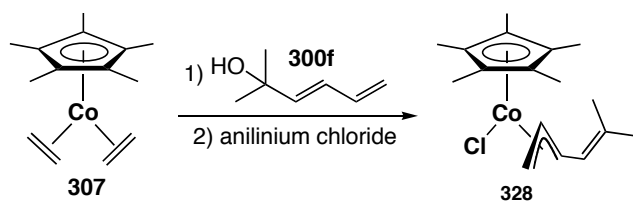


[Cp*Co(η^5 -1,5-dimethylpentadienyl)]⁺BF₄⁻ (297j**). In the dry box, a Schlenk tube was charged with Cp*Co(CH₂CH₂)₂ (89 mg, 0.36 mmol) in acetone (5 mL) and removed to the Schlenk line. To this, *E,E*-2,4-heptadien-6-ol (**300e**) (40 mg, 0.36 mmol) was added via syringe and heated to reflux under an argon atmosphere for 3 hours, resulting in a brown solution. This solution was cooled to -78 °C in a dry ice/acetone bath and HBF₄•OEt₂ (49 μ L, 0.36 mmol) added. Gradual warming to room temperature overnight (\approx 16 hours) was followed by transfer to a reaction bomb and heating at 40 °C for 30 hours. The solvent was removed *in vacuo* and the residue purified on the bench by silica gel chromatography using 3% MeOH/CH₂Cl₂. The red fraction was collected and dried to yield 80 mg (60%) of product as a sticky red solid. Material suitable for combustion and X-ray analysis was obtained via two-chambered liquid diffusion of diethyl ether into CH₂Cl₂. If the final heating stage is omitted, the product is obtained as a 1:1 mixture of **297j** and **319**. Compound **297j**: IR (neat, cm⁻¹): 3142 (w), 3044 (w), 3005 (w), 2966 (m), 2909 (m), 1813 (w), 1459 (m), 1383 (s), 1284 (m), 1249 (w), 1135 (w), 1092 (s), 1044 (s), 994(s), 942 (s), 837 (w), 754 (w); ¹H NMR (400 MHz, CDCl₃): δ 6.48 (t, J_{1-2} = 7.0 Hz, 1H, H₁); 5.04 (dd, J_{2-3} = 12.1 Hz; J_{2-1} = 7.0 Hz, 2H, H₂); 2.06 (dq, J_{3-2} = 12.5 Hz, J_{3-Me} = 6.3 Hz, 2H, H₃); 1.84 (s, 15H, C₅Me₅); 1.45 (d, J_{Me-3} = 6.3 Hz, 6H, Me); ¹H-¹H GCOSY (400 MHz, CDCl₃): δ 6.48 (H₁) \leftrightarrow δ 5.04 (H₂); δ 5.04 (H₂) \leftrightarrow δ 2.06 (H₃), 1.45 (Me); δ 2.06 (H₃) \leftrightarrow δ 1.45 (Me); ¹³C{¹H} NMR (100 MHz, CDCl₃): δ 99.7, 96.9, 90.1, 83.0, 18.5, 9.5; Electrospray MS *m/z* calculated for C₁₇H₂₆Co (M⁺ - BF₄): 289.13610;**

found: 289.13639 (100%); Analysis calculated for C₁₇H₂₆CoBF₄: C, 54.29%, H, 6.97%; found: C, 54.15%, H, 6.99%. Compound **319** (partial data only): ¹H NMR (300 MHz, CDCl₃): δ 5.69 (q, *J*₄₋₃ = *J*₄₋₅ = 7.2 Hz, 1H, H₄), 4.21 (dd, *J*₅₋₆ = 12.4 Hz, *J*₅₋₄ = 7.4 Hz, 1H, H₅), 3.90-3.72 (m, 1H, H₂), 3.41 (d, *J*_{OH-2} = 6.8 Hz, 1H, -OH), 2.88 (dq, *J*₆₋₅ = 12.4 Hz, *J*_{6-Me} = 6.2 Hz, 1H, H₆), 1.79 (s, 15H, C₅Me₅), 1.73 (d, *J*₇₋₆ = 5.8 Hz, 3H, H₇), 0.96 (d, *J*₁₋₂ = 6.0 Hz, 3H, H₁), 0.18-0.07 (m, 2H, H₃).



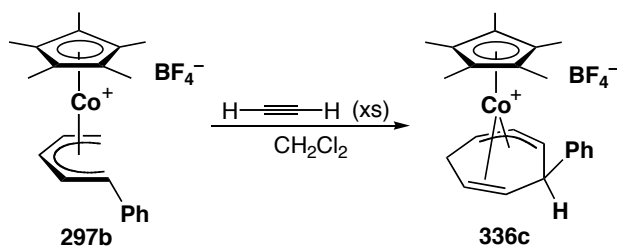
***E*-3-methyl-1,4-hexadien-3-ol (299c).** To a solution of 0.6 M vinyl Grignard (22 mL, 13 mmol) in THF (5 mL), cooled to -78 °C in a dry ice/acetone bath, *E*-3-penten-2-one (1.01 g, 10.1 mmol) in THF (10 mL) was slowly added by syringe. The mixture was allowed to warm to room temperature and stirred for another 15 minutes. The solution was cooled again and quenched with 20 mL of saturated ammonium chloride solution and 10 mL of water. This mixture was extracted with 3x25 mL portions of ether. The resulting solution was concentrated to afford **299c** (1.48 g) as crude yellow oil. Purification via silica gel column chromatography with 10% ethyl acetate/hexanes did not significantly improve the spectroscopic purity. No further purification was attempted and the material was used as is for further reactions. ¹H NMR (300 MHz, CDCl₃): δ 5.93 (dd, *J* = 17.3, 10.6 Hz, 1H), 5.62 (dq, *J* = 15.5, 6.0 Hz, 1H), 5.56 (d, *J* = 16.0 Hz, 1H), 5.20 (dd, *J* = 17.3, 1.2 Hz, 1H), 5.02 (dd, *J* = 10.6, 1.2 Hz, 1H), 1.67 (d, *J* = 5.2 Hz, 3H), 1.33 (s, 3H), -OH proton not seen; ¹³C{¹H} NMR (100 MHz, CDCl₃): δ 144.2, 136.7, 123.7, 111.7, 73.0, 27.9, 17.6.



[Cp*Co(η^3 -1,1-dimethylpentadienyl)]Cl (328). Method 1. In the dry box, a Schlenk tube was charged with Cp*Co(CH₂CH₂)₂ (89 mg, 0.36 mmol) and dissolved in acetone (5 mL), then removed to the Schlenk line. To this, *E*-5-methyl-1,3-hexadien-5-ol (**300f**) (40 mg, 0.36 mmol) was added and heated to reflux under an argon atmosphere for 3 hours resulting in brown solution. This solution was cooled to -78 °C in a dry ice/acetone bath and HBF₄•OEt₂ (49 μ L, 0.36 mmol) added. The solution was then allowed to warm to room temperature gradually overnight (\approx 16 h). The solvent was removed *in vacuo* and purified by filtration through activity IV alumina in the glove box to give 35 mg (26%) of product as a red oil. **Method 2.** In the dry box, a Schlenk tube was charged with Cp*Co(CH₂CH₂)₂ (110 mg, 0.44 mmol) and dissolved in acetone (10 mL), then removed to the Schlenk line. To this, *E*-5-methyl-1,3-hexadien-5-ol (**300f**) (49 mg, 0.44 mmol) was added and heated to reflux under an argon atmosphere for 3 hours producing a brown solution. This solution was cooled to -78 °C in a dry ice/acetone bath and N,N-dimethyl anilinium chloride (69 mg, 0.44 mmol) added. The solution was allowed to warm to room temperature gradually overnight (\approx 16 h). The solvent was removed *in vacuo* and the product purified by filtration through activity IV alumina in the glove box to give **328** as a red/brown oil (80 mg, 56%). A dark purple powder suitable for combustion analysis was obtained via cooling a saturated pentane solution to -80 °C overnight. IR (neat, cm⁻¹): 3068 (m), 2966 (s), 2913 (s), 2721 (m), 2537 (w), 2399 (w), 2040 (w), 1970 (w), 1779 (m), 1743 (w), 1703 (w), 1630 (s), 1512 (s), 1447 (s), 1376 (s), 1358 (s), 1255 (m), 1203

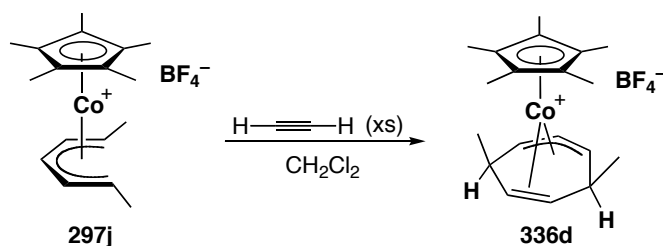
(m), 1185 (s), 1159 (m), 1074 (m), 1051 (m), 1026 (s), 992 (s), 949 (m), 891 (s), 883 (s), 852 (m); ^1H NMR (400 MHz, C_6D_6): δ 5.35 (dsept, $J_{4-3} = 10.8$ Hz, $J_{4-\text{Me}} = J_{4-\text{Me}'} = 1.4$ Hz, 1H, H_4), 4.29 (t, $J_{3.4} = J_{3-2} = 11.4$ Hz, 1H, H_3), 3.89-3.78 (m, 2H, $\text{H}_{1\text{syn}}$, H_2), 3.16 (d, $J_{1\text{trans}-2} = 12.4$ Hz, 1H, $\text{H}_{1\text{trans}}$), 1.59 (s, 3H, Me), 1.52 (s, 3H, Me'), 1.19 (s, 15H, C_5Me_5); ^1H - ^1H GCOSY (400 MHz, C_6D_6): δ 5.35 (H_4) \leftrightarrow δ 4.29 (H_3), 1.59 (Me), 1.52 (Me'); δ 4.29 (H_3) \leftrightarrow δ 3.89-3.78 (H_2); δ 3.89-3.78 (H_2) \leftrightarrow δ 3.16 ($\text{H}_{1\text{trans}}$); $^{13}\text{C}\{^1\text{H}\}$ NMR (100 MHz, C_6D_6): δ 137.7, 95.8, 92.9, 78.2, 56.4, 30.2, 27.1, 20.4, 9.4; Electron impact MS m/z calculated for $\text{C}_{17}\text{H}_{26}\text{CoCl}$ (M^+): 324.10550; found: 324.10566 (22%); Analysis calculated for $\text{C}_{17}\text{H}_{26}\text{CoCl}$: C, 62.87%, H, 8.07%; found: C, 62.78%, H, 8.06%.

II. Chapter 3

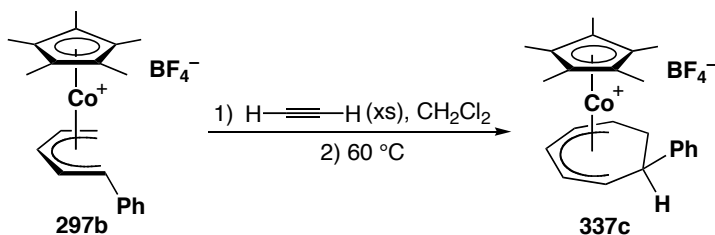


[Cp*Co(η^2, η^3 -1-phenylcycloheptadienyl)] $^+$ BF $_4^-$ (336c). [Cp*Co(η^5 -1-phenylpenta-
dienyl)] $^+$ BF $_4^-$ (**297b**) (16 mg, 0.038 mmol) was dissolved in CH_2Cl_2 (3 mL) and
degassed with argon for 5 minutes. Simultaneously, acetylene was bubbled through
 CH_2Cl_2 in a test-tube for 25 minutes in order to ensure saturation. Then, 2 mL of this
saturated solution was transferred to the bomb via cannula. The bomb was sealed and
allowed to stand at room temperature overnight. During this time, the colour was seen to
change gradually from dark-red to orange-red. The solvent was then removed *in vacuo*

and the product purified by silica gel chromatography using 3% MeOH/CH₂Cl₂. The red fraction was collected and dried providing 15 mg (89%) of product as a thick, red oil. The ¹H NMR spectrum showed that there was a small quantity (ca. 10%) of the fully-conjugated isomer **337c** present. Since the product slowly isomerizes at room temperature, only spectroscopic characterization was obtained. IR (neat, cm⁻¹): 3639 (w), 3552 (w), 3061 (s), 3032 (s), 2964 (s), 2916 (s), 2861 (s), 2262 (s), 1817 (w), 1603 (s), 1552 (w), 1494 (s), 1453 (s), 1430 (s), 1384 (s), 1286 (s), 1184 (w), 1097 (s), 916 (s), 830 (w), 794 (w), 761 (s), 734 (s), 702 (s); ¹H NMR (400 MHz, CDCl₃): δ 7.51 – 7.34 (m, 5H, Ph, overlaps solvent signal), 4.10 (dd, $J_{1-2} = 7.3$ Hz, $J_{1-7} = 4.0$ Hz, 1H, H₁), 4.06 (td, $J_{3-4endo} = J_{3-2} = 8.2$ Hz, $J_{3-4exo} = 4.1$ Hz, 1H, H₃), 3.51 (t, $J_{2-1} = J_{2-3} = 7.7$ Hz, 1H, H₂), 3.40 (t, $J_{7-1} = J_{7-6} = 4.2$ Hz, 1H, H₇), 3.30 (dt, $J_{4endo-4exo} = 14.1$ Hz, $J_{4endo-3} = J_{4endo-5} = 8.6$ Hz, 1H, H_{4endo}), 3.02 (td, $J_{5-4endo} = J_{5-6} = 7.5$ Hz, $J_{5-4exo} = 4.8$ Hz, 1H, H₅), 2.75 (td, $J_{6-5} = J_{6-7} = 6.0$ Hz, $J_{6-4exo} = 0.3$ Hz, 1H, H₆), 2.31 (br. app. dt, $J_{4exo-4endo} = 13.9$ Hz, $J_{4exo-3} = J_{4exo-5} = 4.4$ Hz, 1H, H_{4exo}), 1.84 (s, 15H, C₅Me₅); ¹H-¹H GCOSY (400 MHz, CDCl₃): δ 4.10 (H₁) ↔ δ 3.51 (H₂), 3.40 (H₇); δ 4.06 (H₃) ↔ δ 3.51 (H₂), 3.30 (H_{4endo}), 2.31 (H_{4exo}); δ 3.51 (H₂) ↔ δ 3.30 (H_{4endo}), 2.31 (H_{4exo}); δ 3.40 (H₇) ↔ δ 2.75 (H₆), 2.31 (H_{4exo}); δ 3.30 (H_{4endo}) ↔ δ 3.02 (H₅), 2.75 (H₆), 2.31 (H_{4exo}); δ 3.02 (H₅) ↔ δ 2.75 (H₆), 2.31 (H_{4exo}); δ 2.75 (H₆) ↔ δ 2.31 (H_{4exo}); ¹³C{¹H} NMR (100 MHz, CDCl₃): δ 139.4, 129.4, 128.9, 128.0, 126.5, 98.0, 91.7, 48.7, 45.7, 45.5, 36.2, 21.7, 9.7; Electrospray MS *m/z* calculated for C₂₃H₂₈Co (M⁺ – BF₄): 363.15175; found: 363.15182 (100%).



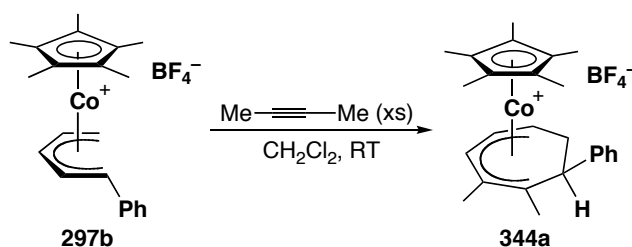
[Cp*Co(η^2, η^3 -1,5-dimethylcycloheptadienyl)]⁺BF₄⁻ (336d). [Cp*Co(η^5 -1,5-dimethylpentadienyl)]⁺ BF₄⁻ (**297j**) (11 mg, 0.029 mmol) was dissolved in CH₂Cl₂ (3 mL) and degassed with argon for 5 minutes. Simultaneously, acetylene was bubbled through CH₂Cl₂ in a test-tube for 25 minutes in order to ensure saturation. Then, 2 mL of this saturated solution was transferred to the bomb via cannula. The bomb was sealed and allowed to stand at room temperature for 3 days. The solvent was removed *in vacuo* and the product purified by silica gel chromatography using 3% MeOH/CH₂Cl₂. The red fraction was collected and dried providing 11 mg (94%) of product as a thick, red oil. Crystallization via two-chambered liquid diffusion using CH₂Cl₂ and Et₂O provided red crystals suitable for combustion and X-ray analysis. IR (neat, cm⁻¹): 2978 (w), 2930 (w), 2878 (w), 1460 (w), 1429 (w), 1383 (m), 1313 (w), 1283 (w), 1263 (w), 1050 (s), 1036 (s), 988 (w), 900 (w), 864 (w), 803 (w); ¹H NMR (400 MHz, CDCl₃): δ 3.59 (dd, $J_{2-1} = 7.6$ Hz, $J_{2-3} = 3.8$ Hz, 2H, H₂), 3.42 (tt, $J_{1-2} = 7.7$ Hz, $J_{1-3} = 0.7$ Hz, 1H, H₁), 2.38 (d, $J_{4-3} = 3.2$ Hz, 2H, H₄), 2.34 (m, 2H, H₃), 1.87 (s, 15H, C₅Me₅), 1.47 (d, $J_{Me-3} = 6.8$ Hz, 6H, Me); ¹H-¹H GCOSY (400 MHz, CDCl₃): δ 3.59 (H₂) \leftrightarrow δ 3.42 (H₁), 2.34 (H₃); δ 3.42 (H₁) \leftrightarrow δ 2.34 (H₃); δ 2.38 (H₄) \leftrightarrow δ 2.34 (H₃); δ 2.34 (H₃) \leftrightarrow δ 1.47 (Me); ¹³C{¹H} NMR (100 MHz, CDCl₃): δ 98.1, 91.7, 54.2, 52.9, 27.8, 19.9, 10.2; Electrospray MS *m/z* calculated for C₁₉H₂₈Co (M⁺ - BF₄): 315.15175; found: 315.15156 (100%); Analysis calculated for C₁₉H₂₈CoBF₄: C, 56.74%; H, 7.02%; found: C, 56.36%, H, 7.33%.



[Cp*Co(η^5 -1-phenylcycloheptadienyl)]⁺BF₄⁻ (337c). [Cp*Co(η^5 -1-phenylpentadi-

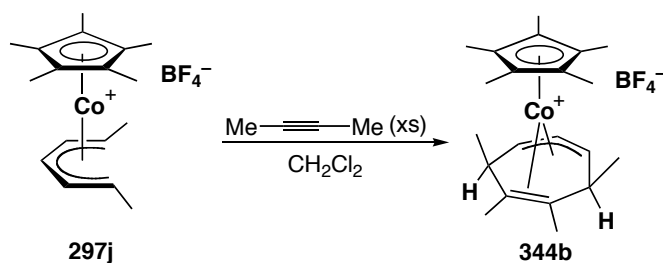
enyl)]⁺BF₄⁻ (**297b**) (105 mg, 0.25 mmol) was dissolved in CH₂Cl₂ (3 mL) in a reaction bomb and degassed with argon for 5 minutes. Simultaneously, acetylene was bubbled through CH₂Cl₂ in a test-tube for 25 minutes in order to ensure saturation. Then, 2 mL of this saturated solution was transferred to the bomb via cannula. The bomb was sealed and allowed to stand at room temperature for 3 days. During this time, the colour was seen to gradually change from dark-red to orange-red. The bomb was then heated at 60 °C in an oil bath for one day and the colour changed back to dark red. The solvent was removed *in vacuo* and the product purified by silica gel chromatography using 3% MeOH/CH₂Cl₂. The red fraction was collected and dried providing 111 mg (100%) of product as a thick, red oil. A sample suitable for combustion analysis was obtained by crystallization via two-chambered liquid diffusion using CH₂Cl₂ and Et₂O to yield a light, orange powder. IR (CH₂Cl₂ cast, cm⁻¹): 3029 (w), 2917 (w), 1601 (w), 1493 (w), 1456 (w), 1384 (w), 1284 (w), 1056 (s), 878 (w), 762 (w), 732 (w), 704 (w); ¹H NMR (400 MHz, CDCl₃): δ 7.36 (m, 2H, Ph), 7.27 (m, 1H, Ph, overlaps solvent signal), 7.12 (m, 2H, Ph), 6.90 (t, $J_{3-2} = J_{3-4} = 6.3$ Hz, 1H, H₃), 5.42 (t, $J_{2-1} = J_{2-3} = 7.1$ Hz, 1H, H₂), 5.16 (t, $J_{4-3} = J_{4-5} = 8.6$ Hz, 1H, H₄), 4.52 (dt, $J_{5-4} = 9.3$ Hz, $J_{5-6endo} = J_{5-6exo} = 3.7$ Hz, 1H, H₅), 4.32 (ddd, $J_{1-2} = 8.1$ Hz, $J_{1-7} = 4.5$ Hz, $J_{1-3} = 1.1$ Hz, 1H, H₁), 2.99 (ddd, $J_{6endo-6exo} = 16.7$ Hz, $J_{6endo-7} = 10.4$ Hz, $J_{6endo-5} = 4.2$ Hz, 1H, H_{6endo}), 2.30 (br. app. dt, $J_{6exo-6endo} = 16.7$ Hz, $J_{6exo-5} = J_{6exo-7} = 3.7$ Hz, 1H, H_{6exo}), 1.91 (s, 15H, C₅Me₅), 1.78 (dt, $J_{7-6endo} = 11.6$, $J_{7-1} =$

$J_{7-6\text{exo}} = 5.2$ Hz, 1H, H₇); $^1\text{H}-^1\text{H}$ GCOSY (400 MHz, CDCl_3): δ 7.36 (Ph) \leftrightarrow δ 7.27 (Ph), 7.12 (Ph); δ 7.27 (Ph) \leftrightarrow δ 7.12 (Ph); δ 6.90 (H₃) \leftrightarrow δ 5.42 (H₂), 5.16 (H₄), 4.32 (H₁); δ 5.42 (H₂) \leftrightarrow δ 4.32 (H₁); δ 5.16 (H₄) \leftrightarrow δ 4.52 (H₅); δ 4.52 (H₅) \leftrightarrow δ 2.99 (H_{6\text{endo}}}), 2.30 (H_{6\text{exo}}}); δ 4.32 (H₁) \leftrightarrow δ 1.78 (H₇); δ 2.99 (H_{6\text{endo}}}) \leftrightarrow δ 2.30 (H_{6\text{exo}}}), 1.78 (H₇); δ 2.30 (H_{6\text{exo}}}) \leftrightarrow δ 1.78 (H₇); $^{13}\text{C}\{^1\text{H}\}$ NMR (100 MHz, CDCl_3): δ 141.8, 129.1, 127.3, 126.9, 101.1, 99.0, 98.1, 97.7, 95.1, 88.8, 49.0, 45.6, 9.8; Electrospray MS m/z calculated for $\text{C}_{23}\text{H}_{28}\text{Co}$ ($\text{M}^+ - \text{BF}_4^-$): 363.15175; found: 363.15171 (100%); Analysis calculated for $\text{C}_{23}\text{H}_{28}\text{CoBF}_4$: C, 61.36%; H, 6.27%; found: C, 61.05%; H, 6.03%.



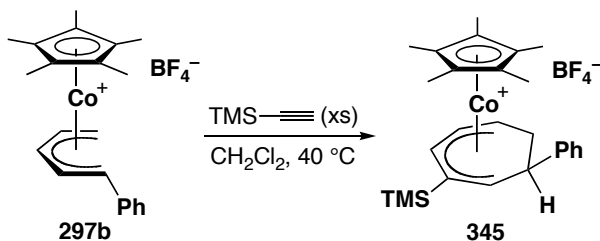
[Cp*Co(η^5 -1-phenyl-2,3-dimethylcycloheptadienyl)]⁺BF₄⁻ (344a). [Cp*Co(η^5 -1-phenylpentadienyl)]⁺BF₄⁻ (**297b**) (101 mg, 0.24 mmol) was dissolved in CH_2Cl_2 (4 mL) in a reaction bomb and degassed with argon for 5 minutes. To this, 2-butyne (100 μL , 1.28 mmol) was added. The bomb was sealed and allowed to stand at room temperature for 3 days. The solvent was then removed *in vacuo* and the product purified by silica gel chromatography using 3% MeOH/ CH_2Cl_2 . The red fraction was collected and dried providing 110 mg (96%) of product as a thick, red oil. A sample suitable for combustion and X-ray analysis was prepared by crystallization via two-chambered liquid diffusion using CH_2Cl_2 and Et_2O to yield red crystals. IR (CH_2Cl_2 cast, cm^{-1}): 2920 (m), 1491 (w), 1456 (m), 1432 (w), 1384 (m), 1054 (s), 775 (m), 732 (m), 706 (m), 520 (w); ^1H

NMR (300 MHz, CDCl₃): δ 7.30-7.17 (m, 3H, Ph, overlaps solvent signal), 6.95 (m, 2H, Ph), 6.75 (d, $J_{1-2} = 7.4$ Hz, 1H, H₁), 4.83 (t, $J_{2-1} = J_{2-3} = 8.3$ Hz, 1H, H₂), 4.52 (dt, $J_{3-2} = 9.2$ Hz, $J_{3-4\text{endo}} = J_{3-4\text{exo}} = 3.4$ Hz, 1H, H₃), 3.25 (ddd, $J_{4\text{endo}-4\text{exo}} = 16.5$ Hz, $J_{4\text{endo}-5} = 12.8$ Hz, $J_{4\text{endo}-3} = 3.1$ Hz, 1H, H_{4\text{endo}}}), 2.39 (br. app. dt, $J_{4\text{exo}-4\text{endo}} = 16.6$ Hz, $J_{4\text{exo}-5} = J_{4\text{exo}-3} = 4.8$ Hz, 1H, H_{4\text{exo}}}, other couplings which do not resolve well are also seen), 2.23 (s, 3H, Me), 1.80 (s, 15H, C₅Me₅), 1.30 (dd, $J_{5-4\text{endo}} = 12.8$ Hz, $J_{5-4\text{exo}} = 4.0$ Hz, 1H, H₅), 0.84 (s, 3H, Me); ¹H-¹H GCOSY (300 MHz, CDCl₃): δ 7.30-7.17 (Ph) ↔ δ 6.95 (Ph); δ 6.75 (H₁) ↔ δ 4.83 (H₂); δ 4.83 (H₂) ↔ δ 4.52 (H₃), 2.39 (H_{4\text{endo}}}); δ 4.52 (H₃) ↔ δ 3.25 (H_{4\text{endo}}}), 2.39 (H_{4\text{exo}}}); δ 3.25 (H_{4\text{endo}}}) ↔ δ 2.39 (H_{4\text{exo}}}), 1.30 (H₅); δ 2.39 (H_{4\text{exo}}}) ↔ δ 1.30 (H₅); ¹³C{¹H} NMR (100 MHz, CDCl₃): δ 137.7, 128.57, 128.55, 127.3, 108.5, 100.3, 99.7, 97.9, 96.5, 86.6, 47.1, 46.6, 21.7, 17.0, 9.1; Electrospray MS *m/z* calculated for C₂₅H₃₂Co (M⁺ – BF₄⁻): 391.18305; found: 391.18328 (100%); Analysis calculated for C₂₅H₃₂CoBF₄: C, 62.78%; H, 6.74%; found: C, 62.95%; H, 6.73%.



[Cp*Co(η^2, η^3 -1,2,3,4-tetramethylcycloheptadienyl)]⁺BF₄⁻ (**344b**). [Cp*Co(η^5 -1,5-dimethylcycloheptadienyl)]⁺BF₄⁻ (**297j**) (80 mg, 0.213 mmol) was dissolved in CH₂Cl₂ (15 mL) in a reaction bomb and degassed with argon for 5 minutes. To this, 2-butyne (80 μ L, 1.02 mmol) was added via syringe. The bomb was sealed and heated at 40 °C for 3 days in an oil bath. The solvent was then removed *in vacuo* and the product purified by

silica gel chromatography using 3% MeOH/CH₂Cl₂. The red fraction was collected and dried providing 78 mg (85%) of product as a thick, red oil. Crystallization attempts led only to decomposition, so spectroscopic characterization alone was obtained. IR (neat, cm⁻¹): 3032 (w), 2966 (m), 2905 (m), 1473 (m), 1390 (m), 1329 (w), 1282 (w), 1259 (s), 1181 (w), 1044 (s), 901 (w), 861 (w), 799 (s); ¹H NMR (400 MHz, CDCl₃): δ 3.67 (dd, *J*₂₋₁ = 7.4 Hz, *J*₂₋₃ = 4.5 Hz, 2H, H₂), 3.12 (t, *J*₁₋₂ = 7.4 Hz, 1H, H₁), 2.69 (qd, *J*_{3-Me} = 6.7 Hz, *J*₃₋₂ = 4.4 Hz, 2H, H₃), 1.73 (s, 15H, C₅Me₅), 1.72 (s, 6H, Me), 1.46 (d, *J*_{Me-3} = 7.1 Hz, 6H, Me); ¹H-¹H GCOSY (400 MHz, CDCl₃): δ 3.67 (H₂) ↔ δ 3.12 (H₁), 2.69 (H₃); δ 3.12 (H₁) ↔ δ 2.69 (H₃); δ 2.69 (H₃) ↔ δ 1.72 (Me), 1.46 (Me); ¹³C{¹H} NMR (100 MHz, CDCl₃): δ 96.6, 89.6, 63.3, 52.1, 32.0, 18.5, 14.2, 9.5; Electrospray MS *m/z* calculated for C₂₁H₃₂Co (M⁺ - BF₄⁻): 343.18305; found: 343.18302 (100%).



[Cp*(η^5 -1-phenyl-3-trimethylsilylcycloheptadienyl)]⁺BF₄⁻ (**345**). [Cp*Co(η^5 -1-phenylpentadienyl)]⁺BF₄⁻ (**297b**) (102 mg, 0.24 mmol) was dissolved in CH₂Cl₂ (4 mL) in a reaction bomb and degassed with argon for 5 minutes. To this, TMS-acetylene (200 μ L, 1.42 mmol) was added. The bomb was sealed and heated at 40 °C for 2 days. The solvent was then removed *in vacuo* and the product purified by silica gel chromatography using 3% MeOH/CH₂Cl₂. The red fraction was collected and dried providing 98 mg of product as a thick, red oil which still contained significant impurities. The product yield (26%) was determined by ¹H NMR using 1,3,5-trimethoxybenzene as an internal

standard. Over several reactions, the yield was inexplicably seen to range from as low as 26% to as high as 55%. A sample suitable for combustion and X-ray analysis was prepared by recrystallizing three times via two-chambered liquid diffusion using CH₂Cl₂ and Et₂O to yield red crystals. IR (CH₂Cl₂ cast, cm⁻¹): 3390 (w), 2957 (w), 2915 (w), 1601 (w), 1493 (m), 1454 (m), 1430 (m), 1383 (m), 1252 (m), 1057 (s), 918 (w), 883 (w), 842 (s), 762 (m), 732 (w), 703 (m); ¹H NMR (400 MHz, CDCl₃): δ 7.36 (t, *J* = 7.4 Hz, 2H, Ph), 7.26 (t, *J* = 7.3 Hz, 1H, Ph, overlaps solvent signal), 7.07 (d, *J* = 7.3 Hz, 2H, Ph), 6.73 (d, *J*₃₋₄ = 6.9 Hz, 1H, H₃), 5.25 (dd, *J*₄₋₅ = 8.8 Hz, *J*₄₋₃ = 7.5 Hz, 1H, H₄), 4.79 (dt, *J*₅₋₄ = 9.5 Hz, *J*_{5-6endo} = *J*_{5-6exo} = 3.6 Hz, 1H, H₅), 3.93 (dd, *J*₂₋₁ = 4.2 Hz, *J*₂₋₃ = 0.7 Hz, 1H, H₂), 3.06 (ddd, *J*_{6endo-6exo} = 17.1 Hz, *J*_{6endo-1} = 11.1 Hz, *J*_{6endo-5} = 4.2 Hz, 1H, H_{6endo}), 2.36 (br. app. dt, *J*_{6exo-6endo} = 17.0 Hz, *J*_{6exo-1} = *J*_{6exo-5} = 3.6 Hz, 1H, H_{6exo}), 1.90 (s, 15H, C₅Me₅), 1.48 (dt, *J*_{1-6endo} = 10.8 Hz, *J*₁₋₂ = *J*_{1-6exo} = 4.8 Hz, 1H, H₁), 0.35 (s, 9H, SiMe₃); ¹H-¹H GCOSY (400 MHz, CDCl₃): δ 7.36 (Ph) ↔ δ 7.26 (Ph), 7.07 (Ph); δ 6.73 (H₃) ↔ δ 5.25 (H₄), 3.93 (H₂); δ 5.25 (H₄) ↔ δ 4.79 (H₅); δ 4.79 (H₅) ↔ δ 3.06 (H_{6endo}), 2.36 (H_{6exo}); δ 3.93 (H₂) ↔ δ 1.48 (H₁); δ 3.06 (H_{6endo}) ↔ δ 2.36 (H_{6exo}), 1.48 (H₁); δ 2.36 (H_{6exo}) ↔ δ 1.48 (H₁); ¹³C{¹H} NMR (100 MHz, CDCl₃): δ 142.1, 129.1, 127.2, 126.6, 107.1, 102.3, 99.1, 98.0, 92.7, 91.6, 47.5, 47.2, 10.2, -0.7; Electrospray MS *m/z* calculated for C₂₆H₃₆SiCo (M⁺ – BF₄): 435.19128; found: 435.19152 (100%); Analysis calculated for C₂₆H₃₆SiCoBF₄: C, 59.78%; H, 6.95%; found: C, 59.98%; H, 7.07%.

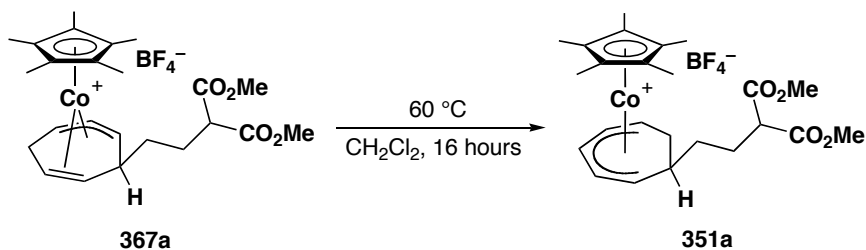
Computations. Computations for the complexation of cyclopropene to Cp*Co(η⁵-1-methylpentadienyl) complex **297d** were performed at the BP86/TZVPP level. The total

electronic energies (E_{elec}), zero-point energies (ZPE), thermal corrections (E_{therm}), and free energies (G) are collected in Table 8.1.

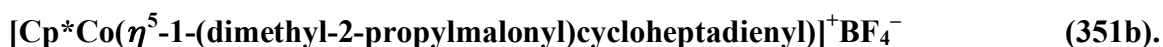
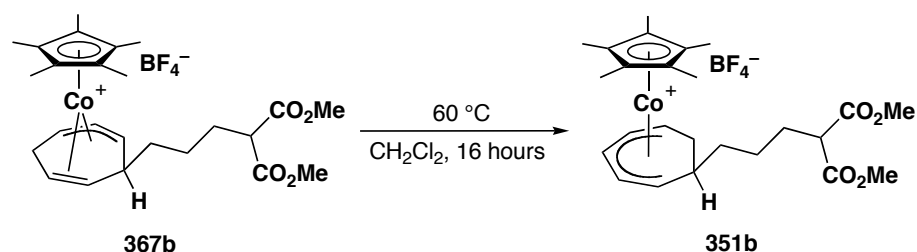
Table 8.1: Thermodynamic Data for Cyclopropene Complexation (hartrees)

	E_{elec}	ZPE	$E_{\text{elec}}+\text{ZPE}$	E_{therm}	G
297d	-2007.33402	0.34698	-2006.98704	0.32567	-2007.00835
Cyclopropene	-116.67194	0.05432	-116.61762	0.04151	-116.63043
TS	-2123.96717	0.40036	-2123.56681	0.37636	-2123.59081

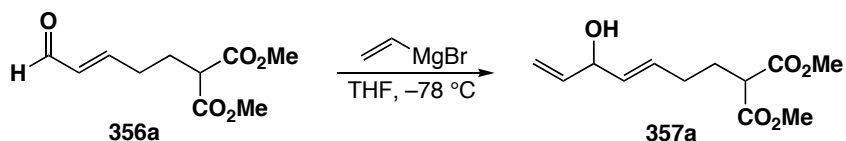
III. Chapter 4



[Cp*Co(η^5 -1-(dimethyl-2-ethylmalonyl)cycloheptadienyl)]⁺BF₄⁻ (351a). Allyl/olefin complex **367a** (10 mg) was dissolved in CH₂Cl₂ (5 mL) in a reaction bomb and heated at 60 °C in an oil bath for 3 days. The solvent was removed and the residue filtered through silica gel using 3% MeOH/CH₂Cl₂ to remove paramagnetic impurities. ¹H NMR spectroscopy indicated quantitative conversion to the fully conjugated isomer. The ¹H NMR spectra were consistent with those previously reported.²²⁵



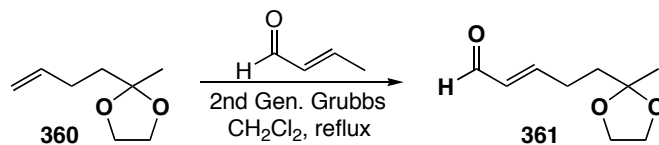
Allyl/olefin complex **367b** (10 mg) was dissolved in CH₂Cl₂ (5 mL) in a reaction bomb and heated at 60 °C in an oil bath for 3 days. The solvent was removed and the residue filtered through silica gel using 3% MeOH/CH₂Cl₂ to remove paramagnetic impurities. ¹H NMR spectroscopy indicated quantitative conversion to the fully conjugated isomer. The ¹H NMR spectra were consistent with those previously reported.²²⁵



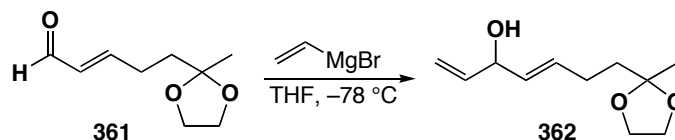
***E*-Dimethyl-2-(5-hydroxyhepta-3,6-dien-1-yl)malonate (357a).** Aldehyde **356a** (1.6 g, 7.5 mmol), was dissolved in THF (5 mL) in a dry Schlenk flask under an argon atmosphere. The flask was cooled to -78 °C in a dry ice/acetone bath and vinyl Grignard (0.34 M in THF, 44 mL, 15 mmol) was added via canula. The mixture was stirred at -78 °C for 30 minutes and then allowed to warm to room temperature. The flask was cooled again and the reaction quenched with aqueous NH₄Cl. This mixture was extracted with diethyl ether, washed with water then brine and dried over NaSO₄. The solvent was removed *in vacuo* and the product purified via triethylamine-neutralized silica gel chromatography with 4:1 hexanes/EtOAc on the bench. The solvent was removed to yield 1.1 g (60%) of dienol **357a** as a clear oil. IR (neat, cm⁻¹): 3447 (br, m), 3008 (w),

crotonaldehyde. The aldehyde product **356b** was unstable to chromatography and was therefore taken directly to the next step. The residue was taken up in THF (25 mL) and transferred to a dry addition funnel under an argon atmosphere and added dropwise to a vinyl Grignard solution (0.34 M in THF, 159 mL, 54 mmol) cooled to $-78\text{ }^{\circ}\text{C}$ in a dry ice/acetone bath. Upon complete addition, the reaction was stirred for an additional 30 minutes at $-78\text{ }^{\circ}\text{C}$ and then allowed to warm to room temperature. The flask was cooled again and the reaction quenched with aqueous NH_4Cl . This mixture was extracted with diethyl ether, washed with water then brine and dried over NaSO_4 . The solvent was removed *in vacuo* and the product purified via triethylamine neutralized silica gel chromatography with 4:1 hexanes/EtOAc on the bench. The solvent was removed to yield 3.8 g (80%) of dienol **357b** as a clear oil. The product upon chromatography is spectroscopically pure, sufficiently so to be carried forward, while additional chromatography was required to obtain the product in analytical purity. IR (neat, cm^{-1}): 3455 (br, s), 3082 (w), 2958 (s), 2850 (s), 1737 (s), 1641 (w), 1438 (s), 1346 (s), 1261 (s), 1156 (s), 1091 (s), 1016 (s), 924 (m), 873 (w), 800 (m), 699 (w); ^1H NMR (400 MHz, CDCl_3): δ 5.87 (ddd, $J_{2\text{-}1\text{trans}} = 17.2\text{ Hz}$, $J_{2\text{-}1\text{cis}} = 10.4\text{ Hz}$, $J_{2\text{-}3} = 5.8\text{ Hz}$, 1H, H_2), 5.65 (dtd, $J_{5\text{-}4} = 15.3\text{ Hz}$, $J_{5\text{-}6} = 6.5\text{ Hz}$, $J_{5\text{-}3} = 0.7\text{ Hz}$, 1H, H_5), 5.50 (ddt, $J_{4\text{-}5} = 15.5\text{ Hz}$, $J_{4\text{-}3} = 6.5\text{ Hz}$, $J_{4\text{-}6} = 1.3\text{ Hz}$, 1H, H_4), 5.23 (dt, $J_{1\text{trans}\text{-}2} = 17.2\text{ Hz}$, $J_{1\text{trans}\text{-}1\text{cis}} = J_{1\text{trans}\text{-}3} = 1.4\text{ Hz}$, 1H, $\text{H}_{1\text{trans}}$), 5.10 (dt, $J_{1\text{cis}\text{-}2} = 10.4$, $J_{1\text{cis}\text{-}1\text{trans}} = J_{1\text{cis}\text{-}3} = 1.4\text{ Hz}$, 1H, $\text{H}_{1\text{cis}}$), 4.56 (br. m, 1H, H_3), 3.72 (s, 6H, -OMe), 3.34 (t, $J_{9\text{-}8} = 7.6\text{ Hz}$, 1H, H_9), 2.06 (q, $J_{6\text{-}5} = J_{6\text{-}7} = 7.1\text{ Hz}$, 2H, H_6), 1.89 (m, 2H, CH_2), 1.57 (d, $J_{\text{HO}\text{-}3} = 3.8\text{ Hz}$, 1H, -OH), 1.40 (m, 2H, CH_2); $^{13}\text{C}\{^1\text{H}\}$ NMR (100 MHz, CDCl_3): δ 169.6, 139.6, 131.7, 131.4, 114.7, 73.6, 52.3, 51.4, 31.6, 28.2, 26.6; Electrospray MS m/z calculated for $\text{C}_{13}\text{H}_{20}\text{O}_5\text{Na}$ ($\text{M}^+ + \text{Na}$): 279.12030;

found: 279.12020 (100%); Analysis calculated for C₁₃H₂₀O₅: C, 60.92%; H, 7.87%;
found: C, 61.21%; H, 7.92%.

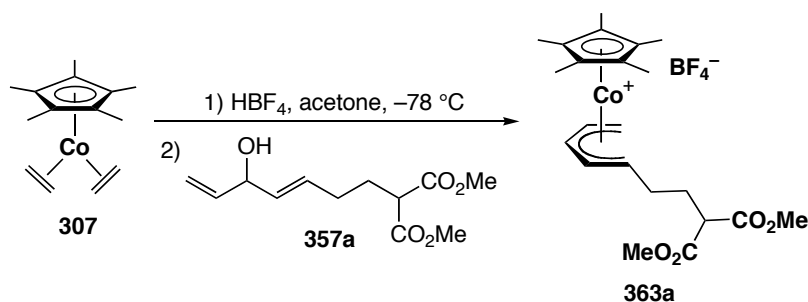


E-5-(2-methyl-1,3-dioxolan-2-yl)pent-2-enal (361). 2-(But-3-en-1-yl)-2-methyl-1,3-dioxolane **360** (1.34 g, 9.43 mmol) and crotonaldehyde (3.9 mL, 47.15 mmol) were dissolved in CH₂Cl₂ (15 mL) under an argon atmosphere. Second generation Grubbs' catalyst (120 mg, 0.14 mmol) was added and the reaction heated under reflux for 90 minutes. The solvent was removed *in vacuo* and the product purified by silica gel chromatography using 4:1 hexanes:EtOAc to provide 1.38 g (86%) of aldehyde **361** as a clear oily liquid. IR (neat, cm⁻¹): 2984 (s), 2956 (m), 2886 (s), 2736 (w), 1690 (s), 1637 (m), 1479 (w), 1449 (w), 1378 (m), 1302 (w), 1255 (s), 1222 (s), 1150 (s), 1053 (s), 979 (m), 949 (m), 867 (s); ¹H NMR (300 MHz, CDCl₃): δ 9.49 (d, *J*₁₋₂ = 7.9 Hz, 1H, H₁), 6.87 (dt, *J*₃₋₂ = 15.6 Hz, *J*₃₋₄ = 6.7 Hz, 1H, H₃), 6.10 (ddt, *J*₂₋₃ = 15.6 Hz, *J*₂₋₁ = 7.9 Hz, *J*₂₋₄ = 1.6 Hz, 1H, H₂), 3.90 (m, 4H, -OCH₂CH₂O-), 2.45 (m, 2H, H₄), 1.86 (m, 2H, H₅), 1.33 (s, 3H, Me); ¹H-¹H GCOSY (400 MHz, CDCl₃): δ 9.49 (H₁) ↔ δ 6.10 (H₂); δ 6.87 (H₃) ↔ δ 6.10 (H₂), 2.45 (H₄); δ 6.10 (H₂) ↔ δ 2.45 (H₄); δ 2.45 (H₄) ↔ δ 1.86 (H₅); Electron impact MS *m/z* calculated for C₉H₁₄O₃ (M⁺): 170.09430; found: 170.09481 (0.28%); ¹³C NMR (100 MHz, CDCl₃): δ 193.8, 158.4, 132.5, 109.1, 64.6, 36.9, 27.1, 23.9; Analysis calculated for C₉H₁₄O₃: C, 63.51%; H, 8.29%; found: C, 63.28%; H, 8.31%.



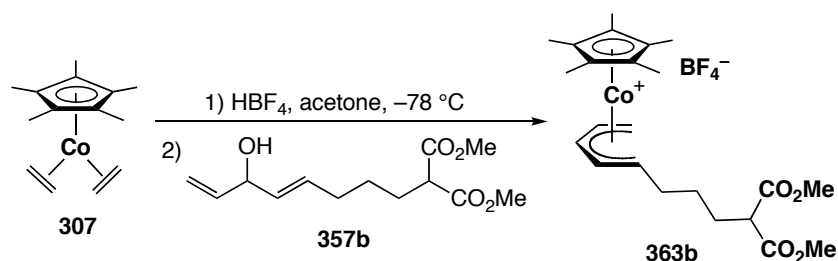
***E*-7-(2-methyl-1,3-dioxolan-2-yl)hepta-1,4-dien-3-ol (362).** A solution of vinyl Grignard (0.34 M in THF, 18.2 mL, 6.18 mmol) was added to a flame dried Schlenk flask under an argon atmosphere and cooled to $-78\text{ }^{\circ}\text{C}$ in a dry ice/acetone bath. To the resulting slurry, aldehyde **361** (1.01 g, 5.88 mmol) was added slowly via syringe. The mixture was stirred at $-78\text{ }^{\circ}\text{C}$ for 30 minutes and then allowed to warm slowly to room temperature and stirred for an additional 15 minutes. The solution was cooled again and quenched slowly with aqueous NH_4Cl . The resulting mixture was extracted with ether, washed with water then brine and dried over NaSO_4 . The solvent was removed *in vacuo* and the product purified by silica gel chromatography with 4:1 hexane/EtOAc to provide 0.88 g (75%) of dienol **362** as a thick, pale yellow oil. IR (neat, cm^{-1}): 3440 (br, s), 3080 (w), 2982 (s), 2947 (s), 2882 (s), 2678 (w), 1845 (w), 1668 (m), 1641 (m), 1477 (m), 1450 (m), 1422 (m), 1377 (s), 1344 (w), 1252 (s), 1221 (s), 1119 (s), 1058 (s), 974 (s), 949 (s), 923 (s), 862 (s), 817 (w), 787 (w), 762 (w), 668 (m); ^1H NMR (400 MHz, CDCl_3): δ 5.82 (ddd, $J_{2-1\text{trans}} = 17.2\text{ Hz}$, $J_{2-1\text{cis}} = 10.4\text{ Hz}$, $J_{2-3} = 5.8\text{ Hz}$, 1H, H_2), 5.65 (dtd, $J_{5-4} = 15.4\text{ Hz}$, $J_{5-6} = 6.6\text{ Hz}$, $J_{5-3} = 1.0\text{ Hz}$, 1H, H_5), 5.46 (ddt, $J_{4-5} = 15.4\text{ Hz}$, $J_{4-3} = 6.6\text{ Hz}$, $J_{4-6} = 1.5\text{ Hz}$, 1H, H_4), 5.18 (dt, $J_{1\text{trans}-2} = 17.3\text{ Hz}$, $J_{1\text{trans}-1\text{cis}} = J_{1\text{trans}-3} = 1.5\text{ Hz}$, 1H, $\text{H}_{1\text{trans}}$), 5.05 (dt, $J_{1\text{cis}-2} = 10.4\text{ Hz}$, $J_{1\text{cis}-1\text{trans}} = J_{1\text{cis}-3} = 1.4\text{ Hz}$, 1H, $\text{H}_{1\text{cis}}$), 4.51 (br. app. t, $J = 6.0\text{ Hz}$, 1H, H_3), 3.87 (m, 4H, $-\text{OCH}_2\text{CH}_2\text{O}-$), 2.09 (m, 3H, H_6 , $-\text{OH}$), 1.68 (m, 2H, H_7), 1.26 (s, 3H, H_8); $^1\text{H}-^1\text{H}$ GCOSY (400 MHz, CDCl_3): δ 5.82 (H_2) \leftrightarrow δ 5.18 ($\text{H}_{1\text{trans}}$), 5.05 ($\text{H}_{1\text{cis}}$), 4.51 (H_3); δ 5.65 (H_5) \leftrightarrow δ 5.46 (H_4), 2.09 (H_6); δ 5.46 (H_4) \leftrightarrow δ 4.51 (H_3), 2.09 (H_6); δ 5.18 ($\text{H}_{1\text{trans}}$) \leftrightarrow δ 5.05 ($\text{H}_{1\text{cis}}$), 4.51 (H_3); δ 5.05 ($\text{H}_{1\text{cis}}$) \leftrightarrow δ 4.51 (H_3); δ 2.09 (H_6)

$\leftrightarrow \delta$ 1.68 (H₇); $^{13}\text{C}\{^1\text{H}\}$ NMR (100 MHz, CDCl_3): δ 139.7, 131.9, 131.0, 114.5, 109.6, 73.5, 64.5, 38.2, 26.6, 23.8; Analysis calculated for $\text{C}_{11}\text{H}_{18}\text{O}_3$: C, 66.64%; H, 9.15%; found: C, 66.55%; H, 9.14%.



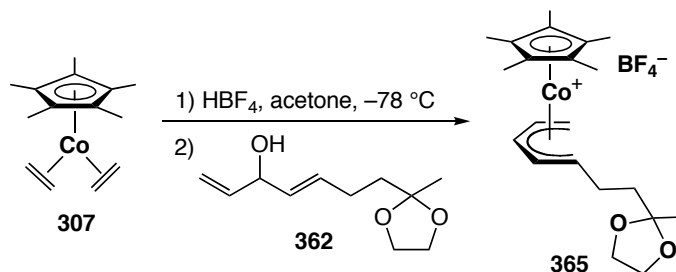
[Cp*Co(η^5 -1-(dimethyl-2-ethylmalonyl)pentadienyl)]⁺BF₄⁻ (363a). In the drybox, Cp*Co(C₂H₄)₂ (0.94 g, 3.75 mmol) was dissolved in acetone (15 mL) and placed in a Schlenk tube equipped with a stir-bar and septum. The sealed flask was removed to the Schlenk line, cooled to $-78\text{ }^\circ\text{C}$ in a dry ice/acetone bath and HBF₄•Et₂O (517 μL , 3.75 mmol) was added. Upon addition of HBF₄, an immediate colour change from red to black was observed. The reaction was allowed to stir under argon for 15 minutes, then *E*-dimethyl-2-(5-hydroxyhepta-3,6-dien-1-yl)malonate (**357a**) (1.00 g, 4.13 mmol) was added via syringe and the reaction mixture allowed to warm to room temperature overnight. A gradual colour change from black to red occurred. The solvent was removed *in vacuo* and the product purified on the bench by silica gel chromatography using 3% MeOH/CH₂Cl₂. The red fraction was collected and dried to yield 1.61 g (85%) of product as a red oil. IR (neat, cm^{-1}): 3539 (w), 2956 (m), 2853 (w), 1731 (s), 1639 (w), 1438 (s), 1382 (w), 1260 (s), 1158 (s), 1078 (w), 1012 (m), 908 (w), 875 (w), 843 (s); ^1H NMR (400 MHz, CDCl_3): δ 6.31 (t, $J_{3-2} = J_{3-4} = 7.0$ Hz, 1H, H₃), 5.07 (dd, $J_{4-5} = 11.7$ Hz, $J_{4-3} = 6.9$ Hz, 1H, H₄), 4.96 (ddd, $J_{2-1\text{anti}} = 11.7$ Hz, $J_{2-3} = 9.8$ Hz, $J_{2-1\text{syn}} = 9.6$

Hz, 1H, H₂), 3.74 (s, 3H, -OMe), 3.72 (s, 3H, -OMe), 3.42 (t, $J_{8-7} = 7.0$ Hz, 1H, H₈), 3.21 (dd, $J_{1\text{syn}-2} = 9.6$ Hz, $J_{1\text{syn}-1\text{anti}} = 3.4$ Hz, 1H, H_{1\text{syn}}}), 2.16-2.03 (m, 2H), 1.99 (m, 2H), 1.82 (s, 15H, C₅Me₅), 1.77 (dd, $J_{1\text{anti}-2} = 12.5$ Hz, $J_{1\text{anti}-1\text{syn}} = 3.9$ Hz, 1H, H_{1\text{anti}}}), 1.50 (m, 1H); ¹³C{¹H} NMR (100 MHz, CDCl₃): δ 169.3, 99.6, 99.0, 98.6, 95.3, 64.4, 52.6, 50.3, 30.3, 29.4, 9.6; Electrospray MS m/z calculated for C₂₂H₃₂O₄Co (M⁺ – BF₄⁻): 419.16271; found: 419.16223 (100%); Analysis calculated for C₂₂H₃₂O₄CoBF₄: C, 52.20%; H, 6.37%; found: C, 52.29%; H, 6.52%.



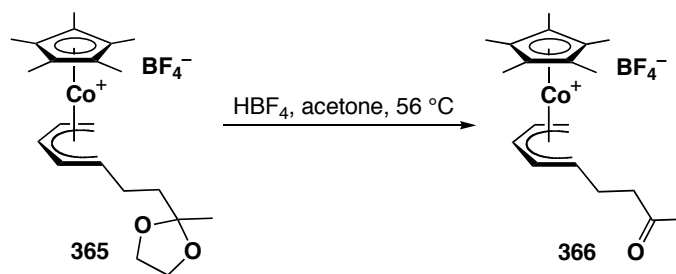
[Cp*Co(η⁵-1-(dimethyl-2-propylmalonyl)pentadienyl)]⁺BF₄⁻ (**363b**). In the drybox, Cp*Co(C₂H₄)₂ (0.720 g, 2.88 mmol) was dissolved in acetone (10 mL) and placed in a Schlenk tube equipped with a stir-bar and septum. The sealed flask was removed to the Schlenk line, cooled to -78 °C in a dry ice/acetone bath and HBF₄•Et₂O (397 μL, 2.88 mmol) was added. Upon addition of HBF₄, an immediate colour change from red to black was observed. The reaction was allowed to stir under argon for 15 minutes, then *E*-dimethyl-2-(6-hydroxyocta-4,7-dien-1-yl)malonate (**357b**) (0.813 g, 3.17 mmol) was added via syringe and the reaction allowed to warm to room temperature overnight. A gradual colour change from black to red occurred. The solvent was removed *in vacuo* and the product purified on the bench by silica gel chromatography using 3% MeOH/CH₂Cl₂. The red fraction was collected and dried to yield 1.20 g (80%) of

product as a red oil. Spectroscopy was not definitive due to the slow decomposition in solution persistently causing paramagnetic broadening, therefore this product was carried forward without further characterization.



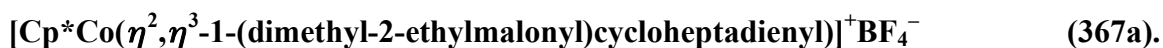
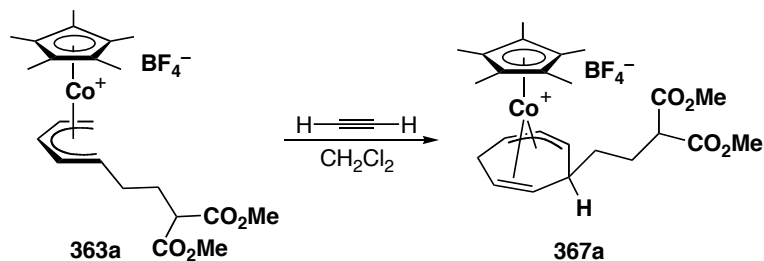
[Cp*Co(η^5 -1-(3-butanoylacetal)pentadienyl)]⁺BF₄⁻ (365). In the drybox, Cp*Co(C₂H₄)₂ (192 mg, 0.77 mmol) was dissolved in acetone (5 mL) and placed in a Schlenk tube equipped with a stir-bar and septum. The sealed flask was removed to the Schlenk line, cooled to -78 °C in a dry ice/acetone bath and HBF₄•Et₂O (105 μ L, 0.77 mmol) was added. Upon addition of HBF₄, an immediate colour change from red to black was observed. The reaction was allowed to stir under argon for 15 minutes, then *E*-7-(2-methyl-1,3-dioxolan-2-yl)hepta-1,4-dien-3-ol (**362**) (163 mg, 0.82 mmol) was added via syringe and the reaction mixture allowed to warm to room temperature overnight. A gradual colour change from black to red occurred. The solvent was removed *in vacuo* and the product purified on the bench by silica gel chromatography using 3% MeOH/CH₂Cl₂. The red fraction was collected and dried to yield 289 mg (81%) of product as a red oil. Crystallization via two-chambered liquid diffusion using CH₂Cl₂ and Et₂O provided red powder suitable for combustion analysis. IR (neat, cm⁻¹): 2981 (w), 1453 (w), 1430 (w), 1383 (w), 1222 (w), 1053 (s), 950 (w), 904 (w), 863 (w); ¹H NMR (400 MHz, CDCl₃): δ 6.46 (t, $J_{3-2} = J_{3-4} = 6.9$ Hz, 1H, H₃), 5.13 (dd, $J_{4-5} = 11.9$ Hz,

$J_{4-3} = 6.8$ Hz, 1H, H₄), 5.03 (ddd, $J_{2-1\text{anti}} = 11.8$ Hz, $J_{2-1\text{syn}} = 9.7$ Hz, $J_{2-3} = 7.1$ Hz, 1H, H₂), 3.94 (m, 4H, -OCH₂CH₂O-), 3.20 (dd, $J_{1\text{syn}-2} = 9.5$ Hz, $J_{1\text{syn}-1\text{anti}} = 3.4$ Hz, 1H, H_{1syn}), 2.10 (m, 1H, H₆), 1.96 (td, $J_{5-4} = J_{5-6} = 10.7$ Hz, $J_{5-6'} = 4.1$ Hz, 1H, H₅), 1.86 (s, 15H, C₅Me₅), 1.80-1.70 (m, 3H, H_{1anti}, H₇), 1.56 (dtd, $J_{6'-6} = 12.5$ Hz, $J_{6'-5} = J_{6'-7} = 10.2$ Hz, $J_{6'-7'} = 5.5$ Hz, 1H, H_{6'}), 1.30 (s, 3H, Me); ¹H-¹H GCOSY (400 MHz, CDCl₃): δ 6.46 (H₃) ↔ δ 5.13 (H₄), 5.03 (H₂), 3.20 (H_{1syn}), 1.96 (H₅), 1.65 (H_{1anti}); δ 5.13 (H₄) ↔ δ 1.96 (H₅); δ 5.03 (H₂) ↔ δ 3.20 (H_{1syn}), 1.65 (H_{1anti}); δ 3.20 (H_{1syn}) ↔ δ 1.65 (H_{1anti}); δ 2.10 (H₆) ↔ δ 1.96 (H₅), 1.70 (H₇), 1.56 (H_{6'}); δ 1.96 (H₅) ↔ δ 1.56 (H_{6'}); δ 1.70 (H₇) ↔ δ 1.56 (H_{6'}); ¹³C{¹H} NMR (100 MHz, CDCl₃): δ 109.3, 99.87, 99.29, 98.7, 95.7, 87.8, 65.0, 64.9, 64.2, 40.2, 28.1, 24.2, 10.0; Electrospray MS *m/z* calculated for C₂₁H₃₂O₂Co (M⁺ – BF₄): 375.17288; found: 375.17293 (100%); Analysis calculated for C₂₁H₃₂O₂CoBF₄: C, 54.57%; H, 6.98%; found: C, 54.46%; H, 7.02%.



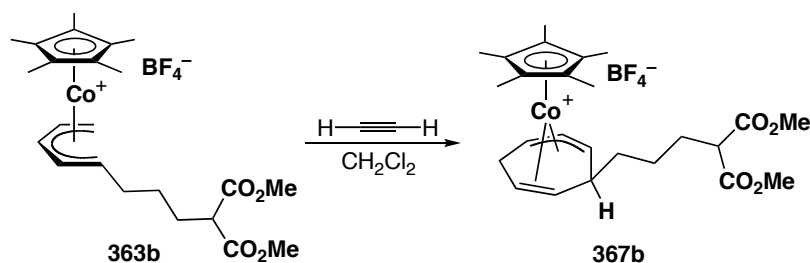
[Cp*Co(η^5 -1-(3-oxobutyl)pentadienyl)]⁺BF₄⁻ (366). Protected pentadienyl complex **365** (52 mg, 0.11 mmol) was placed in a round-bottom flask equipped with a reflux condenser and dissolved in off-the-shelf acetone (15 mL). To this, HBF₄•OEt₂ (10 μ L) was added and heated at reflux overnight (\approx 16 hours). The solvent was removed *in vacuo* and the residue purified via bench top silica gel chromatography using 3% MeOH/CH₂Cl₂ to provide 38 mg (81%) of deprotected pentadienyl complex **366**.

Crystallization via two-chambered liquid diffusion using CH₂Cl₂ and Et₂O provided red crystals suitable for combustion and X-ray analysis. IR (neat, cm⁻¹): 2923 (m), 1709 (s), 1460 (m), 1428 (m), 1391 (m), 1366 (w), 1285 (w), 1270 (m), 1184 (w), 1165 (m), 1054 (s), 951 (w), 920 (w), 895 (w), 817 (w), 736 (w); ¹H NMR (400 MHz, CDCl₃): δ 6.33 (t, $J_{3-2} = J_{3-4} = 7.0$ Hz, 1H, H₃), 5.18 (dd, $J_{4-5} = 11.9$ Hz, $J_{4-3} = 6.8$ Hz, 1H, H₄), 4.98 (ddd, $J_{2-1\text{anti}} = 11.5$ Hz, $J_{2-1\text{syn}} = 9.8$ Hz, $J_{2-3} = 7.2$ Hz, 1H, H₂), 3.18 (dd, $J_{1\text{syn}-2} = 9.6$ Hz, $J_{1\text{syn}-1\text{anti}} = 3.5$ Hz, 1H, H_{1syn}), 2.65 (t, $J_{7-6} = J_{7-6'}$ = 6.9 Hz, 2H, H₇), 2.28 (dtd, $J_{6-6'} = 17.0$ Hz, $J_{6-7} = 6.9$ Hz, $J_{6-5} = 4.0$ Hz, 1H, H₆), 2.08 (s, 3H, Me), 2.01 (m, 1H, H₅), 1.84 (s, 15H, C₅Me₅), 1.80 (dd, $J_{1\text{anti}-2} = 11.8$ Hz, $J_{1\text{anti}-1\text{syn}} = 3.3$ Hz, 1H, H_{1anti}), 1.69 (m, 1H, H_{6'}); ¹H-¹H GCOSY (400 MHz, CDCl₃): δ 6.33 (H₃) ↔ δ 5.18 (H₄), 4.98 (H₂), 3.18 (H_{1syn}), 2.01 (H₅), 1.80 (H_{1anti}); δ 5.18 (H₄) ↔ δ 2.01 (H₅); δ 4.98 (H₂) ↔ δ 3.18 (H_{1syn}), 1.80 (H_{1anti}); δ 3.18 (H_{1syn}) ↔ δ 1.80 (H_{1anti}); δ 2.65 (H₇) ↔ δ 2.28 (H₆), 1.69 (H_{6'}); δ 2.28 (H₆) ↔ δ 2.01 (H₅), 1.69 (H_{6'}); δ 2.01 (H₅) ↔ δ 1.69 (H_{6'}); ¹³C{¹H} NMR (100 MHz, CDCl₃): δ 207.4, 99.7, 99.3, 98.4, 95.2, 86.3, 64.3, 43.6, 30.0, 26.9, 9.7; Electrospray MS *m/z* calculated for C₁₉H₂₈OCo (M⁺ – BF₄⁻): 331.14666; found: 331.14672 (100%); Analysis calculated for C₁₉H₂₈OCoBF₄: C, 54.57%; H, 6.75%; found: C, 54.56%; H, 6.91%.



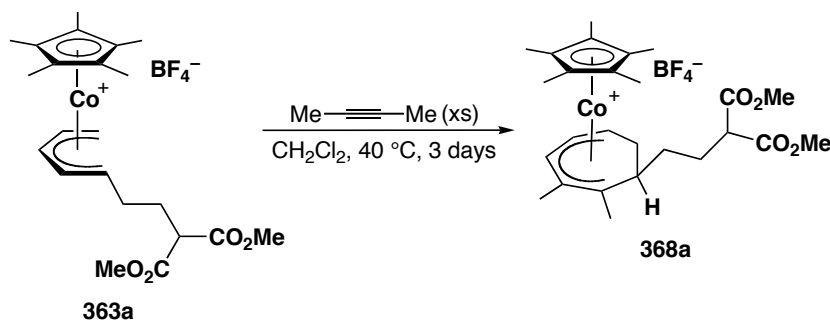
Pentadienyl complex **363a** (127 mg, 0.25 mmol) was dissolved in CH₂Cl₂ (10 mL) and

degassed with argon for 5 minutes. Simultaneously, acetylene was bubbled through CH_2Cl_2 in a test-tube for 25 minutes in order to ensure saturation. Then, 2 mL of this saturated solution was transferred to the bomb via cannula. The bomb was sealed and allowed to stand at room temperature for 3 days. The solvent was removed *in vacuo* and the product purified by silica gel chromatography using 3% MeOH/ CH_2Cl_2 . The red fraction was collected and dried providing 119 mg (89%) of product as a thick, red oil. After repeat crystallizations, we were unable to obtain a sample suitable for combustion analysis. IR (CH_2Cl_2 cast, cm^{-1}): 2957 (m), 2919 (w), 2865 (w), 1732 (s), 1455 (m), 1436 (m), 1389 (m), 1346 (w), 1285 (m), 1225 (m), 1153 (m), 1056 (s), 798 (w), 732 (w); ^1H NMR (400 MHz, CDCl_3): δ 3.92 (td, $J_{3-2} = J_{3-4\text{endo}} = 8.3$ Hz, $J_{3-4\text{exo}} = 4.1$ Hz, 1H, H_3), 3.71 (s, 3H, -OMe), 3.70 (s, 3H, -OMe), 3.60 (dd, $J_{1-2} = 7.6$ Hz, $J_{1-7} = 3.8$ Hz, 1H, H_1), 3.41 (t, $J_{10-9} = 6.9$ Hz, 1H, H_{10}), 3.30 (t, $J_{2-1} = J_{2-3} = 7.6$ Hz, 1H, H_2), 3.10 (dt, $J_{4\text{endo}-4\text{exo}} = 14.1$ Hz, $J_{4\text{endo}-3} = J_{4\text{endo}-5} = 8.5$ Hz, 1H, $\text{H}_{4\text{endo}}$), 2.83 (td, $J_{5-4\text{endo}} = J_{5-6} = 7.3$ Hz, $J_{5-4\text{exo}} = 4.9$ Hz, 1H, H_5), 2.42 (dd, $J_{6-5} = 6.6$ Hz, $J_{6-7} = 4.5$ Hz, 1H, H_6), 2.16 (tt, $J_{7-8} = 7.6$ Hz, $J_{7-1} = J_{7-6} = 3.7$ Hz, 1H, H_7), 2.04 (dt, $J_{4\text{exo}-4\text{endo}} = 14.1$ Hz, $J_{4\text{exo}-3} = J_{4\text{exo}-5} = 4.3$ Hz, 1H, $\text{H}_{4\text{exo}}$), 1.90 (m, 2H, H_9), 1.82-1.78 (m, 2H, H_8 , overlaps Cp^* peak), 1.77 (s, 15H, C_5Me_5); ^1H - ^1H GCOSY (400 MHz, CDCl_3): δ 3.92 (H_3) \leftrightarrow δ 3.60 (H_1), 3.30 (H_2), 3.10 ($\text{H}_{4\text{endo}}$), 2.04 ($\text{H}_{4\text{exo}}$); δ 3.60 (H_1) \leftrightarrow δ 3.30 (H_2), 2.16 (H_7); δ 3.41 (H_{10}) \leftrightarrow δ 1.90 (H_9); δ 3.30 (H_2) \leftrightarrow δ 2.04 ($\text{H}_{4\text{exo}}$); δ 3.10 ($\text{H}_{4\text{endo}}$) \leftrightarrow δ 2.83 (H_5), 2.42 (H_6), 2.04 ($\text{H}_{4\text{exo}}$); δ 2.83 (H_5) \leftrightarrow δ 2.42 (H_6), 2.04 ($\text{H}_{4\text{exo}}$); δ 2.42 (H_6) \leftrightarrow δ 2.16 (H_7); δ 2.16 (H_7) \leftrightarrow δ 1.82-1.78 (H_8); δ 1.90 (H_9) \leftrightarrow δ 1.82-1.78 (H_8); $^{13}\text{C}\{^1\text{H}\}$ NMR (100 MHz, CDCl_3): δ 169.5, 97.8, 92.2, 53.1, 52.6, 50.8, 49.3, 45.8, 44.5, 31.9, 31.1, 25.3, 21.4, 9.5; Electrospray MS m/z calculated for $\text{C}_{24}\text{H}_{34}\text{O}_4\text{Co}$ ($\text{M}^+ - \text{BF}_4$): 445.17836; found: 445.17834 (100%).



Pentadienyl complex **363b** (827 mg, 1.59 mmol) was dissolved in CH₂Cl₂ (10 mL) and degassed with argon for 5 minutes. Simultaneously, acetylene was bubbled through CH₂Cl₂ in a test-tube for 25 minutes in order to ensure saturation. Then, 15 mL of this saturated solution was transferred to the bomb via cannula. The bomb was sealed and allowed to stand at room temperature for 3 days. The solvent was removed *in vacuo* and the product purified by silica gel chromatography using 3% MeOH/CH₂Cl₂. The red fraction was collected and dried providing 702 mg (81%) of product as a thick, red oil. Crystallization via two-chambered liquid diffusion using CH₂Cl₂ and Et₂O provided red crystals suitable for combustion and X-ray analysis. IR (CH₂Cl₂ cast, cm⁻¹): 2955 (m), 2863 (w), 1732 (s), 1653 (w), 1457 (m), 1436 (m), 1388 (m), 1282 (m), 1220 (m), 1156 (m), 1054 (s), 891 (w), 796 (w), 732 (m); ¹H NMR (400 MHz, CDCl₃): δ 3.96 (td, $J_{3-2} = J_{3-4\text{endo}} = 8.4$ Hz, $J_{3-4\text{exo}} = 4.0$ Hz, 1H, H₃), 3.73 (s, 6H, -OMe), 3.58 (dd, $J_{1-2} = 7.6$ Hz, $J_{1-7} = 3.8$ Hz, 1H, H₁), 3.41 (t, $J_{11-10} = 7.5$ Hz, 1H, H₁₁), 3.34 (t, $J_{2-1} = J_{2-3} = 7.6$ Hz, 1H, H₂), 3.15 (dt, $J_{4\text{endo-4exo}} = 14.3$ Hz, $J_{4\text{endo-3}} = J_{4\text{endo-5}} = 8.7$ Hz, 1H, H_{4endo}), 2.87 (td, $J_{5-4\text{endo}} = J_{5-6} = 7.1$ Hz, $J_{5-4\text{exo}} = 5.4$ Hz, 1H, H₅), 2.36 (dd, $J_{6-5} = 6.3$ Hz, $J_{6-7} = 4.7$ Hz, 1H, H₆), 2.18 (tt, $J_{7-8} = 8.0$ Hz, $J_{7-1} = J_{7-6} = 3.7$ Hz, 1H, H₇), 2.10 (dt, $J_{4\text{exo-4endo}} = 14.4$ Hz, $J_{4\text{exo-3}} = J_{4\text{exo-5}} = 4.1$ Hz, 1H, H_{4exo}), 1.93 (q, $J_{10-9} = J_{10-11} = 7.7$ Hz, 2H, H₁₀), 1.88-1.79 (m, 2H, H₈, overlaps Cp* peak), 1.82 (s, 15H, C₅Me₅), 1.44 (m, 2H, H₉); ¹H-¹H GCOSY (400 MHz,

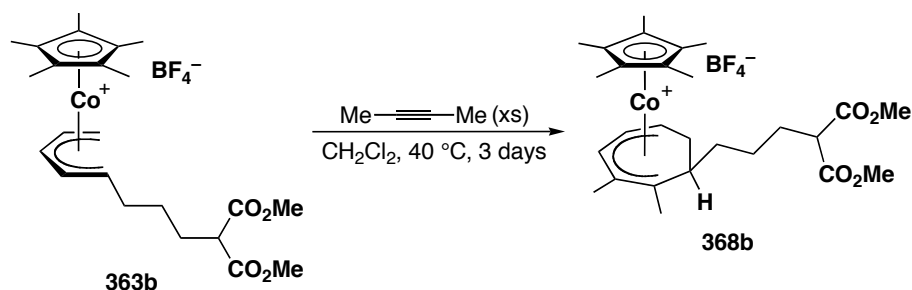
CDCl₃): δ 3.96 (H₃) ↔ δ 3.34 (H₂), 3.15 (H_{4endo}), 2.10 (H_{4exo}); δ 3.58 (H₁) ↔ δ 3.34 (H₂), 2.18 (H₇); δ 3.41 (H₁₁) ↔ δ 1.93 (H₁₀); δ 3.15 (H_{4endo}) ↔ δ 2.87 (H₅), 2.10 (H_{4exo}); δ 2.87 (H₅) ↔ δ 2.36 (H₆), 2.10 (H_{4exo}); δ 2.36 (H₆) ↔ δ 2.18 (H₇); δ 2.18 (H₇) ↔ δ 1.88-1.79 (H₈); δ 1.93 (H₁₀) ↔ δ 1.44 (H₉); ¹³C {¹H} NMR (100 MHz, CDCl₃): δ 169.6, 97.7, 92.2, 53.5, 52.5, 51.1, 49.8, 45.9, 44.7, 33.5, 31.8, 28.2, 23.7, 21.6, 9.6; Electrospray MS *m/z* calculated for C₂₅H₃₆O₄Co (M⁺ – BF₄): 459.19401; found: 459.19432 (100%); Analysis calculated for C₂₅H₃₆O₄CoBF₄: C, 54.97%; H, 6.64%; found: C, 54.52%; H, 6.64%.



[Cp*Co(η⁵-1,2-dimethyl-7-(dimethyl-2-ethylmalonyl)cycloheptadienyl)]⁺BF₄⁻

(368a). Pentadienyl complex **363a** (311 mg, 0.62 mmol) was dissolved in CH₂Cl₂ (10 mL) in a reaction bomb and degassed with argon for 5 minutes. To this, 2-butyne (325 μL, 4.15 mmol) was added via syringe. The bomb was sealed and heated at 40 °C for 3 days in an oil bath. The solvent was then removed *in vacuo* and the product purified by silica gel chromatography using 3% MeOH/CH₂Cl₂. The red fraction was collected and dried providing 241 mg (70%) of product as a thick, red oil. Crystallization via two-chambered liquid diffusion using CH₂Cl₂ and Et₂O provided red crystals suitable for combustion analysis. IR (CH₂Cl₂ cast, cm⁻¹): 2956 (m), 2909 (m), 1732 (s), 1435 (s), 1384 (m), 1345 (w), 1268 (m), 1239 (m), 1199 (m), 1150 (m), 1054 (s), 910 (w), 864 (w),

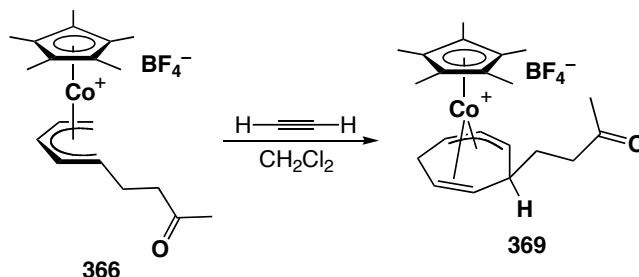
732 (m), 700 (m); ^1H NMR (600 MHz, CDCl_3): δ 6.59 (d, $J_{1-2} = 7.4$ Hz, 1H, H_1), 4.69 (t, $J_{2-1} = J_{2-3} = 8.4$ Hz, 1H, H_2), 4.36 (dt, $J_{3-2} = 9.1$ Hz, $J_{3-4\text{endo}} = J_{3-4\text{exo}} = 3.3$ Hz, 1H, H_3), 3.71 (s, 3H, -OMe), 3.70 (s, 3H, -OMe), 3.21 (t, $J_{8-7} = 7.1$ Hz, 1H, H_8), 2.48 (ddd, $J_{4\text{endo}-4\text{exo}} = 16.7$ Hz, $J_{4\text{endo}-5} = 11.9$ Hz, $J_{4\text{endo}-3} = 2.8$ Hz, 1H, $\text{H}_{4\text{exo}}$), 2.34 (dt, $J_{4\text{exo}-4\text{endo}} = 16.7$ Hz, $J_{4\text{exo}-3} = J_{4\text{exo}-5} = 3.1$ Hz, 1H, $\text{H}_{4\text{exo}}$), 2.22 (s, 3H, Me), 1.75 (s, 15H, C_5Me_5), 1.61 (m, 1H, H_7), 1.48 (dddd, $J_{7'-7} = 18.7$ Hz, $J_{7'-6} = 11.8$ Hz, $J_{7'-8} = 7.2$ Hz, $J_{7'-6'}$ = 4.5 Hz, 1H, $\text{H}_{7'}$), 1.35 (tt, $J_{6-6'} = J_{6-7'} = 12.3$ Hz, $J_{6-5} = J_{6-7} = 5.0$ Hz, 1H, H_6), 1.29 (s, 3H, Me), 1.23 (tdd, $J_{6'-6} = J_{6'-7} = 13.4$ Hz, $J_{6'-5} = 9.0$ Hz, $J_{6'-7'}$ = 5.2 Hz, 1H, $\text{H}_{6'}$), 0.02 (ddt, $J_{5-4\text{endo}} = 12.8$ Hz, $J_{5-6'} = 9.3$ Hz, $J_{5-4\text{exo}} = J_{5-6} = 4.7$ Hz, 1H, H_5); ^1H - ^1H GCOSY (600 MHz, CDCl_3): δ 6.59 (H_1) \leftrightarrow δ 4.69 (H_2); δ 4.69 (H_2) \leftrightarrow δ 4.36 (H_3); δ 4.36 (H_3) \leftrightarrow δ 2.48 ($\text{H}_{4\text{endo}}$), 2.34 ($\text{H}_{4\text{exo}}$); δ 3.21 (H_8) \leftrightarrow δ 1.61 (H_7), 1.48 ($\text{H}_{7'}$); δ 2.48 ($\text{H}_{4\text{endo}}$) \leftrightarrow δ 2.34 ($\text{H}_{4\text{exo}}$), 0.02 (H_5); δ 2.34 ($\text{H}_{4\text{exo}}$) \leftrightarrow δ 0.02 (H_5); δ 1.61 (H_7) \leftrightarrow δ 1.48 ($\text{H}_{7'}$), 1.35 (H_6), 1.23 ($\text{H}_{6'}$); δ 1.48 ($\text{H}_{7'}$) \leftrightarrow δ 1.35 (H_6), 1.23 ($\text{H}_{6'}$); δ 1.35 (H_6) \leftrightarrow δ 1.23 ($\text{H}_{6'}$), 0.02 (H_5); δ 1.23 ($\text{H}_{6'}$) \leftrightarrow δ 0.02 (H_5); $^{13}\text{C}\{^1\text{H}\}$ NMR (100 MHz, CDCl_3): δ 169.4, 108.7, 100.9, 99.1, 97.7, 96.1, 86.6, 52.6, 51.3, 47.9, 41.7, 28.2, 28.0, 19.2, 17.0, 9.0; Electrospray MS m/z calculated for $\text{C}_{26}\text{H}_{38}\text{O}_4\text{Co}$ ($\text{M}^+ - \text{BF}_4$): 473.20966; found: 473.20964 (100%); Analysis calculated for $\text{C}_{26}\text{H}_{38}\text{O}_4\text{CoBF}_4$: C, 55.73%; H, 6.84%; found: C, 55.48%; H, 7.20%.



[Cp*Co(η^5 -1,2-dimethyl-7-(dimethyl-2-propylmalonyl)cycloheptadienyl)]⁺BF₄⁻

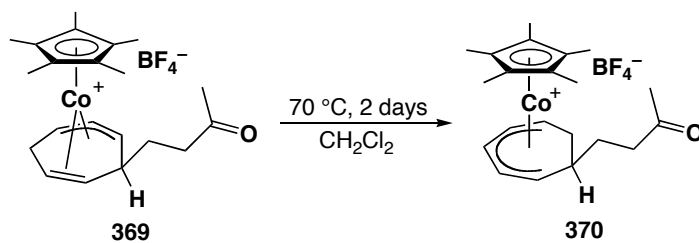
(368b). Pentadienyl complex **363b** (53 mg, 0.10 mmol) was dissolved in CH₂Cl₂ (10 mL) in a reaction bomb and degassed with argon for 5 minutes. To this, 2-butyne (50 μ L, 0.64 mmol) was added via syringe. The bomb was sealed and heated at 40 °C for 3 days in an oil bath. The solvent was then removed *in vacuo* and the product purified by silica gel chromatography using 3% MeOH/CH₂Cl₂. The red fraction was collected and dried providing 54 mg (93%) of product as a thick, red oil. Crystallization was unsuccessful for obtaining analytically pure material despite multiple attempts due to the oily nature of the product. IR (CH₂Cl₂ cast, cm⁻¹): 2955 (m), 1732 (s), 1436 (m), 1384 (m), 1276 (m), 1232 (m), 1152 (m), 1056 (s), 909 (w), 733 (m); ¹H NMR (400 MHz, CDCl₃): δ 6.58 (d, $J_{1-2} = 7.3$ Hz, 1H, H₁), 4.68 (t, $J_{2-1} = J_{2-3} = 8.5$ Hz, 1H, H₂), 4.34 (dt, $J_{3-2} = 9.3$ Hz, $J_{3-4\text{endo}} = J_{3-4\text{exo}} = 3.1$ Hz, 1H, H₃), 3.69 (s, 3H, -OMe), 3.68 (s, 3H, -OMe), 3.23 (t, $J_{9-8} = 7.4$ Hz, 1H, H₉), 2.42 (ddd, $J_{4\text{endo-4exo}} = 16.9$ Hz, $J_{4\text{endo-5}} = 11.7$ Hz, $J_{4\text{endo-3}} = 2.9$ Hz, 1H, H_{4endo}), 2.30 (dt, $J_{4\text{exo-4endo}} = 17.1$ Hz, $J_{4\text{exo-3}} = J_{4\text{exo-5}} = 3.6$ Hz, 1H, H_{4exo}), 2.20 (s, 3H, Me), 1.90-1.70 (m, 2H, H₈, overlaps Cp* peak), 1.74 (s, 15H, C₅Me₅), 1.38-1.19 (m, 2H, H₆, overlaps Me peak), 1.26 (s, 3H, Me), 1.07 (m, 1H, H₇), 0.88 (m, 1H, H₇), 0.00 (m, 1H, H₅); ¹H-¹H GCOSY (400 MHz, CDCl₃): δ 6.58 (H₁) \leftrightarrow δ 4.68 (H₂); δ 4.68 (H₂) \leftrightarrow δ 4.34 (H₃); δ 4.34 (H₃) \leftrightarrow δ 2.42 (H_{4endo}), 2.30 (H_{4exo}); δ 3.23 (H₉) \leftrightarrow δ 1.90-1.70 (H₈); δ 2.42 (H_{4endo}) \leftrightarrow δ 2.30 (H_{4exo}), 0.00 (H₅); δ 2.30 (H_{4exo}) \leftrightarrow δ 0.00 (H₅); δ 1.90-1.70 (H₈) \leftrightarrow δ

1.07 (H₇), 0.88 (H_{7'}); δ 1.38-1.19 (H₆) ↔ δ 1.07 (H₇), 0.88 (H_{7'}), 0.00 (H₅); δ 1.07 (H₇) ↔ δ 0.88 (H_{7'}); ¹³C{¹H} NMR (100 MHz, CDCl₃): δ 169.5, 108.6, 101.0, 99.2, 97.5, 96.3, 86.8, 52.4, 51.2, 48.0, 41.3, 30.3, 28.5, 26.5, 19.1, 16.9, 9.0; Electrospray MS *m/z* calculated for C₂₇H₄₀O₄Co (M⁺ – BF₄): 487.22531; found: 487.22550 (100%).



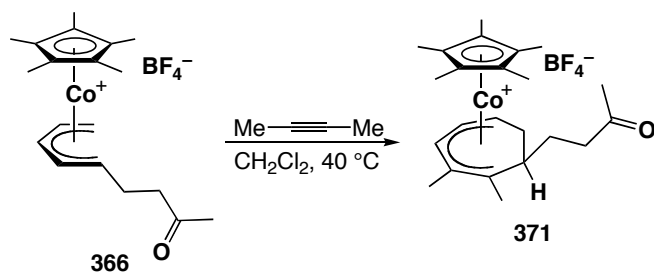
[Cp*Co(η^2, η^3 -1-(3-butanoyl)cycloheptadienyl)]⁺BF₄⁻ (369). Pentadienyl complex **366** (141 mg, 0.34 mmol) was dissolved in CH₂Cl₂ (10 mL) and degassed with argon for 5 minutes. Simultaneously, acetylene was bubbled through CH₂Cl₂ in a test-tube for 25 minutes in order to ensure saturation. Then, 3 mL of this saturated solution was transferred to the bomb via cannula. The bomb was sealed and allowed to stand at room temperature for 3 days. The solvent was removed *in vacuo* and the product purified by silica gel chromatography using 3% MeOH/CH₂Cl₂. The red fraction was collected and dried providing 131 mg (88%) of product as a thick, red oil. Crystallization via two-chambered liquid diffusion using CH₂Cl₂ and Et₂O provided red crystals suitable for combustion and X-ray analysis. IR (CH₂Cl₂ cast, cm⁻¹): 2919 (m), 1711 (s), 1454 (m), 1428 (m), 1384 (s), 1284 (w), 1231 (w), 1170 (w), 1056 (s), 895 (w), 846 (w), 798 (w); ¹H NMR (400 MHz, CDCl₃): δ 3.91 (td, *J*₃₋₂ = *J*_{3-4endo} = 8.4 Hz, *J*_{3-4exo} = 4.0 Hz, 1H, H₃), 3.69 (dd, *J*₁₋₂ = 7.5 Hz, *J*₁₋₇ = 3.7 Hz, 1H, H₁), 3.33 (t, *J*₂₋₁ = *J*₂₋₃ = 7.6 Hz, 1H, H₂), 3.10 (td, *J*_{4endo-4exo} = 14.1 Hz, *J*_{4endo-3} = *J*_{4endo-5} = 8.4 Hz, 1H, H_{4endo}), 2.86 (td, *J*_{5-4endo} = *J*₅₋₆ =

7.2 Hz, $J_{5-4\text{exo}} = 4.8$ Hz, 1H, H₅), 2.69 (t, $J_{9-8} = 7.2$ Hz, 2H, H₉), 2.49 (dd, $J_{6-5} = 6.4$ Hz, $J_{6-7} = 4.6$ Hz, 1H, H₆), 2.21 (m, 1H, H₇, overlaps Me peak), 2.19 (s, 3H, Me), 2.11 (m, 1H, H_{4exo}, overlaps H₈), 2.08 (t, $J_{8-9} = 6.8$ Hz, 2H, H₈), 1.84 (s, 15H, C₅Me₅); ¹H-¹H GCOSY (400 MHz, CDCl₃): δ 3.91 (H₃) ↔ δ 3.33 (H₂), 3.10 (H_{4endo}), 2.11 (H_{4exo}); δ 3.69 (H₁) ↔ δ 3.33 (H₂), 2.21 (H₇); δ 3.33 (H₂) ↔ δ 2.21 (H₇); δ 3.10 (H_{4endo}) ↔ δ 2.86 (H₅), 2.49 (H₆), 2.11 (H_{4exo}); δ 2.86 (H₅) ↔ δ 2.49 (H₆), 2.11 (H_{4exo}); δ 2.69 (H₉) ↔ δ 2.08 (H₈); δ 2.49 (H₆) ↔ δ 2.21 (H₇); ¹³C{¹H} NMR (100 MHz, CDCl₃): δ 208.5, 97.8, 92.2, 53.4, 49.8, 45.8, 44.4, 39.8, 31.6, 30.1, 27.2, 21.6, 9.6; Electrospray MS *m/z* calculated for C₂₁H₃₀OC_o (M⁺ – BF₄⁻): 357.16231; found: 357.16251 (100%); Analysis calculated for C₂₁H₃₀OC_oBF₄: C, 56.78%; H, 6.81%; found: C, 56.69%; H, 6.83%.



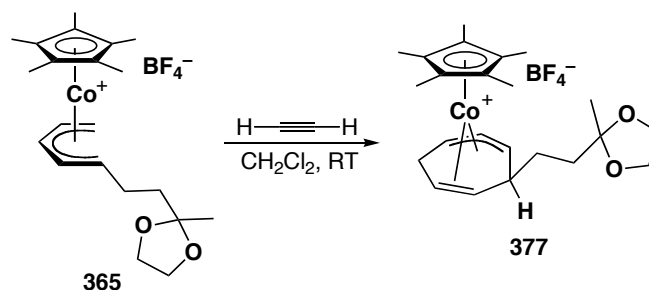
[Cp*Co(η⁵-1-(3-oxobutyl)cycloheptadienyl)]⁺BF₄⁻ (370). Allyl/olefin complex **369** (40 mg, 0.090 mmol) was dissolved in CH₂Cl₂ (5 mL) in a reaction bomb and heated at 70 °C for 2 days. The solvent was removed *in vacuo* and the product purified by silica gel chromatography to provide 36 mg (90%) of the isomerized product **370** as a red oil. Crystallization via two-chambered liquid diffusion using CH₂Cl₂ and Et₂O provided red crystals suitable for combustion and X-ray analysis. IR (neat, cm⁻¹): 3048 (w), 2961 (w), 2919 (w), 2852 (w), 1708 (s), 1489 (w), 1450 (m), 1420 (m), 1388 (m), 1379 (m), 1359 (w), 1318 (w), 1286 (w), 1268 (w), 1227 (w), 1193 (w), 1174 (m), 1154 (m), 1099 (s), 1057 (s), 1038 (s), 964 (m); ¹H NMR (400 MHz, CDCl₃): δ 6.63 (t, $J_{3-2} = J_{3-4} = 6.5$ Hz,

1H, H₃), 5.34 (t, $J_{2-1} = J_{2-3} = 7.2$ Hz, 1H, H₂), 4.94 (t, $J_{4-3} = J_{4-5} = 8.3$ Hz, 1H, H₄), 4.34 (dt, $J_{5-4} = 9.2$ Hz, $J_{5-6endo} = J_{5-6exo} = 3.7$ Hz, 1H, H₅), 4.08 (dd, $J_{1-2} = 8.0$ Hz, $J_{1-7} = 3.8$ Hz, 1H, H₁), 2.45-2.33 (m, 3H, H_{6endo}, H₉), 2.11 (s, 3H, Me), 2.06 (br. dt, $J_{6exo-6endo} = 17.0$ Hz, $J_{6exo-5} = J_{6exo-7} = 3.5$ Hz, 1H, H_{6exo}), 1.88 (s, 15H, C₅Me₅), 1.71-1.51 (m, 2H, H₈), 0.56 (br. m, 1H, H₇); ¹H-¹H GCOSY (400 MHz, CDCl₃): δ 6.63 (H₃) ↔ δ 5.34 (H₂), 4.94 (H₄), 4.08 (H₁); δ 5.34 (H₂) ↔ δ 4.08 (H₁); δ 4.94 (H₄) ↔ δ 4.34 (H₅); δ 4.34 (H₅) ↔ δ 2.35 (H_{6endo}), 2.06 (H_{6exo}); δ 4.08 (H₁) ↔ δ 0.56 (H₇); δ 2.40 (H₉) ↔ δ 1.65 (H₈); δ 2.35 (H_{6endo}) ↔ δ 2.06 (H_{6exo}), 0.56 (H₇); δ 2.06 (H_{6exo}) ↔ δ 0.56 (H₇); δ 1.65 (H₈) ↔ δ 0.56 (H₇); ¹³C{¹H} NMR (100 MHz, CDCl₃): δ 208.3, 100.5, 98.8, 97.9, 97.7, 94.0, 88.4, 46.6, 41.2, 39.3, 30.0, 29.7, 9.7; Electrospray MS *m/z* calculated for C₂₁H₃₀OC_o (M⁺ – BF₄): 357.16231; found: 357.16208 (100%); Analysis calculated for C₂₁H₃₀OC_oBF₄: C, 56.78%; H, 6.81%; found: C, 56.87%; H, 6.75%.



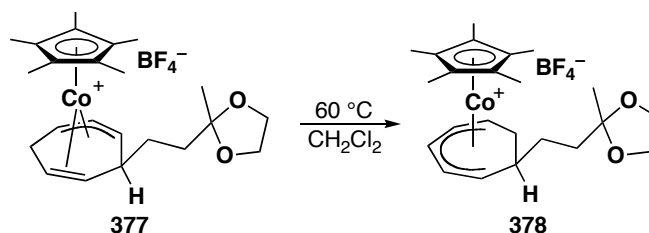
[Cp*Co(η^5 -1,2-dimethyl-7-(3-butanoyl)cycloheptadienyl)]⁺BF₄⁻ (371). Pentadienyl complex **366** (82 mg, 0.20 mmol) was dissolved in CH₂Cl₂ (5 mL) in a reaction bomb and degassed with argon for 3 minutes. To this, 2-butyne (100 μ L, 1.28 mmol) was added via syringe. The bomb was sealed and heated at 40 °C for 3 days in an oil bath. The solvent was then removed *in vacuo* and the product purified by silica gel chromatography using 3% MeOH/CH₂Cl₂. The red fraction was collected and dried

providing 74 mg (80%) of product as a thick, red oil that contained approximately 10% impurity, tentatively characterized as cobaltocenium type products. Crystallization was not successful in producing analytically pure material, despite many attempts, returning only oils. IR (neat, cm^{-1}): 2965 (w), 2912 (w), 1711 (s), 1455 (m), 1432 (m), 1384 (s), 1282 (w), 1163 (w), 1054 (s), 910 (w), 865 (w); ^1H NMR (400 MHz, CDCl_3): δ 6.49 (d, $J_{1-2} = 7.3$ Hz, 1H, H_1), 4.60 (t, $J_{2-1} = J_{2-3} = 7.8$ Hz, 1H, H_2), 4.34 (dt, $J_{3-2} = 9.1$ Hz, $J_{3-4\text{endo}} = J_{3-4\text{exo}} = 3.3$ Hz, 1H, H_3), 2.45 (ddd, $J_{4\text{endo}-4\text{exo}} = 16.7$ Hz, $J_{4\text{endo}-5} = 11.8$ Hz, $J_{4\text{endo}-3} = 3.0$ Hz, 1H, $\text{H}_{4\text{endo}}$), 2.25 (dt, $J_{4\text{exo}-4\text{endo}} = 16.6$ Hz, $J_{4\text{exo}-3} = J_{4\text{exo}-5} = 3.2$ Hz, 1H, $\text{H}_{4\text{exo}}$), 2.19 (s, 3H, Me), 2.15 (m, 1H, H_7), 2.10 (m, 1H, $\text{H}_{7'}$), 2.01 (s, 3H, Me), 1.73 (s, 15H, C_5Me_5), 1.61 (m, 1H, H_6), 1.45 (m, 1H, $\text{H}_{6'}$), 1.30 (s, 3H, Me), -0.01 (tt, $J_{5-4\text{endo}} = J_{5-6} = 9.7$ Hz, $J_{5-4\text{exo}} = J_{5-6'} = 4.5$ Hz, 1H, H_5); ^1H - ^1H GCOSY (400 MHz, CDCl_3): δ 6.49 (H_1) \leftrightarrow δ 4.60 (H_2); δ 4.60 (H_2) \leftrightarrow δ 4.34 (H_3); δ 4.34 (H_3) \leftrightarrow δ 2.45 ($\text{H}_{4\text{endo}}$), 2.25 ($\text{H}_{4\text{exo}}$); δ 2.45 ($\text{H}_{4\text{endo}}$) \leftrightarrow δ 2.25 ($\text{H}_{4\text{exo}}$), -0.01 (H_5); δ 2.25 ($\text{H}_{4\text{exo}}$) \leftrightarrow δ -0.01 (H_5); δ 2.15 (H_7) \leftrightarrow δ 2.10 ($\text{H}_{7'}$), 1.61 (H_6), 1.45 ($\text{H}_{6'}$); δ 2.10 ($\text{H}_{7'}$) \leftrightarrow δ 1.61 (H_6), 1.45 ($\text{H}_{6'}$); δ 1.61 (H_6) \leftrightarrow δ 1.45 ($\text{H}_{6'}$), -0.01 (H_5); δ 1.45 ($\text{H}_{6'}$) \leftrightarrow δ -0.01 (H_5); $^{13}\text{C}\{^1\text{H}\}$ NMR (100 MHz, CDCl_3): δ 208.2, 108.6, 101.2, 99.1, 97.7, 96.2, 86.8, 47.7, 42.5, 41.2, 30.1, 24.3, 19.4, 17.1, 9.1; Electrospray MS m/z calculated for $\text{C}_{23}\text{H}_{34}\text{OC}_5\text{Me}_5$ ($\text{M}^+ - \text{BF}_4$): 385.19362; found: 385.19380 (100%).



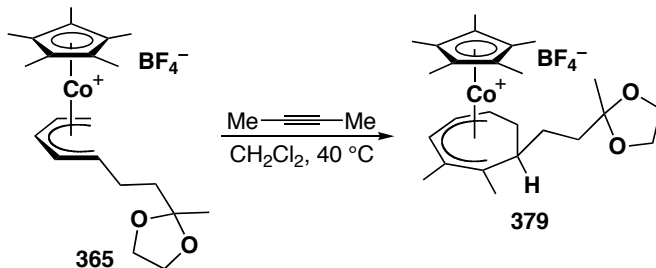
[Cp*Co(η^2, η^3 -1-(3-butanoyl)cycloheptadienyl)]⁺BF₄⁻ (377). Pentadienyl complex **365** (40 mg, 0.087 mmol) was dissolved in CH₂Cl₂ (10 mL) and degassed with argon for 5 minutes. Simultaneously, acetylene was bubbled through CH₂Cl₂ in a test-tube for 25 minutes in order to ensure saturation. Then, 6 mL of this saturated solution was transferred to the bomb via cannula. The bomb was sealed and allowed to stand at room temperature for 3 days. The solvent was removed *in vacuo* and the product purified by silica gel chromatography using 3% MeOH/CH₂Cl₂. The red fraction was collected and dried providing 34 mg (81%) of product as a thick, red oil. Crystallization via two-chambered liquid diffusion using CH₂Cl₂ and Et₂O provided red crystals suitable for combustion and X-ray analysis. IR (neat, cm⁻¹): 3063 (m), 2976 (s), 2930 (s), 1456 (s), 1383 (s), 1372 (s), 1349 (w), 1322 (w), 1280 (w), 1259 (s), 1236 (m), 1172 (w), 1144 (w), 1093 (s), 1048 (s), 1000 (m), 949 (m), 908 (m), 893 (m); ¹H NMR (400 MHz, CDCl₃): δ 3.95 (s, 4H, -OCH₂CH₂O-), 3.93 (m, 1H, H₃, overlaps acetal peak), 3.58 (dd, $J_{1-2} = 7.5$ Hz, $J_{1-7} = 3.7$ Hz, 1H, H₁), 3.34 (t, $J_{2-1} = J_{2-3} = 7.6$ Hz, 1H, H₂), 3.12 (dt, $J_{4\text{endo-}4\text{exo}} = 14.2$ Hz, $J_{4\text{endo-}3} = J_{4\text{endo-}5} = 8.3$ Hz, 1H, H_{4\text{endo}}}), 2.87 (td, $J_{5-4\text{endo}} = J_{5-6} = 7.7$ Hz, $J_{5-4\text{exo}} = 4.8$ Hz, 1H, H₅), 2.36 (dd, $J_{6-5} = 6.2$ Hz, $J_{6-7} = 4.8$ Hz, 1H, H₆), 2.17 (tt, $J_{7-8} = 7.3$ Hz, $J_{7-1} = J_{7-6} = 3.7$ Hz, 1H, H₇), 2.06 (dt, $J_{4\text{exo-}4\text{endo}} = 14.1$ Hz, $J_{4\text{exo-}3} = J_{4\text{exo-}5} = 4.2$ Hz, 1H, H_{4\text{exo}}}), 1.95-1.82 (m, 2H, H₈), 1.80 (s, 15H, C₅Me₅), 1.75-1.64 (m, 2H, H₉), 1.30 (s, 3H, Me); ¹H-¹H GCOSY (400 MHz, CDCl₃): δ 3.93 (H₃) \leftrightarrow δ 3.34 (H₂), 3.12 (H_{4\text{endo}}}),

2.06 (H_{4exo}); δ 3.58 (H₁) \leftrightarrow δ 3.34 (H₂), 2.17 (H₇); δ 3.12 (H_{4endo}) \leftrightarrow δ 2.87 (H₅), 2.06 (H_{4exo}); δ 2.87 (H₅) \leftrightarrow δ 2.36 (H₆), 2.06 (H_{4exo}); δ 2.36 (H₆) \leftrightarrow δ 2.17 (H₇); δ 2.17 (H₇) \leftrightarrow δ 1.95-1.82 (H₈); δ 1.95-1.82 (H₈) \leftrightarrow δ 1.75-1.64 (H₉); ¹³C{¹H} NMR (100 MHz, CDCl₃): δ 109.2, 97.6, 92.2, 64.6, 53.8, 50.3, 46.0, 44.6, 35.2, 31.9, 28.1, 23.8, 21.5, 9.6; Electrospray MS *m/z* calculated for C₂₃H₃₄O₂Co (M⁺ – BF₄⁻): 401.18853; found: 401.18832 (100%); Analysis calculated for C₂₃H₃₄O₂CoBF₄: C, 56.58%; H, 7.02%; found: C, 56.61%; H, 7.17%.



[Cp*Co(η^5 -1-(3-oxobutyl acetal)cycloheptadienyl)]⁺BF₄⁻ (378). Allyl/olefin complex **377** (40 mg, 0.082 mmol) was dissolved in CH₂Cl₂ (5 mL) in a reaction bomb and heated at 60 °C for 16 hours. The solvent was removed *in vacuo* and the product purified by silica gel chromatography to provide 40 mg of product as an inseparable 2:1 mixture of the isomerized product **377** and the unprotected **370** as a red oil. IR (neat, cm⁻¹): 2982 (w), 2921 (w), 1456 (w), 1430 (w), 1382 (w), 1311 (w), 1219 (w), 1054 (s), 952 (w), 857 (w); ¹H NMR (400 MHz, CDCl₃, resonances for **370** omitted): δ 6.64 (t, $J_{3-2} = J_{3-4} = 6.3$ Hz, 1H, H₃), 5.30 (t, $J_{2-1} = J_{2-3} = 7.4$ Hz, 1H, H₂), 4.94 (t, $J_{4-3} = J_{4-5} = 7.9$ Hz, 1H, H₄), 4.34 (dt, $J_{5-4} = 8.6$ Hz, $J_{5-6endo} = J_{5-6exo} = 4.0$ Hz, 1H, H₅), 4.00 (ddd, $J_{1-2} = 8.2$ Hz, $J_{1-7} = 4.1$ Hz, $J_{1-3} = 1.0$ Hz, 1H, H₁), 3.89 (m, 4H, -OCH₂CH₂O-), 2.32 (ddd, $J_{6endo-6exo} = 16.6$ Hz, $J_{6endo-7} = 9.6$ Hz, $J_{6endo-5} = 4.7$ Hz, 1H, H_{6endo}), 2.02 (dt, $J_{6exo-6endo} = 16.5$ Hz, $J_{6exo-5} = J_{6exo-7} = 3.7$ Hz, 1H, H_{6exo}), 1.86 (s, 15H, C₅Me₅), 1.55-1.35 (m, 4H, H₈, H₉), 1.24 (s, 3H,

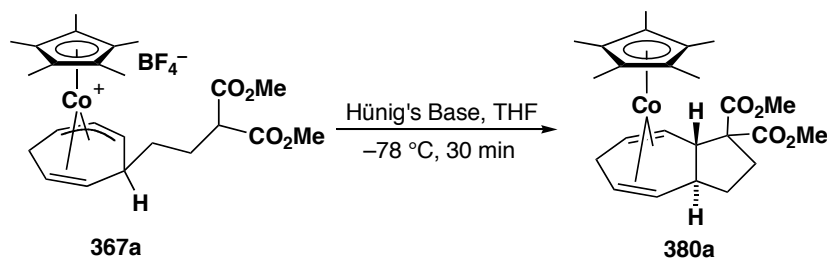
Me), 0.57 (m, 1H, H₇); ¹H-¹H GCOSY (400 MHz, CDCl₃): δ 6.64 (H₃) ↔ δ 5.30 (H₂), 4.94 (H₄), 4.00 (H₁); δ 5.30 (H₂) ↔ δ 4.00 (H₁); δ 4.94 (H₄) ↔ δ 4.34 (H₅); δ 4.34 (H₅) ↔ δ 2.32 (H_{6endo}), 2.02 (H_{6exo}); δ 4.00 (H₁) ↔ δ 0.57 (H₇); δ 2.32 (H_{6endo}) ↔ δ 2.02 (H_{6exo}), 0.57 (H₇); δ 2.02 (H_{6exo}) ↔ δ 0.57 (H₇); δ 1.52 (H₈) ↔ δ 1.38 (H_{8'} and 9), 0.57 (H₇); δ 1.38 (H_{8'}) ↔ δ 0.57 (H₇); ¹³C{¹H} NMR (100 MHz, CDCl₃): δ 109.3, 100.6, 98.8, 97.8, 97.7, 94.4, 88.6, 64.7, 46.5, 40.0, 37.0, 30.5, 23.8, 9.7; Electrospray MS *m/z* calculated for C₂₃H₃₄O₂Co (M⁺ – BF₄⁻): 401.18853; found: 401.18860 (100%).



[Cp*Co(η^5 -1,2-dimethyl-7-(3-butanoylacetal)cycloheptadienyl)]⁺BF₄⁻ (379).

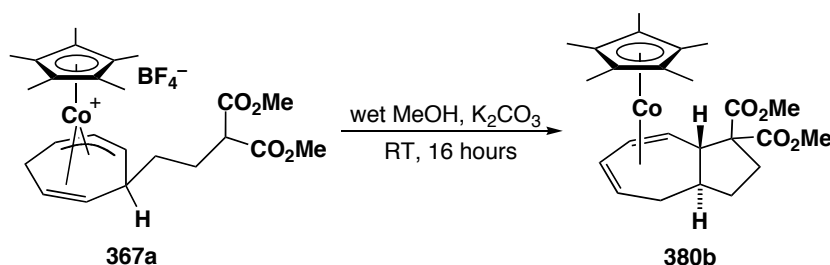
Pentadienyl complex **365** (101 mg, 0.22 mmol) was dissolved in CH₂Cl₂ (5 mL) in a reaction bomb and degassed with argon for 5 minutes. To this, 2-butyne (100 μ L, 1.28 mmol) was added via syringe. The bomb was sealed and heated at 40 °C for 3 days in an oil bath. The solvent was then removed *in vacuo* and the product purified by silica gel chromatography using 3% MeOH/CH₂Cl₂. The red fraction was collected and dried providing 85 mg of a thick, red oil as an inseparable mixture of product **379** and the unprotected **371** in a 2:1 ratio. Fractional crystallization was not successful in producing analytically pure material, despite multiple attempts, giving only impure oils. IR (neat, cm⁻¹): 2878 (m), 1457 (m), 1434 (m), 1382 (m), 1253 (w), 1213 (m), 1138 (w), 1025 (s), 952 (s), 908 (w), 854 (s); ¹H NMR (400 MHz, CDCl₃, resonances for **371** omitted): δ

6.55 (d, $J_{1-2} = 7.2$ Hz, 1H, H₁), 4.66 (t, $J_{2-1} = J_{2-3} = 8.7$ Hz, 1H, H₂, overlaps H₂ of **371**), 4.35 (dt, $J_{3-2} = 9.2$ Hz, $J_{3-4\text{endo}} = J_{3-4\text{exo}} = 3.4$ Hz, 1H, H₃, overlaps H₃ of **371**), 3.85 (m, 4H, -OCH₂CH₂O-), 2.45 (ddd, $J_{4\text{endo-4exo}} = 16.8$ Hz, $J_{4\text{endo-5}} = 12.2$ Hz, $J_{4\text{endo-3}} = 3.2$ Hz, 1H, H_{4\text{endo}}}, overlaps H_{4\text{endo}}} of **371**), 2.30 (dt, $J_{4\text{exo-4endo}} = 16.8$ Hz, $J_{4\text{exo-5}} = J_{4\text{exo-3}} = 3.6$ Hz, 1H, H_{4\text{exo}}}), 2.20 (s, 3H, Me), 1.74 (s, 15H, C₅Me₅), 1.39-1.14 (m, 4H, H₆, H₇, overlaps Me signals), 1.30 (s, 3H, Me), 1.19 (s, 3H, Me), -0.01 (tt, $J_{5-4\text{endo}} = J_{5-6} = 11.8$ Hz, $J_{5-4\text{exo}} = J_{5-6'} = 4.2$ Hz, 1H, H₅, overlaps H₅ of **371**); ¹H-¹H GCOSY (400 MHz, CDCl₃): δ 6.55 (H₁) ↔ δ 4.66 (H₂); δ 4.66 (H₂) ↔ δ 4.35 (H₃); δ 4.35 (H₃) ↔ δ 2.45 (H_{4\text{endo}}}), 2.30 (H_{4\text{exo}}}); δ 2.45 (H_{4\text{endo}}}) ↔ δ 2.30 (H_{4\text{exo}}}), -0.01 (H₅); δ 2.30 (H_{4\text{exo}}}) ↔ δ -0.01 (H₅); δ 1.45 (H₆) ↔ δ 1.25 (H_{6'}), 1.25 (H₉), -0.01 (H₅); δ 1.25 (H_{6'}) ↔ δ -0.01 (H₅); ¹³C{¹H} NMR (100 MHz, CDCl₃): δ 108.7, 101.4, 99.2, 97.6, 97.5, 96.3, 86.8, 64.7, 48.2, 41.8, 38.4, 25.0, 23.7, 19.3, 17.0, 9.1; Electrospray MS *m/z* calculated for C₂₅H₃₈O₂Co (M⁺ - BF₄⁻): 429.21983; found: 429.21965 (100%).



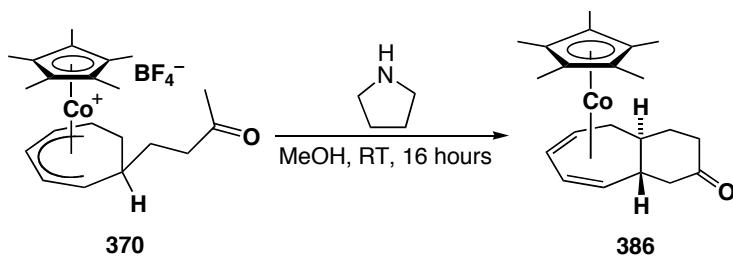
Cp*Co(η²,η²-[5.3.0]-2,2-di(methylcarboxyl)bicyclodeca-7,10-diene) (380a). Allyl/olefin complex **367a** (88 mg, 0.16 mmol) was dissolved in THF (5 mL) in the glove box and removed to the Schlenk line and cooled to -78 °C in a dry ice/acetone bath. To this solution, Hünig's base (28 μL, 0.16 mmol) was added. The reaction was stirred for 30 minutes, then the solvent was removed *in vacuo* and the residue filtered through activity

IV neutral alumina with THF in the glove box. The solvent was removed and the product taken up in a minimal quantity of pentane and cooled to $-30\text{ }^{\circ}\text{C}$. Material slowly came out of solution, providing 62 mg (88%) of product as an impure reddish-brown powder. ^1H NMR (400 MHz, C_6D_6): δ 4.41 (dd, $J = 13.2, 3.7$ Hz, 1H), 3.41 (s, 3H), 3.38 (s, 3H), 3.35 (m, 1H, obscured by other signals), 3.05 (dt, $J = 14.2, 8.7$ Hz, 1H), 2.88 (dt, $J = 13.3, 2.7$ Hz, 1H), 2.35 (m, 3H), 1.99 (td, $J = 7.0, 2.6$ Hz, 1H), 1.58 (s, 15H), remaining signals were overlapping or obscured by impurities. This material was not further characterized.



Cp*Co(η^4 -[5.3.0]-2,2-di(methylcarboxyl)bicyclodeca-7,10-diene) (380b). Allyl/olefin complex **367a** (90 mg, 0.17 mmol) was dissolved in wet MeOH (5 mL) in the glove box. To this solution, K_2CO_3 (26 mg, 0.19 mmol) was added. The reaction was stirred for 16 hours, then the solvent was removed *in vacuo* and the residue filtered through Celite with benzene in the glove box. The solvent was removed to provide 73 mg (97%) of product as a red oil. Analytically pure orange crystals were obtained via cooling a saturated pentane solution to $-30\text{ }^{\circ}\text{C}$. IR (neat, cm^{-1}): 3008 (w), 2986 (w), 2947 (s), 2911 (m), 2859 (m), 2817 (w), 1747 (w), 1724 (s), 1434 (w), 1425 (w), 1376 (w), 1345 (w), 1322 (w), 1262 (m), 1223 (w), 1199 (s), 1152 (m), 1102 (w), 1071 (m), 1050 (w), 1008 (w), 978 (w); ^1H NMR (300 NMR, C_6D_6): δ 4.05 (dd, $J_{3-2} = 6.8$ Hz, $J_{3-4} =$

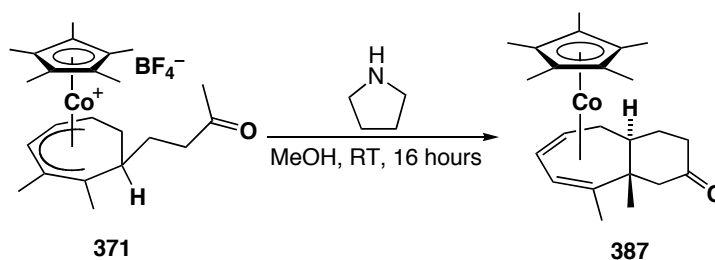
taken up in a minimal quantity of pentane and cooled to $-30\text{ }^{\circ}\text{C}$. Material slowly came out of solution, providing 30 mg (76%) of product as a reddish-brown powder. No further attempts to improve the purity were made. ^1H NMR (400 MHz, C_6D_6): δ 3.52 (dd, $J_{1-7} = 10.8\text{ Hz}$, $J_{1-2} = 4.0\text{ Hz}$, 1H, H_1), 3.39 (s, 3H, -OMe), 3.32 (s, 3H, -OMe), 3.05 (dd, $J_{1-7} = 10.8\text{ Hz}$, $J_{1-2} = 4.0\text{ Hz}$, 1H, H_1), 3.39 (s, 3H, -OMe), 3.32 (s, 3H, -OMe), 3.05 (dd, $J_{1-7} = 10.8\text{ Hz}$, $J_{1-2} = 4.0\text{ Hz}$, 1H, H_1), 2.49 (m, 1H, $\text{H}_{10\text{eq}}$), 2.36 (dt, $J_{4\text{endo-4exo}} = 13.0\text{ Hz}$, $J_{4\text{endo-3}} = J_{4\text{endo-5}} = 7.8\text{ Hz}$, 1H, $\text{H}_{4\text{endo}}$), 2.00 (dd, $J_{2-3} = 8.1\text{ Hz}$, $J_{2-1} = 4.1\text{ Hz}$, 1H, H_2), 1.96 (td, $J_{5-4\text{endo}} = J_{5-4\text{exo}} = 7.2\text{ Hz}$, $J_{5-4\text{endo}} = 3.2\text{ Hz}$, 1H, H_5), 2.02-1.92 (m, 1H, $\text{H}_{9\text{eq}}$, buried by H_2 and H_5), 1.84 (m, 1H, $\text{H}_{8\text{ax}}$), 1.68 (m, 1H, $\text{H}_{9\text{eq}}$), 1.64 (s, 15H, C_5Me_5), 1.62 (m, 1H, H_6), 1.70-1.62 (m, 1H, $\text{H}_{10\text{ax}}$, buried under Cp^* peak), 1.53 (td, $J_{3-2} = J_{3-4\text{endo}} = 8.2\text{ Hz}$, $J_{3-4\text{exo}} = 3.0\text{ Hz}$, 1H, H_3), 1.40 (dt, $J_{7-1} = 9.4\text{ Hz}$, $J_{7-6} = J_{7-8\text{ax}} = 2.9\text{ Hz}$, 1H, H_7), 1.35 (dd, $J_{8\text{eq-8ax}} = 11.9\text{ Hz}$, $J_{8\text{eq-9eq}} = 3.7\text{ Hz}$, 1H, $\text{H}_{8\text{eq}}$); ^1H - ^1H GCOSY (400 MHz, C_6D_6): δ 3.52 (H_1) \leftrightarrow δ 2.00 (H_2), 1.40 (H_7); δ 3.05 ($\text{H}_{4\text{endo}}$) \leftrightarrow δ 2.36 ($\text{H}_{4\text{exo}}$), 1.96 (H_5), 1.53 (H_2); δ 2.49 ($\text{H}_{10\text{eq}}$) \leftrightarrow δ 2.00 ($\text{H}_{9\text{eq}}$), 1.65 ($\text{H}_{10\text{ax}}$); δ 2.36 ($\text{H}_{4\text{exo}}$) \leftrightarrow δ 1.96 (H_5), 1.53 (H_3); δ 1.53 (H_2) \leftrightarrow δ 1.53 (H_3); δ 1.96 (H_5) \leftrightarrow δ 1.62 (H_6); δ 2.02-1.96 ($\text{H}_{9\text{eq}}$) \leftrightarrow δ 1.70-1.62 ($\text{H}_{9\text{ax}}$), 1.35 ($\text{H}_{8\text{eq}}$); δ 1.84 ($\text{H}_{8\text{ax}}$) \leftrightarrow δ 1.40 (H_7), 1.35 ($\text{H}_{8\text{eq}}$), 1.70-1.62 ($\text{H}_{9\text{ax}}$); δ 1.70-1.62 ($\text{H}_{9\text{ax}}$) \leftrightarrow δ 1.35 ($\text{H}_{8\text{eq}}$); δ 1.62 (H_6) \leftrightarrow δ 1.40 (H_7); δ 1.40 (H_7) \leftrightarrow δ 1.35 ($\text{H}_{8\text{eq}}$); $^{13}\text{C}\{^1\text{H}\}$ NMR (100 MHz, C_6D_6): δ 172.5, 170.7, 90.6, 67.0, 66.1, 61.0, 58.0, 51.6, 51.1, 36.5, 34.8, 33.8, 32.6, 29.6, 27.1, 24.4, 9.5; Electron impact MS m/z calculated for $\text{C}_{25}\text{H}_{35}\text{O}_4\text{Co}$ (M^+): 458.18674; found: 458.18695 (5%).



Cp*Co(η^4 -[5.4.0]-bicycloundeca-8,10-dien-3-one) (386). Allyl/olefin complex **370**

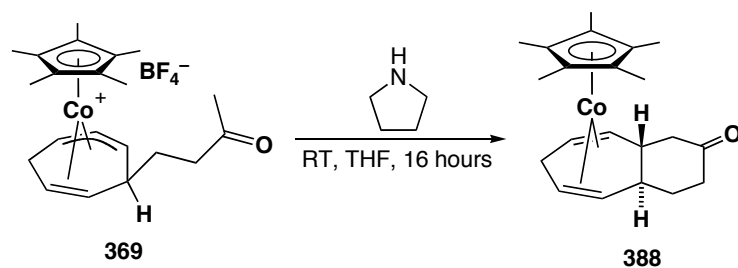
(108 mg, 0.24 mmol) was dissolved in MeOH (5 mL) under an argon atmosphere. To this solution, pyrrolidine (21 μL , 0.25 mmol) was added and stirred at room temperature for 16 hours. The solvent was removed *in vacuo*, the product was taken up in pentane and filtered through activity IV neutral alumina in the glove box. The solvent was removed to yield 47 mg (54%) of product as a red oil. X-ray quality crystals were obtained by cooling a concentrated pentane solution to $-30\text{ }^\circ\text{C}$ in the glove box. Insufficient material for both elemental analysis and further decomplexation chemistry was obtained. ^1H NMR (400 MHz, C_6D_6): δ 3.95 (dd, $J_{4,5} = 7.0\text{ Hz}$, $J_{4,3} = 4.5\text{ Hz}$, 1H, H_4), 3.89 (dd, $J_{3,2} = 6.9\text{ Hz}$, $J_{3,4} = 4.5\text{ Hz}$, 1H, H_3), 2.52 (ddd, $J_{10\text{eq}-10\text{ax}} = 13.4\text{ Hz}$, $J_{10\text{eq}-1} = 3.9\text{ Hz}$, $J_{10\text{eq}-9\text{eq}} = 2.3\text{ Hz}$, 1H, $\text{H}_{10\text{eq}}$), 2.15 (ddt, $J_{9\text{eq}-9\text{ax}} = 13.8\text{ Hz}$, $J_{9\text{eq}-8\text{eq}} = 4.5\text{ Hz}$, $J_{9\text{eq}-8\text{ax}} = J_{9\text{eq}-10\text{eq}} = 2.4\text{ Hz}$, 1H, $\text{H}_{9\text{eq}}$), 2.09 (t, $J_{5,4} = J_{5,6\text{endo}} = 6.8\text{ Hz}$, 1H, H_5), 1.80 (t, $J_{10\text{ax}-10\text{eq}} = J_{10\text{ax}-1} = 13.0\text{ Hz}$, 1H, $\text{H}_{10\text{ax}}$), 1.74 (td, $J_{9\text{ax}-9\text{eq}} = J_{9\text{ax}-8\text{ax}} = 13.9\text{ Hz}$, $J_{9\text{ax}-8\text{eq}} = 6.8\text{ Hz}$, 1H, $\text{H}_{9\text{ax}}$), 1.66 (d, $J_{2,3} = 7.0\text{ Hz}$, 1H, H_2), 1.57 (s, 15H, C_5Me_5), 1.41 (ddd, $J_{6\text{endo}-6\text{exo}} = 16.2\text{ Hz}$, $J_{6\text{endo}-5} = 6.2\text{ Hz}$, $J_{6\text{endo}-7} = 3.4\text{ Hz}$, 1H, $\text{H}_{6\text{endo}}$), 1.26-1.18 (m, 2H, H_1 , $\text{H}_{8\text{eq}}$), 0.94 (ddd, $J_{6\text{exo}-6\text{endo}} = 16.4\text{ Hz}$, $J_{6\text{exo}-7} = 11.6\text{ Hz}$, $J_{6\text{exo}-5} = 1.7\text{ Hz}$, 1H, $\text{H}_{6\text{exo}}$), 0.89 (tdd, $J_{8\text{ax}-8\text{eq}} = J_{8\text{ax}-7} = 13.4\text{ Hz}$, $J_{8\text{ax}-7} = 12.1\text{ Hz}$, $J_{8\text{ax}-9\text{eq}} = 4.4\text{ Hz}$, 1H, $\text{H}_{8\text{ax}}$, overlaps $\text{H}_{6\text{exo}}$), 0.41 (qt, $J_{7,1} = J_{7,6\text{exo}} = J_{7,8\text{ax}} = 11.7\text{ Hz}$, $J_{7,6\text{endo}} = J_{7,8\text{eq}} = 3.4\text{ Hz}$, 1H, H_7); ^1H - ^1H GCOSY (400 MHz, C_6D_6): δ 3.95 (H_4) \leftrightarrow δ 3.89 (H_3), 2.09 (H_5), 1.66 (H_2), 1.41 ($\text{H}_{6\text{endo}}$); δ 3.89 (H_3) \leftrightarrow δ

2.09 (H₅), 1.66 (H₂); δ 2.52 (H_{10eq}) ↔ δ 2.15 (H_{9eq}), 1.80 (H_{10ax}), 1.26-1.18 (H₁); δ 2.15 (H_{9eq}) ↔ δ 1.74 (H_{9ax}), 1.26-1.18 (H_{8eq}); δ 2.09 (H₅) ↔ δ 1.41 (H_{6endo}), 0.94 (H_{6exo}); δ 1.80 (H_{10ax}) ↔ δ 1.26-1.18 (H₁); δ 1.74 (H_{9ax}) ↔ δ 1.26-1.18 (H_{8eq}), 0.89 (H_{8ax}); δ 1.66 (H₂) ↔ δ 1.26-1.18 (H₁); δ 1.41 (H_{6endo}) ↔ δ 0.94 (H_{6exo}), 0.41 (H₇); δ 1.26-1.18 (H₁) ↔ δ 0.41 (H₇); δ 1.26-1.18 (H_{8eq}) ↔ δ 0.89 (H_{8ax}); δ 0.94 (H_{6exo}) ↔ δ 0.41 (H₇); δ 0.89 (H_{8ax}) ↔ δ 0.41 (H₇); ¹³C{¹H} NMR (100 MHz, C₆D₆): δ 208.1, 89.8, 81.7, 79.2, 58.0, 52.4, 51.9, 44.7, 41.2, 37.5, 35.5, 33.4, 9.5; Electron impact MS *m/z* calculated for C₂₁H₂₉OCo (M⁺): 356.15503; found: 356.15547 (51%).



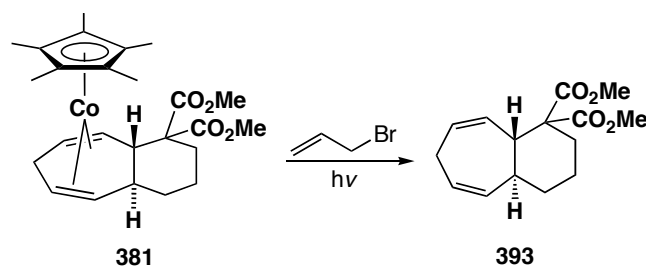
Cp*Co(η⁴-[5.4.0]-1,11-dimethylbicycloundeca-8,10-dien-3-one) (387). Cycloheptadienyl complex **371** (67 mg, 0.14 mmol) was dissolved in MeOH (5 mL) under an argon atmosphere. To this solution, pyrrolidine (12 μL, 0.14 mmol) was added and stirred at room temperature for 16 hours. The solvent was removed *in vacuo*, the product was taken up in pentane and filtered through activity IV neutral alumina in the glove box. The solvent was removed to yield 37 mg (65%) of product as a red oil. Material of improved purity was obtained via cooling a concentrated pentane solution to -30 °C in the glove box. IR (neat, cm⁻¹): 2957 (s), 2907 (s), 2864 (s), 2820 (s), 1706 (s), 1442 (m), 1374 (s), 1361 (m), 1347 (m), 1312 (m), 1277 (m), 1262 (s), 1241 (m), 1214 (w), 1193 (w), 1134 (w), 1114 (w), 1093 (w), 1069 (w), 1059 (w), 1029 (s), 986 (m); ¹H NMR (400

MHz, C₆D₆): δ 3.98 (d, $J_{1-2} = 4.9$ Hz, 1H, H₁), 3.84 (dd, $J_{2-3} = 7.1$ Hz, $J_{2-1} = 4.8$ Hz, 1H, H₂), 2.65 (dd, $J_{8\text{eq}-8\text{ax}} = 12.8$ Hz, $J_{8\text{eq}-7\text{eq}} = 2.4$ Hz, 1H, H_{8eq}), 2.14 (ddt, $J_{7\text{eq}-7\text{ax}} = 13.7$ Hz, $J_{7\text{eq}-6\text{ax}} = 4.5$ Hz, $J_{7\text{eq}-6\text{eq}} = J_{7\text{eq}-8\text{eq}} = 2.0$ Hz, 1H, H_{7eq}), 1.97 (ddd, $J_{3-2} = 7.6$ Hz, $J_{3-4\text{endo}} = 5.7$ Hz, $J_{3-4\text{exo}} = 2.6$ Hz, 1H, H₃), 1.72 (dtd, $J_{6\text{eq}-6\text{ax}} = 13.7$ Hz, $J_{6\text{eq}-7\text{ax}} = J_{6\text{eq}-7\text{eq}} = 7.4$ Hz, $J_{6\text{eq}-5} = 0.8$ Hz, 1H), 1.61 (dt, $J_{8\text{ax}-8\text{eq}} = 12.9$ Hz, $J_{8\text{ax}-7\text{ax}} = J_{8\text{ax}-7\text{eq}} = 1.0$ Hz, 1H, H_{8ax}), 1.54 (s, 15H, C₅Me₅), 1.13 (tdd, $J_{6\text{ax}-6\text{eq}} = J_{6\text{ax}-5/7\text{ax}} = 13.6$ Hz, $J_{6\text{ax}-5/7\text{ax}} = 12.6$ Hz, $J_{6\text{ax}-7\text{eq}} = 4.8$ Hz, 1H, H_{6ax}), 1.02-0.95 (m, 3H, H_{4endo}, H_{4exo}, H_{7ax}), 0.92 (s, 3H, Me), 0.90 (d, $J_{\text{Me}-1} = 1.0$ Hz, 3H, Me), 0.57 (m, 1H, H₅); ¹H-¹H GCOSY (400 MHz, C₆D₆): δ 3.98 (H₁) \leftrightarrow δ 3.84 (H₂), 0.90 (Me); δ 3.84 (H₁) \leftrightarrow δ 1.97 (H₃), 1.02-0.95 (H_{4endo}); δ 2.65 (H_{8eq}) \leftrightarrow δ 2.14 (H_{7eq}), 1.61 (H_{8ax}); δ 2.14 (H_{7eq}) \leftrightarrow δ 1.72 (H_{6eq}), 1.13 (H_{6ax}); δ 1.97 (H₃) \leftrightarrow δ 1.02-0.95 (H_{4endo}, H_{4exo}); δ 1.72 (H_{6eq}) \leftrightarrow δ 1.13 (H_{6ax}), 1.02-0.95 (H_{7ax}); δ 1.13 (H_{6ax}) \leftrightarrow δ 1.02-0.95 (H_{7ax}), 0.57 (H₅); δ 1.02-0.95 (H_{4endo}, H_{4exo}) \leftrightarrow δ 0.57 (H₅); ¹³C{¹H} NMR (100 MHz, C₆D₆): δ 208.9, 90.0, 84.5, 80.8, 66.0, 54.2, 51.7, 43.2, 41.2, 39.8, 30.9, 29.9, 23.8, 18.1, 9.9; Electron impact MS m/z calculated for C₂₃H₃₃OC_o (M⁺): 384.18634; found: 384.18677 (99%).



Cp*Co(η^2, η^2 -[5.4.0]-bicycloundeca-7,10-dien-3-one) (388). Allyl/olefin complex **369** (52 mg, 0.12 mmol) was dissolved in MeOH (5 mL) under an argon atmosphere. To this solution, pyrrolidine (10 μ L, 0.12 mmol) was added and stirred at room temperature for

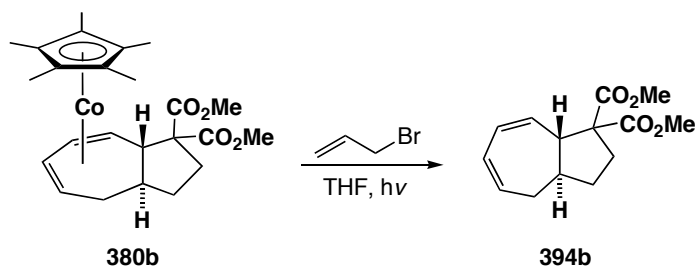
16 hours. The solvent was removed *in vacuo*, the product was taken up in pentane and filtered through activity IV neutral alumina in the glove box. The solvent was removed to yield 33 mg (79%) of product as a red oil and a 4:1 mixture of inseparable **388:386** isomers. Spectroscopic characterization: ^1H NMR (400 MHz, C_6D_6 , resonances for **386** omitted): δ 3.16 (dt, $J_{4\text{endo-4exo}} = 13.1$ Hz, $J_{4\text{endo-3}} = J_{4\text{endo-5}} = 7.7$ Hz, 1H, $\text{H}_{4\text{endo}}$), 2.95 (dddd, $J_{1-10\text{ax}} = 13.8$ Hz, $J_{1-7} = 9.7$ Hz, $J_{1-2} = 4.1$ Hz, $J_{1-10\text{eq}} = 3.1$ Hz, 1H, H_1), 2.51 (dt, $J_{4\text{exo-4endo}} = 13.1$ Hz, $J_{4\text{exo-3}} = J_{4\text{exo-5}} = 2.9$ Hz, 1H, $\text{H}_{4\text{exo}}$), 2.46 (dt, $J_{10\text{eq-10ax}} = 13.7$ Hz, $J_{10\text{eq-1}} = J_{10\text{eq-9eq}} = 2.3$ Hz, 1H, $\text{H}_{10\text{eq}}$), 2.36 (ddt, $J_{9\text{eq-9ax}} = 15.2$ Hz, $J_{9\text{eq-8eq}} = 3.9$ Hz, $J_{9\text{eq-8ax}} = J_{9\text{eq-10eq}} = 1.9$ Hz, 1H, $\text{H}_{9\text{eq}}$), 2.11 (t, $J_{10\text{ax-10eq}} = J_{10\text{ax-1}} = 13.7$ Hz, 1H, $\text{H}_{10\text{ax}}$), 1.92 (td, $J_{5-6} = J_{5-4\text{endo}} = 7.0$ Hz, $J_{5-4\text{exo}} = 2.6$ Hz, 1H, H_5), 1.80 (t, $J_{9\text{ax-9eq}} = J_{9\text{ax-8ax}} = 15.7$ Hz, 1H, $\text{H}_{9\text{ax}}$), 1.56 (m, 2H, H_6 , $\text{H}_{8\text{eq}}$, obscured by **386**), 1.48 (s, 15H, C_5Me_5), 1.42 (m, 1H, H_7 , obscured by **386**), 1.34 (td, $J_{3-2} = J_{3-4\text{endo}} = 8.0$ Hz, $J_{3-4\text{exo}} = 2.9$ Hz, 1H, H_3), 1.23 (m, 1H, $\text{H}_{8\text{ax}}$), 1.14 (dd, $J_{2-3} = 7.8$ Hz, $J_{2-1} = 4.2$ Hz, 1H, H_2); ^1H - ^1H GCOSY (400 MHz, C_6D_6): δ 3.16 ($\text{H}_{4\text{endo}}$) \leftrightarrow δ 2.51 ($\text{H}_{4\text{exo}}$), 1.92 (H_5), 1.31 (H_3); δ 2.95 (H_1) \leftrightarrow δ 2.46 ($\text{H}_{10\text{eq}}$), 2.11 ($\text{H}_{10\text{ax}}$), 1.41 (H_7), 1.14 (H_2); δ 2.51 ($\text{H}_{4\text{exo}}$) \leftrightarrow δ 1.91 (H_5), 1.31 (H_3); δ 2.46 ($\text{H}_{10\text{eq}}$) \leftrightarrow δ 2.36 ($\text{H}_{9\text{eq}}$); δ 2.36 ($\text{H}_{9\text{eq}}$) \leftrightarrow δ 1.80 ($\text{H}_{9\text{ax}}$), 1.56 ($\text{H}_{8\text{eq}}$); δ 1.91 (H_5) \leftrightarrow δ 1.56 (H_6); δ 1.80 ($\text{H}_{9\text{ax}}$) \leftrightarrow δ 1.56 ($\text{H}_{8\text{eq}}$), 1.23 ($\text{H}_{8\text{ax}}$); δ 1.56 ($\text{H}_{8\text{eq}}$) \leftrightarrow δ 1.42 (H_7); δ 1.34 (H_3) \leftrightarrow δ 1.14 (H_2).



***trans*-dimethyl 2,3,4,4a-tetrahydro-1*H*-benzo[7]annulene-1,1(7*H*,9a*H*)-dicarboxylate**

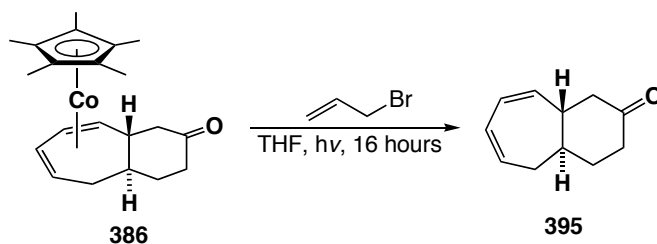
(393). Bicyclic cobalt complex **381** (70 mg, 0.15 mmol) was dissolved in THF (20 mL) in the glove box and placed in a glass reaction bomb. To this, allyl bromide (15 μ L, 0.17 mmol) was added, the bomb sealed and irradiated with UV light in a Rayonet carousel for 16 hours resulting in a green solution. The solvent was removed *in vacuo* and the product purified by silica gel chromatography using 19:1 hexanes/diethyl ether, with the product dissolved in a minimal amount of CH_2Cl_2 for loading onto the column, providing 35 mg (85%) of bicyclic organic product **393** as a clear oil. Reactions run at higher concentration resulted in the formation of a red solution. Again, concentration *in vacuo* followed by careful chromatography allows isolation of the organic product, followed by a red fraction, shown to be $\text{Cp}^*\text{Co}(\eta^3\text{-CH}_2\text{CHCH}_2)\text{Br}$ by comparison with the published spectra. IR (neat, cm^{-1}): 3008 (w), 2951 (m), 2862 (w), 1730 (s), 1434 (m), 1319 (w), 1252 (s), 1208 (m), 1151 (m), 1110 (w), 1084 (w), 1044 (w), 1035 (w), 1025 (w), 1009 (w), 965 (w), 920 (w), 873 (w), 820 (w), 786 (w), 756 (w), 665 (w); ^1H NMR (400 MHz, CDCl_3): δ 5.88-5.76 (m, 2H, H_2 , H_3), 5.62 (dddd, $J_{5-6} = 11.2$ Hz, $J_{5-4} = 6.5$ Hz, $J_{5-4'} = 4.0$ Hz, $J_{5-7} = 2.3$ Hz, 1H, H_5), 5.28 (dt, $J_{6-5} = 11.4$ Hz, $J_{6-4'} = J_{6-7} = 1.8$ Hz, 1H, H_6), 3.76 (s, 3H, -OMe), 3.72 (s, 3H, -OMe), 2.90-2.77 (m, 2H, H_1 , H_4), 2.66-2.55 (m, 2H, H_4' , H_7), 2.35 (dq, $J_{10\text{eq}-10\text{ax}} = 13.2$ Hz, $J_{10\text{eq}-9\text{eq}} = J_{10\text{eq}-9\text{ax}} = J_{10\text{eq}-8\text{eq}} = 3.1$ Hz, 1H, $\text{H}_{10\text{eq}}$), 1.87-1.69 (m, 3H, $\text{H}_{8\text{eq}}$, $\text{H}_{9\text{eq}}$, $\text{H}_{10\text{ax}}$), 1.37-1.21 (m, 2H, $\text{H}_{8\text{ax}}$, $\text{H}_{9\text{ax}}$); ^1H - ^1H GCOSY (400 MHz,

CDCl₃): δ 5.88-5.76 (H₃) ↔ δ 2.90-2.77 (H₄), 2.66-2.55 (H_{4'}); δ 5.88-5.76 (H₂) ↔ δ 2.90-2.77 (H₁); δ 5.62 (H₅) ↔ δ 5.28 (H₆), 2.90-2.77 (H₄), 2.66-2.55 (H_{4'} + H₇); δ 5.28 (H₆) ↔ δ 2.66-2.55 (H₇); δ 2.90-2.77 (H₁) ↔ δ 2.66-2.55 (H₇); δ 2.90-2.77 (H₄) ↔ δ 2.66-2.55 (H_{4'}); δ 2.66-2.55 (H₇) ↔ δ 1.37-1.21 (H_{8ax}); δ 2.35 (H_{10eq}) ↔ δ 1.87-1.69 (H_{8eq} + H_{9eq} + H_{10ax}), 1.37-1.21 (H_{9ax}); δ 1.87-1.69 (H_{8eq} + H_{9eq}) ↔ δ 1.37-1.69 (H_{8ax} + H_{9ax}); ¹³C{¹H} NMR (100 MHz, CDCl₃): δ 173.1, 171.3, 135.5, 132.2, 130.0, 126.8, 59.6, 52.7, 52.2, 45.9, 36.6, 34.1, 33.6, 26.7, 22.3; Electrospray MS *m/z* calculated for C₁₅H₂₀O₄Na (M⁺ + Na): 287.12538; found: 287.12541 (100%).



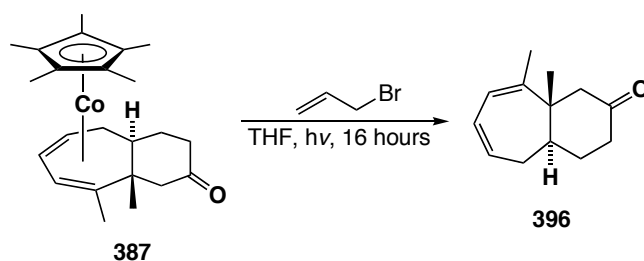
***trans*-dimethyl 2,3,3a,4-tetrahydroazulene-1,1(8a*H*)-dicarboxylate (394b).** Bicyclic cobalt complex **380b** (15 mg, 0.034 mmol) was dissolved in THF (5 mL mL) in the glove box and placed in a glass reaction bomb. To this, allyl bromide (2.9 μL, 0.034 mmol) was added, the bomb sealed and irradiated with UV light in a Rayonet carousel for 16 hours resulting in a red solution. The solvent was removed *in vacuo* and the product purified by silica gel chromatography using 19:1 hexanes/diethyl ether, with the product dissolved in a minimal amount of CH₂Cl₂ for loading onto the column, providing 7.8 mg (92%) of bicyclic organic product **394b** as a pale yellow oil. IR (CH₂Cl₂ cast, cm⁻¹): 3016 (s), 3954 (s), 2870 (s), 1731 (s), 1610 (w), 1435 (s), 1379 (w), 1435 (s), 1329 (w), 1269 (s), 1225 (s), 1172 (s), 1079 (s), 1017 (s), 989 (w); ¹H NMR (400 MHz, CDCl₃): δ

5.82 (m, 1H, H₂), 5.76-5.70 (m, 3H, H₃, H₄, H₅), 3.75 (s, 3H, -OMe), 3.72 (s, 3H, -OMe), 3.03 (dq, $J_{1-7} = 10.4$ Hz, $J_{1-2} = J_{1-3} = J_{1-9} = 1.6$ Hz, 1H, H₁), 2.52 (dddd, $J_{6-6'} = 17.8$ Hz, $J_{6-7} = 6.6$ Hz, $J_{6-5} = 3.2$ Hz, $J_{6-4} = 1.4$ Hz, 1H, H₆), 2.41 (ddd, $J_{9-9'} = 13.7$ Hz, $J_{9-8} = 8.6$ Hz, $J_{9-8'} = 6.9$ Hz, 1H, H₉), 2.38 (m, 1H, H₇), 2.30-2.10 (m, 3H, H_{6'}, H₈, H_{9'}), 1.34 (dddd, $J_{8'-8} = 12.8$ Hz, $J_{8'-7} = 9.4$ Hz, $J_{8'-9'} = 8.4$ Hz, $J_{8'-9} = 6.0$ Hz, 1H, H_{8'}); ¹H-¹H COSY (400 MHz, CDCl₃): δ 5.82 (H₂) ↔ δ 5.76-5.70 (H₃), 3.03 (H₁); δ 5.76-5.70 (H₃) ↔ δ 3.03 (H₁); δ 5.76-5.70 (H₄, H₅) ↔ δ 2.52 (H₆), 2.30-2.10 (H_{6'}); δ 3.03 (H₁) ↔ δ 2.38 (H₇); δ 2.52 (H₆) ↔ δ 2.38 (H₇), 2.30-2.10 (H_{6'}); δ 2.41 (H₉) ↔ δ 2.30-2.10 (H₈, H_{9'}); δ 2.38 (H₇) ↔ δ 2.30-2.10 (H₈), 1.34 (H_{8'}); δ 2.30-2.10 (H₈, H_{9'}) ↔ δ 1.34 (H_{8'}); ¹³C{¹H} NMR (100 MHz, CDCl₃): δ 172.8, 172.3, 132.2, 130.9, 125.0, 124.4, 64.1, 54.3, 52.8, 52.5, 41.2, 37.7, 34.1, 31.7; Electron impact MS *m/z* calculated for C₁₄H₁₈O₄ (M⁺): 250.12051; found: 250.12044 (23%).



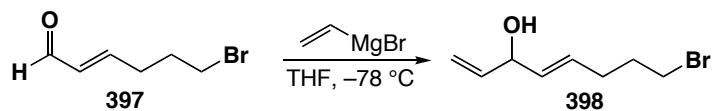
***trans*-3,4,4a,5-tetrahydro-1*H*-benzo[7]annulen-2(9*aH*)-one (395).** Bicyclic cobalt complex **386** (75 mg, 0.21 mmol) was dissolved in THF (20 mL) in the glove box and placed in a glass reaction bomb. To this, allyl bromide (20 μL, 0.23 mmol) was added, the bomb sealed and irradiated with UV light in a Rayonet carousel for 16 hours resulting in a green solution. The solvent was removed *in vacuo* and the product purified by silica gel chromatography using 19:1 hexanes/diethyl ether, with the product dissolved in a

minimal amount of CH₂Cl₂ for loading onto the column, providing 34 mg (100%) of bicyclic organic product **395** as a pale yellow oil. IR (neat, cm⁻¹): 3023 (w), 2930 (s), 2884(m), 1717 (s), 1614 (w), 1453 (w), 1429 (w), 1352 (w), 1325 (w), 1255 (w), 1200 (w), 1170 (w), 1122 (w), 1093 (w), 1073 (w), 997 (w); ¹H NMR (400 MHz, CDCl₃): δ 5.89 (m, 1H, H₅), 5.81 (m, 2H, H₄, H₃), 5.37 (m, 1H, H₂), 2.53 (m, 1H, H₁), 2.45 (ddd, $J_{10\text{eq-}10\text{ax}} = 14.4$ Hz, $J_{10\text{eq-}1} = 4.2$ Hz, $J_{10\text{eq-}9\text{eq}} = 1.8$ Hz, 1H, H_{10eq}), 2.37-2.34 (m, 2H, H₉, H₆), 2.32-2.26 (m, 2H, H_{10ax}, H_{6'}), 2.04 (m, 1H, H₈), 1.98 (m, 1H, H₇), 1.59-1.48 (m, 2H, H_{8'}, H_{9'}); ¹H-¹H COSY (400 MHz, CDCl₃): δ 5.89 (H₅) ↔ δ 5.81 (H₄), 2.37-2.34 (H₆); δ 5.81 (H₄, H₃) ↔ δ 5.37 (H₂), 2.53 (H₁), 2.37-2.34 (H₆); δ 5.37 (H₂) ↔ δ 2.53 (H₁); δ 2.53 (H₁) ↔ δ 2.45 (H_{10eq}), 2.32-2.26 (H_{10ax}), 1.98 (H₇); δ 2.45 (H_{10eq}) ↔ δ 2.32-2.26 (H_{10ax}); δ 2.37-2.34 (H₉) ↔ δ 1.59-1.48 (H_{9'}), 2.04 (H₈), 1.59-1.48 (H_{8'}); δ 2.04 (H₈) ↔ δ 1.59-1.48 (H_{8'}, H_{9'}), 1.98 (H₇); δ 1.98 (H₇) ↔ δ 1.59-1.48 (H_{8'}, H_{9'}); ¹³C{¹H} NMR (100 MHz, CDCl₃): δ 211.1, 135.3, 132.4, 125.1, 124.6, 47.4, 46.8, 40.2, 40.1, 36.1, 33.9; Electron impact MS *m/z* calculated for C₁₁H₁₄O (M⁺): 162.10446; found: 162.10431 (11%).



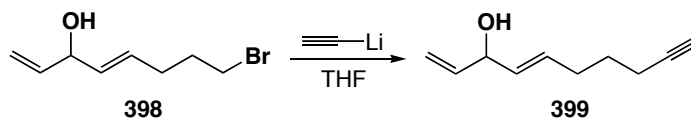
***trans*-9,9a-dimethyl-3,4,4a,5-tetrahydro-1*H*-benzo[7]annulen-2(9a*H*)-one (396).** Bicyclic cobalt complex **387** (5 mg, 0.01 mmol) was dissolved in THF (10 mL) in the glove box and placed in a glass reaction bomb. To this, allyl bromide (1.2 μL, 0.01 mmol) was

added, the bomb sealed and irradiated with UV light in a Rayonet carousel for 16 hours resulting in a green solution. The solvent was removed *in vacuo* and the product purified by silica gel chromatography using 19:1 hexanes/diethyl ether, with the product dissolved in a minimal amount of CH₂Cl₂ for loading onto the column, providing 2.5 mg (100%) of bicyclic organic product **396** as a pale yellow oil. IR (neat, cm⁻¹): 3023 (w), 2965 (s), 2928 (s), 1716 (s), 1611 (w), 1458 (m), 1432 (m), 1375 (w), 1354 (w), 1318 (w), 1294 (w), 1243 (w), 1218 (w), 1178 (w), 1124 (w), 1104 (w), 1000 (w); ¹H NMR (400 MHz, CDCl₃): δ 5.77 (m, 1H, H₃), 5.67 (dd, 1H, *J*₂₋₃ = 7.6 Hz, *J*₂₋₁ = 2.6 Hz, H₂), 5.61 (m, 1H, H₁), 2.53 (dd, *J*_{8eq-8ax} = 13.3 Hz, *J*_{8eq-7eq} = 2.1 Hz, 1H, H_{8eq}), 2.38 (d, *J*_{8ax-8eq} = 13.3 Hz, 1H, H_{8ax}), 2.43-2.31 (m, 3H, H₄, H_{7ax}, H_{7eq}), 2.24 (tdd, *J*_{5-6ax} = *J*₅₋₄ = 12.5 Hz, *J*_{5-6eq} = 4.0 Hz, *J*_{5-4'} = 1.7 Hz, 1H, H₅), 2.12 (ddd, *J*_{4'-4} = 17.8 Hz, *J*_{4'-3} = 7.5 Hz, *J*_{4'-5} = 1.5 Hz, 1H, H_{4'}), 1.97 (dddd, *J*_{6eq-6ax} = 13.8 Hz, *J*_{6eq-7eq} = 6.6 Hz, *J*_{6eq-5} = 4.0 Hz, *J*_{6eq-7ax} = 2.6 Hz, 1H, H_{7eq}), 1.83 (s, 3H, Me), 1.77 (qd, *J*_{6ax-6eq} = *J*_{6ax-5} = *J*_{6ax-7ax} = 13.5 Hz, *J*_{6ax-7eq} = 5.5 Hz, 1H, H_{6ax}), 1.05 (s, 3H, Me); ¹H-¹H GCOSY (400 MHz, CDCl₃): δ 5.77 (H₃) ↔ δ 5.67 (H₂), 2.12 (H_{4'}); δ 5.67 (H₂) ↔ δ 5.61 (H₁); δ 5.61 (H₁) ↔ δ 1.83 (Me); δ 2.53 (H_{8eq}) ↔ δ 2.38 (H_{8ax}), 2.43-2.31 (H_{7eq}); δ 2.43-2.31 (H₄) ↔ δ 2.24 (H₅), 2.12 (H_{4'}); δ 2.43-2.31 (H_{7ax/7eq}) ↔ δ 1.97 (H_{6eq}), 1.77 (H_{6ax}); δ 2.24 (H₅) ↔ δ 2.12 (H_{4'}), 1.97 (H_{6eq}), 1.77 (H_{6ax}); δ 1.97 (H_{6eq}) ↔ δ 1.77 (H_{6ax}); ¹³C{¹H} NMR (100 MHz, CDCl₃): δ 212.1, 146.1, 131.8, 124.8, 122.1, 52.7, 47.4, 42.3, 40.9, 34.4, 31.1, 23.2, 20.1; Electron impact MS *m/z* calculated for C₁₃H₁₈O (M⁺): 190.13577; found: 190.13592 (93%).



***E*-8-bromo-octa-1,4-dien-3-ol (398).** Bromoaldehyde **397** (870 mg, 4.91 mmol) was dissolved in THF (10 mL) and cooled to $-78\text{ }^{\circ}\text{C}$ with a dry ice/acetone bath under an Ar atmosphere. To this, vinyl Grignard (0.61 M in THF, 8 mL, 4.90 mmol) was added slowly via canula and the reaction stirred at $-78\text{ }^{\circ}\text{C}$ for 1 hour and then allowed to warm slowly to room temperature. The mixture was cooled again and quenched with aqueous NH_4Cl . The resultant mixture was then extracted with diethyl ether, washed with water then brine and dried over NaSO_4 . The solvent was removed *in vacuo* and the product purified via silica gel chromatography using straight CH_2Cl_2 . IR (neat, cm^{-1}): 3354 (br, s), 3082 (w), 3011 (w), 2962 (w), 2935 (m), 2848 (m), 1853 (w), 1720 (w), 1669 (w), 1641 (w), 1436 (s), 1353 (w), 1269 (s), 1251 (s), 1203 (w), 1116 (m), 1089 (m), 987 (s), 925 (s), 802 (w), 753 (w), 678 (w); ^1H NMR (400 MHz, CDCl_3): δ 5.89 (ddd, $J_{2-1\text{trans}} = 17.2\text{ Hz}$, $J_{2-1\text{cis}} = 10.4\text{ Hz}$, $J_{2-3} = 5.8\text{ Hz}$, 1H, H_2), 5.68 (dtd, $J_{5-4} = 15.4\text{ Hz}$, $J_{5-6} = 6.6\text{ Hz}$, $J_{5-3} = 0.8\text{ Hz}$, 1H, H_5), 5.58 (ddt, $J_{4-5} = 15.4\text{ Hz}$, $J_{4-3} = 6.2\text{ Hz}$, $J_{4-6} = 1.0\text{ Hz}$, 1H, H_4), 5.26 (dt, $J_{1\text{trans}-2} = 17.2\text{ Hz}$, $J_{1\text{trans}-1\text{cis}} = J_{1\text{trans}-3} = 1.4\text{ Hz}$, 1H, $\text{H}_{1\text{trans}}$), 5.14 (dt, $J_{1\text{cis}-2} = 10.4\text{ Hz}$, $J_{1\text{cis}-1\text{trans}} = J_{1\text{cis}-3} = 1.3\text{ Hz}$, 1H, $\text{H}_{1\text{cis}}$), 4.60 (br. m, 1H, H_3), 3.41 (t, $J_{8-7} = 6.7\text{ Hz}$, 2H, H_8), 2.22 (q, $J_{6-5} = J_{6-7} = 6.4\text{ Hz}$, 2H, H_6), 1.96 (quin, $J_{7-6} = J_{7-8} = 7.0\text{ Hz}$, 2H, H_7), 1.62 (d, $J_{\text{HO}-3} = 3.0\text{ Hz}$, 1H, -OH); $^1\text{H}-^1\text{H}$ GCOSY (400 MHz, CDCl_3): δ 5.89 (H_2) \leftrightarrow δ 5.26 ($\text{H}_{1\text{trans}}$), 5.14 ($\text{H}_{1\text{cis}}$), 4.60 (H_3); δ 5.68 (H_5) \leftrightarrow δ 5.58 (H_4), 4.60 (H_3), 2.22 (H_6); δ 5.58 (H_4) \leftrightarrow δ 4.60 (H_3), 2.22 (H_6); δ 5.26 ($\text{H}_{1\text{trans}}$) \leftrightarrow δ 5.14 ($\text{H}_{1\text{cis}}$), 4.60 (H_3); δ 5.14 ($\text{H}_{1\text{cis}}$) \leftrightarrow δ 4.60 ($\text{H}_{1\text{cis}}$); δ 4.60 (H_3) \leftrightarrow δ 2.22 (H_6), 1.62 (-OH); δ 3.41 (H_8) \leftrightarrow δ 1.96 (H_7); δ 2.22 (H_6) \leftrightarrow δ 1.96 (H_7); $^{13}\text{C}\{^1\text{H}\}$ NMR (100 MHz, CDCl_3): δ 139.5, 132.4, 130.1,

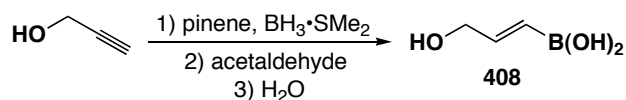
114.9, 73.5, 32.9, 31.8, 30.4; Electrospray MS m/z calculated for $C_8H_{13}OBrNa$ ($M^+ + Na$): 227.00420; found: 227.00418 (35%).



***E*-deca-1,4-dien-9-yn-3-ol (399). Method 1.** Liquid ammonia (30 mL) was gathered in a three-neck round bottom flask equipped with a dry ice condenser, cooled to $-78\text{ }^{\circ}\text{C}$ in a dry ice/acetone bath. Through this, acetylene, purified with an acetone scrubber cooled to $-78\text{ }^{\circ}\text{C}$, was bubbled for 15 minutes. Lithium (100 mg, 14.5 mmol) was added and the mixture stirred until the metal had completely entered the solution. Once completely dissolved, bromodienol **398** (93 mg, 0.45 mmol) was added and the solution allowed to warm to reflux temperature where it was maintained for 4 hours. The condenser was removed and the ammonia allowed to evaporate, assisted via gentle warming in a water bath, whereupon the reaction was carefully quenched with aqueous NH_4Cl . The mixture was extracted with diethyl ether, washed with water and brine, and dried over NaSO_4 . The solvent was removed *in vacuo* and the product purified via silica gel chromatography using straight CH_2Cl_2 to provide 30 mg (45%) of dienol **399** as a pale yellow oil.

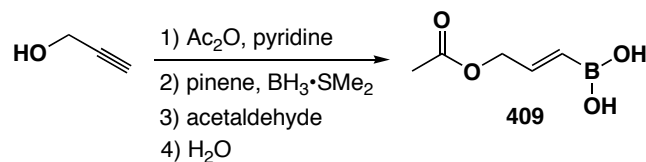
Method 2. Lithium acetylide/ethylene diamine complex (346 mg, 3.76 mmol) was suspended in a 1:1 THF/DMSO mix (5 mL) and cooled to $0\text{ }^{\circ}\text{C}$ under an Ar atmosphere. To this, bromodienol **398** (203 mg, 1.00 mmol) was added and allowed to stir overnight. The reaction was carefully quenched with aqueous NH_4Cl , extracted with diethyl ether, washed with water and brine and dried over NaSO_4 . The solvent was removed *in vacuo* and the product purified by silica gel chromatography using straight CH_2Cl_2 to provide

64 mg (43%) of dienol **399** as a pale yellow oil. IR (neat, cm^{-1}): 3400 (br, s), 3302 (s), 3082 (w), 3013 (w), 2940 (s), 2862 (m), 2117 (w), 1668 (w), 1641 (w), 1454 (w), 1432 (m), 1263 (m), 1117 (m), 990 (s), 970 (s), 925 (s); ^1H NMR (400 MHz, CDCl_3): δ 5.87 (ddd, $J_{2-1\text{trans}} = 17.2$ Hz, $J_{2-1\text{cis}} = 10.4$ Hz, $J_{2-3} = 5.8$ Hz, 1H, H₂), 5.66 (dtd, $J_{5-4} = 15.4$ Hz, $J_{5-6} = 6.7$ Hz, $J_{5-3} = 1.0$ Hz, 1H, H₅), 5.52 (ddt, $J_{4-5} = 15.4$ Hz, $J_{4-3} = 6.4$ Hz, $J_{4-6} = 1.2$ Hz, 1H, H₄), 5.22 (dt, $J_{1\text{trans}-2} = 17.2$ Hz, $J_{1\text{trans}-1\text{cis}} = J_{1\text{trans}-3} = 1.5$ Hz, 1H, H_{1trans}), 5.10 (dt, $J_{1\text{cis}-2} = 10.4$ Hz, $J_{1\text{cis}-1\text{trans}} = J_{1\text{cis}-3} = 1.3$ Hz, 1H, H_{1cis}), 4.56 (br. app. t, $J_{3-2} = J_{3-4} = 5.7$ Hz, 1H, H₃), 2.17 (m, 4H, H₆, H₈), 1.94 (t, $J_{9-8} = 2.7$ Hz, 2H, H₉ and overlaps OH signal), 1.60 (quin, $J_{7-6} = J_{7-8} = 7.2$ Hz, 2H, H₇); ^1H - ^1H GCOSY (400 MHz, CDCl_3): δ 5.87 (H₂) \leftrightarrow δ 5.22 (H_{1trans}), 5.10 (H_{1cis}), 4.56 (H₃); δ 5.66 (H₅) \leftrightarrow δ 5.52 (H₄), 4.56 (H₃), 2.17 (H₆); δ 5.52 (H₄) \leftrightarrow δ 4.56 (H₃), 2.17 (H₆); δ 5.22 (H_{1trans}) \leftrightarrow δ 5.10 (H_{1cis}), 4.56 (H₃); δ 5.10 (H_{1cis}) \leftrightarrow δ 4.56 (H_{1cis}); δ 4.56 (H₃) \leftrightarrow δ 2.17 (H₆); δ 2.17 (H₆) \leftrightarrow δ 1.94 (H₉), δ 1.60 (H₇); $^{13}\text{C}\{^1\text{H}\}$ NMR (100 MHz, CDCl_3): δ 139.7, 132.0, 131.2, 114.8, 84.1, 73.6, 68.6, 31.0, 27.7, 17.8; Electrospray MS m/z calculated for $\text{C}_{10}\text{H}_{14}\text{ONa}$ ($\text{M}^+ + \text{Na}$): 173.09369; found: 173.09371 (100%).



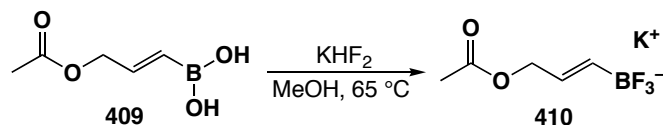
***E*-(3-hydroxyprop-1-en-1-yl)boronic acid (408).** α -Pinene (28 mL, 0.18 mmol) was added dropwise to a solution of $\text{BH}_3\cdot\text{SMe}_2$ (8.7 mL, 0.09 mmol) in THF (25 mL) at 0 °C under an argon atmosphere and then stirred at room temperature for 2 hours. The solution was then cooled to -40 °C in a dry ice/acetone bath and propargyl alcohol (2.5 g, 0.045 mmol) slowly added via syringe. The solution was allowed to warm to room

temperature and stirred overnight (≈ 16 hours). The solution was cooled to $0\text{ }^{\circ}\text{C}$ in an ice bath and acetaldehyde (35 mL) slowly added via syringe followed by heating at reflux for 16 hours. The reaction was then cooled to room temperature and water (68 mL) added, followed by aggressive stirring for 2 hours. The product was extracted with diethyl ether, concentrated and crashed out with hexane. The white solid was isolated by filtration and washing with hexane. Due to the large amounts of boric acid produced as a byproduct, the yield was undetermined. ^1H NMR (300 MHz, D_2O): δ 6.53 (dt, $J_{2-1} = 18.3$ Hz, $J_{2-3} = 4.3$ Hz, 1H, H_2), 5.59 (dt, $J_{1-2} = 18.3$ Hz, $J_{1-3} = 1.9$ Hz, 1H, H_1), 4.13 (dd, $J_{3-2} = 4.3$ Hz, $J_{3-1} = 1.9$ Hz, 2H, H_3); $^{13}\text{C}\{^1\text{H}\}$ NMR (100 MHz, $\text{CD}_3\text{OD} + 5\%$ D_2O): δ 150.1, 122.5, 64.8.



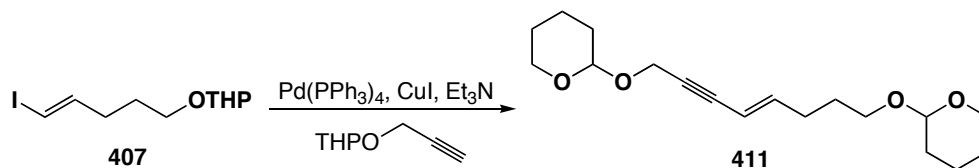
***E*-(3-acetoxyprop-1-en-1-yl)boronic acid (409).** Propargyl alcohol (10 g, 0.18 mol) was dissolved in pyridine (30 mL) and cooled in ice. To this, acetic anhydride (20 g, 0.20 mol) was added dropwise and, upon completion, allowed to stir for 2 hours at room temperature. To this, a 30% aqueous H_2SO_4 solution (320 mL) was slowly added and stirred aggressively for 15 minutes. The solution was then neutralized via successive washing with aqueous NaHCO_3 , then washed with water, diluted with CH_2Cl_2 (30 mL), washed with brine and dried over MgSO_4 to yield 10.8 g (62%) of propargyl acetate. This material was spectroscopically pure and taken forward without further purification. In a separate Schlenk flask, α -pinene (35 mL, 0.22 mol) was added dropwise to a solution of $\text{BH}_3\cdot\text{SMe}_2$ (11 mL, 0.11 mol) in THF (20 mL) at $0\text{ }^{\circ}\text{C}$ under an argon

atmosphere, and upon completion allowed to stir for 2 hours at room temperature. The suspension was cooled to $-40\text{ }^{\circ}\text{C}$ in a dry ice/acetone bath and the propargyl acetate (10.8 g, 0.11 mol) added slowly via syringe then stirred at room temperature overnight (≈ 16 hours). The flask was cooled to $0\text{ }^{\circ}\text{C}$ and acetaldehyde (123 mL) added slowly via syringe, then heated to reflux for 16 hours. The mixture was then cooled to room temperature and water (50 mL) added followed by aggressive stirring for 2 hours. The product was extracted with diethyl ether, concentrated *in vacuo*, precipitated with hexane and collected via filtration. Further washing with hexane and drying yielded 6.3 g (39%) of boronic acid **409** as a sticky white solid. IR (neat, cm^{-1}): 3212 (br, s), 2515 (w), 2361 (w), 2261 (m), 1739 (s), 1646 (m), 1437 (s), 1233 (s), 1195 (s), 1070 (m), 1032 (m), 884 (w), 750 (s); ^1H NMR (400 MHz, $\text{CD}_3\text{OD} + 5\% \text{D}_2\text{O}$): δ 6.55 (dt, $J_{2-1} = 18.4\text{ Hz}$, $J_{2-3} = 4.7\text{ Hz}$, 1H, H_2), 5.71 (dt, $J_{1-2} = 18.3\text{ Hz}$, $J_{1-3} = 1.8\text{ Hz}$, 1H, H_1), 4.73 (dd, $J_{3-2} = 4.6\text{ Hz}$, $J_{3-1} = 1.6\text{ Hz}$, 2H, H_3), 2.18 (s, 3H, H_4); $^{13}\text{C}\{^1\text{H}\}$ NMR (125 MHz, $\text{CD}_3\text{OD} + 5\% \text{D}_2\text{O}$): δ 173.1, 144.3, 125.7, 67.0, 20.8; $^{11}\text{B}\{^1\text{H}\}$ NMR (160 MHz, $\text{CD}_3\text{OD} + 5\% \text{D}_2\text{O}$): δ 19.1; Electrospray MS m/z calculated for $\text{C}_6\text{H}_{11}\text{O}_4\text{BNa}$ (M^+ (as monomethyl ester) + Na): 181.06426; found: 181.06415 (100%).



potassium *E*-(3-acetoxyprop-1-en-1-yl)trifluoro borate (410). Alkenyl boronic acid **409** (0.90 g, 6.3 mmol) and KHF_2 (1.48 g, 19 mmol) were combined in MeOH (25 mL) and heated at reflux for 16 hours. The solution was cooled, concentrated *in vacuo* and redissolved in hot MeCN. Cooling to room temperature provided 0.91 g (75%) of

trifluoroborate **410** as a white powder. IR (neat, cm^{-1}): 3383 (w), 3023 (m), 2970 (m), 2949 (m), 2912 (w), 2887 (w), 1699 (s), 1656 (s), 1544 (w), 1458 (m), 1382 (m), 1354 (m), 1266 (s), 1218 (s), 1108 (s), 1082 (s), 1026 (s), 997 (s), 973 (s), 956 (s), 927 (s), 795 (w), 734 (m); ^1H NMR (400 MHz, CD_3CN): δ 5.53 (dt, $J_{2-1} = 17.9$ Hz, $J_{2-3} = 5.3$ Hz, 1H, H_2), 5.44 (dqt, $J_{1-2} = 17.7$ Hz, $J_{1-\text{F}} = 3.21$ Hz, $J_{1-3} = 1.0$ Hz, 1H, H_1), 4.25 (dt, $J_{3-2} = 5.6$ Hz, $J = 1.1$ Hz, 2H, H_3), 1.80 (s, 3H, H_4); $^{13}\text{C}\{^1\text{H}\}$ NMR (125 MHz, CD_3CN): δ 171.6, 143.1, 129.8 (q, $J_{\text{C-F}} = 4.5$ Hz), 68.7, 21.2; $^{11}\text{B}\{^1\text{H}\}$ NMR (160 MHz, CD_3CN): δ 2.25 (q, $J_{\text{B-F}} = 52$ Hz); $^{19}\text{F}\{^1\text{H}\}$ NMR (376 MHz, CD_3CN): δ -142.4 (1:1:1:1 q, $J_{\text{F-B}} = 49$ Hz); Electrospray MS m/z calculated for $\text{C}_5\text{H}_7\text{O}_2\text{BF}_3$ ($\text{M}^- - \text{K}$): 167.04857; found: 167.04855 (100%); Analysis calculated for $\text{C}_5\text{H}_7\text{BF}_3\text{K}$: C, 29.15%; H, 3.42%; found: C, 29.11%; H, 3.43%.



***E*-2,2'-(oct-4-en-2-yn-1,8-diylbis(oxy))bis(tetrahydro-2H-pyran) (411)**. Vinyl iodide **407** (1.34 g, 4.5 mmol), $\text{Pd}(\text{PPh}_3)_4$ (0.529 g, 0.45 mmol) and CuI (0.172 g, 0.90 mmol) were combined in triethylamine (10 mL) and degassed by bubbling argon through the system for 5 minutes. THP protected propargyl alcohol (0.700 mL, 4.98 mmol) was added slowly via syringe. The mixture was allowed to stir overnight (≈ 16 hours) at room temperature. The solvent was removed *in vacuo* and the residue purified by silica gel chromatography using 9:1 hexanes/ EtOAc to provide 1.04 g (75%) of product as a pale yellow oil. IR (neat, cm^{-1}): 3388 (br, m), 2942 (s), 2870 (s), 2219 (w), 1733 (m), 1442 (m), 1386 (m), 1353 (s), 1323 (m), 1262 (m), 1201 (s), 1183 (m), 1121 (s), 1077 (s),

1026 (s), 972 (s); ^1H NMR (400 MHz, CDCl_3): δ 6.15 (dt, $J_{8-7} = 15.9$ Hz, $J_{8-9} = 7.0$ Hz, 1H, H₈), 5.49 (dq, $J_{7-8} = 15.9$ Hz, $J_{7-6} = J_{7-9} = 1.8$ Hz, 1H, H₇), 4.79 (t, $J_{5-4} = 3.4$ Hz, 1H, H₅), 4.54 (t, $J_{12-13} = 3.6$ Hz, 1H, H₁₂), 4.37 (dd, $J_{6-6'} = 15.7$ Hz, $J_{6-7} = 2.0$ Hz, 1H, H₆), 4.28 (dd, $J_{6'-6} = 15.7$ Hz, $J_{6'-7} = 2.0$ Hz, 1H, H_{6'}), 3.82 (m, 2H, H₁, H₁₆), 3.71 (dt, $J_{11-11'} = 9.7$ Hz, $J_{11-10} = 6.6$ Hz, 1H, H₁₁), 3.48 (m, 2H, H_{1'}, H_{16'}), 3.35 (dt, $J_{11'-11} = 9.7$ Hz, $J_{11'-10} = 6.4$ Hz, 1H, H_{11'}), 2.18 (qt, $J_{9-8} = J_{9-10} = 7.4$ Hz, $J_{9-6/6'} = J_{9-7} = 1.7$ Hz, 2H, H₉), 1.90-1.40 (m, 14H, H₂, H₃, H₄, H₁₀, H₁₃, H₁₄, H₁₅); ^1H - ^1H GCOSY (400 MHz, CDCl_3): δ 6.15 (H₈) \leftrightarrow δ 5.49 (H₇), 2.18 (H₉); δ 5.49 (H₇) \leftrightarrow δ 4.37 (H₆), 4.28 (H_{6'}), 2.18 (H₉); δ 4.79 (H₅) \leftrightarrow δ 1.70 (H₄), 1.60 (H_{4'}); δ 4.54 (H₁₂) \leftrightarrow δ 1.65 (H₁₃), 1.55 (H_{13'}); δ 4.37 (H₆) \leftrightarrow δ 4.28 (H_{6'}); δ 3.82 (H₁, H₁₆) \leftrightarrow δ 3.48 (H_{1'}, H_{16'}), 1.55 (H₂, H₁₅); δ 3.71 (H₁₁) \leftrightarrow δ 3.48 (H_{11'}), 1.65 (H₁₀); δ 3.48 (H_{1'}, H_{16'}) \leftrightarrow δ 1.55 (H₂, H₁₅); δ 3.35 (H_{11'}) \leftrightarrow δ 1.65 (H₁₀); δ 2.18 (H₉) \leftrightarrow δ 1.65 (H₁₀); $^{13}\text{C}\{^1\text{H}\}$ NMR (100 MHz, CDCl_3): δ 144.6, 109.4, 98.7, 96.6, 84.4, 83.5, 66.5, 62.2, 61.8, 54.6, 30.6, 30.1, 29.7, 28.6, 25.35, 25.25, 19.5, 18.9; Electrospray MS m/z calculated for $\text{C}_{18}\text{H}_{28}\text{O}_4\text{Na}$ ($\text{M}^+ + \text{Na}$): 331.18798; found: 331.18780 (100%).

IV. Chapter 6

Computations for the complexation and [5+2] cycloaddition reaction of acetylene with $\text{Cp}^*\text{Co}(\eta^5\text{-1-methylpentadienyl})$ complex **297d**, and the $\eta^2 \rightarrow \eta^3$ isomerization (Figure 6.1) were performed at the BP86/TZVPP level. The total electronic energies (E_{elec}), zero-point energies (ZPE), thermal corrections (E_{therm}), and free energies (G) are collected in Table 8.2.

Table 8.2: Thermodynamic Data for Figure 6.1 (hartrees)

	E _{elec}	ZPE	E _{elec} +ZPE	E _{therm}	G
267d	-2007.33402	0.34690	-2006.98712	0.32567	-2007.00835
Acetylene	-77.36643	0.02678	-77.33965	0.01605	-77.35039
TS0-1	-2084.66455	0.37156	-2084.29299	0.34748	-2084.31707
INT1	-2084.69320	0.37436	-2084.31884	0.35150	-2084.34171
TS1-2	-2084.67658	0.37343	-2084.30315	0.34988	-2084.32670
INT2	-2084.70772	0.37617	-2084.33155	0.35205	-2084.35567
INT3	-2084.73428	0.37899	-2084.35529	0.35672	-2084.37756
TS3-4	-2084.72307	0.37793	-2084.34514	0.35552	-2084.36756
INT4	-2084.77944	0.38171	-2084.39773	0.35985	-2084.41959
TS4-5	-2084.73991	0.37927	-2084.36064	0.35664	-2084.38327
INT5	-2084.75588	0.37973	-2084.37615	0.35723	-2084.39865
TS5-6	-2084.74612	0.37770	-2084.36842	0.35468	-2084.39145
INT6	-2084.74930	0.37783	-2084.37147	0.35539	-2084.39391
TS6-7	-2084.74928	0.37729	-2084.37199	0.35524	-2084.39403
INT7	-2084.76721	0.38047	-2084.38674	0.35815	-2084.40906
TS7-8	-2084.76192	0.37987	-2084.38205	0.35715	-2084.40477
INT8	-2084.79366	0.38251	-2084.41115	0.36056	-2084.43309
TS2-4	-2084.69970	0.37651	-2084.32319	0.35375	-2084.34596
TS1-9	-2084.67663	0.37369	-2084.30294	0.35052	-2084.32611
INT9	-2084.70663	0.37597	-2084.33066	0.35225	-2084.35438
TS9-10	-2084.69746	0.37539	-2084.32207	0.35202	-2084.34544
INT10	-2084.72976	0.37596	-2084.35380	0.35263	-2084.37713
TS10-11	-2084.72874	0.37469	-2084.35405	0.35174	-2084.37700
INT11	-2084.73272	0.37526	-2084.35746	0.35192	-2084.38080
TS2-10	-2084.69348	0.37569	-2084.31779	0.35230	-2084.34118
TS3-12	-2084.68114	0.37665	-2084.30449	0.35506	-2084.32609
INT12	-2084.68627	0.37789	-2084.30838	0.35639	-2084.32988
TS12-13	-2084.66543	0.37753	-2084.28790	0.35584	-2084.30959
INT13	-2084.72770	0.38066	-2084.34704	0.35869	-2084.36901
TS13-4	-2084.71501	0.37905	-2084.33596	0.35742	-2084.35759

Computations for the complexation of methylene chloride with Cp*Co(η^5 -1-methylpentadienyl) complex **297d** (discussed in Note 204) were performed at the BP86/TZVPP level. The total electronic energies (E_{elec}), zero-point energies (ZPE), thermal corrections (E_{therm}), and free energies (G) are collected in Table 8.3.

Table 8.3: Thermodynamic Data for Note 204 (hartrees)

	E _{elec}	ZPE	E _{elec} +ZPE	E _{therm}	G
267d	-2007.33402	0.34698	-2006.98704	0.32567	-2007.00835
CH ₂ Cl ₂	-959.85681	0.02842	-959.82839	0.01392	-959.84288
CH ₂ Cl ₂ TS	-2967.15504	0.37419	-2966.78085	0.34825	-2966.80679
CH ₂ Cl ₂ Comp.	-2967.15839	0.37469	-2966.78370	0.34916	-2966.80923

Computations for the complexation and [5+2] cycloaddition reaction of acetylene with Cp*Co(η^5 -1-methylpentadienyl) complex **297d**, and the $\eta^2 \rightarrow \eta^3$ isomerization (Figure 6.7) were performed at the B3LYP/TZVPP level. The total electronic energies (E_{elec}), zero-point energies (ZPE), thermal corrections (E_{therm}), and free energies (G) are collected in Table 8.4.

Table 8.4: Thermodynamic Data for Figure 6.7 (hartrees)

	E _{elec}	ZPE	E _{elec} +ZPE	E _{therm}	G
297d	-2006.53240	0.35659	-2006.17581	0.33530	-2006.19709
Acetylene	-77.31928	0.02756	-77.29172	0.01683	-77.30245
TS0-1'	-2083.82180	0.03829	-2083.78351	0.35959	-2083.46221
INT1'	-2083.83674	0.38465	-2083.45209	0.36150	-2083.47524
TS1-2'	-2083.81797	0.38426	-2083.43371	0.36107	-2083.45689
INT2'	-2083.85214	0.37598	-2083.47616	0.35135	-2083.50079
INT3'	-2083.87412	0.38985	-2083.48427	0.36767	-2083.50645
TS3-4'	-2083.86087	0.38868	-2083.47219	0.36626	-2083.49462
INT4'	-2083.92070	0.39251	-2083.52819	0.37058	-2083.55012
TS4-5'	-2083.88970	0.39052	-2083.49918	0.36820	-2083.52149
INT5'	-2083.90098	0.39102	-2083.50996	0.36895	-2083.53203
TS5-6'	-2083.88280	0.38788	-2083.49492	0.36556	-2083.51725
INT6'	-2083.91250	0.39139	-2083.52111	0.36901	-2083.54348
INT6'-7'	-2083.88247	0.37680	-2083.50567	0.35596	-2083.52652
INT7'	-2083.91255	0.39154	-2083.52101	0.36934	-2083.54322
TS7-8'	-2083.90938	0.39082	-2083.51856	0.36825	-2083.54113
INT8'	-2083.93557	0.39332	-2083.54225	0.37156	-2083.56401
TS2-4'	-2083.83511	0.38712	-2083.44799	0.36434	-2083.47077

Computations to determine the β -hydride elimination reaction energy of the 2-butyne

[5+2] η^2, η^3 -cycloadducts with both Cp and Cp* ancillary ligands at the BP86/TZVPP level (Figure 6.6). The total electronic energies (E_{elec}), zero-point energies (ZPE), thermal corrections (E_{therm}), and free energies (G) are collected in Table 8.5.

Table 8.5: Thermodynamic Data for Figure 6.6 (hartrees)

	E_{elec}	ZPE	$E_{\text{elec}}+\text{ZPE}$	E_{therm}	G
Cp* Comp.	-2163.42991	0.43605	-2162.99386	0.41400	-2163.01591
Cp* Comp. TS	-2163.39470	0.43317	-2162.96153	0.40911	-2162.98559
Cp Comp.	-1966.76835	0.30237	-1966.46598	0.28232	-1966.48604
Cp Comp. TS	-1966.72160	0.29974	-1966.42186	0.27884	-1966.44276
2-Butyne	-156.04560	0.08154	-155.96406	0.06738	-155.97821

Computations for the complexation and [5+2] cycloaddition reaction of acetylene with the $\text{CpCo}(\eta^5\text{-1-methylpentadienyl})$ complex (Figure 6.9) were performed at the BP86/TZVPP level. The total electronic energies (E_{elec}), zero-point energies (ZPE), thermal corrections (E_{therm}), and free energies (G) are collected in Table 8.6.

Table 8.6: Thermodynamic Data for Figure 6.9 (hartrees)

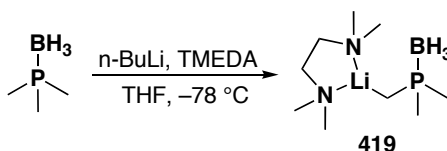
	E_{elec}	ZPE	$E_{\text{elec}}+\text{ZPE}$	E_{therm}	G
Pentadienyl	-1810.66562	0.21306	-1810.45256	0.19453	-1810.47108
Acetylene	-77.36643	0.02678	-77.33965	0.01605	-77.35039
TS0-1''	-1887.99543	0.23815	-1887.75728	0.21686	-1887.77857
INT1''	-1888.02305	0.24037	-1887.78268	0.22008	-1887.80296
TS1-2''	-1887.91522	0.24023	-1887.67499	0.21999	-1887.78559
INT2''	-1888.03523	0.24289	-1887.79234	0.22224	-1887.81299
INT3''	-1888.06470	0.24541	-1887.81929	0.22631	-1887.83838
TS3-4''	-1888.05477	0.24470	-1887.81007	0.22569	-1887.82909
INT4''	-1888.11222	0.24819	-1887.86403	0.22896	-1887.88326
TS2-4''	-1888.03247	0.24253	-1887.78994	0.22280	-1887.80968
INT14''	-1888.03632	0.24394	-1887.79238	0.22412	-1887.81221
TS14-15''	-1888.03161	0.24364	-1887.78797	0.22439	-1887.80722
INT15''	-1888.05106	0.24578	-1887.80528	0.22663	-1887.82443
TS15-4''	-1888.01911	0.24329	-1887.77582	0.22434	-1887.79476
TS2-4a''	-1888.02270	0.24246	-1887.78024	0.22288	-1887.79982
INT4a''	-1888.10848	0.24840	-1887.86008	0.22921	-1887.87928

Computations to determine the complexation transition state energies of η^5 -pentadienyl complexes **297** (Table 6.1) were performed at the BP86/TZVPP level. The total electronic energies (E_{elec}), zero-point energies (ZPE), thermal corrections (E_{therm}), and free energies (G) are collected in Table 8.7.

Table 8.7: Thermodynamic Data for Table 6.1 (hartrees)

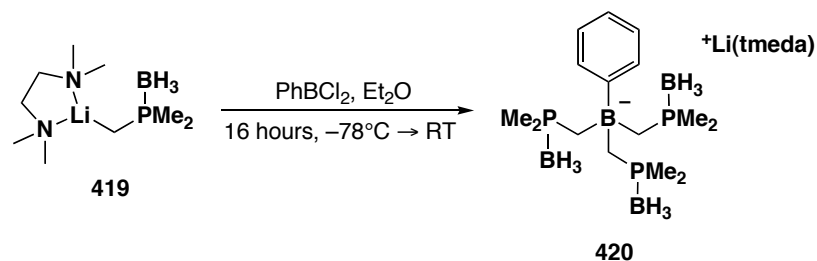
	E_{elec}	ZPE	$E_{\text{elec}}+\text{ZPE}$	E_{therm}	G
297a	-2007.33842	0.34691	-2006.99151	0.32589	-2007.01253
297a TS	-2084.65634	0.37164	-2084.28470	0.34852	-2084.30783
297k	-2046.66755	0.37346	-2046.29409	0.35187	-2046.31568
297k TS	-2123.98927	0.39853	-2123.21609	0.37464	-2123.61462
297c	-2046.66693	0.37361	-2046.29332	0.35174	-2046.31519
297c TS	-2123.99169	0.39865	-2123.59304	0.37476	-2123.61693
297f	-2007.33621	0.34626	-2006.98995	0.32567	-2007.01054
297f TS	-2084.66034	0.37143	-2084.28891	0.34764	-2084.31270
297e	-1968.00497	0.32010	-1967.68487	0.29954	-1967.70544
297e TS	-2045.32915	0.34449	-2044.98466	0.32106	-2045.00809
297l	-2085.99438	0.40063	-2085.59375	0.37801	-2085.61638
297l TS	-2163.32141	0.42596	-2162.89545	0.40187	-2162.91954
297h	-2085.99362	0.40060	-2085.59302	0.37796	-2085.61566
297h TS	-2162.32113	0.42552	-2161.89561	0.40031	-2162.92082
297i	-2046.66488	0.37368	-2046.29120	0.35167	-2046.31321
297i TS	-2123.99316	0.39874	-2123.59442	0.37458	-2123.61859
297g	-2046.66322	0.37393	-2046.28929	0.35166	-2046.31155
297g TS	-2123.99266	0.39831	-2123.59435	0.37285	-2123.61980
297d	-2007.33402	0.34690	-2006.98712	0.32567	-2007.00835
297d TS	-2084.66455	0.37156	-2084.29299	0.34748	-2084.31707
297b	-2199.15125	0.39811	-2198.75314	0.37454	-2198.77671
297b TS	-2276.48455	0.42323	-2276.06132	0.39820	-2276.08634
297j	-2046.66216	0.37405	-2046.28811	0.35200	-2046.31016
297j TS	-2123.99565	0.39857	-2123.59708	0.37385	-2123.62180
297m	-2085.99075	0.40093	-2085.58982	0.37884	-2085.61191
297m TS	-2163.32365	0.42525	-2162.89840	0.39941	-2162.92424
Acetylene	-77.36643	0.02678	-77.33965	0.01605	-77.35039

IV. Chapter 7



Lithiomethyldimethylphosphine borane/tetramethylethylenediamine complex (419).

A solution of $\text{BH}_3 \cdot \text{SMe}_2$ (3.7 mL, 39 mmol) in diethyl ether (30 mL) was prepared and cooled to 0 °C in an ice bath under an argon atmosphere. To this, trimethylphosphine (4 mL, 39 mmol) was added slowly via syringe and then stirred for 15 minutes at room temperature. TMEDA (5.9 mL, 39 mmol) was added and the solution cooled to -78 °C in a dry ice/acetone bath. *n*-BuLi (2.4 M in hexanes, 16 mL, 39 mmol) was added slowly via syringe and the mixture allowed to warm to room temperature slowly over night. The solvent was removed *in vacuo* and the collected in the glove box to provide 8.13 g (97%) of product as a sticky, off-white powder. ^1H NMR (400 MHz, C_6D_6): δ 1.95 (s, 12H, - NMe_2), 1.72 (s, 4H, - $\text{NCH}_2\text{CH}_2\text{N}$ -), 1.37 (d, $J_{\text{Me-P}} = 10.0$ Hz, 6H, - PMe_2), 1.14 (1:1:1:1 qd, $J_{\text{H-B}} = 88.1$ Hz, $J_{\text{H-P}} = 12.4$ Hz, 3H, BH_3), -0.37 (d, $J_{\text{CH}_2\text{-P}} = 11.9$ Hz, 2H, CH_2); $^{13}\text{C}\{^1\text{H}\}$ NMR (100 MHz, C_6D_6): δ 56.4, 45.8, 20.2 (d, $J_{\text{Me-P}} = 30.3$ Hz), 1.72 (br. s); $^{31}\text{P}\{^1\text{H}\}$ NMR (162 MHz, C_6D_6): δ -4.25 (1:1:1:1 q, $J_{\text{P-B}} = 90.8$ Hz); $^{11}\text{B}\{^1\text{H}\}$ NMR (128 MHz, C_6D_6): δ -33.5 (d, $J_{\text{B-P}} = 90.7$ Hz).



Tris(methylenedimethylphosphino)phenyl borate triborane (420). Lithiophoshtine complex **419** (1.00 g, 4.72 mmol) was dissolved in diethyl ether (15 mL) in the glove box and removed to the Schlenk line where it was cooled to -78°C in a dry ice/acetone bath under an argon atmosphere. To this, PhBCl_2 (204 μL , 1.57 mmol) in toluene (2 mL) was added slowly via syringe. The solution was allowed to stir for 16 hours, then the solvent was removed *in vacuo* and the residue taken into the glove box. The material was suspended in benzene, filtered and concentrated to provide 1.63 g (74%) of spectroscopically pure product. This material would darken with time to a purple colour, even when stored in the glove box. This colour would disappear upon dissolution of the material in solvent. An analytical sample was prepared through iterative slow evaporations from hexanes. ^1H NMR (400 MHz, C_6D_6): δ 7.64 (br. d, $J = 7.0$ Hz, 2H, Ph), 7.32 (t, $J = 7.3$ Hz, 2H, Ph), 7.18 (tt, $J = 6.8, 1.3$ Hz, 1H, Ph), 1.95 (s, 12H, $-\text{NMe}_2$), 1.76 (s, 4H, $-\text{NCH}_2\text{CH}_2\text{N}-$), 1.31 (br. d, $J_{\text{CH}_2-\text{P}} = 9.2$ Hz, 6H, $-\text{CH}_2-$), 1.08 (d, $J_{\text{Me}-\text{P}} = 10.6$ Hz, 18H, $-\text{PMe}_2$); $^{13}\text{C}\{^1\text{H}\}$ NMR (100 MHz, C_6D_6): δ 133.5, 127.0, 124.4, 56.7, 46.1, 15.5 (d, $J = 39$ Hz) (note: signals for the carbon atoms bonded to B are not seen); $^{31}\text{P}\{^1\text{H}\}$ NMR (162 MHz, C_6D_6): δ 1.40 (app. q, $J_{\text{P}-\text{B}} \approx 70$ Hz); $^{11}\text{B}\{^1\text{H}\}$ NMR (128 MHz, C_6D_6): δ -14.1 (s), -33.6 (br. d, $J_{\text{B}-\text{P}} = 74.5$ Hz); Electrospray MS m/z calculated for $\text{C}_{15}\text{H}_{38}\text{B}_4\text{P}_3$ ($\text{M}^- - \text{Li}(\text{tmeda})$): 355.25641; found: 355.25642; Analysis calculated for

C₂₁H₅₄B₄P₃N₂Li: C, 52.79%; H, 11.39%; N, 5.86%; found: C, 52.66%; H, 11.31%; N, 5.85%.

Computations. Computations to determine the feasibility of [5+2] cycloaddition reactivity in the tripodalphosphine complexes and the transition state energy of DABCO mediated deprotection of tripodalphosphine borane complexes were performed at the BP86/TZVPP level. The total electronic energies (E_{elec}), zero-point energies (ZPE), thermal corrections (E_{therm}), and free energies (G) are collected in Table 8.8.

Table 8.8: Thermodynamic Data for Tripodal Phosphine Cycloaddition Reaction and Phosphine Deprotection (hartrees)

	E_{elec}	ZPE	$E_{\text{elec}}+\text{ZPE}$	E_{therm}	G
Figure 7.1 a	-3024.39006	0.45054	-3023.93952	0.42801	-3023.96205
Figure 7.2	-3101.71205	0.47662	-3101.23543	0.45239	-3101.25966
Figure 7.1 b	-3101.62946	0.47495	-3101.15451	0.44973	-3101.17972
DABCO	-345.47199	0.17728	-344.99704	0.16201	-345.30998
PMe ₃ •BH ₃	-487.87171	0.13978	-487.73193	0.13978	-487.74764
DABCO TS	-833.31423	0.31759	-832.99664	0.29382	-833.02041
420	-1718.49281	0.48402	-1718.00879	0.45684	-1718.03598
420 TS	-2063.93175	0.66208	-2063.26967	0.62964	-2063.30211
422	-2214.91500	0.41544	-2214.49956	0.41544	-2214.49956
422 TS	-2560.35378	0.62290	-2559.73088	0.58851	-2559.76527

Notes and References

- ¹ For a review on synthetic efforts, see: Kuwajima, I.; Tanino, K. *Chem. Rev.* **2005**, *105*, 4661-4670.
- ² For a review of inside/outside stereochemistry, see: Alder, R. W.; East, S. P. *Chem. Rev.* **1996**, *96*, 2097-2112.
- ³ Brady, S. F.; Singh, M. P.; Janso, J. E.; Clardy, J. *J. Am. Chem. Soc.* **2000**, *122*, 2116-2117.
- ⁴ For a review on tropolonoids, see: Bentley, R. *Nat. Prod. Rep.* **2008**, *25*, 118-138.
- ⁵ Anschütz, R.; Leather, W. *Chem. Ber.* **1885**, *18*, 715-717.
- ⁶ Sanders, J. M. *Proc. Chem. Soc.* **1906**, *22*, 134-135.
- ⁷ Remfry, F. G. P. *J. Chem. Soc.* **1913**, *103*, 1076-1088.
- ⁸ (a) Walls, F.; Padilla, J.; Joseph-Nathan, P.; Giral, F.; Romo, J. *Tetrahedron Lett.* **1965**, *21*, 1577-1582. (b) Walls, F.; Padilla, J.; Joseph-Nathan, P.; Giral, F. *Tetrahedron* **1966**, *22*, 2387-2399.
- ⁹ (a) Archer, D. A.; Thomson, R. H. *Chem. Commun.* **1965**, *15*, 354. (b) Wagner, E. R.; Moss, R. D.; Brooker, R. M.; Heeschen, J. P.; Potts, W. J.; Dilling, M. L. *Tetrahedron Lett.* **1965**, *47*, 4233-4239. (c) Bates, R. B.; Paknikar, S. K.; Thalacker, V. P. *Chem. Ind.* **1965**, 1793.
- ¹⁰ Joseph-Nathan, P.; Mendoza, V.; García, E. *Tetrahedron* **1977**, *33*, 1573-1576.
- ¹¹ (a) Sánchez, I. H.; Yáñez, R.; Enríquez, R.; Joseph-Nathan, P. *J. Org. Chem.* **1981**, *46*, 2818-2819. (b) Joseph-Nathan, P.; Garibay, M. E.; Santillan, R. L. *J. Org. Chem.* **1987**, *52*, 759-763.
- ¹² (a) Sánchez, I. H.; Basurto, F.; Joseph-Nathan, P. *J. Nat. Prod.* **1984**, *47*, 382-383. (b) Sánchez, I. H.; Larraza, M. I.; Basurto, F.; Yáñez, R.; Avila, S.; Tovar, R.; Joseph-Nathan, P. *Tetrahedron* **1985**, *41*, 2355-2359.
- ¹³ Cuadrado, M. J. S.; de la Torre, M. C.; Lin, L.-Z.; Cordell, G. A.; Rodríguez, B.; Perales, A. *J. Org. Chem.* **1992**, *57*, 4722-4728.
- ¹⁴ (a) Mamont, P. *Bull. Soc. Chim. Fr.* **1970**, 1557-1564. (b) Mamont, P. *Bull. Soc. Chim. Fr.* **1970**, 1564-1568. (c) Mamont, P. *Bull. Soc. Chim. Fr.* **1970**, 1568-

1570.

- 15 (a) Büchi, G.; Mak, C.-P. *J. Am. Chem. Soc.* **1977**, *99*, 8073-8075. (b) Büchi, G.; Chu, P.-S. *J. Org. Chem.* **1978**, *43*, 3717-3719. For related work, see: Mortlock, S. V.; Seckington, J. K.; Thomas, E. J. *J. Chem. Soc., Perkin Trans. 1* **1988**, 2305-2307.
- 16 Angle, S. R.; Turnbull, K. D. *J. Org. Chem.* **1993**, *58*, 5360-5369.
- 17 (a) Engler, T. A.; Combrink, K. D.; Takusagawa, F. *J. Chem. Soc., Chem. Commun.* **1989**, 1573-1576. (b) Engler, T. A.; Letavic, M. A.; Combrink, K. D.; Takusagawa, F. *J. Org. Chem.* **1990**, *55*, 5810-5812. (c) Engler, T. A.; Combrink, K. D.; Letavic, M. A.; Lynch, K. O., Jr.; Ray, J. E. *J. Org. Chem.* **1994**, *59*, 6567-6587.
- 18 (a) Collins, J. L.; Grieco, P. A.; Walker, J. K. *Tetrahedron Lett.* **1997**, *38*, 1321-1324. (b) Grieco, P. A.; Walker, J. K. *Tetrahedron* **1997**, *53*, 8975-8996.
- 19 Hellmann, W.; Koschinsky, R.; Mayr, H. *J. Org. Chem.* **1987**, *52*, 1989-1993.
- 20 For a review, see: Yamamura, S.; Nishiyama, S. *Synlett* **2002**, 533-543.
- 21 (a) Shizuri, Y.; Nakamura, K.; Yamamura, S. *J. Chem. Soc., Chem. Commun.* **1985**, 530-531. (b) Maki, S.; Suzuki, T.; Kosemura, S.; Shizuri, Y.; Yamamura, S. *Tetrahedron Lett.* **1991**, *32*, 4973-4976. (c) Maki, S.; Toyoda, K.; Kosemura, S.; Yamamura, S. *Chem. Lett.* **1993**, 1059-1062. (d) Takakura, H.; Yamamura, S. *Tetrahedron Lett.* **1998**, *39*, 3717-3720.
- 22 (a) Shizuri, Y.; Yamamura, S. *Tetrahedron Lett.* **1983**, *24*, 5011-5012. (b) Shizuri, Y.; Suyama, K.; Yamamura, S. *J. Chem. Soc., Chem. Commun.* **1986**, 63-64. (c) Shizuri, Y.; Okuno, Y.; Shigemori, H.; Yamamura, S. *Tetrahedron Lett.* **1987**, *28*, 6661-6664. (d) Shizuri, Y.; Maki, S.; Ohkubo, M.; Yamamura, S. *Tetrahedron Lett.* **1990**, *31*, 7167-7168. (e) Yamamura, S.; Shizuri, Y.; Shigemori, H.; Okuno, Y.; Ohkubo, M. *Tetrahedron* **1991**, *47*, 635-644. (f) Takakura, H.; Toyoda, K.; Yamamura, S. *Tetrahedron Lett.* **1996**, *37*, 4043-4046. (g) Takakura, H.; Yamamura, S. *Tetrahedron Lett.* **1999**, *40*, 299-302.
- 23 Hienuki, Y.; Tsuji, T.; Nishida, S. *Tetrahedron Lett.* **1981**, *22*, 867-870.
- 24 (a) Büchi, G.; Chu, P.-S. *J. Am. Chem. Soc.* **1979**, *101*, 6767-6768. (b) Büchi, G.; Chu, P.-S. *Tetrahedron* **1981**, *37*, 4509-4513.
- 25 Mak, C.-P.; Büchi, G. *J. Org. Chem.* **1981**, *46*, 1-3.
- 26 (a) Ishibashi, M.; Tsuyuki, T.; Takahashi, T. *Tetrahedron Lett.* **1983**, *24*, 4843-

4846. (b) Ishibashi, M.; Tsuyuki, T.; Takahashi, T. *Bull. Chem. Soc. Jpn.* **1985**, *58*, 2357-2360.
- 27 (a) Kim, A. I.; Rychnovsky, S. D. *Angew. Chem. Int. Ed.* **2003**, *42*, 1267-1270.
(b) Harrowven, D. C.; Pascoe, D. D.; Demurtas, D.; Bourne, H. O. *Angew. Chem. Int. Ed.* **2005**, *44*, 1221-1222.
- 28 For reviews, see: (a) Sammes, P. G. *Gazz. Chim. Ital.* **1986**, *119*, 109-114. (b) Mascareñas, J. L. *Advances in Cycloaddition* **1999**, *6*, 1-54. (c) Singh, V.; Krishna, U. M.; Vikrant; Trivedi, G. K. *Tetrahedron* **2008**, *64*, 3405-3428.
- 29 For lead references, see: (a) Ullman, E. F.; Milks, J. E. *J. Am. Chem. Soc.* **1962**, *84*, 1315-1316. (b) Ullman, E. F.; Henderson, W. A., Jr. *J. Am. Chem. Soc.* **1966**, *88*, 4942-4960. (c) Zimmerman, H. E.; Simkin, R. D. *Tetrahedron Lett.* **1964**, *28*, 1847-1851. (d) Lown, J. W.; Matsumoto, K. *Can. J. Chem.* **1971**, *49*, 3993-3455. (e) Feldman, K. S. *Tetrahedron Lett.* **1983**, *24*, 5585-5586. (f) Ramaiah, D.; Rajadurai, S.; Das, P. K.; George, M. V. *J. Org. Chem.* **1987**, *52*, 1082-1089.
- 30 For a related [5+2] process from cellulose pyrolysis products, see: Furneaux, R. H.; Mason, J. M.; Miller, I. J. *J. Chem. Soc., Perkin Trans. 1* **1984**, 1923-1928.
- 31 For lead references, see: (a) Padwa, A.; Carter, S. P.; Nimmegern, H. *J. Org. Chem.* **1986**, *51*, 1157-1158. (b) Padwa, A. *Acc. Chem. Res.* **1991**, *24*, 22-28. (c) Padwa, A.; Hornbuckle, S. F.; Fryxell, G. E.; Zhang, Z. J. *J. Org. Chem.* **1992**, *57*, 5747-5757. (d) Oh, C. H.; Lee, J. H.; Lee, S. M.; Yi, H. J.; Hong, C. S. *Chem. Eur. J.* **2009**, *15*, 71-74. (e) Shu, X.-Z.; Zhao, S.-C.; Ji, K.-G.; Zheng, Z.-J.; Liu, X.-Y.; Liang, Y.-M. *Eur. J. Org. Chem.* **2009**, 117-122. Also, see ref. 28c.
- 32 Katritzky, A. R.; Dennis, N. *Chem. Rev.* **1989**, *89*, 827-861.
- 33 Woods, L. L. *J. Am. Chem. Soc.* **1952**, *74*, 3959.
- 34 Woods, L. L. *J. Am. Chem. Soc.* **1953**, *75*, 1510.
- 35 Hurd, C. D.; Trofimenko, S. *J. Am. Chem. Soc.* **1958**, *80*, 2526-2527.
- 36 Hurd, C. D.; Sims, R. J.; Trofimenko, S. *J. Am. Chem. Soc.* **1959**, *81*, 1684-1687.
- 37 Hurd, C. D.; Trofimenko, S. *J. Am. Chem. Soc.* **1959**, *81*, 2430-2437.
- 38 Volkmann, R. A.; Weeks, P. D.; Kuhla, D. E.; Whipple, E. B.; Chmurny, G. N. *J. Org. Chem.* **1977**, *42*, 3976-3978.
- 39 Garst, M. E.; McBride, B. J.; Douglass, J. G., III. *Tetrahedron Lett.* **1983**, *24*, 1675-1678.

- 40 Wender, P. A.; McDonald, F. E. *J. Am. Chem. Soc.* **1990**, *112*, 4956-4958.
- 41 For another early example using group transfer methods, see: McBride, B. J.; Garst, M. E. *Tetrahedron* **1993**, *49*, 2839-2854.
- 42 (a) Domingo, L. R.; Zaragoza, R. J. *J. Org. Chem.* **2000**, *65*, 5480-5486. (b) Domingo, L. R.; Zaragoza, R. J. *Tetrahedron* **2001**, *57*, 5597-5606. (c) Zaragoza, R. J.; Aurell, M. J.; Domingo, L. R. *J. Phys. Org. Chem.* **2005**, *18*, 610-615.
- 43 Rumbo, A.; Castedo, L.; Mourino, A.; Mascareñas, J. L. *J. Org. Chem.* **1993**, *58*, 5585-5586.
- 44 (a) Mascareñas, J. L.; Rumbo, A.; Castedo, L. *J. Org. Chem.* **1997**, *62*, 8620-8621. (b) Rodríguez, J. R.; Rumbo, A.; Castedo, L.; Mascareñas, J. L. *J. Org. Chem.* **1999**, *64*, 4560-4563.
- 45 (a) Rodríguez, J. R.; Rumbo, A.; Castedo, L.; Mascareñas, J. L. *J. Org. Chem.* **1999**, *64*, 966-970. (b) Rodríguez, J. R.; Castedo, L.; Mascareñas, J. L. *J. Org. Chem.* **2000**, *65*, 2528-2531.
- 46 (a) Rumbo, A.; Castedo, L.; Mascareñas, J. L. *Tetrahedron Lett.* **1997**, *38*, 5885-5886. (b) López, L.; Castedo, L.; Mascareñas, J. L. *Org. Lett.* **2000**, *2*, 1005-1007. (c) López, F.; Castedo, L.; Mascareñas, J. L. *Org. Lett.* **2001**, *3*, 623-625. (d) López, F.; Castedo, L.; Mascareñas, J. L. *Org. Lett.* **2002**, *4*, 3683-3685. (e) López, F.; Castedo, L.; Mascareñas, J. L. *Chem. Eur. J.* **2002**, *8*, 884-899. (f) López, F.; Castedo, L.; Mascareñas, J. L. *J. Org. Chem.* **2003**, *68*, 9780-9786.
- 47 Also, note that tethers bearing chiral malonates can be used to achieve moderate levels of diastereoselectivity: Ohmori, N.; Yoshimura, M.; Ohkata, K. *Heterocycles* **1997**, *45*, 2097-2100.
- 48 (a) Wender, P. A.; Mascareñas, J. L. *J. Org. Chem.* **1991**, *56*, 6267-6269. (b) Wender, P. A.; Mascareñas, J. L. *Tetrahedron Lett.* **1992**, *33*, 2115-2118.
- 49 Nogueira, E.; Guitián, E.; Castedo, L.; Castiñeiras, A. *Aust. J. Chem.* **1997**, *50*, 751-754.
- 50 Hendrickson, J. B.; Farina, J. S. *J. Org. Chem.* **1980**, *45*, 3359-3361.
- 51 Achmatowicz, O. Jr.; Bukowski, P.; Szechner, B.; Zwierzchowska, Z.; Zamojski, A. *Tetrahedron* **1971**, *27*, 1973-1996.
- 52 For another synthetic pathway to oxidopyrylium species involving elimination and their applications in [5+2] cycloaddition, see: Potts, K. T.; Elliott, A. J.; Sorm, M. *J. Org. Chem.* **1972**, *37*, 3838-3845.

- 53 For an additional example, see: Aggarwal, V. K.; Grainger, R. S.; Newton, G. K.; Spargo, P. L.; Hobson, A. D.; Adams, H. *Org. Biomol. Chem.* **2003**, *1*, 1884-1893.
- 54 For reaction with allenes, see: Lee, H.-Y.; Sohn, J.-H.; Kim, H. Y. *Tetrahedron Lett.* **2001**, *42*, 1695-1698.
- 55 (a) Sammes, P. G.; Street, L. J. *J. Chem. Soc., Perkin Trans. 1* **1983**, 1261-1265.
(b) Sammes, P. G.; Street, L. J.; Kirby, P. *J. Chem. Soc., Perkin Trans. 1* **1983**, 2729-2734.
- 56 Ohmori, N.; Miyazaki, T.; Kojima, S.; Ohkata, K. *Chem. Lett.* **2001**, 906-907.
- 57 (a) Ohmori, N. *Chem. Commun.* **2001**, 1552-1553. (b) Ohmori, N. *J. Chem. Soc., Perkin Trans. 1* **2002**, 755-767.
- 58 Delgado, A. D.; Castedo, L.; Mascareñas, J. L. *Org. Lett.* **2002**, *4*, 3091-3094.
- 59 (a) Sammes, P. G.; Street, L. J. *J. Chem. Soc., Chem. Commun.* **1983**, 666-668.
(b) Bromidge, S. M.; Sammes, P. G.; Street, L. J. *J. Chem. Soc., Chem. Commun.* **1985**, 1725-1730. (c) Sammes, P. G.; Street, L. J.; Whitby, R. J. *J. Chem. Soc., Perkin Trans. 1* **1986**, 281-289.
- 60 (a) Wender, P. A.; Rice, K. D.; Schnute, M. E. *J. Am. Chem. Soc.* **1997**, *119*, 7897-7898. (b) Wender, P. A.; Jesudason, C. D.; Nakahira, H.; Tamura, N.; Tebbe, A. L.; Ueno, Y. *J. Am. Chem. Soc.* **1997**, *119*, 12976-12977. (c) Wender, P. A.; Martin-Cantelejo, Y.; Carpenter, A. J.; Chiu, A.; De Brabander, J.; Harran, P. G.; Jimenez, J.-M.; Koehler, M. F. T.; Lippa, B.; Morrison, J. A.; Müller, S. G.; Müller, S. N.; Park, C.-M.; Shiozaki, M.; Siedenbiedel, C.; Skalitzky, D. J.; Tanaka, M.; Irie, K. *Pure & Appl. Chem.* **1998**, *70*, 539-546.
- 61 (a) Wender, P. A.; Lee, H. Y.; Wilhelm, R. S.; Williams, P. D. *J. Am. Chem. Soc.* **1989**, *111*, 8954-8957. (b) Wender, P. A.; Bi, F. C.; Buschmann, N.; Gosselin, F.; Kan, C.; Kee, J.-M.; Ohmura, H. *Org. Lett.* **2006**, *8*, 5373-5376. (c) Wender, P. A.; D'Angelo, N.; Elitzin, V. I.; Ernst, M.; Jackson-Ugueto, E. E.; Kowalski, J. A.; McKendry, S.; Rehfeuter, M.; Sun, R.; Voigtlaender, D. *Org. Lett.* **2007**, *9*, 1829-1832.
- 62 (a) Bauta, W.; Booth, J.; Bos, M. E.; DeLuca, M.; Diorazio, L.; Donohoe, T.; Magnus, N.; Magnus, P.; Mendoza, J.; Pye, P.; Tarrant, J.; Thom, S.; Ujjainwalla, F. *Tetrahedron Lett.* **1995**, *36*, 5327-5330. (b) Bauta, W. E.; Booth, J.; Bos, M. E.; DeLuca, M.; Diorazio, L.; Donohoe, T. J.; Frost, C.; Magnus, N.; Magnus, P.; Mendoza, J.; Pye, P.; Tarrant, J. G.; Thom, S.; Ujjainwalla, F. *Tetrahedron* **1996**, *52*, 14081-14102. (c) Magnus, P.; Shen, L. *Tetrahedron* **1999**, *55*, 3553-3560.

- (d) Magnus, P.; Waring, M. J.; Ollivier, C.; Lynch, V. *Tetrahedron Lett.* **2001**, *42*, 4947-4950.
- 63 For other approaches to the oxabicycloundecane framework, see: (a) Williams, D. R.; Benbow, J. W.; Allen, E. E. *Tetrahedron Lett.* **1990**, *31*, 6769-6772. (b) Williams, D. R.; Benbow, J. W.; McNutt, J. G.; Allen, E. E. *J. Org. Chem.* **1995**, *60*, 833-843. For an asymmetric route see: Krishna, U. M.; Deodhar, K. D.; Trivedi, G. K. *Tetrahedron Lett.* **2004**, *60*, 4829-4836.
- 64 Roethle, P. A.; Hernandez, P. T.; Trauner, D. *Org. Lett.* **2006**, *8*, 5901-5904.
- 65 (a) Tang, B.; Bray, C. D.; Pattenden, G. *Tetrahedron Lett.* **2006**, *47*, 6401-6404. (b) Tang, B.; Bray, C. D.; Pattenden, G. *Org. Biomol. Chem.* **2009**, *7*, 4448-4457.
- 66 (a) Adlington, R. M.; Baldwin, J. E.; Mayweg, A. V. W.; Pritchard, G. J. *Org. Lett.* **2002**, *4*, 3009-3011. (b) Baldwin, J. E.; Mayweg, A. V. W.; Pritchard, G. J.; Adlington, R. M. *Tetrahedron Lett.* **2003**, *44*, 4543-4545.
- 67 Celanire, S.; Marlin, F.; Baldwin, J. E.; Adlington, R. M. *Tetrahedron* **2005**, *61*, 3025-3032.
- 68 (a) Snider, B. B.; Grabowski, J. F. *Tetrahedron Lett.* **2005**, *46*, 823-825. (b) Snider, B. B.; Grabowski, J. F. *Tetrahedron* **2006**, *62*, 5171-5177. (c) Snider, B. B.; Wu, X.; Nakamura, S.; Hashimoto, S. *Org. Lett.* **2007**, *9*, 873-874.
- 69 Krishna, U. M.; Trivedi, G. K. *Tetrahedron Lett.* **2004**, *45*, 257-259.
- 70 Marshall, K. A.; Mapp, A. K.; Heathcock, C. H. *J. Org. Chem.* **1996**, *61*, 9135-9145.
- 71 Sarel, S.; Breuer, E. *J. Am. Chem. Soc.* **1959**, *81*, 6522-6523.
- 72 Pasto, D. J.; Borchardt, J. K.; Fehlner, T. P.; Baney, H.; Schwartz, M. E. *J. Am. Chem. Soc.* **1976**, *98*, 526-529.
- 73 (a) Sarel, S.; Felzenstein, A.; Yovell, J. *J. Chem. Soc., Chem. Commun.* **1973**, 859-860. (b) Sarel, S.; Felzenstein, A.; Yovell, J. *J. Chem. Soc., Chem. Commun.* **1974**, 753-754. (c) Felzenstein, A.; Sarel, S.; Yovell, J. *J. Chem. Soc., Chem. Commun.* **1975**, 918-919.
- 74 (a) Fowler, F. W. *Angew. Chem. Int. Ed.* **1971**, *10*, 135-136. (b) Herges, R.; Ugi, I. *Angew. Chem. Int. Ed.* **1985**, *24*, 594-596.
- 75 For reviews, see: (a) Wender, P. A.; Love, J. A. *Advances in Cycloaddition* **1999**, *5*, 1-45. (b) Wender, P. A.; Gamber, G. G.; Williams, T. J. *Modern Rhodium-*

- Catalyzed Organic Reactions*, P. A. Evans, Ed.; Wiley-VCH: New York, **2005**.
- 76 (a) Ashfeld, B. L.; Miller, K. A.; Smith, A. J.; Tran, K.; Martin, S. F. *Org. Lett.* **2005**, *7*, 1661-1663. (b) Ashfeld, B. L.; Miller, K. A.; Smith, A. J.; Tran, K.; Martin, S. F. *J. Org. Chem.* **2007**, *72*, 9018-9031.
- 77 Wender, P. A.; Takahashi, H.; Witulski, B. *J. Am. Chem. Soc.* **1995**, *117*, 4720-4721.
- 78 Wender, P. A.; Sperandio, D. *J. Org. Chem.* **1998**, *63*, 4164-4165.
- 79 Wender, P. A.; Williams, T. J. *Angew. Chem. Int. Ed.* **2002**, *41*, 4550-4553.
- 80 Wender, P. A.; Love, J. A.; Williams, T. J. *Synlett* **2003**, 1295-1298.
- 81 Gómez, F. J.; Kamber, N. E.; Deschamps, N. M.; Cole, A. P.; Wender, P. A.; Waymouth, R. M. *Organometallics* **2007**, *26*, 4541-4545. For a variant NHC catalyst see: Lee, S. I.; Park, S. Y.; Park, J. H.; Jung, I. G.; Choi, S. Y.; Chung, Y. K.; Lee, B. Y. *J. Org. Chem.* **2006**, *71*, 91-96.
- 82 Gilbertson, S. R.; Hoge, G. S. *Tetrahedron Lett.* **1998**, *39*, 2975-2078.
- 83 Saito, A.; Ono, T.; Hanzawa, Y. *J. Org. Chem.* **2006**, *71*, 6437-6443.
- 84 Wang, B.; Cao, P.; Zhang, X. *Tetrahedron Lett.* **2000**, *41*, 8041-8044.
- 85 (a) Wender, P. A.; Husfeld, C. O.; Langkopf, E.; Love, J. A. *J. Am. Chem. Soc.* **1998**, *120*, 1940-1941. (b) Wender, P. A.; Husfeld, C. O.; Langkopf, E.; Love, J. A.; Pleuss, N. *Tetrahedron* **1998**, *54*, 7203-7220. (c) Wang, Y.; Wang, J.; Su, J.; Huang, F.; Jiao, L.; Liang, Y.; Yang, D.; Zhang, S.; Wender, P. A.; Yu, Z.-X. *J. Am. Chem. Soc.* **2007**, *129*, 10060-10061.
- 86 Wender, P. A.; Glorius, F.; Husfeld, C. O.; Langkopf, E.; Love, J. A. *J. Am. Chem. Soc.* **1999**, *121*, 5348-5349.
- 87 Wender, P. A.; Haustedt, L. O.; Lim, J.; Love, J. A.; Williams, T. J.; Yoon, J.-Y. *J. Am. Chem. Soc.* **2006**, *128*, 6302-6303.
- 88 Shintani, R.; Nakatsu, H.; Takatsu, K.; Hayashi, T. *Chem. Eur. J.* **2009**, *15*, 8692-8694.
- 89 Wender, P. A.; Dyckman, A. *J. Org. Lett.* **1999**, *1*, 2089-2092.
- 90 Wender, P. A.; Dyckman, A. J.; Husfeld, C. O.; Kadereit, D.; Love, J. A.; Rieck, H. *J. Am. Chem. Soc.* **1999**, *121*, 10442-10443.

- 91 Jiao, L.; Ye, S.; Yu, Z.-X. *J. Am. Chem. Soc.* **2008**, *130*, 7178-7179.
- 92 Binger, P.; Wedemann, P.; Kozhushkov, S. I.; de Meijere, A. *Eur. J. Org. Chem.* **1998**, 113-119.
- 93 Wender, P. A.; Rieck, H.; Fuji, M. *J. Am. Chem. Soc.* **1998**, *120*, 10976-10977.
- 94 (a) Wender, P.A.; Dyckman, A. J.; Husfeld, C. O.; Scanio, M. J. C. *Org. Lett.* **2000**, *2*, 1609-1611. (b) Wender, P. A.; Gamber, G. G.; Scanio, M. J. C. *Angew. Chem. Int. Ed.* **2001**, *40*, 3895-3897.
- 95 Wender, P. A.; Barzilay, C. M.; Dyckman, A. J. *J. Am. Chem. Soc.* **2001**, *123*, 179-180.
- 96 Wegner, H. A.; de Meijere, A.; Wender, P. A. *J. Am. Chem. Soc.* **2005**, *127*, 6530-6531.
- 97 Wender, P. A.; Fuji, M.; Husfeld, C. O.; Love, J. A. *Org. Lett.* **1999**, *1*, 137-139.
- 98 Wender, P. A.; Zhang, L. *Org. Lett.* **2000**, *2*, 2323-2326.
- 99 Wender, P. A.; Bi, F. C.; Brodney, M. A.; Gosselin, F. *Org. Lett.* **2001**, *3*, 2105-2108.
- 100 (a) Ashfeld, B. L.; Martin, S. F. *Org. Lett.* **2005**, *7*, 4535-4537. (b) Ashfeld, B. L.; Martin, S. F. *Tetrahedron* **2006**, *62*, 10497-10506.
- 101 Trost, B. M.; Waser, J.; Meyer, A. *J. Am. Chem. Soc.* **2007**, *129*, 14556-14557.
- 102 (a) Yu, Z.-X.; Wender, P. A.; Houk, K. N. *J. Am. Chem. Soc.* **2004**, *126*, 9154-9155. (b) Yu, Z.-X.; Cheong, P. H.-Y.; Liu, P.; Legault, C. Y.; Wender, P. A.; Houk, K. N. *J. Am. Chem. Soc.* **2008**, *130*, 2378-2379. (c) Liu, P.; Cheong, P. H.-Y.; Yu, Z.-X.; Wender, P. A.; Houk, K. N. *Angew. Chem. Int.* **2008**, *47*, 3939-3941.
- 103 (a) Trost, B. M.; Toste, F. D.; Shen, H. *J. Am. Chem. Soc.* **2000**, *122*, 2379-2380. (b) Trost, B. M.; Shen, H. C. *Org. Lett.* **2000**, *2*, 2523-2525. (c) Trost, B. M.; Shen, H. C.; Schulz, T.; Korandin, C.; Schirok, H. *Org. Lett.* **2003**, *5*, 4149-4151. (d) Trost, B. M.; Shen, H. C.; Horne, D. B.; Toste, F. D.; Steinmetz, B. G.; Korandin, C. *Chem. Eur. J.* **2005**, *11*, 2577-2590.
- 104 Trost, B. M.; Shen, H. C. *Angew. Chem. Int. Ed.* **2001**, *40*, 2313-2316.
- 105 Trost, B. M.; Hu, Y.; Horne, D. B. *J. Am. Chem. Soc.* **2007**, *129*, 11781-11790.

- 106 Zuo, G.; Louie, J. *J. Am. Chem. Soc.* **2005**, *127*, 5798-5799.
- 107 Fürstner, A.; Majima, K.; Martín, R.; Krause, H.; Kattnig, E.; Goddard, R.;
Lehmann, C. W. *J. Am. Chem. Soc.* **2008**, *130*, 1992-2004.
- 108 Barluenga, J.; Alonso, J.; Fañanás, F. J.; Borge, J.; García-Granda, S. *Angew.
Chem. Int. Ed.* **2004**, *43*, 5510-5513.
- 109 (a) Lee, T. V.; Boucher, R. J.; Rockell, C. J. M. *Tetrahedron Lett.* **1988**, *29*, 689-
692. (b) Lee, T. V.; Boucher, R. J.; Porter, J. R.; Rockell, C. J. M. *Tetrahedron*
1989, *45*, 5887-5894. (c) Lee, T. V.; Cregg, C. *Synlett* **1990**, 317-319.
- 110 (a) Tanino, K.; Shimizu, T.; Miyama, M.; Kuwajima, I. *J. Am. Chem. Soc.* **2000**,
122, 6116-6117. (b) Tanino, K.; Kondo, F.; Shimizu, T.; Miyashita, M. *Org. Lett.*
2002, *4*, 2217-2219.
- 111 For a review of (cycloheptyne)dicobalt complexes, see: Green, J. R. *Eur. J. Org.
Chem.* **2008**, 6053-6062.
- 112 Nicholas, K. M. *Acc. Chem. Res.* **1987**, *20*, 207-214.
- 113 (a) Yin, J.; Liebeskind, L. S. *J. Am. Chem. Soc.* **1999**, *121*, 5811-5812. (b)
Malinakova, H. C.; Liebeskind, L. S. *Org. Lett.* **2000**, *2*, 3909-3911. (c)
Malinakova, H. C.; Liebeskind, L. S. *Org. Lett.* **2000**, *2*, 4083-4086.
- 114 Garnier, E. C.; Liebeskind, L. S. *J. Am. Chem. Soc.* **2008**, *130*, 7449-7458.
- 115 Zhang, Y.; Liebeskind, L. S. *J. Am. Chem. Soc.* **2006**, *128*, 465-472.
- 116 Yueh, T.-C.; Lush, S.-F.; Lee, G.-H.; Peng, S.-M.; Liu, R.-S. *Organometallics*
1996, *15*, 5669-5673.
- 117 Wilson, A. M.; Waldman, T. E.; Rheingold, A. L.; Ernst, R. D. *J. Am. Chem. Soc.*
1992, *114*, 6252-6254.
- 118 (a) Tomaszewski, R.; Hyla-Kryspin, I.; Mayne, C. L.; Arif, A. M.; Gleiter, R.;
Ernst, R. D. *J. Am. Chem. Soc.* **1998**, *120*, 2959-2960. (b) Harvey, B. G.; Mayne,
C. L.; Arif, A. M.; Tomaszewski, R.; Ernst, R. D. *J. Am. Chem. Soc.* **2005**, *127*,
16426-16435.
- 119 Basta, R.; Harvey, B. G.; Arif, A. M.; Ernst, R. D. *Inorg. Chim. Acta* **2004**, *357*,
3883-3888.
- 120 (a) Kreiter, C. G.; Koch, E.-C.; Frank, W.; Reiss, G. *Inorg. Chim. Acta* **1994**, *220*,
77-83. (b) Kreiter, C. G.; Fiedler, C.; Frank, W.; Reiss, G. *J. Chem. Ber.* **1995**,

- 128, 515-518. (c) Kreiter, C. G.; Fiedler, C.; Frank, W.; Reiss, G. J. *J. Organomet. Chem.* **1995**, *490*, 133-141. (d) Kreiter, C. G.; Koch, E.-C.; Frank, W.; Reiss, G. J. *Z. Naturforsch. B* **1996**, *51B*, 1473-1485.
- 121 (a) Wang, C.; Sheridan, J. B.; Chung, H.-J.; Coté, M. L.; Lalancette, R. A.; Rheingold, A. L. *J. Am. Chem. Soc.* **1994**, *116*, 8966-8972. (b) Chung, H.-J.; Sheridan, J. B.; Coté, M. L.; Lalancette, R. A. *Organometallics* **1996**, *15*, 4575-4585.
- 122 Chen, W.; Chung, H.-J.; Wang, C.; Sheridan, J. B.; Coté, M. L.; Lalancette, R. A. *Organometallics* **1996**, *15*, 3337-3344.
- 123 Witherell, R. D.; Ylijoki, K. E. O.; Stryker, J. M. *J. Am. Chem. Soc.* **2008**, *130*, 2176-2177.
- 124 Schwiebert, K. E.; Stryker, J. M. *J. Am. Chem. Soc.* **1995**, *117*, 8275-8276.
- 125 Nehl, H. *Chem. Ber.* **1993**, *126*, 1519-1527.
- 126 Etkin, N.; Dzwiniel, T. L.; Schweibert, K. E.; Stryker, J. M. *J. Am. Chem. Soc.* **1998**, *120*, 9702-9703.
- 127 Dzwiniel, T. L.; Etkin, N.; Stryker, J. M. *J. Am. Chem. Soc.* **1999**, *121*, 10640-10641.
- 128 Dzwiniel, T. L.; Stryker, J. M. *J. Am. Chem. Soc.* **2004**, *126*, 9184-9185.
- 129 (a) Bennett, M. A.; Nicholls, J. C.; Rahman, A. K. F.; Redhouse, A. D.; Spencer, J. L.; Willis, A. C. *J. Chem. Soc., Chem. Commun.* **1989**, 1328-1330. (b) Nicholls, J. C.; Spencer, J. L. *Organometallics* **1994**, *13*, 1781-1787.
- 130 For reviews, see: (a) Ernst, R. D. *Chem. Rev.* **988**, *88*, 1255-1291. (b) Ernst, R. D. *Comments Inorg. Chem.* **1999**, *21*, 285-325. (c) Stahl, L.; Ernst, R. D. *Adv. Organomet. Chem.* **2008**, *55*, 137-199.
- 131 White, C.; Thompson, S. J.; Maitlis, P. M. *J. Organomet. Chem.* **1977**, *134*, 319-325.
- 132 (a) Powell, P.; Russell, L. J. *J. Chem. Research* **1978**, *283*, 3652-3672. (b) Powell, P. *J. Organomet. Chem.* **1979**, *165*, C43-C46. (c) Powell, P. *J. Organomet. Chem.* **1981**, *206*, 239-255. (d) Powell, P. *J. Organomet. Chem.* **1983**, *244*, 393-399. (e) Powell, P.; Stephens, M.; Muller, A. *J. Organomet. Chem.* **1986**, *310*, 255-268.
- 133 (a) Mahler, J. E.; Pettit, R. *J. Am. Chem. Soc.* **1963**, *85*, 3955-3959. (b) Mahler,

- J. E.; Gibson, D. H.; Pettit, R. *J. Am. Chem. Soc.* **1963**, *85*, 3959-3963.
- 134 (a) Bleeke, J. R.; Donaldson, A. *J. Organometallics* **1988**, *7*, 1588-1596. (b) Bleeke, J. R.; Luaders, S. T. *Organometallics* **1995**, *14*, 1667-1673.
- 135 Müller, J.; Schiller, C.; Gaede, P. E.; Kempf, M. *Z. Anorg. Allg. Chem.* **2005**, *631*, 38-46.
- 136 (a) Bleeke, J. R.; Peng, W.-J. *Organometallics* **1984**, *3*, 1422-1426. (b) Wilson, D. R.; Ernst, R. D.; Kralik, M. S. *Organometallics* **1984**, *3*, 1442-1444. (c) Bleeke, J. R.; Peng, W.-J. *Organometallics* **1986**, *5*, 635-644. (d) Lee, G.-H.; Peng, S.-M.; Liao, M.-Y.; Liu, R.-S. *J. Organomet. Chem.* **1986**, *312*, 113-120. (e) Bleeke, J. R.; Donaldson, A. J.; Peng, W.-J. *Organometallics* **1988**, *7*, 33-37.
- 137 Kirk, A. D. "Ancillary Ligand Effects in the Cobalt-Mediated [5+2] Pentadienyl/Alkyne Cycloaddition Reactions" *MSc. Thesis*, University of Alberta, **2007**.
- 138 Ernst, R. D.; Ma, H.; Sergeson, G.; Zahn, T.; Ziegler, M. L. *Organometallics* **1987**, *6*, 848-853.
- 139 Cracknell, R. B.; Nicholls, J. C.; Spencer, J. L. *Organometallics* **1996**, *15*, 446-448.
- 140 Butovskii, M. V.; Englert, U.; Herberich, G. E.; Kirchner, K.; Koelle, U. *Organometallics* **2003**, *22*, 1989-1991.
- 141 For reviews, see: (a) Pellissier, H. *Tetrahedron* **2005**, *61*, 6479-6517. (b) Frontier, A. J.; Collison, C. *Tetrahedron* **2005**, *61*, 7577-7606.
- 142 Ylijoki, K. E. O.; Witherell, R. D.; Kirk, A. D.; Böcklein, S.; Lofstrand, V. A.; McDonald, R.; Ferguson, M. J.; Stryker, J. M. *Organometallics* **2009**, *28*, 6907-6822.
- 143 Witherell, R. D. "Seven-Membered Ring Compounds from [3+2+2] and [5+2] Cobalt-Mediated Cycloadditions" *Ph.D. Dissertation*, University of Alberta, **2007**.
- 144 Shing, T. K. M.; Zhu, X. Y.; Yeung, Y. Y. *Chem. Eur. J.* **2003**, *9*, 5489.
- 145 Bertus, P.; Drouin, L.; Laroche, C.; Szymoniak, J. *Tetrahedron* **2004**, *60*, 1375.
- 146 Cao, X.-P. *Tetrahedron* **2002**, *58*, 1301-1307.
- 147 Hu, Q.; Rege, P. D.; Corey, E. J. *J. Am. Chem. Soc.* **2004**, *126*, 5984-5986.

- 148 Piers, E.; Jung, G. L.; Ruediger, E. H. *Can. J. Chem.* **1986**, *65*, 670-682.
- 149 Martelli, J.; Grée, D.; Kessadi, J.; Grée, R. *Tetrahedron* **1989**, *45*, 4213-4226.
- 150 Ishii, T.; Kawamura, N.; Matsubara, S.; Utimoto, K. *J. Org. Chem.* **1987**, *52*, 4416-4418.
- 151 Bobbitt, J. M.; Amundsen, L. H.; Steiner, R. I. *J. Org. Chem.* **1960**, *25*, 2230-2231.
- 152 (a) Braude, E. A.; Timmons, C. J. *J. Chem. Soc.* **1950**, 2007-2011. (b) Andersson, P. G.; Bäckvall, J.-E. *J. Org. Chem.* **1991**, *56*, 5349-5353.
- 153 Coelho, P. J.; Blanco, L. *Eur. J. Org. Chem.* **2000**, 3039-3046.
- 154 (a) Brookhart, M.; Green, M. L. H.; Pardy, R. B. A. *J. Chem. Soc., Chem. Commun.* **1983**, 691-693. (b) Brookhart, M.; Lincoln, D. M.; Volpe, A. F.; Schmidt, G. F. *Organometallics* **1989**, *8*, 1212-1218. (c) Brookhart, M.; Lincoln, D. M.; Bennett, M. A.; Pelling, S. *J. Am. Chem. Soc.* **1990**, *112*, 2691-2694.
- 155 Wang, Y.; Schill, B. D.; Arif, A. M.; West, F. G. *Org. Lett.* **2003**, *5*, 2747-2750.
- 156 Lenges, C. P.; Brookhart, M.; Grant, B. E. *J. Organomet. Chem.* **1997**, *528*, 199-203.
- 157 Krivykh, V. V.; Gusev, O. V.; Petrovskii, P., V.; Rybinskaya, M. I. *J. Organomet. Chem.* **1989**, *366*, 129-145.
- 158 (a) Margulis, T. N.; Schiff, L.; Rosenblum, M. *J. Am. Chem. Soc.* **1965**, *87*, 3269-3270. (b) Eisenstadt, A.; Winstein, S. *Tetrahedron Lett.* **1970**, *11*, 4603-4606. (c) Johnson, B. F. G.; Lewis, J.; Randall, G. L. P. *J. Chem. Soc., (A)* **1971**, 422-429. (d) Eisenstadt, A. *J. Organomet. Chem.* **1972**, *38*, C32-C34. (e) Domingos, A. J. P.; Johnson, B. F. G.; Lewis, J. L. *J. Chem. Soc., Dalton Trans.* **1974**, 145-149. (f) Charles, A. D.; Diversi, P.; Johnson, B. F. G.; Karlin, K. D.; Lewis, J.; Rivera, A. V.; Sheldrick, G. M. *J. Organomet. Chem.* **1977**, *128*, C31-C34. (g) Rivera, A. V.; Sheldrick, G. M. *Acta Crystallogr., Sect. B: Struct. Sci.* **1978**, *B34*, 1716-1718. (h) Charles, A. D.; Diversi, P.; Johnson, B. F. G.; Lewis, J. *J. Chem. Soc., Dalton Trans.* **1981**, 1906-1917. (i) Bluemel, J.; Hertkorn, N.; Kanellakopoulos, B.; Koehler, F. H.; Lachmann, J.; Mueller, G.; Wagner, F. E. *Organometallics* **1993**, *12*, 3896-3905.
- 159 Lewis, J.; Parkins, A. W. *J. Chem. Soc. (A)* **1969**, 953-957.
- 160 Salzer, A.; Bigler, P. *Inorg. Chim. Acta* **1981**, *48*, 199-203.

- 161 Older, C. M.; McDonald, R.; Stryker, J. M. *J. Am. Chem. Soc.* **2005**, *127*, 14202-14203.
- 162 Lambert, L. B.; Wang, G.; Finzel, R. B.; Teramura, D. H. *J. Am. Chem. Soc.* **1987**, *109*, 7838-7845.
- 163 Chengebroyen, J.; Linke, M.; Robitzer, M.; Sirlin, C.; Pfeffer, M. *J. Organomet. Chem.* **2003**, *687*, 313-321.
- 164 Breslow, R.; Pecoraro, J.; Sugimoto, T. *Org. Syn., Coll. Vol. 6* **1988**, 361-364.
- 165 Iwamoto, M.; Warita, Y.; Tamura, H.; Ito, M. Jpn. Patent 11130705, **1999**.
- 166 Hoye, T. R.; van Veidhuizen, J. J.; Vos, T. J.; Zhao, P. *Synth. Comm.* **2001**, *31*, 1367-1371.
- 167 Brillon, D.; Deslongchamps, P. *Can. J. Chem.* **1987**, *65*, 43-55.
- 168 Arnett, E. M.; Maroldo, S. G.; Schilling, S. L.; Harrelson, J. A. *J. Am. Chem. Soc.* **1984**, *106*, 6759-6767.
- 169 Chatterjee, A. K.; Morgan, J. P.; Scholl, M.; Grubbs, R. H. *J. Am. Chem. Soc.* **2000**, *122*, 3783-3784.
- 170 Ballini, R.; Bosica, G.; Frullanti, B.; Maggi, R.; Sartori, G.; Schroer, F. *Tetrahedron Lett.* **1998**, *39*, 1615-1618.
- 171 Using sufficiently electron-deficient olefins, thermally stable 1,4-diene complexes can be prepared: Holland, R. L.; Bunker, K. D.; Chen, C. H.; DiPasquale, A. G.; Rheingold, A. L.; Baldrige, K. K.; O'Connor, J. M. *J. Am. Chem. Soc.* **2008**, *130*, 10093-10095.
- 172 Stork, G.; Brizzolara, A.; Landesman, H.; Szmuskovicz, J.; Terrell, R. *J. Am. Chem. Soc.* **1963**, *85*, 207-222. For recent reviews see: (a) Mukherjee, S.; Yang, J. W.; Hoffmann, S.; List, B. *Chem. Rev.* **2007**, *107*, 5471-5569. (b) List, B. *Acc. Chem. Res.* **2004**, *37*, 548-557. (c) *The Chemistry of Enamines*, Rappoport, Z., Ed.; Wiley: New York, **1994**.
- 173 (a) Boger, D. L.; Panek, J. S. *J. Org. Chem.* **1981**, *46*, 2179-2182. (b) Sainz, Y. F.; Raw, S. A.; Taylor, R. J. K. *J. Org. Chem.* **2005**, *70*, 10086-10095.
- 174 Crampton, M. R.; Robotham, I. A. *J. Chem. Res. (S)* **1997**, 22-23.
- 175 (a) Bordwell, F. G. *Acc. Chem. Res.* **1988**, *21*, 456-463. (b) Taft, R.; Bordwell, F. G. *Acc. Chem. Res.* **1988**, *21*, 463-469.

- 176 Davies, S. G.; Green, M. L. H.; Mingos, D. M. P. *Tetrahedron* **1978**, *34*, 3047-3077.
- 177 Aponick, A.; Li, C.-Y.; Biannic, B. *Org. Lett.* **2008**, *10*, 669-671.
- 178 Brandsma, L.; Verkruijsse, H. D. *Synthesis of Acetylenes, Allenes and Cumulenes: A Laboratory Manual*, Elsevier, **1981**.
- 179 Menzel, K.; Fu, G. C. *J. Am. Chem. Soc.* **2003**, *125*, 3718-3719.
- 180 Roush, W. R.; Champoux, J. A.; Peterson, B. C. *Tetrahedron Lett.* **1996**, *37*, 8989-8992.
- 181 Champoux, J. A. *Ph. D. Dissertation*, Indiana University, **1997**.
- 182 Clarke, P. A.; Rolla, G. A.; Cridland, A. P.; Gill, A. A. *Tetrahedron* **2007**, *63*, 9124-9128.
- 183 Gravel, M.; Touré, B. B.; Hall, D. G. *Org. Prep. Proc. Intl.* **2004**, *36*, 573-579.
- 184 Uenishi, J.; Beau, J. M.; Armstrong, R. W.; Kishi, Y. *J. Am. Chem. Soc.* **1987**, *109*, 4756-4758.
- 185 (a) Molander, G. A.; Felix, L. A. *J. Org. Chem.* **2005**, *70*, 3950-3956. (b) Molander, G. A.; Yokoyama, Y. *J. Org. Chem.* **2006**, *71*, 2493-2498. (c) Molander, G. A.; Ellis, N. *Acc. Chem. Res.* **2007**, *40*, 275-286.
- 186 Vedejs, E.; Chapman, R. W.; Fields, S. C.; Lin, S.; Schrimpf, M. R. *J. Org. Chem.* **1995**, *60*, 3020-3027.
- 187 (a) Tsuji, J.; Takahashi, H.; Morikawa, M. *Tetrahedron Lett.* **1965**, *6*, 4387-4388. (b) Trost, B. M.; Fullerton, T. J. *J. Am. Chem. Soc.* **1973**, *95*, 292-294. (c) Trost, B. M.; Van Vranken, D. L. *Chem. Rev.* **1996**, *96*, 395-422. (d) Trost, B. M.; Crawley, M. L. *Chem. Rev.* **2003**, *103*, 2921-2944.
- 188 (a) Trost, B. M.; Ball, Z. T. *J. Am. Chem. Soc.* **2001**, *123*, 12726-12727. (b) Trost, B. M.; Ball, Z. T.; Jöge, T. *J. Am. Chem. Soc.* **2002**, *124*, 7922-7923. (c) Trost, B. M.; Ball, Z. T. *J. Am. Chem. Soc.* **2003**, *125*, 30-31. (d) Trost, B. M.; Ball, Z. T.; Jöge, T. *Angew. Chem. Int. Ed.* **2003**, *42*, 3415-3418. (e) Chung, L. W.; Wu, Y.-D.; Trost, B. M.; Ball, Z. T. *J. Am. Chem. Soc.* **2003**, *125*, 11578-11582. (f) Crabtree, R. H. *New J. Chem.* **2003**, *27*, 771-772.
- 189 Steinmetz, B.; Schenk, W. A. *Organometallics* **1999**, *18*, 943-946.

- 190 Daeuble, J. F.; McGettigan, C.; Stryker, J. M. *Tetrahedron Lett.* **1990**, *31*, 2397-2400.
- 191 Dzwiniel, T. L. "Seven-Membered Carbocycle Synthesis by Cobalt-Mediated [3+2+2] Alkyl/Alkyne Cycloaddition Reactions and Novel [5+2] Cyclopentadienyl/Alkyne Ring Expansions" *Ph.D. Dissertation*, University of Alberta, **1999**.
- 192 (a) Koch, W.; Holthausen, M. C. *A Chemist's Guide to Density Functional Theory*, Wiley-VCH, **2000**. (b) Ziegler, T. *Can. J. Chem.* **1995**, *73*, 743-761. (c) Ziegler, T. *Chem. Rev.* **1991**, *91*, 651-667.
- 193 Hohenberg, P.; Kohn, W. *Phys. Rev.* **1964**, *136*, B864-B871.
- 194 Kohn, W.; Sham, L. J. *Phys. Rev.* **1965**, *140*, A1133-A1138.
- 195 (a) Becke, A. D. *Phys. Rev. A* **1988**, *38*, 3098-3100. (b) Perdew, J. P. *Phys. Rev. B* **1986**, *33*, 8822-8824.
- 196 (a) Lee, C.; Yang, W.; Parr, R. G. *Phys. Rev. B* **1988**, *37*, 785-789. (b) Becke, A. D. *J. Chem. Phys.* **1993**, *98*, 1372-1377. (c) Becke, A. D. *J. Chem. Phys.* **1993**, *98*, 5648-5652. (d) Note, for the purpose of this work, we will use the standard B3LYP notation, however the functional "b3-lyp" as implemented in *Turbomole* is not identical with the Gaussian "B3LYP" functional.
- 197 (a) Ahlrichs, R.; Bär, M.; Häser, M.; Horn, H.; Kölmel, C. *Chem. Phys. Lett.* **1989**, *162*, 165-169. (b) Treutler, O.; Ahlrichs, R. *J. Chem. Phys.* **1995**, *102*, 346. (c) Arnim, M. A.; Ahlrichs, R. *J. Comput. Chem.* **1998**, *19*, 1746-1757. (d) Ahlrichs, R.; Bär, M.; Baron, H.-P.; Bauernschmitt, R.; Böcker, S.; Ehrig, M.; Eichkorn, K.; Elliott, S.; Furche, F.; Haase, F.; Häser, M.; Hättig, C.; Horn, H.; Huber, C.; Huniar, U.; Kattannek, M.; Köhn, A.; Kölmel, C.; Kollwitz, M.; May, K.; Ochsenfeld, C.; Ohm, H.; Schäfer, A.; Schneider, U.; Treutler, O.; Tsereteli, K.; Unterreiner, B.; Von Arnim, M.; Weigend, F.; Weis, P.; Weiss, H. *Turbomole* Version 5; Theoretical Chemistry Group, University of Karlsruhe, **2002**.
- 198 Schäfer, A.; Horn, H.; Ahlrichs, R. *J. Chem. Phys.* **1992**, *97*, 2571-2577.
- 199 Schäfer, A.; Huber, C.; Ahlrichs, R. *J. Chem. Phys.* **1994**, *100*, 5829-5835.
- 200 Weigend, F.; Furche, F.; Ahlrichs, R. *J. Chem. Phys.* **2003**, *119*, 12753-12762.
- 201 Klamt, A.; Schüürmann, G. *J. Chem. Soc., Perkin Trans. 2* **1993**, 799-805.
- 202 (a) Tobisch, S.; Ziegler, T. *J. Am. Chem. Soc.* **2004**, *126*, 9059-9071. (b) Raucoles, R.; de Bruin, T.; Raybaud, P.; Adamo, C. *Organometallics* **2009**, *28*,

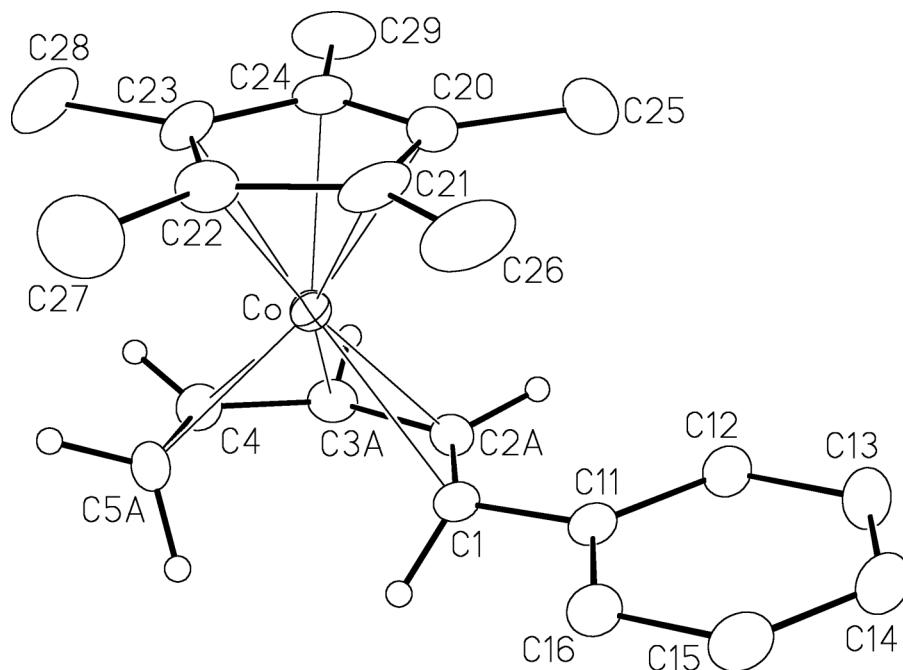
5358-5367.

- 203 For related work suggesting the entropy drops to nearly half the gas-phase value in polar solvents, see: Cooper, J.; Ziegler, T. *Inorg. Chem.* **2002**, *41*, 6614-6622.
- 204 We also explored the possibility of CH₂Cl₂ assisted $\eta^5 \rightarrow \eta^3$ isomerization. The TS energy for CH₂Cl₂ complexation is 27.89 kcal/mol with the product complex being only slightly lower energy at 26.25 kcal/mol. Given the high energies, this pathway is considered unlikely.
- 205 Beck, R.; Frey, M.; Camadanli, S.; Klein, H.-F. *Dalton Trans.* **2008**, 4981-4983.
- 206 (a) Brookhart, M.; Grant, B. E.; Lenges, C. P.; Prosenc, M. H.; White, P. S. *Angew. Chem. Int. Ed.* **2000**, *39*, 1676-1679. (b) Ingleson, M.; Fan, H.; Pink, M.; Tomaszewski, J.; Caulton, K. G. *J. Am. Chem. Soc.* **2006**, *128*, 1804-1805.
- 207 Note, this value is lower than the energy of INT6; prior to entropy correction, a barrier of 0.20 kcal/mol was computed, suggesting this correction does not adequately represent entropy at all points on the PES.
- 208 Gandon, V.; Agenet, N.; Vollhardt, K. P. C.; Malacria, M.; Aubert, C. *J. Am. Chem. Soc.* **2009**, *131*, 3007-3015.
- 209 (a) Fouqueau, A.; Mer, S.; Casida, M. E.; Daku, L. M. L.; Hauser, A.; Mineva, T.; Neese, F. *J. Chem. Phys.* **2004**, *120*, 9473-9486. (b) Fouqueau, A.; Casida, M. E.; Daku, L. M. L.; Hauser, A.; Neese, F. *J. Chem. Phys.* **2005**, *122*, 044110-1-04110-13.
- 210 Deeth, R. J.; Fey, N. *J. Comput. Chem.* **2004**, *25*, 1840-1848.
- 211 Reiher, M.; Salomon, O.; Hess, B. A. *Theor. Chem. Acc.* **2001**, *107*, 48-55.
- 212 For some of these intermediate points, closed-shell SCF convergence was problematic and an unrestricted, broken symmetry solution was lower in energy. However, the stationary points all preferred closed shell descriptions.
- 213 Kirk, A. D.; Stryker, J. M. *Unpublished results.*
- 214 Ammal, S. C.; Nakamura, E.-I.; Stryker, J. M. *Unpublished results.*
- 215 (a) Glueck, D. S.; Wu, J.; Hollarnder, F. J.; Bergman, R. G. *J. Am. Chem. Soc.* **1991**, *113*, 2041-2054. (b) Glueck, D. S.; Winslow, L. J. N.; Bergman, R. G. *Organometallics* **1991**, *10*, 1462-1479. (c) Bergman, R. G. *Polyhedron* **1995**, *14*, 3227-3237. (d) Martín-Matute, B.; Åberg, J. B.; Edin, M.; Bäckvall, J.-E. *Chem. Eur. J.* **2007**, *13*, 6063-6072.

- 216 Cibura, K. *Ph.D. Dissertation*, Max-Planck-Institut für Kohlenforschung, **1985**.
- 217 For lead references, see: (a) Peters, J. C.; Feldman, J. D.; Tilley, T. D. *J. Am. Chem. Soc.* **1999**, *121*, 9871-9872. (b) Barney, A. A.; Heyduk, A. F.; Nocera, D. G. *Chem. Commun.* **1999**, 2379-2380. (c) Shapiro, I. R.; Jenkins, D. M.; Thomas, J. C.; Day, M. W.; Peters, J. C. *Chem. Commun.* **2001**, 2152-2153. (d) Jenkins, D. M.; Betley, T. A.; Peters, J. C. *J. Am. Chem. Soc.* **2002**, *124*, 11238-11239. (e) Betley, T. A.; Peters, J. C. *Inorg. Chem.* **2003**, *42*, 5074-5084. (f) Peters, J. C.; Thomas, J. C.; Dupont, J. A.; Riordan, C. G. *Inorg. Synth.* **2004**, *34*, 8-14.
- 218 Karsch, H. H.; Appelt, A. *Z. Naturforsch. Teil B* **1983**, *38B*, 1399-1405.
- 219 Thomas, J. C.; Peters, J. C. *Inorg. Chem.* **2003**, *42*, 5055-5073.
- 220 (a) Karsch, H. H.; Appelt, A.; Müller, G. *J. Chem. Soc., Chem. Commun.* **1984**, 1415-1416. (b) Karsch, H. H.; Appelt, A.; Köhler, F. H.; Müller, G. *Organometallics* **1985**, *4*, 231-238. (c) Karsch, H. H.; Appelt, A.; Müller, G. *Organometallics* **1985**, *4*, 1624-1632. (d) Karsch, H. H.; Appelt, A.; Riede, J.; Müller, G. *Organometallics* **1987**, *6*, 316-323.
- 221 Mente, D. C.; Mills, J. L. *Inorg. Chem.* **1975**, *14*, 1862-1865.
- 222 Cairncross, A.; Sheppard, W. A.; Wonchoba, E. *Org. Synth.* **1979**, *59*, 122-129.
- 223 Sundararaman, A.; Jäkle, F. *J. Organomet. Chem.* **2003**, *681*, 134-142.
- 224 Nicholls, J. C.; Spencer, J. L. *Inorg. Synth.* **1990**, *28*, 278.
- 225 Endeshaw, M.; Stryker, J. M. *Unpublished results*.

Appendix

Crystallographic Information for Complex **297b**. For the full structure report see reference no. 142.



Perspective view of the $[(\eta^5\text{-C}_5\text{Me}_5)\text{Co}(\eta^5\text{-1-phenylpenta-2,4-dien-1-yl})]^+$ complex ion showing the atom labelling scheme. Non-hydrogen atoms are represented by Gaussian ellipsoids at the 20% probability level. Hydrogen atoms of the penta-2,4-dien-1-yl unit are shown with arbitrarily small thermal parameters; phenyl and pentamethylcyclopentadienyl hydrogens are not shown.

Crystallographic Experimental Details

A. Crystal Data

formula	$\text{C}_{21}\text{H}_{26}\text{BCoF}_4$
formula weight	424.16
crystal dimensions (mm)	$0.75 \times 0.39 \times 0.24$
crystal system	monoclinic
space group	$P2_1/c$ (No. 14)
unit cell parameters ^a	
<i>a</i> (Å)	7.4627 (7)
<i>b</i> (Å)	15.6724 (14)
<i>c</i> (Å)	16.9431 (15)
β (deg)	92.6467 (12)
<i>V</i> (Å ³)	1979.5 (3)
<i>Z</i>	4

ρ_{calcd} (g cm ⁻³)	1.423
μ (mm ⁻¹)	0.905

B. Data Collection and Refinement Conditions

diffractometer	Bruker PLATFORM/SMART 1000 CCD ^b
radiation (λ [Å])	graphite-monochromated Mo K α (0.71073)
temperature (°C)	-80
scan type	ω scans (0.4°) (10 s exposures)
data collection 2θ limit (deg)	52.82
total data collected	12112 ($-8 \leq h \leq 9, -19 \leq k \leq 19, -21 \leq l \leq 21$)
independent reflections	4052 ($R_{\text{int}} = 0.0178$)
number of observed reflections (<i>NO</i>)	3411 [$F_o^2 \geq 2\sigma(F_o^2)$]
structure solution method	Patterson search/structure expansion (<i>DIRDIF-99</i> ^c)
refinement method	full-matrix least-squares on F^2 (<i>SHELXL-93</i> ^d)
absorption correction method	multi-scan (<i>SADABS</i>)
range of transmission factors	0.8120–0.5500
data/restraints/parameters	4052 [$F_o^2 \geq -3\sigma(F_o^2)$] / 10 ^e / 292
goodness-of-fit (S) ^f	1.049 [$F_o^2 \geq -3\sigma(F_o^2)$]
final R indices ^g	
R_1 [$F_o^2 \geq 2\sigma(F_o^2)$]	0.0534
wR_2 [$F_o^2 \geq -3\sigma(F_o^2)$]	0.1601
largest difference peak and hole	0.668 and -0.463 e Å ⁻³

^aObtained from least-squares refinement of 6197 reflections with $4.82^\circ < 2\theta < 52.04^\circ$.

^bPrograms for diffractometer operation, data collection, data reduction and absorption correction were those supplied by Bruker.

^cBeurskens, P. T.; Beurskens, G.; de Gelder, R.; Garcia-Granda, S.; Israel, R.; Gould, R. O.; Smits, J. M. M. (1999). The *DIRDIF-99* program system. Crystallography Laboratory, University of Nijmegen, The Netherlands.

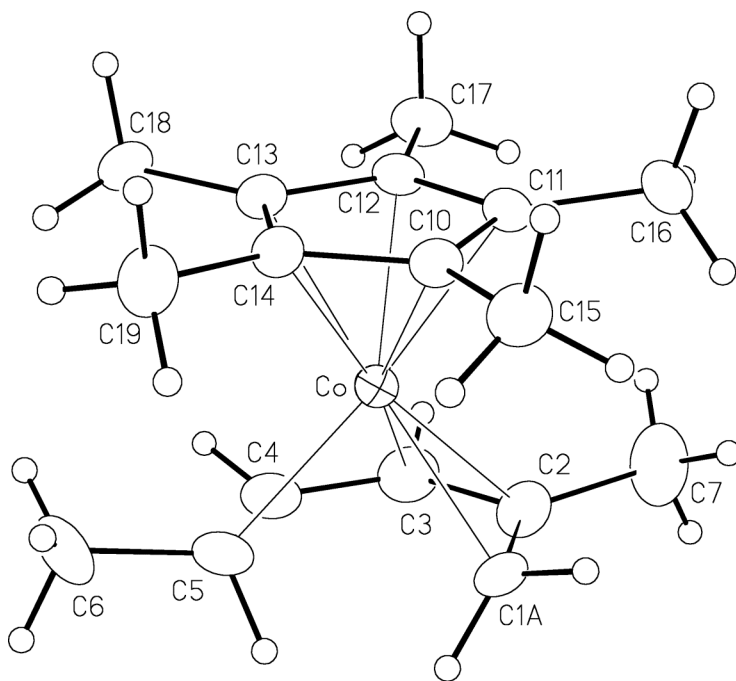
^dSheldrick, G. M. *SHELXL-93*. Program for crystal structure determination. University of Göttingen, Germany, 1993.

^eThe F–B and F…F distances within the minor (35%) conformer of the disordered tetrafluoroborate ion were given fixed idealized values: $d(\text{F1B–B1B}) = d(\text{F2B–B1B}) = d(\text{F3B–B1B}) = d(\text{F4B–B1B}) = 1.35 \text{ \AA}$; $d(\text{F1B}\cdots\text{F2B}) = d(\text{F1B}\cdots\text{F3B}) = d(\text{F1B}\cdots\text{F4B}) = d(\text{F2B}\cdots\text{F3B}) = d(\text{F2B}\cdots\text{F4B}) = d(\text{F3B}\cdots\text{F4B}) = 2.20 \text{ \AA}$.

^f $S = [\sum w(F_o^2 - F_c^2)^2 / (n - p)]^{1/2}$ (n = number of data; p = number of parameters varied; $w = [\sigma^2(F_o^2) + (0.0959P)^2 + 1.8344P]^{-1}$ where $P = [\text{Max}(F_o^2, 0) + 2F_c^2]/3$).

^g $R_1 = \sum ||F_o| - |F_c|| / \sum |F_o|$; $wR_2 = [\sum w(F_o^2 - F_c^2)^2 / \sum w(F_o^4)]^{1/2}$.

Crystallographic Information for Complex **297i**. For the full structure report see reference no. 142.



Perspective view of the $[(\eta^5\text{-C}_5\text{Me}_5)\text{Co}(\eta^5\text{-2-methylhexa-2,4-dien-1-yl})]^+$ complex ion showing the atom labelling scheme. Non-hydrogen atoms are represented by Gaussian ellipsoids at the 20% probability level. Hydrogen atoms are shown with arbitrarily small thermal parameters.

Crystallographic Experimental Details

A. Crystal Data

formula	$\text{C}_{17}\text{H}_{26}\text{BCoF}_4$
formula weight	376.12
crystal dimensions (mm)	$0.48 \times 0.19 \times 0.17$
crystal system	monoclinic
space group	$P2_1/n$ (an alternate setting of $P2_1/c$ [No. 14])
unit cell parameters ^a	
<i>a</i> (Å)	7.6610 (5)
<i>b</i> (Å)	15.8621 (11)
<i>c</i> (Å)	14.4805 (10)
β (deg)	91.9520 (10)
<i>V</i> (Å ³)	1758.6 (2)
<i>Z</i>	4
ρ_{calcd} (g cm ⁻³)	1.421
μ (mm ⁻¹)	1.009

B. Data Collection and Refinement Conditions

diffractometer Bruker	PLATFORM/SMART 1000 CCD ^b
radiation (λ [Å])	graphite-monochromated Mo K α (0.71073)
temperature (°C)	-80
scan type	ω scans (0.3°) (20 s exposures)
data collection 2θ limit (deg)	55.00
total data collected	15178 ($-9 \leq h \leq 9$, $-20 \leq k \leq 20$, $-18 \leq l \leq 18$)
independent reflections	4023 ($R_{\text{int}} = 0.0272$)
number of observed reflections (NO)	3296 [$F_o^2 \geq 2\sigma(F_o^2)$]
structure solution method	Patterson search/structure expansion (<i>DIRDIF-99</i> ^c)
refinement method	full-matrix least-squares on F^2 (<i>SHELXL-97</i> ^d)
absorption correction method	multi-scan (<i>SADABS</i>)
range of transmission factors	0.8472–0.6431
data/restraints/parameters	4023 [$F_o^2 \geq -3\sigma(F_o^2)$] / 10^e / 264
goodness-of-fit (S) ^f	1.050 [$F_o^2 \geq -3\sigma(F_o^2)$]
final R indices ^g	
R_1 [$F_o^2 \geq 2\sigma(F_o^2)$]	0.0440
wR_2 [$F_o^2 \geq -3\sigma(F_o^2)$]	0.1162
largest difference peak and hole	0.604 and -0.221 e Å ⁻³

^aObtained from least-squares refinement of 7700 reflections with $5.14^\circ < 2\theta < 54.44^\circ$.

^bPrograms for diffractometer operation, data collection, data reduction and absorption correction were those supplied by Bruker.

^cBeurskens, P. T.; Beurskens, G.; de Gelder, R.; Garcia-Granda, S.; Israel, R.; Gould, R. O.; Smits, J. M. M. (1999). The *DIRDIF-99* program system. Crystallography Laboratory, University of Nijmegen, The Netherlands.

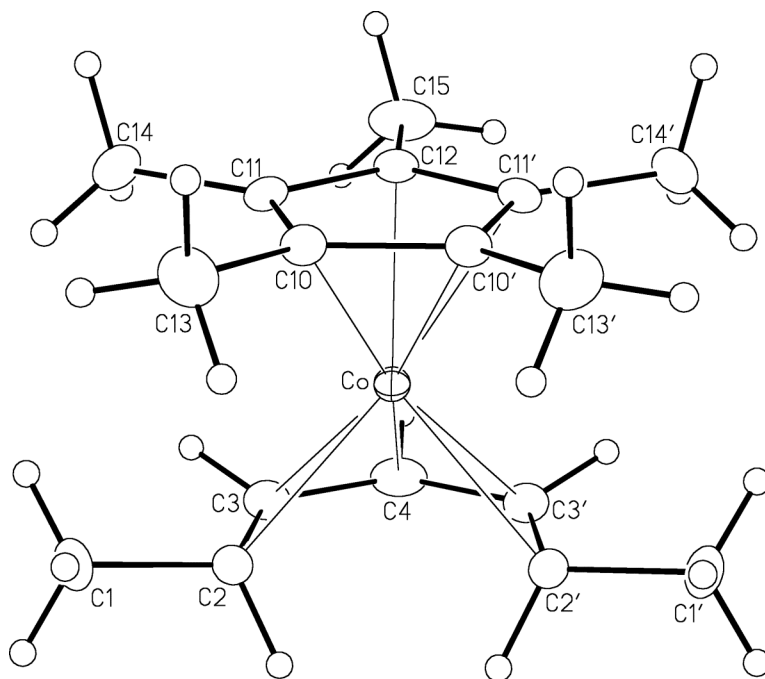
^dSheldrick, G. M. *SHELXL-97*. Program for crystal structure determination. University of Göttingen, Germany, 1997.

^eAnalogous distances within two conformers of the disordered tetrafluoroborate were constrained to be equal (within 0.001 Å) during refinement: $d(\text{F1A-B1A}) = d(\text{F1B-B1B})$; $d(\text{F2A-B1A}) = d(\text{F2B-B1B})$; $d(\text{F3A-B1A}) = d(\text{F3B-B1B})$; $d(\text{F4A-B1A}) = d(\text{F4B-B1B})$; $d(\text{F1A}\cdots\text{F2A}) = d(\text{F1B}\cdots\text{F2B})$; $d(\text{F1A}\cdots\text{F3A}) = d(\text{F1B}\cdots\text{F3B})$; $d(\text{F1A}\cdots\text{F4A}) = d(\text{F1B}\cdots\text{F4B})$; $d(\text{F2A}\cdots\text{F3A}) = d(\text{F2B}\cdots\text{F3B})$; $d(\text{F2A}\cdots\text{F4A}) = d(\text{F2B}\cdots\text{F4B})$; $d(\text{F3A}\cdots\text{F4A}) = d(\text{F3B}\cdots\text{F4B})$.

^f $S = [\sum w(F_o^2 - F_c^2)^2 / (n - p)]^{1/2}$ (n = number of data; p = number of parameters varied; $w = [\sigma^2(F_o^2) + (0.0661P)^2 + 0.6264P]^{-1}$ where $P = [\text{Max}(F_o^2, 0) + 2F_c^2]/3$).

^g $R_1 = \sum ||F_o| - |F_c|| / \sum |F_o|$; $wR_2 = [\sum w(F_o^2 - F_c^2)^2 / \sum w(F_o^4)]^{1/2}$.

Crystallographic Information for Complex **297j**. For the full structure report see reference no. 142.



Perspective view of the $[\text{Cp}^*\text{Co}(\text{hepta-3,5-dienyl-2-yl})]^+$ ion showing the atom labelling scheme. Primed atoms are related to the unprimed ones by the crystallographic mirror plane located at $(0, y, z)$. Non-hydrogen atoms are represented by Gaussian ellipsoids at the 20% probability level. Hydrogen atoms are shown with arbitrarily small thermal parameters.

Crystallographic Experimental Details

A. Crystal Data

formula	$\text{C}_{17}\text{H}_{26}\text{BCoF}_4$
formula weight	376.12
crystal dimensions (mm)	$0.38 \times 0.22 \times 0.12$
crystal system	orthorhombic
space group	$Cmc2_1$ (No. 36)
unit cell parameters ^a	
<i>a</i> (Å)	9.1007 (6)
<i>b</i> (Å)	14.7533 (10)
<i>c</i> (Å)	13.0941 (9)
<i>V</i> (Å ³)	1758.1 (2)
<i>Z</i>	4
ρ_{calcd} (g cm ⁻³)	1.421
μ (mm ⁻¹)	1.009

B. Data Collection and Refinement Conditions

diffractometer	Bruker PLATFORM/SMART 1000 CCD ^b
radiation (λ [Å])	graphite-monochromated Mo K α (0.71073)
temperature (°C)	-80
scan type	ω scans (0.3°) (20 s exposures)
data collection 2θ limit (deg)	54.96
total data collected	7529 ($-11 \leq h \leq 11$, $-19 \leq k \leq 19$, $-17 \leq l \leq 16$)
independent reflections	2134 ($R_{\text{int}} = 0.0232$)
number of observed reflections (NO)	2081 [$F_o^2 \geq 2\sigma(F_o^2)$]
structure solution method	direct methods (<i>SHELXS-97</i> ^c)
refinement method	full-matrix least-squares on F^2 (<i>SHELXL-97</i> ^d)
absorption correction method	multi-scan (<i>SADABS</i>)
range of transmission factors	0.8885–0.7004
data/restraints/parameters	2134 [$F_o^2 \geq -3\sigma(F_o^2)$] / 0 / 119
Flack absolute structure parameter ^e	-0.005(19)
goodness-of-fit (S) ^f	1.112 [$F_o^2 \geq -3\sigma(F_o^2)$]
final R indices ^g	
R_1 [$F_o^2 \geq 2\sigma(F_o^2)$]	0.0312
wR_2 [$F_o^2 \geq -3\sigma(F_o^2)$]	0.0781
largest difference peak and hole	0.473 and -0.234 e Å ⁻³

^aObtained from least-squares refinement of 6037 reflections with $5.26^\circ < 2\theta < 54.78^\circ$.

^bPrograms for diffractometer operation, data collection, data reduction and absorption correction were those supplied by Bruker.

^cSheldrick, G. M. *Acta Crystallogr.* **1990**, *A46*, 467–473.

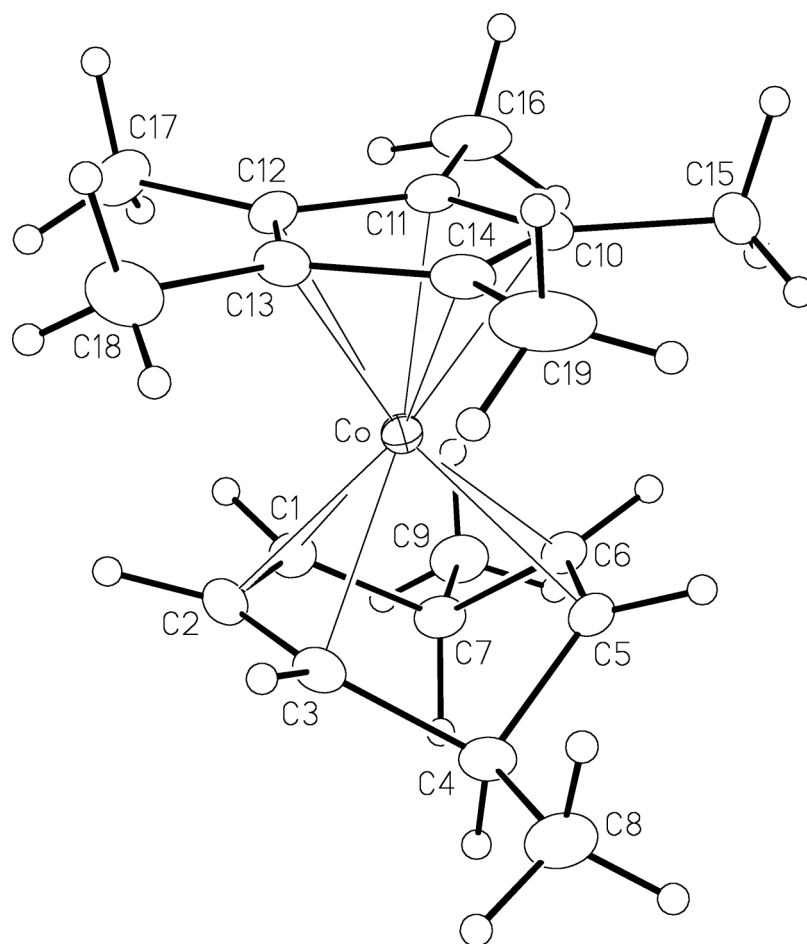
^dSheldrick, G. M. *SHELXL-97*. Program for crystal structure determination. University of Göttingen, Germany, 1997.

^eFlack, H. D. *Acta Crystallogr.* **1983**, *A39*, 876–881; Flack, H. D.; Bernardinelli, G. *Acta Crystallogr.* **1999**, *A55*, 908–915; Flack, H. D.; Bernardinelli, G. *J. Appl. Cryst.* **2000**, *33*, 1143–1148. The Flack parameter will refine to a value near zero if the structure is in the correct configuration and will refine to a value near one for the inverted configuration.

^f $S = [\sum w(F_o^2 - F_c^2)^2 / (n - p)]^{1/2}$ (n = number of data; p = number of parameters varied; $w = [\sigma^2(F_o^2) + (0.0484P)^2 + 0.4223P]^{-1}$ where $P = [\text{Max}(F_o^2, 0) + 2F_c^2] / 3$).

^g $R_1 = \sum |F_o| - |F_c| / \sum |F_o|$; $wR_2 = [\sum w(F_o^2 - F_c^2)^2 / \sum w(F_o^4)]^{1/2}$.

Crystallographic Information for Complex **336d**. University of Alberta Department of Chemistry Structure Determination Laboratory Report #JMS0743.



Perspective view of the $[(\eta^5\text{-C}_5\text{Me}_5)\text{Co}(\eta^3, \eta^2\text{-4,7-dimethylcyclohepta-2,5-dien-1-yl})]^+$ complex ion showing the atom labelling scheme. Non-hydrogen atoms are represented by Gaussian ellipsoids at the 20% probability level. Hydrogen atoms are shown with arbitrarily small thermal parameters.

Crystallographic Experimental Details

A. Crystal Data

formula	$\text{C}_{19}\text{H}_{28}\text{BCoF}_4$
formula weight	402.15
crystal dimensions (mm)	$0.53 \times 0.49 \times 0.38$
crystal system	monoclinic
space group	$P2_1/n$ (an alternate setting of $P2_1/c$ [No. 14])
unit cell parameters ^a	
<i>a</i> (Å)	8.5841 (8)

b (Å)	17.6785 (17)
c (Å)	12.6769 (12)
β (deg)	99.8617 (10)
V (Å ³)	1895.3 (3)
Z	4
ρ_{calcd} (g cm ⁻³)	1.409
μ (mm ⁻¹)	0.941

B. Data Collection and Refinement Conditions

diffractometer	Bruker PLATFORM/SMART 1000 CCD ^b
radiation (λ [Å])	graphite-monochromated Mo K α (0.71073)
temperature (°C)	-80
scan type	ω scans (0.4°) (10 s exposures)
data collection 2θ limit (deg)	54.96
total data collected	11459 ($-11 \leq h \leq 11$, $-15 \leq k \leq 22$, $-16 \leq l \leq 16$)
independent reflections	4315 ($R_{\text{int}} = 0.0198$)
number of observed reflections (NO)	3650 [$F_o^2 \geq 2\sigma(F_o^2)$]
structure solution method	Patterson search/structure expansion (<i>DIRDIF-99</i> ^c)
refinement method	full-matrix least-squares on F^2 (<i>SHELXL-97</i> ^d)
absorption correction method	multi-scan (<i>SADABS</i>)
range of transmission factors	0.7163–0.6354
data/restraints/parameters	4315 [$F_o^2 \geq -3\sigma(F_o^2)$] / 0 / 271
goodness-of-fit (S) ^e	1.044 [$F_o^2 \geq -3\sigma(F_o^2)$]
final R indices ^f	
R_1 [$F_o^2 \geq 2\sigma(F_o^2)$]	0.0409
wR_2 [$F_o^2 \geq -3\sigma(F_o^2)$]	0.1122
largest difference peak and hole	0.643 and -0.305 e Å ⁻³

^aObtained from least-squares refinement of 6938 reflections with $4.60^\circ < 2\theta < 54.90^\circ$.

^bPrograms for diffractometer operation, data collection, data reduction and absorption correction were those supplied by Bruker.

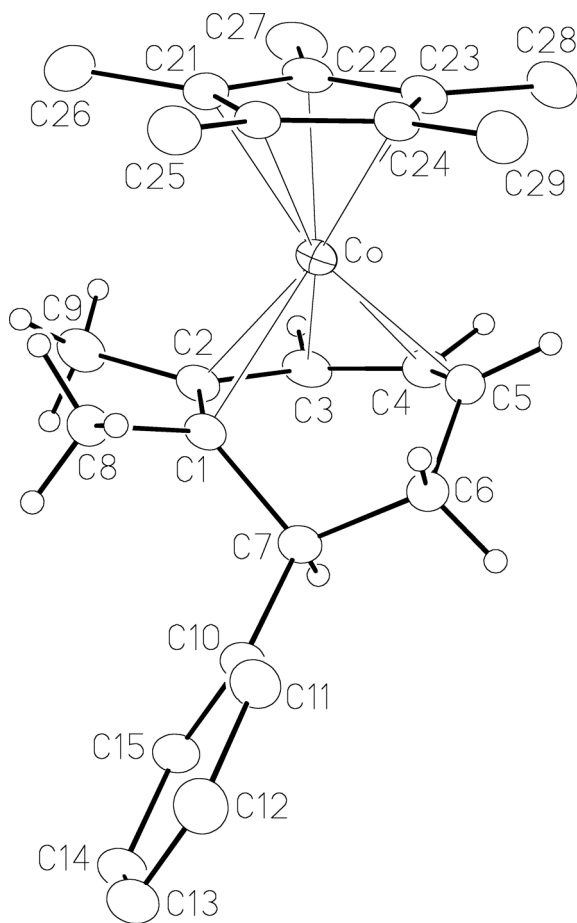
^cBeurskens, P. T.; Beurskens, G.; de Gelder, R.; Garcia-Granda, S.; Israel, R.; Gould, R. O.; Smits, J. M. M. (1999). The *DIRDIF-99* program system. Crystallography Laboratory, University of Nijmegen, The Netherlands.

^dSheldrick, G. M. *SHELXL-97*. Program for crystal structure determination. University of Göttingen, Germany, 1997.

^e $S = [\sum w(F_o^2 - F_c^2)^2 / (n - p)]^{1/2}$ (n = number of data; p = number of parameters varied; $w = [\sigma^2(F_o^2) + (0.0668P)^2 + 0.7740P]^{-1}$ where $P = [\text{Max}(F_o^2, 0) + 2F_c^2]/3$).

^f $R_1 = \sum ||F_o| - |F_c|| / \sum |F_o|$; $wR_2 = [\sum w(F_o^2 - F_c^2)^2 / \sum w(F_o^4)]^{1/2}$.

Crystallographic Information for Complex **344a**. University of Alberta Department of Chemistry Structure Determination Laboratory Report #JMS0617.



Perspective view of the $[(\eta^5\text{-C}_5\text{Me}_5)\text{Co}(\eta^5\text{-1,2-dimethyl-7-phenylcyclohepta-2,4-dien-1-yl})]^+$ complex ion showing the atom labelling scheme. Non-hydrogen atoms are represented by Gaussian ellipsoids at the 20% probability level. Hydrogen atoms are shown with arbitrarily small thermal parameters except for those of the phenyl and pentamethylcyclopentadienyl groups, which are not shown.

Crystallographic Experimental Details

A. Crystal Data

formula	$\text{C}_{25}\text{H}_{32}\text{BCoF}_4$
formula weight	478.25
crystal dimensions (mm)	$0.47 \times 0.33 \times 0.29$
crystal system	monoclinic
space group	$P2_1/n$ (an alternate setting of $P2_1/c$ [No. 14])
unit cell parameters ^a	
<i>a</i> (Å)	12.9507 (9)

b (Å)	12.9074 (9)
c (Å)	13.8127 (10)
β (deg)	100.3505 (11)
V (Å ³)	2271.4 (3)
Z	4
ρ_{calcd} (g cm ⁻³)	1.399
μ (mm ⁻¹)	0.798

B. Data Collection and Refinement Conditions

diffractometer	Bruker PLATFORM/SMART 1000 CCD ^b
radiation (λ [Å])	graphite-monochromated Mo K α (0.71073)
temperature (°C)	-80
scan type	ω scans (0.3°) (15 s exposures)
data collection 2θ limit (deg)	52.74
total data collected	17635 ($-16 \leq h \leq 16$, $-16 \leq k \leq 16$, $-17 \leq l \leq 17$)
independent reflections	4645 ($R_{\text{int}} = 0.0172$)
number of observed reflections (NO)	3952 [$F_o^2 \geq 2\sigma(F_o^2)$]
structure solution method	direct methods (<i>SHELXS-86</i> ^c)
refinement method	full-matrix least-squares on F^2 (<i>SHELXL-93</i> ^d)
absorption correction method	multi-scan (<i>SADABS</i>)
range of transmission factors	0.8016–0.7055
data/restraints/parameters	4645 [$F_o^2 \geq -3\sigma(F_o^2)$] / 0 / 314
goodness-of-fit (S) ^e	1.037 [$F_o^2 \geq -3\sigma(F_o^2)$]
final R indices ^f	
R_1 [$F_o^2 \geq 2\sigma(F_o^2)$]	0.0479
wR_2 [$F_o^2 \geq -3\sigma(F_o^2)$]	0.1374
largest difference peak and hole	1.797 and -0.352 e Å ⁻³

^aObtained from least-squares refinement of 5103 reflections with $4.36^\circ < 2\theta < 52.74^\circ$.

^bPrograms for diffractometer operation, data collection, data reduction and absorption correction were those supplied by Bruker.

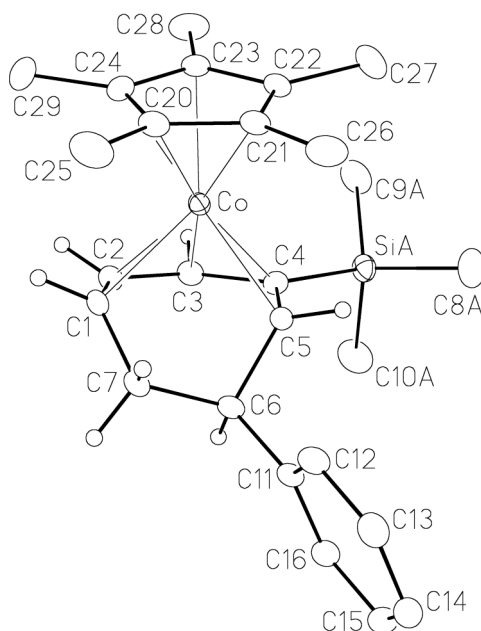
^cSheldrick, G. M. *Acta Crystallogr.* **1990**, *A46*, 467–473.

^dSheldrick, G. M. *SHELXL-93*. Program for crystal structure determination. University of Göttingen, Germany, 1993.

^e $S = [\sum w(F_o^2 - F_c^2)^2 / (n - p)]^{1/2}$ (n = number of data; p = number of parameters varied; $w = [\sigma^2(F_o^2) + (0.0791P)^2 + 1.6921P]^{-1}$ where $P = [\text{Max}(F_o^2, 0) + 2F_c^2]/3$).

^f $R_1 = \sum ||F_o| - |F_c|| / \sum |F_o|$; $wR_2 = [\sum w(F_o^2 - F_c^2)^2 / \sum w(F_o^4)]^{1/2}$.

Crystallographic Information for Complex **345**. For the full structure report see reference no. 123.



Perspective view of the $[(\eta^5\text{-C}_5\text{Me}_5)\text{Co}(\eta^5\text{-6-phenyl-4-trimethylsilylcyclohepta-2,4-dien-1-yl})]^+$ complex ion showing the atom labelling scheme. Non-hydrogen atoms are represented by Gaussian ellipsoids at the 20% probability level. Hydrogen atoms of the cyclohepta-2,4-dien-1-yl ring are shown with arbitrarily small thermal parameters; all other hydrogens are not shown.

Crystallographic Experimental Details

A. Crystal Data

formula	$\text{C}_{26}\text{H}_{36}\text{BCoF}_4\text{Si}$
formula weight	522.38
crystal dimensions (mm)	$0.62 \times 0.36 \times 0.34$
crystal system	orthorhombic
space group	$P2_12_12_1$ (No. 19)
unit cell parameters ^a	
<i>a</i> (Å)	9.8585 (10)
<i>b</i> (Å)	11.2388 (11)
<i>c</i> (Å)	23.172 (2)
<i>V</i> (Å ³)	2567.4 (4)
<i>Z</i>	4
ρ_{calcd} (g cm ⁻³)	1.351
μ (mm ⁻¹)	0.756

B. Data Collection and Refinement Conditions

diffractometer	Bruker PLATFORM/SMART 1000 CCD ^b
radiation (λ [Å])	graphite-monochromated Mo K α (0.71073)
temperature (°C)	-80
scan type	ω scans (0.3°) (20 s exposures)
data collection 2θ limit (deg)	52.80
total data collected	20531 ($-12 \leq h \leq 12$, $-14 \leq k \leq 14$, $-28 \leq l \leq 28$)
independent reflections	5264 ($R_{\text{int}} = 0.0150$)
number of observed reflections (NO)	5129 [$F_o^2 \geq 2\sigma(F_o^2)$]
structure solution method	Patterson search/structure expansion (<i>DIRDIF-99</i> ^c)
refinement method	full-matrix least-squares on F^2 (<i>SHELXL-93</i> ^d)
absorption correction method	multi-scan (<i>SADABS</i>)
range of transmission factors	0.7831–0.6514
data/restraints/parameters	5264 [$F_o^2 \geq -3\sigma(F_o^2)$] / 0 / 334
Flack absolute structure parameter ^e	0.538 (13)
goodness-of-fit (S) ^f	1.055 [$F_o^2 \geq -3\sigma(F_o^2)$]
final R indices ^g	
R_1 [$F_o^2 \geq 2\sigma(F_o^2)$]	0.0313
wR_2 [$F_o^2 \geq -3\sigma(F_o^2)$]	0.0884
largest difference peak and hole	0.649 and -0.390 e Å ⁻³

^aObtained from least-squares refinement of 6132 reflections with $5.42^\circ < 2\theta < 52.72^\circ$.

^bPrograms for diffractometer operation, data collection, data reduction and absorption correction were those supplied by Bruker.

^cBeurskens, P. T.; Beurskens, G.; de Gelder, R.; Garcia-Granda, S.; Israel, R.; Gould, R. O.; Smits, J. M. M. (1999). The *DIRDIF-99* program system. Crystallography Laboratory, University of Nijmegen, The Netherlands.

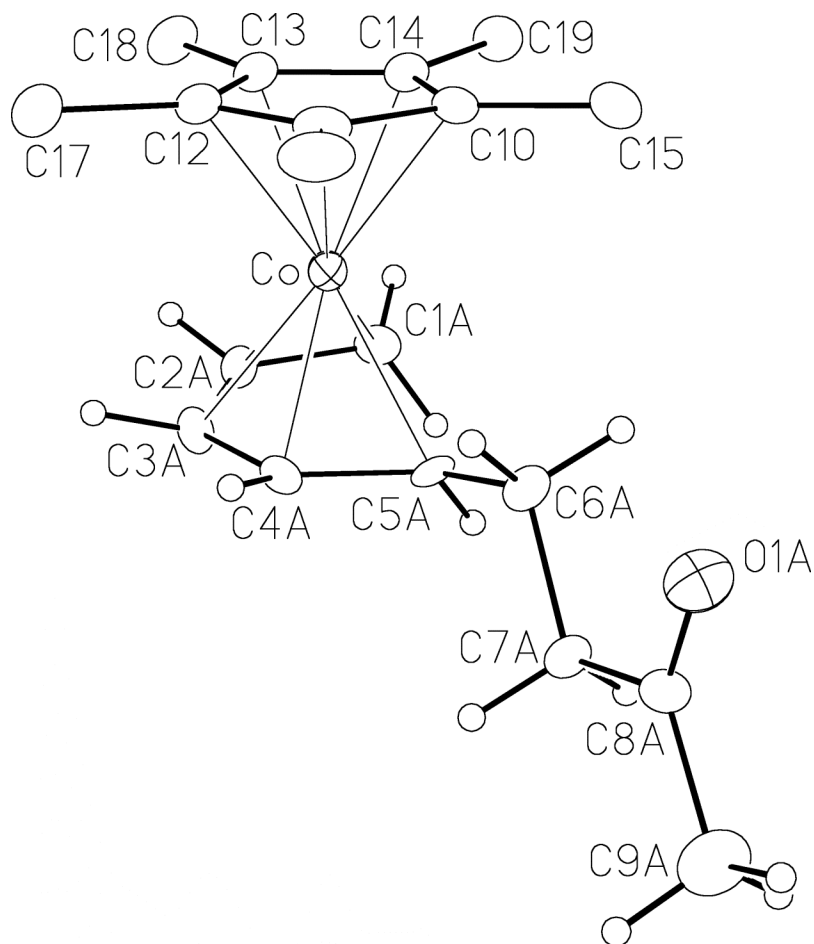
^dSheldrick, G. M. *SHELXL-93*. Program for crystal structure determination. University of Göttingen, Germany, 1993.

^eFlack, H. D. *Acta Crystallogr.* **1983**, *A39*, 876–881; Flack, H. D.; Bernardinelli, G. *Acta Crystallogr.* **1999**, *A55*, 908–915; Flack, H. D.; Bernardinelli, G. *J. Appl. Cryst.* **2000**, *33*, 1143–1148. The Flack parameter will refine to a value near zero if the structure is in the correct configuration and will refine to a value near one for the inverted configuration. The value observed herein is indicative of racemic twinning, and was accommodated during the refinement (using the *SHELXL-93* TWIN instruction [see reference *d*]).

^f $S = [\sum w(F_o^2 - F_c^2)^2 / (n - p)]^{1/2}$ (n = number of data; p = number of parameters varied; $w = [\sigma^2(F_o^2) + (0.0569P)^2 + 0.8796P]^{-1}$ where $P = [\text{Max}(F_o^2, 0) + 2F_c^2] / 3$).

^g $R_1 = \sum ||F_o| - |F_c|| / \sum |F_o|$; $wR_2 = [\sum w(F_o^2 - F_c^2)^2 / \sum w(F_o^4)]^{1/2}$.

Crystallographic Information for Complex **366**. University of Alberta Department of Chemistry Structure Determination Laboratory Report #JMS0561.



Perspective view of the $[(\eta^5\text{-C}_5\text{Me}_5)\text{Co}(\eta^5\text{-8-oxonona-2,4-dien-1-ide})]^+$ complex ion showing the atom labelling scheme. Non-hydrogen atoms are represented by Gaussian ellipsoids at the 20% probability level. Hydrogen atoms of the 8-oxonona-2,4-dien-1-ide ligand are shown with arbitrarily small thermal parameters, while hydrogens of the pentamethylcyclopentadienyl ligand are not shown.

Crystallographic Experimental Details

A. Crystal Data

formula	$\text{C}_{19}\text{H}_{28}\text{BCoF}_4\text{O}$
formula weight	418.15
crystal dimensions (mm)	$0.56 \times 0.21 \times 0.11$
crystal system	orthorhombic
space group	$Pna2_1$ (No. 33)
unit cell parameters ^a	
<i>a</i> (Å)	16.9258 (14)

b (Å)	14.2819 (12)
c (Å)	8.2379 (7)
V (Å ³)	1991.4 (3)
Z	4
ρ_{calcd} (g cm ⁻³)	1.395
μ (mm ⁻¹)	0.902

B. Data Collection and Refinement Conditions

diffractometer	Bruker PLATFORM/SMART 1000 CCD ^b
radiation (λ [Å])	graphite-monochromated Mo K α (0.71073)
temperature (°C)	-80
scan type	ω scans (0.3°) (20 s exposures)
data collection 2θ limit (deg)	52.84
total data collected	14440 ($-21 \leq h \leq 21$, $-17 \leq k \leq 17$, $-10 \leq l \leq 10$)
independent reflections	4107 ($R_{\text{int}} = 0.0364$)
number of observed reflections (NO)	3412 [$F_o^2 \geq 2\sigma(F_o^2)$]
structure solution method	direct methods (<i>SHELXS-86</i> ^c)
refinement method	full-matrix least-squares on F^2 (<i>SHELXL-93</i> ^d)
absorption correction method	multi-scan (<i>SADABS</i>)
range of transmission factors	0.9073–0.6320
data/restraints/parameters	4107 [$F_o^2 \geq -3\sigma(F_o^2)$] / 27 ^e / 333
Flack absolute structure parameter ^f	0.019 (18)
goodness-of-fit (S) ^g	1.051 [$F_o^2 \geq -3\sigma(F_o^2)$]
final R indices ^h	
R_1 [$F_o^2 \geq 2\sigma(F_o^2)$]	0.0363
wR_2 [$F_o^2 \geq -3\sigma(F_o^2)$]	0.0953
largest difference peak and hole	0.293 and -0.207 e Å ⁻³

^aObtained from least-squares refinement of 6040 reflections with $4.82^\circ < 2\theta < 51.54^\circ$.

^bPrograms for diffractometer operation, data collection, data reduction and absorption correction were those supplied by Bruker.

^cSheldrick, G. M. *Acta Crystallogr.* **1990**, *A46*, 467–473.

^dSheldrick, G. M. *SHELXL-93*. Program for crystal structure determination. University of Göttingen, Germany, 1993.

^ePairs of analogous Co–C distances involving analogous carbon positions of the disordered pentadienyl moiety were constrained to be equal (within 0.001 Å) during refinement: $d(\text{Co}-\text{C1A}) = d(\text{Co}-\text{C1B})$; $d(\text{Co}-\text{C2A}) = d(\text{Co}-\text{C2B})$; $d(\text{Co}-\text{C3A}) = d(\text{Co}-\text{C3B})$; $d(\text{Co}-\text{C4A}) = d(\text{Co}-\text{C4B})$; $d(\text{Co}-\text{C5A}) = d(\text{Co}-\text{C5B})$. Analogous bond lengths and 1,3-distances within the 8-oxonona-2,4-dien-1-ide ligand were also constrained to be equal: $d(\text{O1A}-\text{C8A}) = d(\text{O1B}-\text{C8B})$; $d(\text{C1A}-\text{C2A}) = d(\text{C1B}-\text{C2B})$; $d(\text{C2A}-\text{C3A}) = d(\text{C2B}-\text{C3B})$; $d(\text{C3A}-\text{C4A}) = d(\text{C3B}-\text{C4B})$; $d(\text{C4A}-\text{C5A}) = d(\text{C4B}-\text{C5B})$.

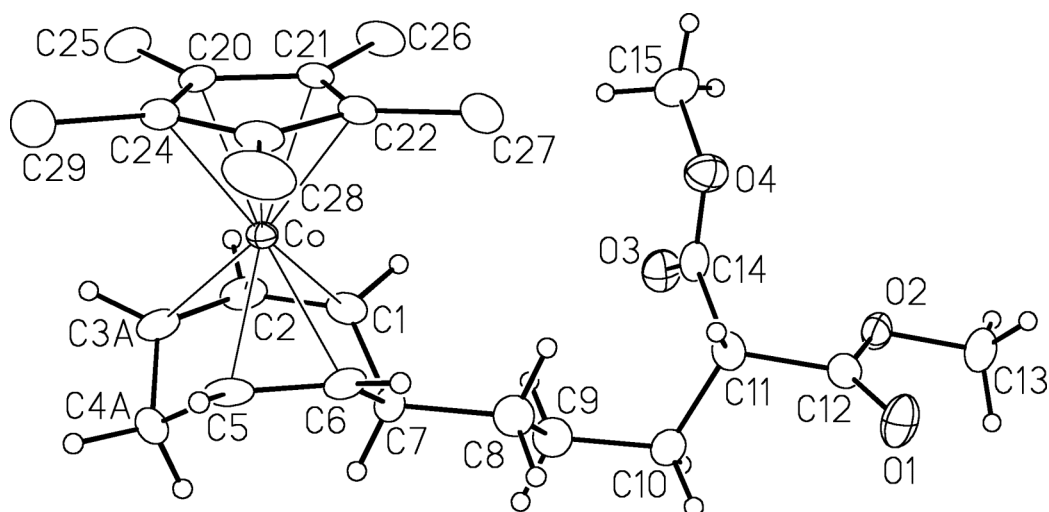
d(C5B); d(C5A–C6A) = d(C5B–C6B); d(C6A–C7A) = d(C6B–C7B); d(C7A–C8A) = d(C7B–C8B); d(C8A–C9A) = d(C8B–C9B); d(O1A···C7A) = d(O1B···C7B); d(O1A···C9A) = d(O1B···C9B); d(C1A···C3A) = d(C1B···C3B); d(C2A···C4A) = d(C2B···C4B); d(C3A···C5A) = d(C3B···C5B); d(C4A···C6A) = d(C4B···C6B); d(C5A···C7A) = d(C5B···C7B); d(C6A···C8A) = d(C6B···C8B); d(C7A···C9A) = d(C7B···C9B).

Flack, H. D. *Acta Crystallogr.* **1983**, *A39*, 876–881; Flack, H. D.; Bernardinelli, G. *Acta Crystallogr.* **1999**, *A55*, 908–915; Flack, H. D.; Bernardinelli, G. *J. Appl. Cryst.* **2000**, *33*, 1143–1148. The Flack parameter will refine to a value near zero if the structure is in the correct configuration and will refine to a value near one for the inverted configuration.

$$gS = [\sum w(F_o^2 - F_c^2)^2 / (n - p)]^{1/2} \quad (n = \text{number of data}; p = \text{number of parameters varied}; w = [\sigma^2(F_o^2) + (0.0556P)^2 + 0.1387P]^{-1} \text{ where } P = [\text{Max}(F_o^2, 0) + 2F_c^2] / 3).$$

$$^hR_1 = \sum |F_o| - |F_c| / \sum |F_o|; wR_2 = [\sum w(F_o^2 - F_c^2)^2 / \sum w(F_o^4)]^{1/2}.$$

Crystallographic Information for Complex **367b**. University of Alberta Department of Chemistry Structure Determination Laboratory Report #JMS0553.



Perspective view of the $[(\eta^5\text{-C}_5\text{Me}_5)\text{Co}(\eta^3, \eta^2\text{-4-}\{4,4\text{-bis(methoxycarbonyl)-butyl}\}\text{cyclohepta-1,5-dien-3-yl})]^+$ complex ion showing the atom labelling scheme. Non-hydrogen atoms are represented by Gaussian ellipsoids at the 20% probability level. Hydrogen atoms are shown with arbitrarily small thermal parameters except for those of the pentamethylcyclopentadienyl group, which are not shown.

Crystallographic Experimental Details

A. Crystal Data

formula	$\text{C}_{25}\text{H}_{36}\text{BCoF}_4\text{O}_4$
formula weight	546.28
crystal dimensions (mm)	$0.60 \times 0.50 \times 0.04$
crystal system	monoclinic
space group	$P2_1/c$ (No. 14)
unit cell parameters ^a	
<i>a</i> (Å)	17.9718 (15)
<i>b</i> (Å)	8.2619 (7)
<i>c</i> (Å)	17.3504 (15)
β (deg)	98.0824 (15)
<i>V</i> (Å ³)	2550.6 (4)
<i>Z</i>	4
ρ_{calcd} (g cm ⁻³)	1.423
μ (mm ⁻¹)	0.731

B. Data Collection and Refinement Conditions

diffractometer	Bruker PLATFORM/SMART 1000 CCD ^b
radiation (λ [Å])	graphite-monochromated Mo $K\alpha$ (0.71073)

temperature (°C)	-80
scan type	ω scans (0.3°) (20 s exposures)
data collection 2θ limit (deg)	52.90
total data collected	19647 ($-22 \leq h \leq 22$, $-10 \leq k \leq 10$, $-21 \leq l \leq 21$)
independent reflections	5249 ($R_{\text{int}} = 0.0551$)
number of observed reflections (NO)	3858 [$F_o^2 \geq 2\sigma(F_o^2)$]
structure solution method	direct methods (<i>SHELXS-86</i> ^c)
refinement method	full-matrix least-squares on F^2 (<i>SHELXL-93</i> ^d)
absorption correction method	multi-scan (<i>SADABS</i>)
range of transmission factors	0.9713–0.6681
data/restraints/parameters	5249 [$F_o^2 \geq -3\sigma(F_o^2)$] / 0 / 356
goodness-of-fit (S) ^e	1.068 [$F_o^2 \geq -3\sigma(F_o^2)$]
final R indices ^f	
R_1 [$F_o^2 \geq 2\sigma(F_o^2)$]	0.0549
wR_2 [$F_o^2 \geq -3\sigma(F_o^2)$]	0.1584
largest difference peak and hole	1.095 and $-0.477 \text{ e } \text{Å}^{-3}$

^aObtained from least-squares refinement of 5774 reflections with $4.96^\circ < 2\theta < 51.80^\circ$.

^bPrograms for diffractometer operation, data collection, data reduction and absorption correction were those supplied by Bruker.

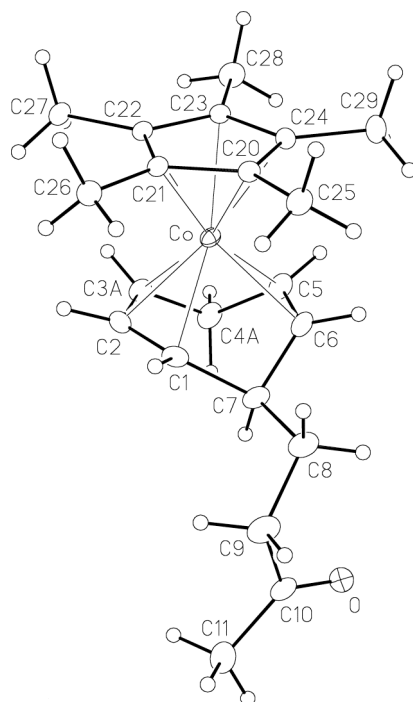
^cSheldrick, G. M. *Acta Crystallogr.* **1990**, *A46*, 467–473.

^dSheldrick, G. M. *SHELXL-93*. Program for crystal structure determination. University of Göttingen, Germany, 1993.

^e $S = [\sum w(F_o^2 - F_c^2)^2 / (n - p)]^{1/2}$ (n = number of data; p = number of parameters varied; $w = [\sigma^2(F_o^2) + (0.0820P)^2 + 1.9699P]^{-1}$ where $P = [\text{Max}(F_o^2, 0) + 2F_c^2] / 3$).

^f $R_1 = \sum ||F_o| - |F_c|| / \sum |F_o|$; $wR_2 = [\sum w(F_o^2 - F_c^2)^2 / \sum w(F_o^4)]^{1/2}$.

Crystallographic Information for Complex **369**. University of Alberta Department of Chemistry Structure Determination Laboratory Report #JMS0864.



Perspective view of one of the two crystallographically-independent $[(\eta^5\text{-C}_5\text{Me}_5)\text{-Co}\{\eta^3, \eta^2\text{-7-(3-oxobutyl)cyclohepta-2,4-dien-1-yl}\}]^+$ complex ions (moiety A) showing the atom labelling scheme. Non-hydrogen atoms are represented by Gaussian ellipsoids at the 20% probability level. Hydrogen atoms are shown with arbitrarily small thermal parameters.

Crystallographic Experimental Details

A. Crystal Data

formula	$\text{C}_{21}\text{H}_{30}\text{BCoF}_4\text{O}$
formula weight	444.19
crystal dimensions (mm)	$0.69 \times 0.21 \times 0.16$
crystal system	triclinic
space group	$P\bar{1}$ (No. 2)
unit cell parameters ^a	
<i>a</i> (Å)	8.3978 (6)
<i>b</i> (Å)	10.5938 (8)
<i>c</i> (Å)	24.6587 (18)
<i>α</i> (deg)	87.4032 (9)
<i>β</i> (deg)	88.7435 (8)
<i>γ</i> (deg)	70.2237 (8)

V (Å ³)	2062.2 (3)
Z	4
ρ_{calcd} (g cm ⁻³)	1.431
μ (mm ⁻¹)	0.876
<i>B. Data Collection and Refinement Conditions</i>	
diffractometer	Bruker D8/APEX II CCD ^b
radiation (λ [Å])	graphite-monochromated Mo K α (0.71073)
temperature (°C)	-100
scan type	ω scans (0.3°) (20 s exposures)
data collection 2θ limit (deg)	54.92
total data collected	18171 ($-10 \leq h \leq 10$, $-13 \leq k \leq 13$, $-31 \leq l \leq 31$)
independent reflections	9330 ($R_{\text{int}} = 0.0158$)
number of observed reflections (NO)	8358 [$F_o^2 \geq 2\sigma(F_o^2)$]
structure solution method	Patterson/structure expansion (<i>DIRDIF-2008</i> ^c)
refinement method	full-matrix least-squares on F^2 (<i>SHELXL-97</i> ^d)
absorption correction method	Gaussian integration (face-indexed)
range of transmission factors	0.8697–0.5841
data/restraints/parameters	9330 [$F_o^2 \geq -3\sigma(F_o^2)$] / 12^e / 556
goodness-of-fit (S) ^f	1.096 [$F_o^2 \geq -3\sigma(F_o^2)$]
final R indices ^g	
R_1 [$F_o^2 \geq 2\sigma(F_o^2)$]	0.0613
wR_2 [$F_o^2 \geq -3\sigma(F_o^2)$]	0.1641
largest difference peak and hole	1.232 and -0.656 e Å ⁻³

^aObtained from least-squares refinement of 9857 reflections with $4.47^\circ < 2\theta < 54.86^\circ$.

^bPrograms for diffractometer operation, data collection, data reduction and absorption correction were those supplied by Bruker.

^cBeurskens, P. T.; Beurskens, G.; de Gelder, R.; Smits, J. M. M.; Garcia-Granda, S.; Gould, R. O. (2008). The *DIRDIF-2008* program system. Crystallography Laboratory, Radboud University Nijmegen, The Netherlands.

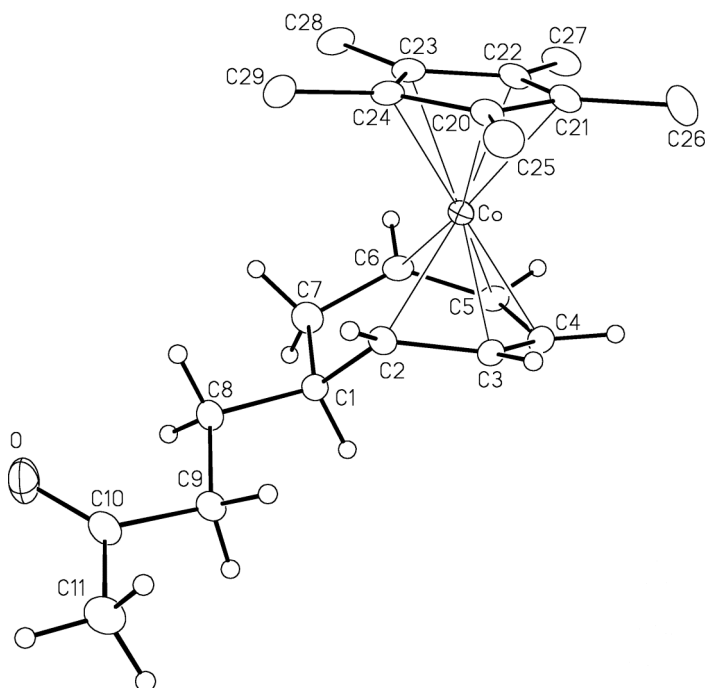
^dSheldrick, G. M. *Acta Crystallogr.* **2008**, *A64*, 112–122.

^eDistances involving the disordered ring carbons were constrained to be equal (within 0.05 Å) during refinement: $d(C2-C3A)_A = d(C4B-C5)_A = d(C2-C3A)_B = d(C4B-C5)_B$; $d(C3A-C4A)_A = d(C3B-C4B)_A = d(C3A-C4A)_B = d(C3B-C4B)_B$; $d(C4A-C5)_A = d(C2-C3B)_A = d(C4A-C5)_B = d(C2-C3B)_B$ (the A and B subscripts refer to distances within the crystallographically-independent complex ions [moieties A and B]).

^f $S = [\sum w(F_o^2 - F_c^2)^2 / (n - p)]^{1/2}$ (n = number of data; p = number of parameters varied; $w = [\sigma^2(F_o^2) + (0.0759P)^2 + 4.0333P]^{-1}$ where $P = [\text{Max}(F_o^2, 0) + 2F_c^2]/3$).

^g $R_1 = \sum ||F_o| - |F_c|| / \sum |F_o|$; $wR_2 = [\sum w(F_o^2 - F_c^2)^2 / \sum w(F_o^4)]^{1/2}$.

Crystallographic Information for Complex **370**. University of Alberta Department of Chemistry Structure Determination Laboratory Report #JMS0903.



Perspective view of the $[\text{Cp}^*\text{Co}\{7\text{-(3-oxobutyl)cyclohepta-2,4-dien-1-yl}\}]^+$ ion showing the atom labelling scheme. Non-hydrogen atoms are represented by Gaussian ellipsoids at the 20% probability level. Hydrogen atoms are shown with arbitrarily small thermal parameters, and are not shown for the Cp^* ligand.

Crystallographic Experimental Details

A. Crystal Data

formula	$\text{C}_{21}\text{H}_{30}\text{BCoF}_4\text{O}$
formula weight	444.19
crystal dimensions (mm)	$0.58 \times 0.22 \times 0.18$
crystal system	orthorhombic
space group	$P2_12_12_1$ (No. 19)
unit cell parameters ^a	
<i>a</i> (Å)	7.6504 (4)
<i>b</i> (Å)	15.5039 (7)
<i>c</i> (Å)	17.5002 (8)
<i>V</i> (Å ³)	2075.72 (17)
<i>Z</i>	4
ρ_{calcd} (g cm ⁻³)	1.421
μ (mm ⁻¹)	0.870

B. Data Collection and Refinement Conditions

diffractometer	Bruker D8/APEX II CCD ^b
radiation (λ [Å])	graphite-monochromated Mo K α (0.71073)
temperature (°C)	-100
scan type	ω scans (0.3°) (20 s exposures)
data collection 2θ limit (deg)	55.00
total data collected	18108 ($-9 \leq h \leq 9, -20 \leq k \leq 20, -22 \leq l \leq 22$)
independent reflections	4763 ($R_{\text{int}} = 0.0192$)
number of observed reflections (NO)	4642 [$F_o^2 \geq 2\sigma(F_o^2)$]
structure solution method	direct methods (<i>SIR97</i> ^c)
refinement method	full-matrix least-squares on F^2 (<i>SHELXL-97</i> ^d)
absorption correction method	multi-scan (<i>SADABS</i>)
range of transmission factors	0.8591–0.6305
data/restraints/parameters	4763 [$F_o^2 \geq -3\sigma(F_o^2)$] / 0 / 260
Flack absolute structure parameter ^e	0.491(16)
goodness-of-fit (S) ^f	1.115 [$F_o^2 \geq -3\sigma(F_o^2)$]
final R indices ^g	
R_1 [$F_o^2 \geq 2\sigma(F_o^2)$]	0.0361
wR_2 [$F_o^2 \geq -3\sigma(F_o^2)$]	0.0961
largest difference peak and hole	0.668 and -0.353 e Å ⁻³

^aObtained from least-squares refinement of 9992 reflections with $5.26^\circ < 2\theta < 56.58^\circ$.

^bPrograms for diffractometer operation, data collection, data reduction and absorption correction were those supplied by Bruker.

^cAltomare, A.; Burla, M. C.; Camalli, M.; Cascarano, G. L.; Giacovazzo, C.; Guagliardi, A.; Moliterni, A. G. G.; Polidori, G.; Spagna, R. *J. Appl. Cryst.* **1999**, *32*, 115–119.

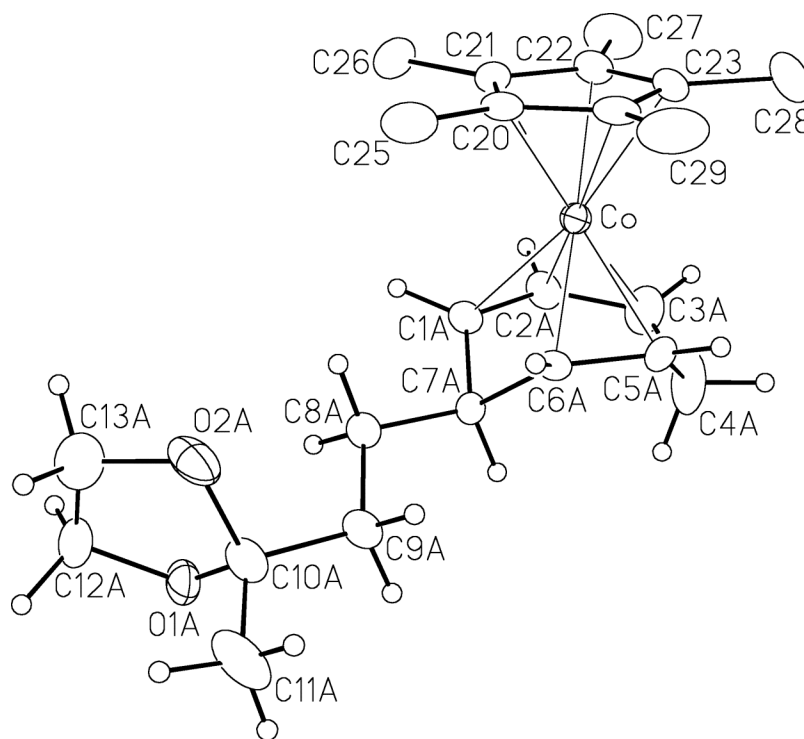
^dSheldrick, G. M. *Acta Crystallogr.* **2008**, *A64*, 112–122.

^eFlack, H. D. *Acta Crystallogr.* **1983**, *A39*, 876–881; Flack, H. D.; Bernardinelli, G. *Acta Crystallogr.* **1999**, *A55*, 908–915; Flack, H. D.; Bernardinelli, G. *J. Appl. Cryst.* **2000**, *33*, 1143–1148. The Flack parameter will refine to a value near zero if the structure is in the correct configuration and will refine to a value near one for the inverted configuration. The value observed herein is indicative of racemic twinning, and was accommodated during the refinement (using the *SHELXL-93* TWIN instruction [see reference *d*]).

^f $S = [\sum w(F_o^2 - F_c^2)^2 / (n - p)]^{1/2}$ (n = number of data; p = number of parameters varied; $w = [\sigma^2(F_o^2) + (0.0507P)^2 + 1.0999P]^{-1}$ where $P = [\text{Max}(F_o^2, 0) + 2F_c^2]/3$).

^g $R_1 = \sum ||F_o| - |F_c|| / \sum |F_o|$; $wR_2 = [\sum w(F_o^2 - F_c^2)^2 / \sum w(F_o^4)]^{1/2}$.

Crystallographic Information for Complex **377**. University of Alberta Department of Chemistry Structure Determination Laboratory Report #JMS0562.



Perspective view of the $[(\eta^5\text{-C}_5\text{Me}_5)\text{Co}\{\eta^3,\eta^2\text{-7-(2-(2-methyl-1,3-dioxolan-2-yl)ethyl)cyclohepta-2,5-dien-1-yl}\}]^+$ complex ion showing the atom labelling scheme. Non-hydrogen atoms are represented by Gaussian ellipsoids at the 20% probability level. Hydrogen atoms are shown with arbitrarily small thermal parameters except for pentamethylcyclopentadienyl hydrogens, which are not shown.

Crystallographic Experimental Details

A. Crystal Data

formula	$\text{C}_{23}\text{H}_{34}\text{BCoF}_4\text{O}_2$
formula weight	488.24
crystal dimensions (mm)	$0.58 \times 0.14 \times 0.14$
crystal system	monoclinic
space group	$P2_1/n$ (an alternate setting of $P2_1/c$ [No. 14])
unit cell parameters ^a	
<i>a</i> (Å)	11.2392 (17)
<i>b</i> (Å)	16.482 (3)
<i>c</i> (Å)	12.5865 (19)
β (deg)	91.496 (4)
<i>V</i> (Å ³)	2330.8 (6)
<i>Z</i>	4

ρ_{calcd} (g cm ⁻³)	1.391
μ (mm ⁻¹)	0.785

B. Data Collection and Refinement Conditions

diffractometer	Bruker PLATFORM/SMART 1000 CCD ^b
radiation (λ [Å])	graphite-monochromated Mo K α (0.71073)
temperature (°C)	-80
scan type	ω scans (0.3°) (20 s exposures)
data collection 2θ limit (deg)	50.00
total data collected	8933 ($-13 \leq h \leq 13$, $0 \leq k \leq 19$, $0 \leq l \leq 14$)
independent reflections	8933 ($R_{\text{int}} = 0.0000$)
number of observed reflections (NO)	5837 [$F_o^2 \geq 2\sigma(F_o^2)$]
structure solution method	direct methods (<i>SHELXS-86</i> ^c)
refinement method	full-matrix least-squares on F^2 (<i>SHELXL-93</i> ^d)
absorption correction method	multi-scan (<i>TWINABS</i>)
range of transmission factors	0.8981–0.6589
data/restraints/parameters	8933 [$F_o^2 \geq -3\sigma(F_o^2)$] / 41 ^e / 377
goodness-of-fit (S) ^f	0.980 [$F_o^2 \geq -3\sigma(F_o^2)$]
final R indices ^g	
R_1 [$F_o^2 \geq 2\sigma(F_o^2)$]	0.0582
wR_2 [$F_o^2 \geq -3\sigma(F_o^2)$]	0.1601
largest difference peak and hole	0.991 and -0.300 e Å ⁻³

^aObtained from least-squares refinement of 4575 reflections with $9.28^\circ < 2\theta < 52.27^\circ$.

^bPrograms for diffractometer operation, data collection, data reduction and absorption correction were those supplied by Bruker. The crystal used for data collection was found to display non-merohedral twinning. Both components of the twin were indexed with the program *CELL_NOW* (Bruker AXS Inc., Madison, WI, 2004). The first twin component can be related to the second component by 180° rotation about the [0 0 1] axis in both real and reciprocal space. Integrated intensities for the reflections from the two components were written into a *SHELXL-93* HKLF 5 reflection file with the data integration program *SAINTE* (version 7.06A), using all reflection data (exactly overlapped, partially overlapped and non-overlapped).

^cSheldrick, G. M. *Acta Crystallogr.* **1990**, *A46*, 467–473.

^dSheldrick, G. M. *SHELXL-93*. Program for crystal structure determination. University of Göttingen, Germany, 1993.

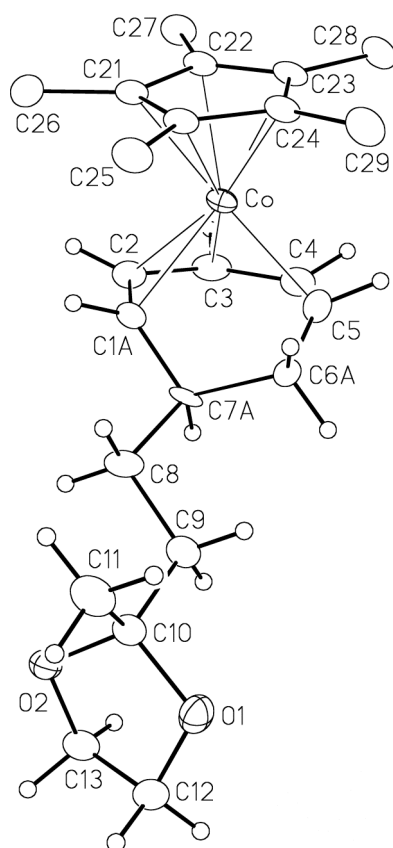
^eAnalogous bond lengths and 1,3-distances within the disordered 7-(2-(2-methyl-1,3-dioxolan-2-yl)ethyl)cyclohepta-2,5-dien-1-yl ligand were constrained to be equal (within 0.001 Å) during refinement: $d(\text{O1A}-\text{C10A}) = d(\text{O1B}-\text{C10B})$; $d(\text{O1A}-\text{C12A}) = d(\text{O1B}-\text{C12B})$; $d(\text{O2A}-\text{C10A}) = d(\text{O2B}-\text{C10B})$; $d(\text{O2A}-\text{C13A}) = d(\text{O2B}-\text{C13B})$; $d(\text{C1A}-\text{C2A}) = d(\text{C1B}-\text{C2B})$; $d(\text{C1A}-\text{C7A}) = d(\text{C1B}-\text{C7B})$; $d(\text{C2A}-\text{C3A}) = d(\text{C2B}-\text{C3B})$.

C3B); $d(C3A-C4A) = d(C3B-C4B)$; $d(C4A-C5A) = d(C4B-C5B)$; $d(C5A-C6A) = d(C5B-C6B)$; $d(C6A-C7A) = d(C6B-C7B)$; $d(C7A-C8A) = d(C7B-C8B)$; $d(C8A-C9A) = d(C8B-C9B)$; $d(C9A-C10A) = d(C9B-C10B)$; $d(C10A-C11A) = d(C10B-C11B)$; $d(C12A-C13A) = d(C12B-C13B)$; $d(O1A \cdots O2A) = d(O1B \cdots O2B)$; $d(O1A \cdots C9A) = d(O1B \cdots C9B)$; $d(O1A \cdots C11A) = d(O1B \cdots C11B)$; $d(O1A \cdots C13A) = d(O1B \cdots C13B)$; $d(O2A \cdots C9A) = d(O2B \cdots C9B)$; $d(O2A \cdots C11A) = d(O2B \cdots C11B)$; $d(O1A \cdots C12A) = d(O1B \cdots C12B)$; $d(C1A \cdots C3A) = d(C1B \cdots C3B)$; $d(C1A \cdots C6A) = d(C1B \cdots C6B)$; $d(C1A \cdots C8A) = d(C1B \cdots C8B)$; $d(C2A \cdots C4A) = d(C2B \cdots C4B)$; $d(C2A \cdots C7A) = d(C2B \cdots C7B)$; $d(C3A \cdots C5A) = d(C3B \cdots C5B)$; $d(C4A \cdots C6A) = d(C4B \cdots C6B)$; $d(C5A \cdots C7A) = d(C5B \cdots C7B)$; $d(C6A \cdots C8A) = d(C6B \cdots C8B)$; $d(C7A \cdots C9A) = d(C7B \cdots C9B)$; $d(C8A \cdots C10A) = d(C8B \cdots C10B)$; $d(C9A \cdots C11A) = d(C9B \cdots C11B)$; $d(C10A \cdots C12A) = d(C10B \cdots C12B)$; $d(C10A \cdots C13A) = d(C10B \cdots C13B)$.

$$fS = [\sum w(F_o^2 - F_c^2)^2 / (n - p)]^{1/2} \quad (n = \text{number of data}; p = \text{number of parameters varied}; w = [\sigma^2(F_o^2) + (0.0938P)^2]^{-1} \text{ where } P = [\text{Max}(F_o^2, 0) + 2F_c^2]/3).$$

$$gR_1 = \Sigma |F_o| - |F_c| / \Sigma |F_o|; \quad wR_2 = [\sum w(F_o^2 - F_c^2)^2 / \sum w(F_o^4)]^{1/2}.$$

Crystallographic Information for Complex **378**. University of Alberta Department of Chemistry Structure Determination Laboratory Report #JMS0870.



Perspective view of the $[(\eta^5\text{-C}_5\text{Me}_5)\text{Co}(\eta^5\text{-7-}\{2\text{-}(2\text{-methyl-1,3-dioxolan-2-yl)ethyl}\}\text{-cyclohepta-2,4-dien-1-yl})]^+$ ion showing the atom labelling scheme. Non-hydrogen atoms are represented by Gaussian ellipsoids at the 20% probability level. Hydrogen atoms are shown with arbitrarily small thermal parameters except for pentamethylcyclopentadienyl hydrogens, which are not shown.

Crystallographic Experimental Details

A. Crystal Data

formula	$\text{C}_{23}\text{H}_{34}\text{BCoF}_4\text{O}_2$
formula weight	488.24
crystal dimensions (mm)	$0.39 \times 0.34 \times 0.16$
crystal system	monoclinic
space group	$P2_1/c$ (No. 14)
unit cell parameters ^a	
<i>a</i> (Å)	10.0330 (8)
<i>b</i> (Å)	13.7352 (11)
<i>c</i> (Å)	16.5907 (13)

β (deg)	94.0237 (12)
V (Å ³)	2280.7 (3)
Z	4
ρ_{calcd} (g cm ⁻³)	1.422
μ (mm ⁻¹)	0.802

B. Data Collection and Refinement Conditions

diffractometer	Bruker D8/APEX II CCD ^b
radiation (λ [Å])	graphite-monochromated Mo K α (0.71073)
temperature (°C)	-100
scan type	ω scans (0.3°) (25 s exposures)
data collection 2θ limit (deg)	52.86
total data collected	9344 ($-12 \leq h \leq 12$, $0 \leq k \leq 17$, $0 \leq l \leq 20$)
independent reflections	9344 ($R_{\text{int}} = 0.0000$)
number of observed reflections (NO)	7625 [$F_o^2 \geq 2\sigma(F_o^2)$]
structure solution method	direct methods (<i>SHELXS-97</i> ^c)
refinement method	full-matrix least-squares on F^2 (<i>SHELXL-97</i> ^c)
absorption correction method	multi-scan (<i>TWINABS</i>)
range of transmission factors	0.8810–0.7460
data/restraints/parameters	9344 [$F_o^2 \geq -3\sigma(F_o^2)$] / 0 / 313
goodness-of-fit (S) ^d	1.054 [$F_o^2 \geq -3\sigma(F_o^2)$]
final R indices ^e	
R_1 [$F_o^2 \geq 2\sigma(F_o^2)$]	0.0436
wR_2 [$F_o^2 \geq -3\sigma(F_o^2)$]	0.1189
largest difference peak and hole	0.671 and -0.456 e Å ⁻³

^aObtained from least-squares refinement of 9186 reflections with $5.04^\circ < 2\theta < 48.80^\circ$.

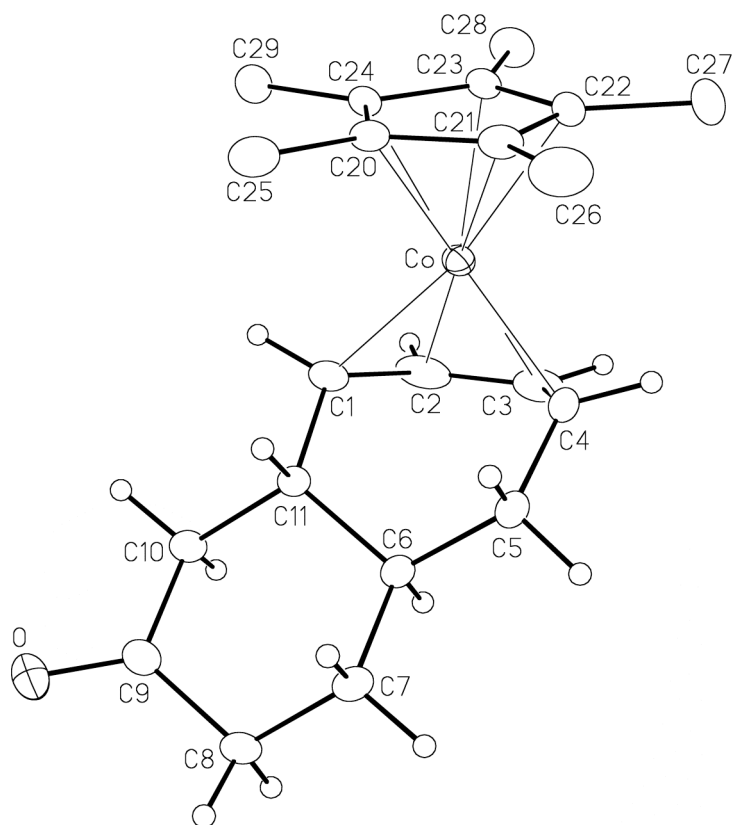
^bPrograms for diffractometer operation, data collection, data reduction and absorption correction were those supplied by Bruker. The crystal used for data collection was found to display non-merohedral twinning. Both components of the twin were indexed with the program *CELL_NOW* (Bruker AXS Inc., Madison, WI, 2004). The second twin component can be related to the first component by 180° rotation about the [0.11 0 1] axis in real space and about the [0 0 1] axis in reciprocal space. Integrated intensities for the reflections from the two components were written into a *SHELXL-93* HKLF 5 reflection file with the data integration program *SAINTE* (version 7.53A), using all reflection data (exactly overlapped, partially overlapped and non-overlapped).

^cSheldrick, G. M. *Acta Crystallogr.* **2008**, *A64*, 112–122.

^d $S = [\sum w(F_o^2 - F_c^2)^2 / (n - p)]^{1/2}$ (n = number of data; p = number of parameters varied; $w = [\sigma^2(F_o^2) + (0.0590P)^2 + 0.9767P]^{-1}$ where $P = [\text{Max}(F_o^2, 0) + 2F_c^2] / 3$).

^e $R_1 = \sum ||F_o| - |F_c|| / \sum |F_o|$; $wR_2 = [\sum w(F_o^2 - F_c^2)^2 / \sum w(F_o^4)]^{1/2}$.

Crystallographic Information for Complex **386**. University of Alberta Department of Chemistry Structure Determination Laboratory Report #JMS0913.



Perspective view of the [Cp*Co(1,3,4,4a,5,9a-hexahydro-2H-benzo[7]annulen-2-one)] molecule showing the atom labelling scheme. Non-hydrogen atoms are represented by Gaussian ellipsoids at the 20% probability level. Hydrogen atoms are shown with arbitrarily small thermal parameters, and are not shown for the Cp* methyl groups.

Crystallographic Experimental Details

A. Crystal Data

formula	C ₂₁ H ₂₉ CoO
formula weight	356.37
crystal dimensions (mm)	0.43 × 0.40 × 0.17
crystal system	monoclinic
space group	<i>P</i> 2 ₁ / <i>c</i> (No. 14)
unit cell parameters ^a	
<i>a</i> (Å)	14.0561 (14)
<i>b</i> (Å)	8.6637 (9)
<i>c</i> (Å)	16.6265 (16)
β (deg)	113.9090 (10)
<i>V</i> (Å ³)	1851.0 (3)

Z	4
ρ_{calcd} (g cm ⁻³)	1.279
μ (mm ⁻¹)	0.930
<i>B. Data Collection and Refinement Conditions</i>	
diffractometer	Bruker D8/APEX II CCD ^b
radiation (λ [Å])	graphite-monochromated Mo K α (0.71073)
temperature (°C)	-100
scan type	ω scans (0.3°) (20 s exposures)
data collection 2θ limit (deg)	50.50
total data collected	6668 ($-16 \leq h \leq 15$, $0 \leq k \leq 10$, $0 \leq l \leq 19$)
independent reflections	6668 ($R_{\text{int}} = 0.0351$)
number of observed reflections (<i>NO</i>)	5903 [$F_o^2 \geq 2\sigma(F_o^2)$]
structure solution method	direct methods (<i>SHELXS-97</i> ^c)
refinement method	full-matrix least-squares on F^2 (<i>SHELXL-97</i> ^c)
absorption correction method	multi-scan (<i>TWINABS</i>)
range of transmission factors	0.8610–0.6917
data/restraints/parameters	6668 [$F_o^2 \geq -3\sigma(F_o^2)$] / 0 / 215
goodness-of-fit (<i>S</i>) ^d	1.079 [$F_o^2 \geq -3\sigma(F_o^2)$]
final <i>R</i> indices ^e	
R_1 [$F_o^2 \geq 2\sigma(F_o^2)$]	0.0294
wR_2 [$F_o^2 \geq -3\sigma(F_o^2)$]	0.0778
largest difference peak and hole	0.227 and $-0.159 \text{ e \AA}^{-3}$

^aObtained from least-squares refinement of 4658 reflections with $5.36^\circ < 2\theta < 52.84^\circ$.

^bPrograms for diffractometer operation, data collection, data reduction and absorption correction were those supplied by Bruker. The crystal used for data collection was found to display non-merohedral twinning. Both components of the twin were indexed with the program *CELL_NOW* (Bruker AXS Inc., Madison, WI, 2004). The second twin component can be related to the first component by 180° rotation about the $[1\ 0\ -1/2]$ axis in reciprocal space and about the $[1\ 0\ 0]$ axis in real space. Integrated intensities for the reflections from the two components were written into a *SHELXL-93* HKLF 5 reflection file with the data integration program *SAINT* (version 7.60A), using all reflection data (exactly overlapped, partially overlapped and non-overlapped).

^cSheldrick, G. M. *Acta Crystallogr.* **2008**, *A64*, 112–122.

^d $S = [\sum w(F_o^2 - F_c^2)^2 / (n - p)]^{1/2}$ (n = number of data; p = number of parameters varied; $w = [\sigma^2(F_o^2) + (0.0356P)^2 + 0.5114P]^{-1}$ where $P = [\text{Max}(F_o^2, 0) + 2F_c^2] / 3$).

^e $R_1 = \sum |F_o| - |F_c| / \sum |F_o|$; $wR_2 = [\sum w(F_o^2 - F_c^2)^2 / \sum w(F_o^4)]^{1/2}$.